Sensitivity based planning and operation of modern distribution systems

by

Mohammad Abujubbeh

B.S., Eastern Mediterranean University, 2016

M.S., Middle East Technical University, 2019

AN ABSTRACT OF A DISSERTATION

submitted in partial fulfillment of the
requirements for the degree

DOCTOR OF PHILOSOPHY

Mike Wiegers Department of Electrical and Computer Engineering
Carl R. Ice College of Engineering

KANSAS STATE UNIVERSITY
Manhattan, Kansas

2023

Abstract

The power system is undergoing numerous changes due to the rapid increase in energy demand, rising concerns of climate change, and increased engagement of consumers in the energy market. Consumers are now motivated to invest in distributed energy resources (DERs), e.g., rooftop photovoltaic systems, due to their environmental advantages. The number of electric vehicles (EVs) is also increasing due to their reliability and low carbon footprint. Despite their numerous benefits, the rapid onset of DERs and EVs introduces new technical challenges to distribution systems including (1) complex system operation due to reverse power flows, (2) voltage instability issues; and (3) increased power losses due to poor DER and EV planning as well as their temporal uncertainty. Existing methods to improve the planning and operation of distribution systems in the presence of these technologies use available data from measurement devices in the grid together with traditional load flow analysis. However, some of the major limitations of existing impact-analysis techniques include (1) inability to capture uncertainty, (2) high computational burden; and (3) lack of foresight. This dissertation addresses these research gaps by proposing computationally efficient, yet accurate, sensitivity frameworks that help simplify planning and operation of modern distribution systems.

First, a novel probabilistic sensitivity framework is developed to quantify the impact of grid-edge technologies, e.g., DERs and EVs, on line losses for balanced and unbalanced distribution systems. Results show that the developed approaches offer high approximation accuracy and four-orders faster execution time when compared to classical approaches. Secondly, this dissertation develops a novel preemptive voltage monitoring approach based on low-complexity probabilistic voltage sensitivity analysis that predicts the probability distribution of node voltage magnitudes, which is then used to identify nodes that may violate the nominal operational limits with high probability. The proposed approach offers over 95%

accuracy in predicting voltage violations. To address the complexity-accuracy trade-off with existing planning methods, this dissertation develops a novel spatio-temporal sensitivity approach to analyze both spatial and temporal uncertainties associated with DER injections. The spatio-temporal framework is used to quantify voltage violations for various PV penetration levels and subsequently determine the hosting capacity of the system without the need to examine a large number of scenarios. This framework is further extended for EV charging station allocation to ensure minimum active power losses and voltage deviations. Thirdly, this dissertation develops a new system voltage influencer (SVI) paradigm that identifies strategic locations in the system that have the highest influence on node voltages. The SVI nodes are ranked and used within a stochastic control setup to eliminate voltage violations. The development of SVI paradigm is essential given the increased number of behind-the-meter and utility-controlled DERs, where it is becoming difficult to select optimal control points and counter the impact of the introduced uncertainties. The developed approaches in this dissertation help system operators quickly reveal impending voltage and loss issues resulting from power changes at the grid edge.

Sensitivity based planning and operation of modern distribution systems

by

Mohammad Abujubbeh

B.S., Eastern Mediterranean University, 2016

M.S., Middle East Technical University, 2019

A DISSERTATION

submitted in partial fulfillment of the
requirements for the degree

DOCTOR OF PHILOSOPHY

Mike Wiegers Department of Electrical and Computer Engineering
Carl R. Ice College of Engineering

KANSAS STATE UNIVERSITY
Manhattan, Kansas

2023

Approved by:

Major Professor
Balasubramaniam Natarajan

Copyright

© Mohammad Abujubbeh 2023.

Abstract

The power system is undergoing numerous changes due to the rapid increase in energy demand, rising concerns of climate change, and increased engagement of consumers in the energy market. Consumers are now motivated to invest in distributed energy resources (DERs), e.g., rooftop photovoltaic systems, due to their environmental advantages. The number of electric vehicles (EVs) is also increasing due to their reliability and low carbon footprint. Despite their numerous benefits, the rapid onset of DERs and EVs introduces new technical challenges to distribution systems including (1) complex system operation due to reverse power flows, (2) voltage instability issues; and (3) increased power losses due to poor DER and EV planning as well as their temporal uncertainty. Existing methods to improve the planning and operation of distribution systems in the presence of these technologies use available data from measurement devices in the grid together with traditional load flow analysis. However, some of the major limitations of existing impact-analysis techniques include (1) inability to capture uncertainty, (2) high computational burden; and (3) lack of foresight. This dissertation addresses these research gaps by proposing computationally efficient, yet accurate, sensitivity frameworks that help simplify planning and operation of modern distribution systems.

First, a novel probabilistic sensitivity framework is developed to quantify the impact of grid-edge technologies, e.g., DERs and EVs, on line losses for balanced and unbalanced distribution systems. Results show that the developed approaches offer high approximation accuracy and four-orders faster execution time when compared to classical approaches. Secondly, this dissertation develops a novel preemptive voltage monitoring approach based on low-complexity probabilistic voltage sensitivity analysis that predicts the probability distribution of node voltage magnitudes, which is then used to identify nodes that may violate the nominal operational limits with high probability. The proposed approach offers over 95%

accuracy in predicting voltage violations. To address the complexity-accuracy trade-off with existing planning methods, this dissertation develops a novel spatio-temporal sensitivity approach to analyze both spatial and temporal uncertainties associated with DER injections. The spatio-temporal framework is used to quantify voltage violations for various PV penetration levels and subsequently determine the hosting capacity of the system without the need to examine a large number of scenarios. This framework is further extended for EV charging station allocation to ensure minimum active power losses and voltage deviations. Thirdly, this dissertation develops a new system voltage influencer (SVI) paradigm that identifies strategic locations in the system that have the highest influence on node voltages. The SVI nodes are ranked and used within a stochastic control setup to eliminate voltage violations. The development of SVI paradigm is essential given the increased number of behind-the-meter and utility-controlled DERs, where it is becoming difficult to select optimal control points and counter the impact of the introduced uncertainties. The developed approaches in this dissertation help system operators quickly reveal impending voltage and loss issues resulting from power changes at the grid edge.

Table of Contents

List of Figures

List of Tables

List of Nomenclature

ADMS	Advanced distribution management system
CLF	Classical load flow
DER	Distributed energy resources
ELF	Exact loss formula
EV	Electric vehicle
EVCS	EV charging station
HC	Hosting capacity
JSD	Jensen-Shannon distance
LSA	Loss sensitivity analysis
LSM	Loss sensitivity factor
MC	Matrix completion
MDS	Modern distribution system
MILP	Mixed integer linear program
MPC	Model predictive control
NAF	Nodal allocation factor
NSF	Nodal sensitivity factor
PL	Penetration level
PLSA	Probabilistic loss sensitivity analysis
PV	Photovoltaic
PVSA	Probabilistic voltage sensitivity analysis
QP	Quadratic program
SE	State estimation
ST-PVSA	Spatio-temporal PVSA

STS	Standard test system
SVI	System voltage influencer
VC	Voltage controller
VVP	Voltage violation prediction

Acknowledgments

Foremost, I would like to express my sincere gratitude to my supervisor Dr. Bala Natarajan for his continuous support, encouragement, and patience during my Ph.D. study and research. His knowledge, passion for work, and ability to inspire are truly remarkable. I am very thankful to him for his interest in my research and for being always available despite his busy schedule. I would like to extend my thanks and special appreciation to my doctoral committee members, Dr. Anil Pahwa, Dr. Hongyu Wu, and Dr. Cen Wu for their time and comments to improve the quality of my research.

Special thanks to my colleagues Dr. Kumarsinh Jhala, Dr. Loiy Al-Ghussain, and Dr. James Rajasekaran for working alongside me and providing constant motivation. I would like to also thank members of the CPSWin group, Hazhar Sufi Karimi, Sai Munikoti, Shweta Dahale, Dylan Wheeler, Biswajeet Rout, Deepesh Agarwal, Priyanka Gautam, Aabila Tharzeen, and Prudhviraj Dhanapala for their support, encouragement, and guidance. Thanks to my dear friends Eda Kaya, Arman Malekloo, Mohammad Abu Saleh, Erfan Saydanzad, Aysu Deniz, Aziz Alrwaili, Mohammad Alabed, Mehmetcan Gursoy, Shima Soleimani, Mohanish Andurkar, and Ingrid Lindal. I will always miss the moments we shared.

I am forever grateful to my parents Fayzeh Qaddoura and Abdullah Abujubbeh for their unconditional love, support, and unwavering trust in me. Special thanks to my supportive siblings, Wael, Shareef, Sahar, and Mousa for their support despite the long distance. I dedicate this dissertation to my father (Rest in Peace) that had been and will always be my role model and my greatest teacher. I hope that I made you proud.

This work is partly supported by the Department of Energy, Office of Energy Efficiency and Renewable Energy (EERE), Solar Energy Technologies Office, under Award DE-EE0008767 and National Science Foundation under award #1855216.

Dedication

To my parents.

Preface

This dissertation, "Sensitivity based operation and planning of modern distribution systems," is submitted for the degree of Doctor of Philosophy in the Mike Weigers Department of Electrical and Computer Engineering at Kansas State University. The research was conducted under the supervision of Professor Balasubramaniam Natarajan. This work is original to the best of my knowledge, except where acknowledgments and references are indicated. Most of the work has been presented in the following published peer-reviewed journals and conferences:

1. M. Abujubbeh, S. Munikoti, A. Pahwa, and B. Natarajan, "Probabilistic loss sensitivity analysis in power distribution systems," IEEE Transactions on Power Systems, 2022.

2. M. Abujubbeh and B. Natarajan, "Overview of loss sensitivity analysis in modern distribution systems," IEEE Access, vol. 10, pp. 16037-16051, 2022.

3. M. Abujubbeh, S. Munikoti, and B. Natarajan, "Analytical power loss sensitivity analysis in distribution systems," in 2021 IEEE Power & Energy Society General Meeting (PESGM), pp. 1-5, IEEE, 2021.

4. M. Abujubbeh and B. Natarajan, "A novel stochastic framework to quantify losses in unbalanced distribution systems," in IEEE Transactions on Power Systems, Under Review, 2023.

5. M. Abujubbeh, S. Dahale, and B. Natarajan, "Voltage violation prediction in unobservable distribution systems," in 2022 IEEE Power & Energy Society General Meeting (PESGM), pp. 1-5, IEEE, 2022.

6. M. Abujubbeh, S. Munikoti, and B. Natarajan, "Probabilistic voltage sensitivity based preemptive voltage monitoring in unbalanced distribution networks," in 2020 52nd North American Power Symposium (NAPS), pp. 1-6, IEEE, 2021.

7. M. Abujubbeh and B. Natarajan, "A new probabilistic framework for ev charging station planning in distribution systems considering spatio-temporal uncertainties," in IEEE Kansas Power and Energy Conference (KPEC), Under Review, 2023.

8. S. Munikoti, M. Abujubbeh, K. Jhala, and B. Natarajan, "A novel framework for hosting capacity analysis with spatio-temporal probabilistic voltage sensitivity analy-11sis,"International Journal of Electrical Power & Energy Systems, vol. 134, p. 107426, 2022.

9. M. Abujubbeh, M. Sai, K. Jhala, and B. Natarajan, "A new analytical voltage influencer paradigm for voltage control in power distribution systems," in International Journal of Electrical Power & Energy Systems, Under Review, 2023.

10. M. Abujubbeh and B. Natarajan, "A novel dynamic voltage influencing metric for cost-effective voltage control in unbalanced distribution systems," in 2023 IEEE PES GTD, Accepted, 2023.

11. M. Abujubbeh, R. K. James, A. Pahwa, B. Natarajan, "Optimal voltage control in lowobservable unbalanced distribution systems," in 2022 IEEE Power & Energy Society Innovative Smart Grid Technologies Conference (ISGT), pp. 1-5, IEEE, 2022.

12. S. Munikoti, M. Abujubbeh, K. Jhala, and B. Natarajan, "An information theoretic approach to identify dominant voltage influencers for unbalanced distribution systems," IEEE Transactions on Power Systems, 2022.

Chapter 1

Introduction

Power systems are the backbone of modern life. These energy infrastructure enables multiple other infrastructures that societies use to function and prosper. However, power systems across the globe are witnessing various structural changes as a response to the exponential growth in energy demand, increased impacts of climate change and aging system infrastructure. For instance, there is growing investment in green distributed energy resources (DERs), e.g., rooftop solar photovoltaic (PV) systems, for the numerous environmental, technical and economic advantages they provide [1]. The number of Electric Vehicles (EVs) is also increasing due to their reliability and low carbon footprint [2]. This motivated the inclusion of sensory devices to obtain measurements of voltage states, current flows, and energy consumption patterns at the grid-edge [3]. Fig. 1.1 shows a simple illustration of a modern power distribution system that accommodates DERs, EVs, and sensors for different entities such as residential and industrial consumers. Consumers in modern distribution systems are no longer perceived as static entities. In the modern framework, consumers are able to actively participate in the energy market through local energy management, home automation, energy storage and usage, EV charging and many other ancillary services [4]. In addition, consumers will be able to schedule their loads based on dynamic prices of electricity [5]. The motives for consumers to engage in such activities can be: (1) reducing carbon footprint; (2) economic profitability, or (3) raising living standards through seeking comfort [6]. However,

the increased engagement of consumers in such activities may impose new challenges to the operation of the system. For example, the rapid onset of DER and EV integration may cause abrupt power changes that introduce technical challenges to system operation such as (1) reverse power flow [7], (2) voltage instability issues [8]; and (3) increased power losses [9]. Therefore, system operators are motivated to plan, monitor, control the integration of grid-edge resources and consumer activities to improve overall system efficiency.

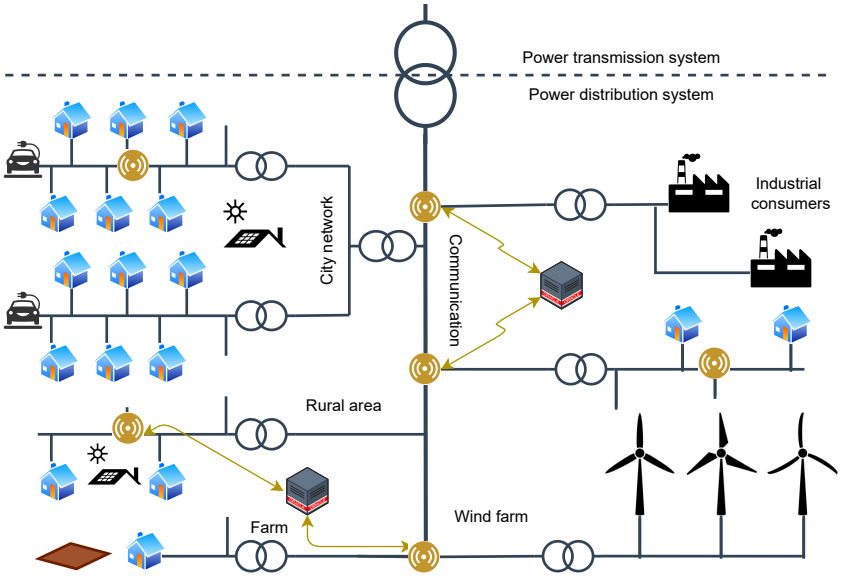

Figure 1.1: Illustration of a modern distribution system.

In this regard, sensitivity analysis (also known as impact-analysis study [10]) has garnered a huge attention due to three main reasons: (1) abrupt power changes can lead to unanticipated voltage issues that are difficult to handle with classical approaches [11], (2) large contribution to economic losses and degradation of system efficiency [12]; and (3) strict compliance requirements of emerging distribution system regulatory standards (e.g., the IEEE Std 1547-2018 indicates that inverter-based DERs shall be equipped with reactive power demand and injection functionality up to 44% of their power ratings for voltage support [13]). Specifically, sensitivity analysis exploits topological information and available system states (via sensory devices or state estimation) to study the relationship between power changes induced by grid-edge technologies and the resulting change in system parameters such as voltage profiles and line current flow or losses [14]. The first step toward

successful implementation of sensitivity analysis in modern systems involves capturing the dependencies between grid-edge technologies, which in turn serves as a tool to quantifying their impact on system performance. For instance, a positive increase in power at the grid-edge could represent an increase in local load or a decrease in PV power injection. Similarly, a negative power change could represent a decrease in EV power demand or an increase in PV generation. Given the interconnected structure of power distribution systems, when these changes occur at any node, voltage fluctuates at other nodes, which increases the possibility of voltage magnitudes exceeding safe operational limits - a detrimental scenario that causes power disruptions. In addition to voltage fluctuations, line current flow can increase/decrease depending on the change in power, which leads to excessive power losses. Furthermore, sensitivity analysis involves analyzing the impact of system imbalance due to heavy concentration of consumers on any of system phases, resulting in a holistic framework that incorporates practical scenarios.

Several works have used sensitivity analysis to enable various downstream applications. Essentially, system operators use this sensitivity information to monitor power losses and voltage states [10], implement hosting capacity analysis, enable optimal DER [15, 16] and capacitor placement and sizing [17], feeder reconstruction and network configuration [18] or optimal allocation of EV charging stations [2]. Additionally, sensitivity analysis can be used to implement efficient volt-var control algorithms to bring voltage states within the permissible limits by adjusting the active and reactive power setpoints of DERs at the grid edge [19]. Therefore, the development of simple and accurate techniques to quantify the impact of power changes on the system is an essential need for the successful adaptation of reliable and efficient power systems. Although there have been various methods developed under each downstream application, the shortcomings of these sensitivity methods make them inadequate to address the requirements of modern power distribution systems. The shortcomings of existing methods are summarized below.

- **Inability to capture uncertainty:** Power changes caused by the integration of grid-edge technologies are random due to variable load changes, variable EV charging

patterns, and weather-related fluctuation of DER power output. The major drawback of existing sensitivity methods that compute the impact of grid-edge technologies on voltage change and power losses, is that they are deterministic and do not incorporate this random behavior. The inability to model the random behavior of power changes heavily impacts the accuracy of results obtained with such methods and causes them to miss important details that otherwise may hinder system reliability.

- **High computational burden:** Existing approaches on computing the sensitivity are computationally complex, which make intractable for large practical systems. This is because such methods require recomputing system states whenever a change occurs at the grid-edge. For example, the Jacobian matrix provides a deterministic sensitivity metric between different nodes in the system. This matrix is not valid when a change in the system state occurs, e.g., a new PV or EV charging station is integrated, which increases the computational requirement of existing methods. Additionally, to capture the uncertainty of power changes, classical approaches require simulating a large number of Monte-Carlo scenarios. For example, to approximate the distribution of voltage magnitude, multiple load-flow scenarios must be simulated with existing approaches, making them intractable for preemptive voltage monitoring.

- **Lack of foresight:** Conventional impact-analysis studies, e.g., voltage sensitivity for control applications via traditional capacitor banks and tap changers, represent reactionary approaches and do not exploit any knowledge of voltage state based on anticipated power fluctuations. One reason for resorting to such reactive approaches is the difficulty in estimating the states of a distribution system due to lack of foresight on system states. That is, the efficacy of classical methods is dependent on the ability to accurately predict voltage violations in the system so that operational setpoints of the PV inverters can be appropriately set in advance. The development of quick voltage violation prediction techniques provides more insights to system operators and removes the reliance on reactionary control approaches.

- **Modeling inefficiencies:** While traditional methods can provide basic topological sensitivity metrics (usually static metrics valid for a given system state), they do not provide any additional information on strategic locations for efficient system planning or control applications. For example, in the case of PV/EV hosting capacity analysis, existing methods rely on large number of scenarios to capture both spatial (e.g., location of PV/EV charging station installation) and temporal uncertainties. Since these methods are simulation-based, their accuracy is heavily impacted by the number of scenarios created, i.e., a higher accuracy requires a higher number of simulated scenarios. This creates a trade-off between accuracy and computational efficiency, making such methods inadequate for system planning. Additionally, the continuous growth in field controllers (i.e., inverter-based DERs) makes it difficult to implement real-time control due to limited communication bandwidth and lack of interoperability standards (see section II-B of the recent tutorial [12]). Unfortunately, classical control approaches cannot identify a subset of strategic locations to provide voltage support via inverter-based DERs, which otherwise could help reduce control cost and communication requirements.

Based on these shortcomings in literature, this dissertation aims to address a few fundamental research questions. The research questions of this dissertation as well as the resulting scientific contributions are discussed below in sections 1.1 and 1.2, respectively. The organization of chapters is explained in 1.3.

1.1 Research questions

Question 1: *Analytical approximation of change in line losses: Can we remove the reliance on multiple load-flow simulations to capture uncertainties caused by grid-edge technologies? Is there a way to bound the approximation error resulting from the analytical sensitivity approach?*

Question 2: *Can the developed analytical approximation hold promise for unbalanced distribution systems? For example, can we compute the probability distribution of line losses*

for any phase in the system?

Question 3: *Preemptive voltage monitoring:*

(a) *Is it possible to predict voltage violations based on anticipated power fluctuations?*

(b) *How robust is the voltage violation prediction rule against missing/erroneous measurements?*

Question 4: *Efficient system planning:*

(a) *Can we exploit topology information to simplify the accuracy-complexity trade-off with existing hosting capacity analysis methods?*

(b) *How does analytical sensitivity-based metrics help in EV charging station planning? Can we find a strategic location that minimizes losses and voltage deviations?*

Question 5: *Inverter-based DER control:*

(a) *Distribution systems typically lack measurements, rendering them unobservable. Can we maintain adequate control performance even when the system is unobservable?*

(b) *Can we identify strategic locations in the system to implement voltage control programs?*

(c) *Can we dynamically identify a set of strategic locations that can be used in dynamic control applications?*

1.2 Contributions

To address research question 1, Chapter 4 of this dissertation proposes a novel analytical approximation of line loss sensitivity analysis. The proposed framework models power changes due to grid-edge technologies as a stochastic process and computes the resulting probability distribution of line losses, which removes the need to run multiple load flow scenarios to capture power uncertainties. The developed probabilistic sensitivity approach is then used in 7

for probabilistic EV charging station planning. The major contributions of these chapters are listed below.

- This work derives, for the first time, an analytical expression that approximates the changes in line current flows due to deterministic complex power variations at any node in the system (Theorem 1).
- This work further develops analytical expressions to study the aggregate impact of multiple active consumers changing their complex power simultaneously on power losses in the system (Corollary 2).
- The derived analytical expressions of line current and power loss changes are extended to account for variability associated with DER power injections at active consumer sites in the system resulting in a unique probabilistic sensitivity result.
- The approximation error of the deterministic approximation is shown to be upper bounded as shown in Corollary 3. In addition, the Jensen-Shannon distance between the proposed and simulated loss probability distributions is in the order of 10^{-2}, which demonstrates the high accuracy of the proposed method.
- The computational complexity of the proposed method is significantly lower than existing load flow-based methods, i.e., four-orders faster execution time.

More details on the probabilistic loss sensitivity analysis can be found in Chapters 3 and 4, and in the following articles:

- M. Abujubbeh, S. Munikoti, A. Pahwa, and B. Natarajan, "Probabilistic loss sensitivity analysis in power distribution systems," in *IEEE Transactions on Power Systems*, 2022 [20].
- M. Abujubbeh and B. Natarajan, "Overview of loss sensitivity analysis in modern distribution systems," in *IEEE Access*, vol. 10, pp. 16037-16051, 2022 [21].

- M. Abujubbeh, S. Munikoti, and B. Natarajan, "Analytical power loss sensitivity analysis in distribution systems," in *2021 IEEE Power & Energy Society General Meeting (PESGM)*, pp. 1-5, IEEE, 2021[22].

An analytical sensitivity framework is derived in Chapter 5 to address research question 2. Specifically, Chapter 5 of this dissertation extends the probabilistic sensitivity to the generic case, i.e., three-phase unbalanced distribution systems. This extension accounts for the effect of mutual coupling impedance across different phases, which further increases the generalizibility of the proposed approach. The generalizibility of this framework allows accurate modeling of grid-edge technologies with the presence of system imbalance due to higher concentration of consumer activities on any of the three phases [23, 24]. The key contributions of this work can be listed as follows.

- Proposes a new analytical approximation of the change in line flow due complex power changes at a single and multiple node(s) in three-phase unbalanced distribution systems as shown in Theorem 2 and Eq. (5.8), respectively.

- Derives an analytical expression for the change in line losses due to consumer activities at multiple locations in three-phase unbalanced distribution systems as shown in Eq. (5.13).

- Extends the probabilistic sensitivity framework to derive the probability distribution of change in current flow and change in line losses. The resulting unique probability distributions can be used to simplify planning applications in unbalanced power distribution systems as shown in Chapter 7.

- Estimates the deterministic and stochastic changes in line current flows as well as losses with a high accuracy when compared to classical load-flow based method. It has been shown that the deterministic approximation offers over 98% accuracy via the mean absolute percentage error (MAPE) and the probability distributions can be estimated with very low Jensen-Shannon distances.

- The proposed method is validated against conventional approaches in the standard IEEE 37-node and IEEE 123-node test systems.

More details on the probabilistic framework for three phase-unbalanced distribution systems can be found in Chapters 5 and in the following article:

- M. Abujubbeh and B. Natarajan, "A novel stochastic framework to quantify losses in unbalanced distribution systems," in *IEEE Transactions on Power Systems*, Under Review, 2023. [25].

To address research question 3-a, a voltage violation prediction (VVP) framework is developed with a focus on identifying nodes with high probability of violating voltage limits at different time instances. Leveraging existing knowledge of voltage states along with uncertain forecasts of power generation/demand, probabilistic voltage sensitivity analysis is used to reveal impending voltage issues at any node in the system. Unlike existing probabilistic sensitivity methods, the proposed approach focuses on computing the probability distribution of voltage magnitude rather than the distribution of magnitude of voltage change. Research question 3-b focuses on studying the robustness of the proposed preemptive monitoring tool in cases where voltage measurements are missing. Therefore, to address this research question, we incorporate Bayesian matrix completion (BMC)-based state estimation within the probabilistic voltage sensitivity framework. The key contributions of these methods are summarized as follows.

- A probabilistic voltage sensitivity analysis based approach that predicts the probability of future voltage violations due to change in complex power injection is proposed. The approach is used to predict the number of violations in the system at any time instant (based on forecasted PV generation).

- The complexity of the proposed analytical approach is significantly lower than traditional load flow-based methods.

- The efficacy of the proposed VVP approach is generic to low-observable unbalanced distribution systems.

- The proposed approach that integrates state estimation and forecast-based probabilistic voltage sensitivity to account for distribution system unobservability and measurement errors.

- The proposed approach provides 90% VVP accuracy with 50% fraction of available data, which makes it a suitable tool for predictive voltage control applications in modern distribution systems.

More details on the probabilistic voltage violation prediction can be found in Chapter 6 and in the following articles:

- M. Abujubbeh, S. Dahale, and B. Natarajan, "Voltage violation prediction in unobservable distribution systems," in *2022 IEEE Power & Energy Society General Meeting (PESGM)*, pp. 1-5, IEEE, 2022 [26].

- M. Abujubbeh, S. Munikoti, and B. Natarajan, "Probabilistic voltage sensitivity based preemptive voltage monitoring in unbalanced distribution networks," in *2020 52nd North American Power Symposium (NAPS)*, pp. 1-6, IEEE, 2021 [27].

In Chapter 7, a generic spatio-temporal framework is proposed to address the accuracy-complexity trade-off with existing distribution system planning methods, e.g., for PV hosting capacity analysis (question 4-a) or EV charging station allocation (question 4-b). In addition to temporal uncertainty in power changes, the spatio-temporal framework exploits topology information to derive an analytical relationship between power changes and nodal voltage changes and line current losses. The development of the spatio-temporal framework helps improve the efficiency of existing grid planning initiatives. For example, using the proposed spatio-temporal sensitivity, it is possible to evaluate PV hosting capacity in the system without the need to evaluate every possible spatial allocation scenario of PV systems. Similarly, one can use the spatio-temporal framework to find the most suitable location of EV charging station that minimizes losses or voltage deviations. The key contributions of this work are listed below.

- For the first time, the probability distribution of voltage change due to random change in complex power (temporal) across random locations (spatial) of a three phase unbalanced distribution system is derived analytically.

- The proposed approach method is used to (1) analyze the aggregate effect of spatial random distribution of PVs on the feeder voltage, and (2) determine the probability of node voltages exceeding allowable limits.

- This method involves a substantial change in the formulation compared to [26] since incorporating both spatial and temporal randomness in a three phase setting requires extensive mathematical and statistical analysis for obtaining the probability distribution of voltage change.

- The proposed approach is employed to efficiently and accurately determine PV hosting capacity in a significantly faster way. For e.g., three orders faster in IEEE 123-node system relative to the existing load flow-based approach.

- The proposed approach also accounts for spatio-temporal uncertainties of EV load and computes the distribution of total changes in power losses and voltage deviation as shown in Eq. (7.33) and (7.34), which is then used to strategic locations of EV charging station placement.

- Analytical results are validated using simulation on the IEEE 37-node and 123-node test systems.

More details on the spatio-temporal sensitivity frameworks can be found in Chapter 7 and in the following articles:

- M. Abujubbeh and B. Natarajan, "A new probabilistic framework for ev charging station planning in distribution systems considering spatio-temporal uncertainties," in *IEEE Kansas Power and Energy Conference (KPEC)*, Under Review, 2023 [28].

- S. Munikoti, M. Abujubbeh, K. Jhala, and B. Natarajan, "A novel framework for hosting capacity analysis with spatio-temporal probabilistic voltage sensitivity analysis,"

in *International Journal of Electrical Power & Energy Systems*, vol. 134, p. 107426, 2022 [14].

To address question 5-a, Chapter 8 proposes a model predictive control (MPC)-based method for optimal voltage control in unobservable distribution systems with the presence of PV injections. Unlike existing approaches, this method uses only 50% fraction of available data to estimate missing states using matrix completion approach. As for question 5-b, a new system voltage influencers (SVI) paradigm is developed based on dominant influencer of voltage fluctuations (DIVF) paradigm to identify the most dominant nodes that significantly impact system voltages. Using these nodes within the control program helps improve the efficiency of existing control algorithms in terms of computational effort and control cost. There could be scenarios where power changes due to grid-edge technologies are high, which might impact the rank of nodes within the SVI set. Therefore, we compute the SVI set dynamically using analytically derived probabilistic voltage sensitivity approach, which addresses question 5-c. The contributions of this work can be summarized as follows.

- Unlike existing methods, this work does not assume full availability of state measurements at all nodes and uses matrix completion based approach to estimate the states of nodes where measurements are missing.

- This work remove the reliance on scenario based analysis and Jacobian sensitivity matrix calculations where it uses an analytical voltage sensitivity framework to update voltage states.

- A new analytical approach is proposed to compute the SVI set of inverter-based DERs to participate in distribution system voltage control applications as shown in Eq. (8.36). The set contains the most dominant nodes that impact voltage services across the system.

- The proposed approach utilizes a stochastic control framework to account for uncertainty related to DER variability and changeable load patterns. The results demon-

strate that using the stochastic framework, it is possible to minimize voltage violations caused by DER uncertainty.

- This work outperforms existing methods in terms of computational efficiency with at least an order faster execution time (Proposition 1).
- This work accounts for controller constraints and provides effective voltage support with significantly lower control cost compared to traditional methods (Proposition 2).

More details on the developed inverter-based DER control can be found in Chapter 8 and in the following articles:

- M. Abujubbeh, M. Sai, K. Jhala, and B. Natarajan, "A new analytical voltage influencer paradigm for voltage control in power distribution systems," in *International Journal of Electrical Power & Energy Systems*, Under Review, 2023 [29].
- M. Abujubbeh and B. Natarajan, "A novel dynamic voltage influencing metric for cost-effective voltage control in unbalanced distribution systems," in *2023 IEEE PES GTD*, Accepted, 2023 [30].
- M. Abujubbeh, R. K. James, A. Pahwa, B. Natarajan, "Optimal voltage control in low-observable unbalanced distribution systems," in *2022 IEEE Power & Energy Society Innovative Smart Grid Technologies Conference (ISGT)*, pp. 1-5, IEEE, 2022 [31].
- S. Munikoti, M. Abujubbeh, K. Jhala, and B. Natarajan, "An information theoretic approach to identify dominant voltage influencers for unbalanced distribution systems," in *IEEE Transactions on Power Systems*, 2022 [32].

1.3 Organization of this dissertation

The structure of this dissertation is outlined in figure 1.2. Chapter 2 discusses the related literature work. Chapter 3 provides a comparative analysis of existing methods on loss sensitivity analysis and discusses the research gaps and future research directions. Chapter

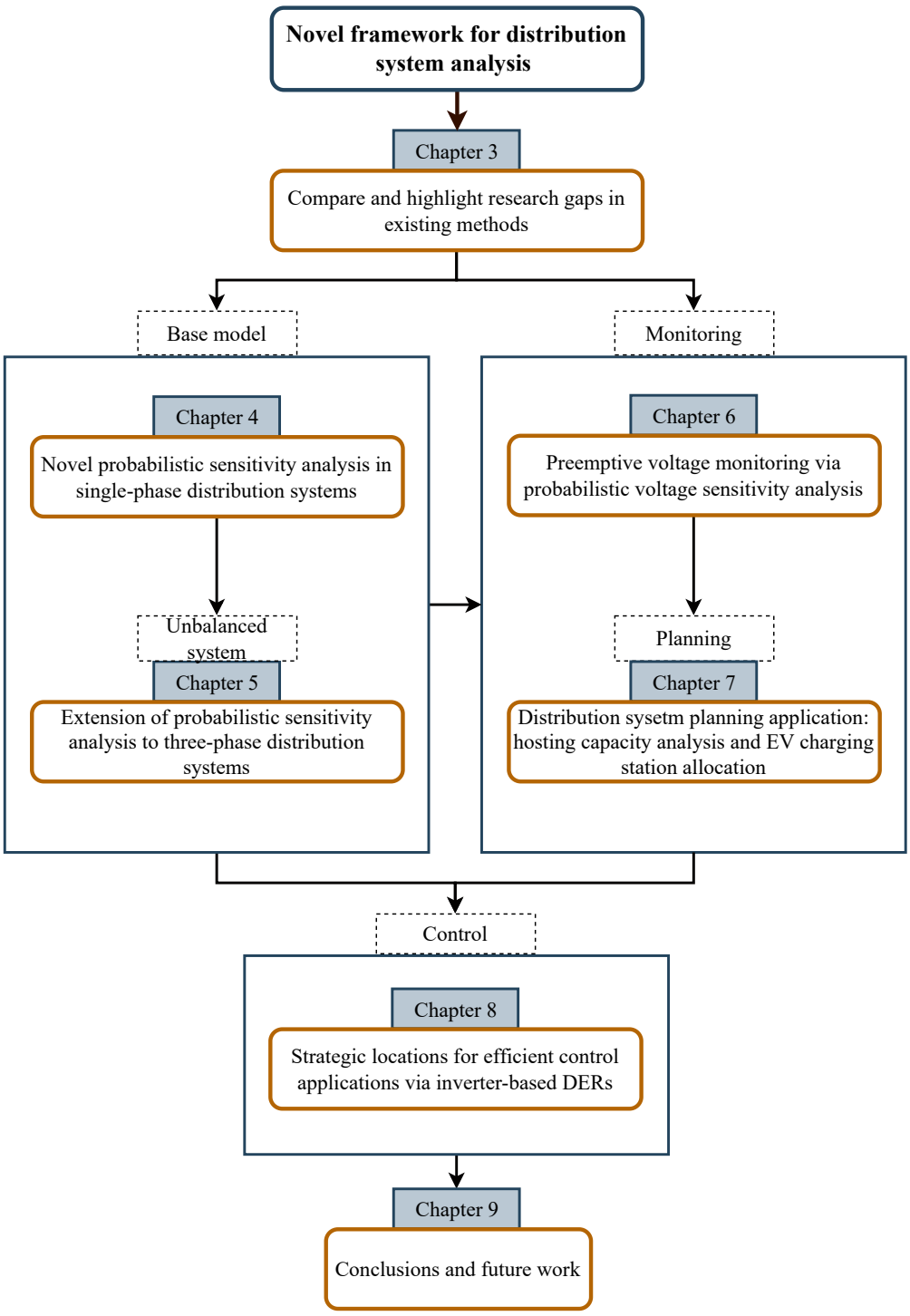

Figure 1.2: Outline of the dissertation.

4 develops a novel probabilistic loss sensitivity analysis framework for single-phase power distribution systems. By leveraging the fundamental work of Chapter 3, a generic probabilistic sensitivity framework is developed for three-phase unbalanced distribution systems in

Chapter 5. Chapter 6 proposes an analytical framework for preemptive voltage monitoring applications. In this chapter the voltage violation prediction rule is updated using Bayesian matrix completion for maintaining adequate prediction accuracy in unobservable systems. Chapter 7 proposes a novel spatio-temporal sensitivity approach to simplify complexity-accuracy trade-off with existing approaches. The developed spatio-temporal approach is then used for downstream planning applications such as PV hosting capacity analysis and EV charging station allocation. Chapter 8 discusses the proposed state-estimation based voltage control approach and develops static and dynamic SVI paradigm for efficient voltage control applications. Finally, Chapter 9 concludes this dissertation and suggests possible future research directions.

Chapter 2

Literature review

This chapter provides details on the research gaps of existing works and provides a review of the literature of the topics discussed in this dissertation.

2.1 Loss sensitivity analysis

Prior work on loss sensitivity analysis in distribution systems can be broadly grouped into two main categories: (1) analytical methods, and (2) classical load flow-based methods. As far as analytical methods are concerned, the most widely used method in the literature is based on computing nodal sensitivity factors [33, 34]. In this analytical method, the sensitivity of system losses is related to complex nodal changes through partial derivatives of line losses with respect to active or reactive power injection [35, 36]. The nodal sensitivity factor list helps reduce the search space when applying heuristic optimization algorithms for finding the best location or size of the DER [36]. For instance, in [16, 37] an analytical method is presented to find the optimal bus for installing DG in a power distribution system based on bus admittance matrix, generation information and load distribution of the system. Similarly, authors in [38, 39] propose a loss sensitivity-based method for placement of DERs in distribution systems. Here, loss sensitivity is used to examine the impact of DER injection on active power losses, which helps to determine optimal locations for DERs in the system

[40]. Similar to nodal sensitivity factors, there are few analytical methods that focus on nodal allocation factors. The main idea of nodal allocation factors is to study the contribution of nodal complex power changes to system losses. Under this category, three popular types are typically used in literature: (1) incremental allocation method [41]; (2) Z-bus allocation [42] method, and (3) proportional sharing method [43]. In [41], nodal allocation factors are based on generator domains (the set of nodes that are supplied by each generator) and the set of commons (the set of nodes supplied by the same generator). The set of domains and commons are computed to determine the contribution of each generator to line flows, and thereby determine the contribution to line losses. Similarly, the z-bus allocation method is based on Z-bus matrix of the system (inverse of admittance matrix Y-bus). Authors in [42] use the Z-bus allocation method to determine incentive or penalties to nodal load increments considering system losses. However, such methods do not scale very-well with regard to computational complexity when the analysis is extended to large systems. When the size of the test system is small (e.g., 6 nodes [42]), it is difficult to generalize any method to real-world practical systems that are characterized by a large number of nodes. This is especially problematic when the method involves running multiple loops such as in (1) classical load flow analysis to capture DER variability [44], or (2) in the Z-bus allocation method to compute the set of domains and commons in the system. In addition, the incremental sharing method requires an algorithmic extension to be applicable for systems larger than 4 nodes [41]. Although nodal sensitivity factors help guide optimal DER planning strategies [45], results obtained from such methods are valid for a given scenario of power change. In this case, the nodal sensitivity factor list may differ across time considering dynamic load analysis, which unfortunately cannot be captured by traditional analytical loss sensitivity methods. Other approaches in the literature use polynomial chaos theory to compute voltage sensitivity in distribution systems [46]. Here, the approach involves finding basis polynomial functions to approximate the voltage change as a way to replace brute-force Monte Carlo simulations. However, the accuracy of this method depends greatly on the number of basis polynomials used to compute the voltage sensitivity. For example, for a 2 node distribution system with 4 loads, 15 polynomials are required to compute voltage sensitivity [46]. Additionally, the

computational complexity of this method directly varies with the number of polynomials, resulting in an accuracy-complexity trade-off [46, 47]. Power loss sensitivity can also be determined using the classical load flow-based approach [48]. Here, the loss sensitivity is computed based on the voltage change due to complex power changes at different locations. In this regard, the change in voltage can be determined based on the Jacobian matrix of the system [49], i.e., partial derivatives of power flow equations with respect to nodal voltage magnitude and angles [44]. This can be used to determine the change in line current flows, which enables computing the changes in line power losses.

Most of the prior work on loss sensitivity considers computationally complex traditional methods of sensitivity analysis or traditional power flow equations. Such methods may not be adequate to address the needs of modern distribution systems for the following reasons. First, results obtained from such methods are scenario-specific and the inclusion of dynamic behavior of active consumers impacts their consistency. This hinders their applicability in real-time applications like finding the optimal location for EV charging or power loss monitoring [50]. Second, traditional sensitivity methods are computationally complex and require simulating a large number of scenarios to obtain the sensitivity of each scenario. It is important to note that the computational complexity of these methods increases with the increase in system size. Finally, in distribution systems, complex power changes at active consumer sites can be random due to variability in PV power outputs or dynamic load behaviors. This is unfortunately not considered in traditional analytical and load flow-based sensitivity methods. It should be noted that uncertainties of PV units (or DERs in general) can be captured by simulating a large number of scenarios, where the sensitivity can be computed. However, scenario-based analyses do not scale very well with increasing dimensions of variability. As we witness an increase in DER penetration, the number of scenarios needed for valid statistical inference grows exponentially. Alternatively, the proposed probabilistic approach in this dissertation is accurate, simple to implement, and scalable to large systems. This is because computing the parameters of well-established probability distributions is relatively (and consistently) faster.

2.2 Preemptive voltage monitoring

The integration of smart grid technologies such as electric vehicles, energy storage facilities, and distributed generation, introduces advantages as well as system operational challenges [3]. Renewable energy sources are characterized by variable power outputs that increase system vulnerability to operational inefficiencies [51]. In particular, distribution grids become highly vulnerable to random voltage fluctuations especially when there is a high penetration of distributed solar PV generation [52] [53]. Conventional voltage regulation methods such as capacitor banks [54] and tap changers [55] represent reactionary approaches and do not exploit any knowledge of voltage state based on anticipated power fluctuations. One reason for resorting to such reactive approaches is the difficulty in estimating the states of a distribution network due to lack of observability. However, recent efforts on sparsity-based estimation strategies (see [56, 57, 58]) have opened up new possibilities for more proactive methods for voltage regulation [52]. Additionally, the classic voltage regulation methods are not designed for bi-directional current flow and typically provide reactive support after an event is detected [59]. Many recent research efforts have explored the possibility of using reactive power capabilities of PV generators through smart inverters in either a centralized [60], [61] or decentralized [62] scheme. The efficacy of these methods is dependent on the ability to accurately predict voltage violations in the system so that operational setpoints of the PV inverters can be appropriately set in advance. Load flow based look-ahead prediction approaches are cumbersome, computationally complex and not scalable. Therefore, the development of a computationally efficient, yet accurate voltage-violation prediction approach that predicts future violations as well as their uncertainty bounds is critically important for control and management of distribution grids.

Early work on voltage monitoring involves learning from historical data, through which optimal system operation is implemented [63][64]. More recent approaches in literature use traditional load flow based voltage sensitivity to derive a look-ahead prediction of nodal voltage states for predictive control purposes [65, 66, 67, 68]. However, these methods do not account for uncertainty related to DER injections or load variability and their reliance

on classical load flow based sensitivity makes them (1) computationally complex; and (2) non-scalable. Alternatively, authors in [69, 70] use Monte-Carlo based approaches to account for different DER sizes and derive the probability of nodal voltage violation. For example, [69] creates a large number of scenarios with different electric vehicle deployment capacities considering random spatial distribution. Similarly, [70] analyzes multiple scenarios to select the best load model for voltage regulation and loss minimization applications. It is important to note that such methods still do not consider temporal uncertainty of DERs or changeable load patterns but rather focus on analyzing the impact of multiple scenarios of DER capacities on voltage states, making them suitable only for planning applications. Few other methods focus on deep learning based prediction models for voltage violations such as deep neural network [71]. However, the hidden layers of such models makes it difficult to provide guarantee of performance against known or unknown errors in voltage states. Newer approaches introduce the paradigm of probabilistic voltage sensitivity analysis (PVSA) that is accurate and more computationally efficient when compared to classical load flow sensitivity [72][10][52]. However, these studies do not consider distribution system unobservability. Specifically, [10][52] assume full knowledge of temporal voltage states (e.g., voltage current updates) to derive the probability distribution of predicted voltage states. However, this is not a realistic assumption since distribution systems are characterized with low-observability [73].

2.3 Hosting capacity analysis

Authors in [74] and [75] have reviewed the literature related to HC and fundamentally classified the efforts into four major categories (deterministic, stochastic ([76], [77]), optimization-based ([78]), and streamlined ([79])) based on the available data and the type of study to be performed. Most of these approaches for HC depend on numerical load flow-based methods [80, 81, 82, 83], and involve the analysis of multiple PV deployment scenarios. For instance, a rigorous framework is developed in [76], where authors have incorporated both aleatoric (base voltages, solar PV production, local consumption) and epistemic uncertainty (installed

capacity per customer, number of customers with solar PV, phase to which single-phase units are connected) of active distribution network individually. Similarly, in [81], a scenario is generated by randomly allocating PVs in the network, and then load flow is executed for each penetration level until a voltage violation is encountered. To cover all possible locations, the complete process is repeated for multiple scenarios, thereby presenting a huge computational burden. [82] assigns each feeder a minimum and maximum HC, corresponding to the most conservative and most optimistic HC value. However, the overvoltage risk within the range of two HC endpoint values is not quantified. Furthermore, authors in [79], propose a quasi-static-time-series (QSTS) based dynamic PV HC methodology. Here, power flow analysis is conducted on the load and PV data over one year, where the time duration of violation is also monitored along with the total violations count. For a real distribution model with thousands of nodes and one-second resolution data, an annual simulation could take a few days [79]. Furthermore, the PV and load uncertainties have significant influences upon HC values. As a result, probabilistic HC methods have gained attention [84, 85, 86]. The authors in [85] determine HC by incorporating uncertainties associated with PV, Wind turbines, and loads while. However, the approach does not consider the stochastic random distribution of DGs along the target feeder. Though the probabilistic approaches can effectively describe the uncertainty in fluctuations of PVs and loads, most of these approaches are simulation-based and thus are computationally inefficient. More importantly, the performance of these approaches relies heavily on the availability of data.

In addition to HC, numerical VSA methods have also been used to guide various grid applications such as voltage regulation, DER allocations, etc. [87, 88]. For instance, authors in [87] propose a method for analyzing voltage variations due to PV generation fluctuations, considering a variety of factors. However, its dependency on the inefficient simulation method limits its applications to large scale distribution networks. Similarly, authors in [88] develop an optimization model for the electric vehicle charging schedule based on VSA approaches. Still, the requirements of iterative executions of power flow calculations and optimization models hinder its application in real-world scenarios. Thus, traditional methods suffer from high computational complexity and do not provide analytical insight into the un-

derlying physics of the system. Therefore, to overcome the drawbacks of numerical methods, there are some limited analytical approaches for VSA that have been proposed. Authors in [89, 90], develop an algorithm based on VSA which optimally manages active and reactive power of DGs to keep the system voltages inside the limits. Here, instead of repeating load flow calculations to solve the optimization problem, a sensitivity matrix is used to conduct load flow computation in a non-iterative manner, reducing the computational burden significantly. However, the algorithms proposed are not properly validated with standard test systems. Authors in [91], have taken a probabilistic approach where smart meter data is used along with sensitivity analysis to define boundary values of various operation indices. This approach does not account for unbalanced load conditions. The authors in [57], develop a new probabilistic voltage sensitivity approach to quantify voltage change in a computationally efficient way and accounts for the temporal uncertainties associated with random power change at fixed locations of the grid. However, the assumption of a fixed location is not generic enough to account for unknown locations of PV installations. Therefore, in [53], authors provide a quick and efficient tool for estimating the distribution of voltage change in a distribution system with spatial randomness in PV installations. However, the proposed framework is valid only for single phase balanced systems and does not hold true for an unbalanced distribution systems. Therefore, in this dissertation, a generic computationally efficient framework for probabilistic voltage sensitivity is developed for an unbalanced distribution system that systematically accounts for both spatial and temporal uncertainty associated with PV generation.

2.4 EV charging station planning

The integration of electric vehicles (EVs) in modern distribution systems has rapidly increased due to their low carbon footprint, long term reliability, and grid support functionalities [92]. For example, the integration of EVs helps smoothing load curves by participating in peak shaving programs, which in turn, enhance the reliability of the system [93, 94]. It has also been shown that coordinated EV charging may counteract the intermittency in-

troduced by distributed energy resources (DERs) [95]. However, without proper planning, EV charging stations can create additional challenges that limit efficient operation of power distributions systems. This includes excessive power losses and increased voltage deviations, which may contribute to large economic losses [96]. For example, the charging peak of most commercial EV stations occurs during load-peak hours, which is a detrimental scenario that has been shown to cause voltage violations [21]. In addition to these challenges, EV charging pattern is random due to varying consumer needs, variety in charger types (e.g., residential or commercial chargers), and uncertainties of EV arrival/departure times. To mitigate these challenges, EV charging station planning has garnered a huge interest from researchers and EV industry practitioners.

EV charging station planning involves identifying the optimum location and size of charging stations to meet EV charging needs while keeping system constraints within acceptable limits. Existing EV charging station planning approaches can be broadly categorized into two main categories: (1) model-based planning approaches; and (2) approximate meta-heuristic optimization approaches. The first category uses topology information to quantify the impact of installing a charging station on the system. Load flow solution is the most popular model-based impact-analysis technique where system performance indicators, e.g., power loss and voltage profiles, are evaluated before and after the integration of charging stations [97]. For example, in [98] a multi-objective optimization framework is formulated to minimize annualized social cost of EV charging while keeping distribution system parameters within safe operational limits. Here, classical load-flow equations are used to analyze the impact of EV integration on system parameters. Similarly, [2] uses forward/backward sweep-based load flow equations within the EV planning framework. Alternatively, [99] uses load flow solution within an iterative search method to evaluate the impact of EV integration on the system. Other model-based planning approaches include sensitivity factors where the change in system parameters is computed as the partial derivative with respect to incremental power change at any node in the system. For example, [45, 100, 101] use sensitivity factors to compute the change in voltage and losses due to EV charging stations. In this framework, nodes are ranked based on their sensitivities and the least sensitive nodes are chosen as candidate

nodes for charging station placement. While existing model-based approaches may provide a fast evaluation of topology-related impacts on the placement, these methods typically do not consider the spatio-temporal uncertainties introduced by EV load, which may lead to inaccurate EV planning results. In addition, whenever system state changes (e.g., there is integration of a new DER or a change in topology information), the solution has to be reevaluated because these indicators depend on current system states. To overcome these issues, there has been a large focus on meta-heuristic optimization algorithms [102]. These algorithms include genetic [103], particle-swarm [104], whale [105], or grasshopper [106] optimization algorithms. While meta-heuristics can provide accurate approximations if a global optimum is found, their main drawback is the lack of performance guarantees, especially when the algorithm is exposed to practical assumptions such as system reconfiguration, the addition of DERs, and change in topology structure, e.g., radial/meshed topology. Additionally, these approaches tend to be very complex compared model-based analysis, which limits their integration into existing planning frameworks. Therefore, the aim of this research is to solve these challenges by proposing a new model-based probabilistic framework for planning EV charging stations in modern distribution systems. The proposed approach builds off of our prior work on probabilistic sensitivity analysis [20, 72] to compute the probability distribution of change in power losses and voltage deviation, which then can be used to identify the best location for charging station placement. Next, a quadratic optimization problem is formulated to determine the size of charging stations to meet EV demand while satisfying system constraints.

2.5 Voltage control via inverter-based DERs

Numerous studies view the voltage control problem through inverter-based DERs as an optimal power flow (OPF) problem where, instead of the operational cost, the voltage deviation as well as power losses are minimized [107]. This approach assumes the full availability of system information and allocates optimal reactive power set points to satisfy the OPF constraints. For example, [108] proposes new sparsity-based regularization technique to ensure

convexity of optimal PV dispatch as an OPF problem for voltage support whereas [109] uses convex relaxation techniques for improved accuracy. While these methods can provide voltage support, their computational complexity is a barrier and the increased number of control points in the system adds further operational burden, making them intractable for practical implementation [12]. Additionally, since these methods depend on communication infrastructure, communication delays can be an obstacle to solving voltage issues caused by abrupt DER complex power changes. Multiple distributed control algorithms have been introduced to overcome the aforementioned challenges. To guarantee optimality and fast convergence, the PV-curtailment approach proposed in [110] relies on dual ascent. In [111] the consensus-based information sharing via model predictive control (MPC) has been advocated whereas [112] proposes a robust policy-based day-ahead implementation that considers PV-battery inverters. Alternatively, in [113, 114] the alternating-direction method-of-multipliers (ADMM) has been used and shown in [113] to outperform the dual ascent in terms of convergence. The voltage control problem has also been extensively solved with the traditional droop-based control. In this approach the reactive power control signals are determined based on a linearized droop curve using instantaneous nodal voltages [115]. For example, in [116], an adaptive droop-based control scheme is proposed to update the droop coefficient and synchronize current measurements. For nodal voltages, an observer model is considered to estimate voltage states of neighbor nodes. Furthermore, in [117] the droop-based control has been implemented for overvoltage mitigation and tested on different droop schemes, e.g., active power control and coordinated active and reactive power control. Recently, in [118], a droop-based control framework has been proposed for medium voltage distribution systems. Here, the control framework switches seamlessly between a master-slave control and droop-control modes to achieve the required voltage support. However, it has been shown in [119] that, with droop-based controllers, it is important to maintain a small droop slope to guarantee system stability. This is a condition that severely penalizes the reactive power output of controllers [120]. Therefore, this approach may not completely eliminate voltage violations, especially in cases where voltage violations are significant due to large variability in complex power changes. The convergence and stability has been analyzed in [121] and

[122]. However, the models do not consider reactive power constraints at control nodes, which is not a realistic scenario.

Therefore, it is evident that most of the prior work either suffers high computational burden, lacks attention to control cost and reactive power constraints, or inadequate to provide effective voltage support in the presence of DER uncertainties. Thus, the aim of this dissertation is to address these research gaps by providing a general framework that utilizes the control participation factors (CPFs) of nodes integrated with inverter-based DERs to identify the optimal set of nodes that participate in the control program, which we refer to in this dissertation as the *system voltage influencer* set (SVI). In our prior work on dominant influencer of voltage fluctuations (DIVF) [32], we have shown that it is possible to compute and rank the set of dominant nodes that influences voltage variations at any given node in the system. Inspired by the DIVF approach, the SVI set in this dissertation contains the most dominant nodes that influence voltage fluctuations across the entire system. We show in this dissertation that, using the SVI set for voltage control applications via inverter-based DERs provides, (1) faster execution time than using all DERs for control, (2) significantly lower control cost compared to the same number of non-SVI controllers; and (3) high robustness against uncertainty of complex power changes, which can be due to loads or DER injections. It is important to note that the proposed approach in this dissertation is generic and can be applied with any existing voltage control architecture.

Chapter 3

Overview of sensitivity analysis in power distribution systems

Modern distribution systems (MDSs) are facing major challenges due to the rapid growth in energy demand and the engagement of consumers in energy markets. Consumers can participate in the energy market through local energy management, home automation, energy storage and usage, electric vehicle (EV) charging, distributed energy resources (DER) integration, and many other ancillary services [4]. Through this participation, consumers can also schedule their loads based on dynamic electricity prices [5]. The motives for consumers to engage in such activities include: (1) reducing carbon footprint, (2) economic profitability; and/or (3) raising living standards through seeking comfort [6]. However, the increased engagement of consumers in such activities may impose new challenges to the operation of the system. If such consumer activities are not properly accounted for, technical challenges like increased power losses [9], nodal under-voltages [8], and reverse power flow [7] will arise. High levels of power losses in the distribution system results in economic losses and degradation of overall system efficiency. It is estimated that the average power loss across the globe is approximately 8% of the total produced electricity [123], which is a non-negligible amount of economic loss that utilities strive to minimize. Therefore, real-time loss monitoring through loss sensitivity analysis (LSA) will become a necessary tool to determine the

impact of these technologies on system losses [124]. LSA studies the change in line losses due to complex power changes at any location in the distribution system. This chapter presents a comprehensive review of existing methods and helps direct the focus of future research efforts in this important domain.

3.1 Existing LSA methods

Power in distribution systems is transferred either via overhead lines or underground cables. In both types, the system is susceptible to power losses due to the increased heat in conductors [125]. Power loss can be categorized into either technical (TL) or non-technical losses (NTL) [126]. The first category includes losses due to resistance of system lines and the relative amount of current flow, leakage and transformer losses and corona losses [127]. NTLs in the system can be caused by several factors such as inaccurate meter readings, device malfunctioning, and billing cycle errors. In other words, NTLs occur when energy is efficiently delivered but not accurately measured at the consumer end due to device errors [128]. TLs contribute the highest to total system losses as they are related to system mode of operation. Therefore, this section thoroughly explains existing methods for technical LSA in distribution systems.

3.1.1 Exact loss formula (ELF)

The ELF is based on system topology and the change in system states such as nodal voltages, line impedance, and the change in complex power [129]. According to the ELF, the total real power loss in the system can be computed as [1],

$$\begin{aligned} L_s = \sum_{m\in\mathcal{N}}\sum_{n\in\mathcal{N}} [&\alpha_{mn}(P_mP_n + Q_mQ_n) \\ &+ \beta_{mn}(Q_mP_n - P_mQ_n)], \end{aligned} \tag{3.1}$$

where $\alpha_{mn} = \frac{R_{mn}}{V_m V_n}\cos(\delta_m - \delta_n)$, $\beta_{mn} = \frac{X_{mn}}{V_m V_n}\sin(\delta_m - \delta_n)$. Here, V_m and V_n are the voltage magnitudes whereas δ_m and δ_n are the voltage angles of nodes m and n, respectively. When complex power at node m changes from $S_m = P_m + jQ_m$ to $S_m^{'} = P_m^{'} + jQ_m^{'}$ with $\Delta S_m = S_m^{'} - S_m = \Delta P_m + j\Delta Q_m$, the ELF can be rewritten as,

$$\begin{aligned} L_s = \sum_{m\in\mathcal{N}}\sum_{n\in\mathcal{N}} [&\alpha_{mn}(\Delta P_m P_n + \Delta Q_m Q_n) \\ &+ \beta_{mn}(\Delta Q_m P_n - \Delta P_m Q_n)]. \end{aligned} \tag{3.2}$$

3.1.2 Nodal sensitivity factors (NSFs)

NSFs relate the sensitivity of system losses to individual nodes given a particular static complex power change profile. This method is used as a way of reducing the search space when selecting candidate nodes for DER placement algorithms (with lower complexity and execution time) [131]. For instance, nodes with high NSFs are selected as candidate nodes for optimal placement of DERs and SCs [132, 133]. NSFs are computed using partial derivatives

Table 3.1: A summary of NSF-based methods.

Ref.	Control variable					Test system		Load model	
	P	Q	V	θ	Hyb.	SC	LS	Static	Dynamic
[130]	✗	✓	✗	✗	✗	✓	✓	✓	✗
[131]	✗	✓	✗	✗	✗	✓	✓	✓	✗
[132]	✗	✓	✗	✗	✗	✓	✗	✓	✗
[133]	✗	✓	✗	✗	✗	✓	✓	✓	✗
[134]	✗	✓	✗	✗	✗	✓	✗	✓	✗
[135]	✓	✗	✗	✗	✗	✗	✓	✗	✓
[136]	✓	✗	✗	✗	✗	✓	✗	✓	✗
[137]	✓	✗	✗	✗	✗	✗	✓	✗	✓
[138]	✓	✗	✗	✗	✗	✓	✗	✓	✗
[139]	✓	✓	✗	✗	✓	✓	✓	✓	✗
[140]	✗	✗	✓	✓	✓	✓	✗	✓	✗
[141]	✓	✓	✗	✗	✓	✓	✗	✓	✗
[142]	✓	✓	✗	✗	✓	✗	✓	✓	✗
[143]	✓	✓	✗	✗	✓	✓	✗	✓	✓

of system line losses. Consider again nodes m and n that are shown in Fig. **??** connected by line impedance Z_{mn}. The active and reactive power losses on this line can be written as [130] [134] [131],

$$L_{mn,p} = \frac{(P_n^2 + Q_n^2)R_{mn}}{(V_n)^2} \tag{3.3}$$

$$L_{mn,q} = \frac{(P_n^2 + Q_n^2)X_{mn}}{(V_n)^2}. \tag{3.4}$$

Using (3.3) and (3.4), one can compute NSFs based on partial derivatives [130, 132] of system losses with respect to reactive power demand at the destination n node as follows,

$$NSF_P = \frac{\partial L_{mn,p}}{\partial Q_n} = \frac{2Q_n R_{mn}}{(V_n)^2} \tag{3.5}$$

$$NSF_q = \frac{\partial L_{mn,q}}{\partial Q_n} = \frac{2Q_n X_{mn}}{(V_n)^2}. \tag{3.6}$$

Other NSF approaches are used in literature [135, 136, 137] where the partial derivatives are taken with respect to the active power at node n. In this way, the active power NSF can be formulated as,

$$NSF_P = \frac{\partial L_{mn,P}}{\partial P_n} = \frac{2P_n R_{mn}}{(V_n)^2}. \tag{3.7}$$

Further studies propose the concept of combined-NSFs [139, 140, 141], which takes into account both real and reactive power losses into the sensitivity criteria, which results in the following loss sensitivity matrix (LSM),

$$LSM = \begin{bmatrix} \frac{\partial L_{mn,p}}{\partial P_n} & \frac{\partial L_{mn,q}}{\partial P_n} \\ \frac{\partial L_{mn,p}}{\partial Q_n} & \frac{\partial L_{mn,q}}{\partial Q_n} \end{bmatrix}. \tag{3.8}$$

The control variables in this case are both active and reactive power change. In [139, 140, 141, 142], NSFs are computed considering peak demand at a particular node. This can also be extended to accommodate time-series analysis with a given consumption profile [143]. Finally, NSFs can be computed in the presence of DERs where the analysis is based on the change in system loss before and after DER integration. In this case, NSF is the ratio

of power loss change to the change in active power injection at that particular node [138]. Accordingly, NSF_P can be formulated as,

$$NSF_P = \frac{\Delta L_s}{\Delta P_n} \tag{3.9}$$

where ΔL_s is the change in system active power losses after DER placement and ΔP_n is the increase in DER capacity at node n.

NSFs provide useful insights on critical locations in the system and therefore help enhance its performance. NSFs depend on power flow solution to obtain the base nodal voltages. Therefore, these factors are generally used in planning applications as prior information for various control purposes. It can also be noticed that, NSFs do not account for any uncertainty associated with the knowledge of system states or DER power outputs, which is why these factors are typically used at the planning stage. The literature on NSFs is briefly summarized in Table 3.1 based on the control variable, test system used, and load model.

3.1.3 Nodal allocation factors (NAFs)

Along with NSFs, there have been few studies that propose the concept of NAFs to study the impact of nodal power changes on losses in the system including incremental allocation method, proportional sharing method and Z-bus allocation. This subsection briefly describes each of these methods.

Incremental allocation method

The main goal of this method is to identify the contribution of node power changes to total system losses. First appearing in [41], this method is based on determining three components given a certain scenario of power change:

- **Generator domain:** for a generating node $k \in \mathcal{N}$, the domain is the set of nodes that are supplied by power injections at k.
- **Commons:** represents the set of nodes supplied by the same generating node.

- **State graph:** Line flows are determined to form a directed state graph.

Using the domains and commons in a given state graph, it is possible to determine the contribution of each generator to line flows, which helps to determine its contribution to line losses. Some nodes may contribute low power to loads but high contribution in line losses [41]. This method has been shown to be effective in determining the contribution of nodes (either negative or positive) to system losses. Yet, computing the domains and commons is complex for large systems. Moreover, MDSs typically experience stochastic complex power changes at different locations as well as variable system configurations, which may lead to topology changes of the state graph.

Z-bus allocation method

This method is based on the Z-bus matrix of the system, which is the inverse of the Y-bus (admittance matrix). The main idea of the Z-bus method is to determine whether a node receives incentives or penalties for load increments based on loss contribution to the system. The active power loss in the system can be expressed as,

$$L_s = \sum_{k \in n} L_k, \tag{3.10}$$

where L_k stands for the loss contribution due to current injections at node k. This can be expressed in terms of Y and V or Z and I through,

$$L_s = \sum_{k \in \mathcal{N}} V_k \sum_{j \in \mathcal{N}} Y_{kj} V_j^* \tag{3.11}$$

$$L_s = \sum_{k \in \mathcal{N}} I_k^* \sum_{j \in \mathcal{N}} Z_{kj} I_j, \tag{3.12}$$

where, Y_{kj} and Z_{kj} correspond to the kj^{th} element of the Y-bus and Z-bus matrices, respectively. This method uses the Newton-Raphson power flow solution to determine current flows. The Z-bus allocation method can provide insights on node contributions to system losses similar to IA method. For instance, in [42], the method is used to determine the

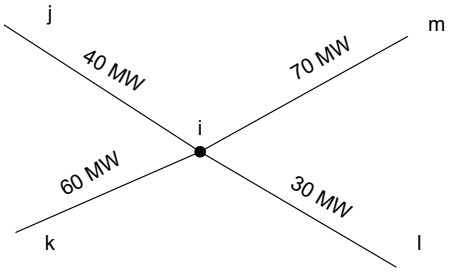

Figure 3.1: Proportional sharing method illustration.

loss sensitivity using the IEEE 14 node and the IEEE 118 node transmission test systems. For the first system, only one scenario is considered where a 100 MW generator is added, and the loss is monitored. Another alternative to this method is discussed in the following subsection where the proportion of nodal power injections with respect to neighboring lines is considered.

Proportional sharing method

Unlike the previous NAFs, this proportional sharing method is based on determining the proportion of node generation to line flows [43]. This can be computed using the proportional sharing matrix that helps determine contribution of nodes to line losses. To demonstrate the underlying principle, consider the nodal illustration in Fig. 3.1. The proportional method says that the 70 MW on $i-m = \frac{40}{100}70 + \frac{60}{100}70$, which means, 28 MW from line $j-i$ and 42 MW from $k-i$. Similarly, the 30 MW on $i-l = \frac{40}{100}30 + \frac{60}{100}30$. In other words, 12 MW from line $j-i$ and 18 MW from $k-i$. In [43], the method is implemented on an arbitrary 4 node test system to demonstrate its effectiveness. Nevertheless, this method requires details derivation for systems greater than 4 nodes, which increases the complexity of this method. It is important to mention that this method works very well with transmission systems due to the existence of multiple generating nodes.

3.2 Applications of loss sensitivity analysis

One of the goals of modern distribution systems is to integrate consumer level activities with core distribution planning and optimal operation tools [3]. This integration results in various advantages, one of which is consumer flexibility. In the modern framework, consumers are more engaged in the energy market by exchanging information over the communication infrastructure [4]. Other benefits include improving system situational awareness and providing accurate measures regarding the impact of consumer activities on system operation [10]. Fig. 3.2 illustrates an MDS architecture, where utilities leverage the capabilities of the communication infrastructure to transfer information from consumer level to a sensor data management system (SDMS) [144]. The main goal of SDMS is to filter incoming data from consumer resources [3]. This information can then be transferred to distribution system state estimation (DSSE). DSSE provides the asset management center with the required information about nodal voltages, power measurements and line current flows [145][146][147]. Such information can be used as the input to outage management systems (OMS)[148]. Functionalities of OMS include managing planned/unplanned outages, outage call reports, field maintenance crews and reliability index analysis [149][150][151]. Additionally, secondary-level DSSE information enable home energy management systems (HEMS) [152], which can include applications like demand side management [153] and load shifting [154][155]. Home automation features can also be embedded into HEMS, in which consumers can remotely control household appliances [156]. Finally, customer-level information can be fed to the advanced distribution management system (ADMS). ADMS include the distribution system optimal planning, operational applications, and sensitivity analysis that optimize system operation and study system dynamics in the presence of consumer-level resources [157][158] [72]. In the light of LSA, ADMS accommodates different types of applications such as optimal system reconfiguration, DER planning, SC allocation and EV charging station management [159][160]. The following subsections summarize state of the art and provides a glimpse at future pathways. Table 3.2.3 includes a summary of LSA applications on IEEE standard test systems (STS).

3.2.1 System reconfiguration

System reconfiguration - also known as optimal topology identification (OTI) - can be defined as the process of changing the status (open or close) of system switches in order to find the optimal topology that keeps power losses minimum and voltage profiles within permissible limits [161]. Many research efforts in literature have proposed algorithms to solve this reconfiguration problem based on different sensitivity metrics [162]. One of the early attempts appeared in [163] where authors focused on loss minimization by searching for the optimal spanning tree configuration. Later on, different optimization techniques have been developed based on leveraging various loss sensitivity techniques. For example, [164, 165, 166, 167, 168, 169] use CLF-based sensitivity analysis (**??**) to find the optimal configuration of the system. [18, 161, 170, 171, 172] use NSF-based sensitivity analysis (3.1.2). Most of LSA-based system reconfiguration studies rely on base load analysis [18, 166, 171]. In the last decade, however, researchers have started incorporating the impact of system assets on optimal reconfiguration. [161, 167], for example, consider the impact of DERs on system losses and propose new heuristic optimization algorithms to solve the reconfiguration problem. In addition to DERs, [170] takes int account the impact of SCs on system reconfiguration. Except [170], most of the prior work on LSA-based system reconfiguration studies are based on static load models. However, it is desired to address the reconfiguration problem from an operational point of view because static analysis may not fully capture actual MDS dynamics.

3.2.2 DER management

DER integration into distribution systems is complex and requires in-depth assessment and efficient operational and planning tools. This is mainly because DERs are not dispatchable by distribution system operators and can have a large impact on losses, power flow, voltage stability and power quality [34, 173]. Numerous algorithms have been employed for DER optimal allocation, resulting in the best location and size of DERs considering loss reduction [174]. These algorithms are broadly based on analytical techniques, optimization algorithms,

or heuristics [1, 175]. Additionally, the existing work on DER allocation considers either single [176] or multiple allocation [177, 178]. For computing loss sensitivity, the vast majority of existing work uses PQ-based NSFs where the factors are computed based on active and reactive power injections (or withdrawal) by the DER unit [179] [180] [181] [182] [183] [184][185] [35]. Few works [178][176][186] use the ELF whereas others determine the loss sensitivity using CLF method [187][173][188] [189] [190]. Despite the efficacy of existing methods for DER planning based on loss sensitivity, MDSs require system performance analysis with different penetration levels of DERs. In this regard, DER hosting capacity (HC) attracts the attention of MDS practitioners. HC can be defined as the maximum amount of DERs (such as PV or wind) that MDS can accommodate without the need for infrastructure upgrades while keeping system performance indicators within safe limits [81]. A comprehensive HC analysis framework must incorporate different system performance indicators such as power losses, line thermal loading or nodal voltage stability [75]. The adoption of different DER resources, ESSs and EVs motivates hybrid HC analysis due to the differential impact of these technologies [174]. For example, while rooftop PV systems inject power, EVs form additional loading at different locations in the system. This introduces spatio-temporal randomness in power injections (or withdrawals) that classical sensitivity methods failed to address.

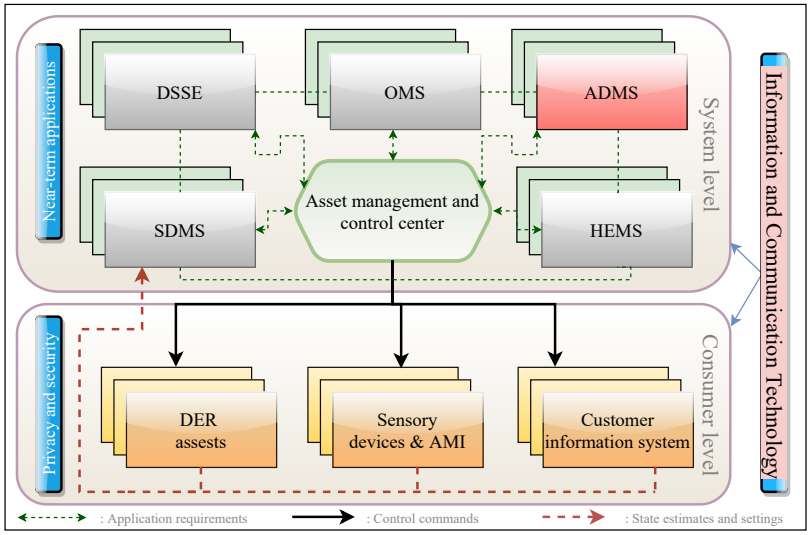

Figure 3.2: Architecture of MDS.

3.2.3 Shunt capacitor allocation

SC placement in distribution systems can significantly help reduce system losses and stabilize voltage by improving the power factor of the system[191]. SCs can be connected to primary or lateral feeders and/or secondary level loads depending on system topology. The installation of SC at secondary feeder indeed provides enhanced system efficiency in terms of voltage support and loss minimization. However, in some cases, the resources can be limited and the installation of additional SCs can be an expensive alternative to minimize losses (or provide voltage support) [133]. Therefore, it is possible in such scenarios to integrate SCs at the primary feeder. In this scheme, losses at the secondary level can be minimized through controllable DER assets. This scheme may also have adverse impacts on different locations in the system since some nodes can be very sensitive to complex power changes at other nodes [132]. For this reason, several research efforts in literature propose optimal SC placement and sizing algorithms for loss minimization [192] [193][194]. To determine the loss sensitivity, ELF [17], PQ-based NSF [180][182][170] [195][196], or CLF method [191][197][198] can be used. Few studies focus on loss minimization by optimal placement and sizing of SCs with the presence of DERs [180][182][191] or system optimal reconfiguration [197]. The effectiveness of SCs (as well as other regulatory devices such as tap changers [55] and static var compensators[54]) is limited by their maximum allowable limits in the system. In addition, the installation of such devices might be very expensive, especially for large systems. Recent research utilizes PQ-based DERs instead of complete reliance on the deployment of regulatory devices [19]. Utilities can adjust the PQ setpoints of inverters in order to maintain system indicators within safe operational limits. In cases where DERs operate at maximum power point tracking (MPPT) mode, i.e., PQ setpoints are not controllable by utilities, assistive SCs can be installed with DERs and operated as needed.

Table 3.2: Application summary.
†: system reconfiguration, ‡: DER management, ⊙: SC allocation, ⊗: EV coordination, *: applicable to transmission system.

			Test system			Load model		Hybrid
Category	Reference	LSA						

			Type	Scale				
				Small	Large	Static	Dynamic	
	[161]	NSF	IEEE STS	✓	✓	✓	✗	‡
	[170]	NSF	IEEE STS*	✗	✓	✓	✓	‡ ⊙
	[164]	CLF	IEEE STS	✓	✓	✓	✗	✗
	[165]	CLF	IEEE STS*	✓	✗	✓	✗	✗
	[171]	NSF	IEEE STS	✗	✓	✓	✗	✗
†	[166]	CLF	IEEE STS	✓	✗	✓	✗	✗
	[167]	CLF	IEEE STS	✗	✓	✓	✗	‡
	[168]	CLF	Non IEEE	✓	✓	✓	✗	‡
	[18]	NSF	IEEE STS	✗	✓	✓	✗	✗
	[172]	NSF	IEEE STS*	✓	✓	✓	✓	‡
	[169]	CLF	IEEE STS	✓	✓	✓	✗	✗
	[179]	NSF	IEEE STS	✓	✗	✓	✗	⊙
	[180]	NSF	IEEE STS	✓	✗	✓	✗	⊙
	[181]	NSF	IEEE STS*	✓	✓	✓	✗	✗
	[182]	NSF	IEEE STS*	✓	✓	✓	✗	⊙
	[187]	CLF	IEEE STS	✓	✓	✓	✗	†
	[199]	NSF	IEEE STS	✓	✗	✓	✗	†
	[173]	CLF	IEEE STS	✓	✗	✓	✗	✗
	[188]	CLF	IEEE STS	✓	✗	✓	✗	✗
‡	[185]	NSF	IEEE STS	✗	✓	✓	✗	✗
	[178]	ELF	IEEE STS	✓	✓	✓	✗	✗
	[183]	NSF	IEEE STS	✓	✓	✓	✗	✗
	[184]	NSF	IEEE STS	✓	✗	✓	✗	⊙
	[189]	CLF	IEEE STS	✓	✓	✓	✗	✗
	[190]	CLF	IEEE STS	✓	✗	✓	✗	✗

	[176]	ELF	IEEE STS	✓	✗	✓	✗	✗
	[35]	NSF	IEEE STS	✓	✗	✓	✗	†
	[186]	ELF	IEEE STS	✗	✓	✓	✓	✗
	[180]	NSF	IEEE STS	✓	✗	✓	✗	‡
	[17]	ELF	IEEE STS	✓	✓	✓	✗	✗
	[182]	NSF	IEEE STS*	✓	✓	✓	✗	‡
	[191]	CLF	IEEE STS	✓	✗	✓	✗	‡
⊙	[197]	CLF	IEEE STS	✓	✗	✓	✗	†
	[198]	CLF	IEEE STS	✓	✗	✓	✗	⊗
	[170]	NSF	IEEE STS*	✓	✓	✓	✗	† ‡
	[195]	NSF	IEEE STS	✓	✓	✓	✗	†
	[196]	NSF	IEEE STS*	✓	✓	✓	✗	✗
	[2]	NSF	IEEE STS	✓	✗	✓	✗	‡
	[198]	CLF	IEEE STS	✓	✗	✓	✗	⊙
	[200]	CLF	IEEE STS	✓	✗	✓	✗	✗
	[98]	CLF	IEEE STS	✓	✗	✓	✗	✗
	[94]	CLF	IEEE STS	✓	✓	✓	✓	✗
	[99]	CLF	IEEE STS	✓	✓	✓	✗	✗
⊗	[201]	NSF	IEEE STS	✓	✗	✓	✓	✗
	[202]	CLF	IEEE STS	✓	✗	✓	✗	✗
	[203]	CLF	IEEE STS	✓	✗	✓	✓	‡
	[204]	CLF	IEEE STS	✗	✓	✓	✗	✗
	[205]	NSF	IEEE STS	✓	✗	✓	✓	✗
	[206]	NSF	IEEE STS	✓	✗	✓	✓	✗
	[207]	CLF	IEEE STS	✓	✗	✓	✓	✗
	[208]	CLF	Non IEEE	✓	✗	✓	✓	†
	[209]	NSF	IEEE STS	✗	✗	✓	✓	‡

3.2.4 EV coordination

The decay in natural fuel reserves, increase in gasoline prices and the stringent governmental regulations on adopting greener technologies have spanned the growth of EVs [210]. Compared to classical fuel-based vehicles, EVs are fuel efficient and environmental friendly [211]. Yet, the integration of EVs into distribution systems brings new challenges to utilities in order to maintain system efficiency. A typical, yet detrimental scenario of EV operation occurs when consumers charge their EVs during peak-load hours such as early morning and after work hours. Such uncontrolled grid-to-vehicle (G2V) charging patterns increase the stress on nodal power demand and has been linked to voltage violations [212], active power losses [213] and increased likelihood of blackouts due to system overloading [214]. EVs can also be operated in vehicle-to-grid (V2G) mode in which the EV is regarded as a controllable resource that provides ancillary services to system operation such as active loss reduction [215, 216], voltage control [217], peak shaving [208, 218] or demand response programs [219].

With the technological advancements in communication infrastructures and computational resources, efficient G2V or V2G coordination algorithms are currently being developed to limit EV impacts on distribution systems. Many EV coordination studies consider active loss reduction in distribution systems. For instance, [94, 98, 99, 201, 202] propose optimal planning strategies of G2V-based EV planning for improving system indicators including loss reduction. The planning problem can be formulated as optimal placement and sizing of charging stations across the system [203, 220]. For loss sensitivity calculations in G2V planning, few studies use linear approximation of annual losses [94, 204, 208] whereas others use CLF analysis [99, 202] or NSFs [201]. In addition to planning, the system optimal operation is widely studied in the literature. Typically, the interaction between EVs and system is modeled with a temporal profile of complex power dynamics. For example, [206] shows that system losses can be minimized by integrating ESSs with different levels of EV penetration. The study uses NSFs for computing the sensitivity. Similarly, [205] shows that optimal control of EV charging locations can significantly reduce system losses using classical load flow loss sensitivity. In addition to G2V scheme, research has shown with LSA that

it is possible to reduce power losses in V2G scheme [221] [222] [223]. For example, authors in [207] propose a new placement and sizing approach of V2G facilities using CLF-based LSA. Similarly, [208] studies V2G coordination via optimal placement and sizing but with integrated DERs across the system. In [209], system optimal reconfiguration is considered with V2G coordination, where the objective is to minimize losses and ensure system reliability. The last block of Table 3.2.3 summarizes the EV management studies based on loss sensitivity.

3.3 Research gaps and future trends

This section discusses the major shortcomings of existing loss sensitivity methods from the perspective of MDSs and provides future recommendations to direct the focus of new research efforts in this domain.

3.3.1 Enabling real-time monitoring

Classical loss sensitivity methods have shown value at system planning stage for various applications such as DER and SC placement. For example, it can be seen from Tables 3.1 and 3.2.3 that the most commonly used load model is the static model. This implies the that loss sensitivity has been widely used in distribution system planning. The diverse structure of MDS in terms of end-user technologies motivates the need for real-time monitoring tools that are able to quantify the impact of consumer level activities on system losses. This is mainly due to the difference in the impact that different technologies may have on the system. For instance, PV units supply active power to local loads and thereby, reduce system losses since less power is withdrawn from the source. EVs, on the other hand, increase local loading and therefore, may lead to excess losses during existing peak demand hours. Therefore, real-time monitoring of loss is important to ensure system efficiency.

3.3.2 Incorporating uncertainty

The variable nature of DER power outputs and load profiles in MDSs can cause adverse impacts on system operation and reliability. This uncertainty can result from changing weather conditions, partial shading over PV panels, or sudden peak in local loads. All of the aforementioned factors can contribute to excessive amounts of power losses. This obligates the inclusion of uncertainty analysis to loss sensitivity methods. Uncertainty analysis with real-time monitoring enables system operators to apply optimal consumer asset management, e.g., G2V charging scheduling or real-time allocation, to maintain minimum losses during peak hours. Unfortunately, based on the review in this section, uncertainty analysis is still a knowledge gap that must be addressed by exploring new methods of loss sensitivity or by innovating existing frameworks in a accurate and a computationally efficient manner.

3.3.3 Alleviating computational burden

MDS optimal operation with minimum losses entails a wide range of time-sensitive and data-intensive tools for sensitivity analysis. Based on the review in this section, there are two major areas where computational complexity requires further attention: (1) the requirement for algorithmic extensions, and (2) complexity of scenario based sensitivity analysis for realistic systems, especially at system operation stage. For instance, the set of domains and commons in 3.1.3 requires significant algorithmic extensions for systems larger than 4 nodes. In addition, although a majority of the reviewed methods consider large IEEE STSs in the analysis, the results must be validated against realistic unbalanced distribution systems along with the secondary feeder level to efficiently capture the impacts of active consumers on losses. This inevitably increases the computational complexity, especially when uncertainty is incorporated in the analysis because it requires running multiple scenarios to obtain the desired accuracy for CLF-based sensitivity.

3.3.4 State estimation and measurement devices

System states are obtained via measurement devices at the main feeder side such as the SCADA system that provide nodal active/reactive power and real/imaginary voltage readings, through which loss sensitivity can be computed. Yet, distribution systems are mostly constrained with few measurement devices at select locations, rendering the system unobservable. One solution to this can be the installation of additional measurement devices at every location in the system. However, this approach is not cost-effective. In this regard, state estimation of low observable distribution systems is an attractive alternative. Based on the literature analysis, the majority of works consider full availability of system states for computing the sensitivity. Breaking the barriers between state estimation and sensitivity analysis is a key element in MDSs that can result in efficient planning, monitoring and optimal asset control.

3.3.5 Other research pathways

Legacy distribution systems were designed in a top-down structure with limited coordination between management systems. Such coordination is important for impact assessment of consumer resources on both device and system level. Therefore, the dynamic nature of MDSs calls for advanced frameworks to collaboratively foresee the evolving needs of the system. In this regard, loss sensitivity can be integrated with other frameworks (e.g., voltage sensitivity analysis) to predict system response and guide optimal management strategies. As far as asset management is concerned, fairness to consumers participating in the management program is another aspect that will draw the attention of system operators. Finally, cybersecurity and data privacy will also be relevant areas with sensitivity analysis, especially during the process of communicating control commands from system operators to the consumer level.

3.4 Summary

This chapter proposes a comprehensive analysis on existing literature work on LSA and reviews the state of the art to identify future research directions. Theoretical formulations of LSA are initially summarized. Then, the applications of LSA are thoroughly discussed and categorized based on the LSA framework used. After extensive analysis on literature, this chapter discusses existing research gaps and provides a vision for future research directions. It is found that the development of computationally efficient sensitivity frameworks is essential to achieve real-time monitoring and enable efficient planning applications in modern distribution systems. Moreover, DER uncertainty and lack of measurement devices are two important aspects that can help provide realistic results for system planning and operation using LSA. Next chapter proposes an analytical LSA framework that accounts for power uncertainties.

Chapter 4

Analytical approaches for Loss Sensitivity Analysis

It is evident from Chapters 2 and 3 that prior work on loss sensitivity analysis (LSA) considers computationally complex traditional methods of sensitivity analysis or traditional power flow equations. Such methods may not be adequate to address the needs of modern distribution systems for the following three reasons. First, results obtained from such methods are scenario-specific and the inclusion of dynamic behavior of active consumers impacts their consistency. Second, traditional sensitivity methods are computationally complex and require simulating a large number of scenarios to obtain the sensitivity of each scenario. Finally, in distribution systems, complex power changes at active consumer sites can be random due to variability in PV power outputs or dynamic load behaviors. This is unfortunately not considered in traditional analytical and load flow-based sensitivity methods. While it is possible to capture uncertainties with classical methods by simulating a large number of scenarios, such methods do not scale very well with increasing dimensions of variability. As we witness an increase in DER penetration, the number of scenarios needed for valid statistical inference grows exponentially. Therefore, this Chapter derives an analytical approximation of LSA that quantifies the impact of grid-edge technologies on change in line losses. The proposed approach accounts for uncertainties associated with power changes and derives the distribu-

tion of change in power losses in balanced distribution systems. The proposed framework will be used in Chapter 5 to derive the distribution of change in line losses for the general case, i.e., unbalanced three-phase distribution systems.

4.1 Analytical framework for loss sensitivity

Consider a power distribution system with $\mathcal{N}$ nodes and $\mathcal{L}$ lines as illustrated in Fig. 4.1. The change in complex power at any node in the system causes changes in current flow in all lines, and thereby, causes changes in line power losses. Nodes where complex power varies are called *actor nodes* and lines where the change in current flow or power loss is monitored are called *monitored lines*. This section presents an analytical approximation for the change in line currents and losses at any monitored line (M) due to change in complex power at actor nodes (A) in the system. When power at actor node A changes from S_A to $S_A + \Delta S_A$, the current at the monitored line changes from I_M to $I_M + \Delta I_{MA}$, where ΔI_{MA} is the change in current flow on the monitored line M due to complex power changes at actor node A. The reference node throughout this chapter is assumed to operate at a unity voltage, i.e., $1\angle 0°$ p.u. Considering a single actor node, the change in current flow at the monitored line M can be approximated using Theorem 1.

Theorem 1. *For a single-phase distribution system, the change in current flow at a monitored line (M) due to change in complex power at an actor node (A) is approximated by,*

$$\Delta I_{MA} \approx \frac{\Delta S_A^* \Psi_{MA}}{V_A^*}, \tag{4.1}$$

where, ΔS_A^* is the complex conjugate of complex power change at actor node A, V_A^* is the complex conjugate of base voltage at the actor node A and Ψ_{MA} represents the influence indicator between node A and the origin node of line M. For nodes impacting the current flow on M, Ψ_{MA} can be set to 1 and 0 otherwise.

Proof. Consider a single-phase radial distribution system with $\mathcal{N}$ nodes and $\mathcal{L}$ lines with l_{m-n} representing the line connecting nodes m and n as shown in Fig. 4.1. Let e be the line

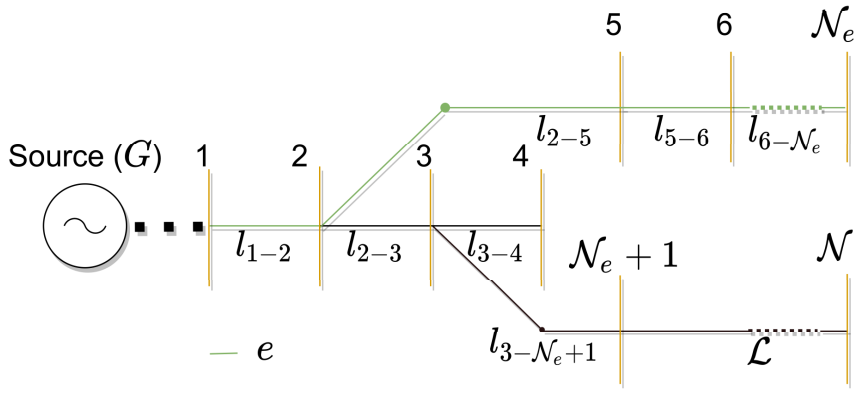

Figure 4.1: An illustration of a distribution system.

connecting the set of nodes $\mathcal{N}_e$ with the source node G. The downstream current flowing through e can be written in terms of complex conjugate of power injections and nodal voltages as,

$$I_e = \sum_{k \in \mathcal{N}_e} I_k = \sum_{k \in \mathcal{N}_e} \frac{S_k^*}{V_k^*}. \tag{4.2}$$

When complex power changes at active consumer locations ($k \in \mathcal{N}_e$) from S_k to $S_k + \Delta S_k$, the voltage also changes from V_k to $V_k + \Delta V_k$. Therefore, the current flowing through e changes from I_e to $I_e^{'}$ and can be rewritten as,

$$I_e^{'} = \sum_{k \in \mathcal{N}_e} I_k^{'} = \sum_{k \in \mathcal{N}_e} \frac{S_k^* + \Delta S_k^*}{V_k^* + \Delta V_k^*}. \tag{4.3}$$

The change in line flow ($\Delta I_e = I_e^{'} - I_e$) at line e can be written as follows,

$$\begin{aligned} \Delta I_e &= \sum_{k \in \mathcal{N}_e} \frac{S_k^* + \Delta S_k^*}{V_k^* + \Delta V_k^*} - \sum_{k \in \mathcal{N}_e} \frac{S_k^*}{V_k^*} \\ &= \sum_{k \in \mathcal{N}_e} \frac{V_k^*(S_k^* + \Delta S_k^*) - S_k^*(V_k^* + \Delta V_k^*)}{V_k^*(V_k^* + \Delta V_k^*)} \end{aligned}$$

Using assumption 2, we can rewrite ΔI_e as,

$$\Delta I_e \approx \sum_{k \in \mathcal{N}_e} \frac{\Delta S_k^*}{V_k^* + \Delta V_k^*} \tag{4.4}$$

Now assume that only one node (say node $A \in \mathcal{N}_e$) is changing its complex power. The corresponding change in line current can be written as,

$$\Delta I_e \approx \frac{\Delta S_A^*}{V_A^* + \Delta V_A^*} \tag{4.5}$$

The change in line flow can be written in terms of real and imaginary parts as follows,

$$\begin{aligned}\Delta I_e \approx & \frac{\Delta P_A V_A^r (1 + \frac{\Delta V_A^r}{V_A^r}) + \Delta Q_A V_A^i (1 + \frac{\Delta V_A^i}{V_A^i})}{(V_A^r (1 + \frac{\Delta V_A^r}{V_A^r}))^2 + (V_A^i (1 + \frac{\Delta V_A^i}{V_A^i}))^2} \\ & + j \frac{\Delta P_A V_A^i (1 + \frac{\Delta V_A^i}{V_A^i}) - \Delta Q_A V_A^r (1 + \frac{\Delta V_A^r}{V_A^r})}{(V_A^r (1 + \frac{\Delta V_A^r}{V_A^r}))^2 + (V_A^i (1 + \frac{\Delta V_A^i}{V_A^i}))^2},\end{aligned} \tag{4.6}$$

where, V_A^r and V_A^i are the real and imaginary parts of actor node voltage, respectively. ΔP_A and ΔQ_A are the real and reactive power changes at actor node A. Now, using assumption 2, the change in real and imaginary parts of line current flow can be written as,

$$\Delta I_e \approx \frac{\Delta P_A V_A^r + \Delta Q_A V_A^i}{(V_A^r)^2 + (V_A^i)^2} + j \frac{\Delta P_A V_A^i - \Delta Q_A V_A^r}{(V_A^r)^2 + (V_A^i)^2} = \frac{\Delta S_A^*}{V_A^*} \tag{4.7}$$

For any monitored line $M \in e$, the change in current flow will only occur due to complex power changes at $A \in \mathcal{N}_e$ as shown in Fig. 4.1. Therefore, for any actor node $A \notin \mathcal{N}_e$, the influence factor Ψ_{MA} can be set to zero. That is,

$$\Delta I_{MA} \approx \frac{\Delta S_A^* \Psi_{MA}}{V_A^*}, \tag{4.8}$$

which completes the proof of Theorem 1. Below is a summary of the assumptions used throughout the proof of Theorem 1. □

Assumption 1. *The reference node operates at unity voltage, i.e.,* $1\angle 0^\circ$ *p.u.*

Assumption 2. *In distribution systems, the change in nodal voltage relative to the actual nodal voltage is small.*

Assuming multiple actor nodes in the system change their complex power, the change in current flow through the monitored line M can be written as the sum effect of all individual changes as given in Corollary 1.

Corollary 1. *For a single-phase distribution system, the aggregate impact of complex power change at multiple actor nodes ($A \in \mathcal{A}$) on the change in current flow at a monitored line (M) is approximated by,*

$$\Delta I_M \approx \sum_{A \in \mathcal{A}} \frac{\Delta S_A^* \Psi_{MA}}{V_A^*}, \tag{4.9}$$

The current sensitivity due to multiple actor nodes is used to derive the loss sensitivity due to complex power change at active consumer sites.

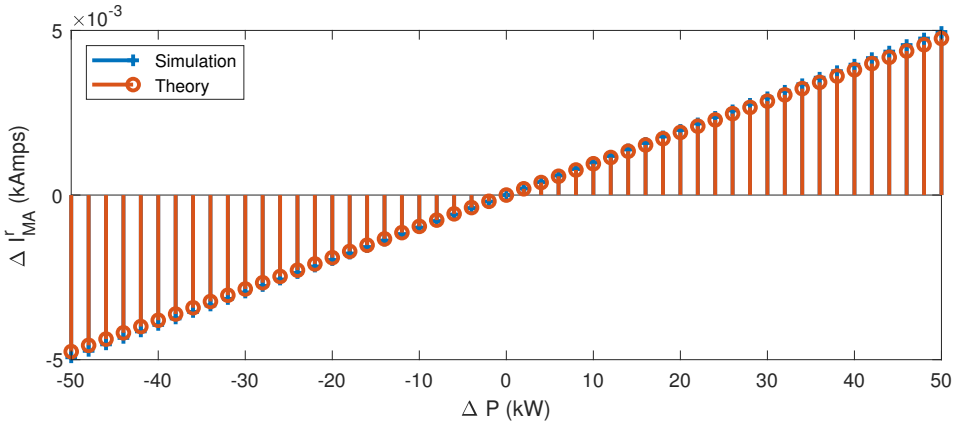

(a)

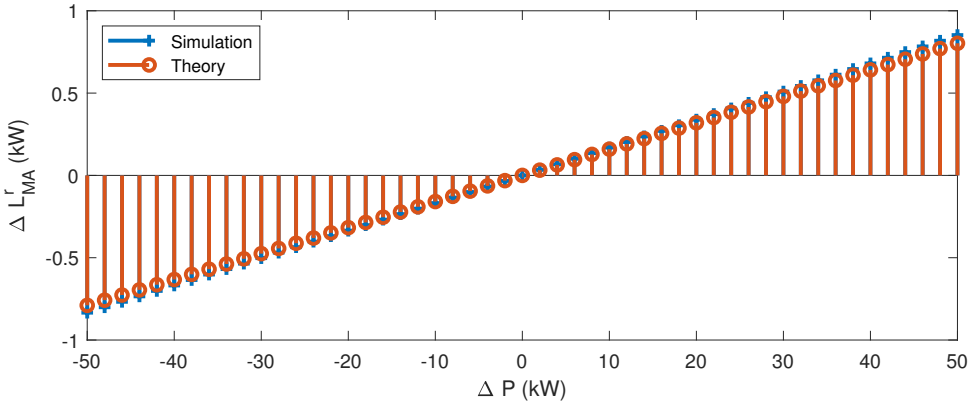

(b)

Figure 4.2: Sensitivity due to a single actor node: (a) change in line flow ΔI_{MA}. (b) change in active power losses ΔL_{MA}.

Corollary 2. *For a single-phase distribution system, the aggregate impact of complex power change at multiple actor nodes ($A \in \mathcal{A}$) on the change in power loss at a monitored line (M) is approximated by,*

$$\Delta L_M \approx \Bigg[\Big| \sum_{A \in \mathcal{A}} \frac{\Delta S_A^* \Psi_{MA}}{V_A^*} \Big|^2 + 2\Re\Big(I_M^* \sum_{A \in \mathcal{A}} \frac{\Delta S_A^* \Psi_{MA}}{V_A^*} \Big) \Bigg] Z_M. \tag{4.10}$$

where, $Z_M = R_M + jX_M$ is the impedance of the monitored line M and I_M^* is the complex conjugate of base current flow at line M.

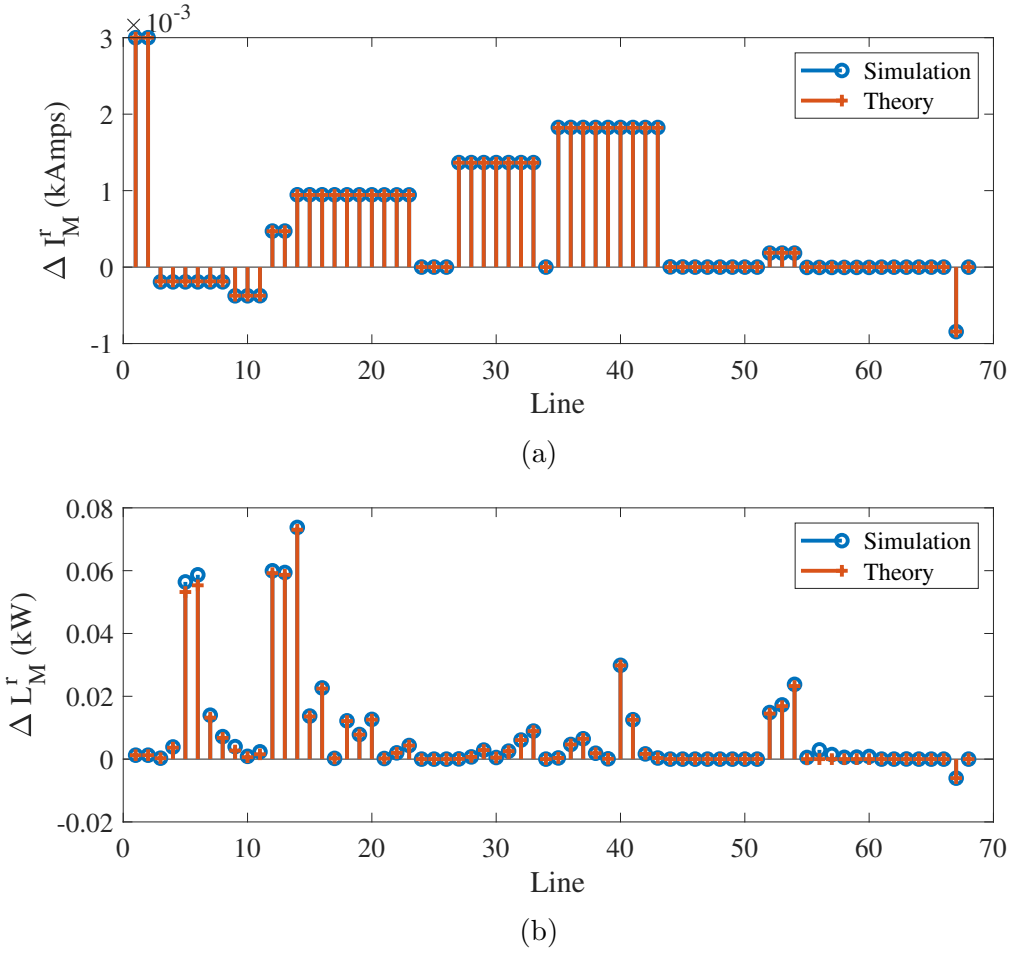

Figure 4.3: Sensitivity due to multiple actor nodes: (a) change in line flow ΔI_M. (b) change in active power losses ΔL_M.

Proof. Consider again the system shown in Fig. 4.1. Power loss at a monitored line M can be written as [224],

$$L_M = |I_M|^2 Z_M \tag{4.11}$$

$$= L_{M,P} + jL_{M,Q} \tag{4.12}$$

$$= |I_M|^2 R_M + j|I_M|^2 X_M, \tag{4.13}$$

where $L_{M,P}$ and $L_{M,Q}$ are the active and reactive power losses at monitored line M, respectively. When the current flow at a monitored line M changes by ΔI_M, power loss at that line changes by ΔL_M and can be written as,

$$\Delta L_M = \Big[|I_M + \Delta I_M|^2 - |I_M|^2\Big] Z_M \tag{4.14}$$

$$= \Big[|\Delta I_M|^2 + 2\Re(I_M^* \Delta I_M)\Big] Z_M. \tag{4.15}$$

The change in current flow on that line (ΔI_M) can be computed using the analytical expression derived in Eq. (4.9). Therefore, the change in power loss at a monitored line M becomes,

$$\Delta L_M \approx \Bigg[\Big|\sum_{A\in\mathcal{A}} \frac{\Delta S_A^* \Psi_{MA}}{V_A^*}\Big|^2 + 2\Re\Big(I_M^* \sum_{A\in\mathcal{A}} \frac{\Delta S_A^* \Psi_{MA}}{V_A^*}\Big)\Bigg] Z_M. \tag{4.16}$$

□

4.1.1 Validation of analytical approximation

In this section, the proposed analytical approximation of the change in power losses is validated on the IEEE 69 node test system [225]. The base voltage of this test system is 12.66 kV and standard base loads are used for the analysis. Classical load flow method is used as

Table 4.1: Complex power change at multiple actor nodes.

Node	ΔS (kVA)	Base loading (kVA)
14	-5+j3	8+j5.5
24	10+j7	28+j20
34	15-j5	19.5+j14
44	20+j20	0
55	2+j2	24+j17.2
68	-9-j4	28+j20

a benchmark to evaluate the accuracy of the proposed analytical approach. Two scenarios are created to show the accuracy of approximating the change in line current flow as well as losses. For the first scenario, node 15 is chosen randomly to change its complex power and the current and loss changes are monitored at line $5-6$, i.e., $\Delta I^r_{5,15}$ and $\Delta L^r_{5,15}$, where the superscript r represents the real part. Negative power change could represent increased DER injections (such as PV) or decreased load power. Similarly, positive power change can result from increased consumption or decrease in DER injection. Fig. 4.2 shows the changes in real line current and active losses where theory represents the proposed analytical expression and simulation is the result obtained via classical load flow-based method. It can be seen that the proposed analytical approach is accurate in approximating the change in line current and active power losses. The second scenario presents a case where power changes at randomly selected actor nodes. Table 4.1 reports the actor nodes and the respective values of complex power change as well as the base kVA loading. The change in real part of current flow and active losses for this scenario are illustrated in Fig. 4.3. As can be seen from the figure, the proposed method can approximate not only positive changes but also negative changes due to increased PV injection. This demonstrates the accuracy of the proposed method in approximating the change in line current flow and power loss. The proposed approach is generic and can also be applied in the presence of various binary equipment such as switches, tap changers, and switched capacitors. Such equipment are control action enablers that ensure optimal system operation, whereas the proposed sensitivity approach could be used as a precursor to such control actions. Specifically, the proposed analytical approach does not change due to the presence of switches, tap changers, or switching capacitors. However,

thanks to the analytical nature of the proposed approach, it is a trivial task to account for such cases. Specifically, we only need to run the load flow once (or use recently proposed sparsity based distribution system state estimation approaches [145]) to get the base values of voltage, and thereafter the proposed analytical method can be applied to compute loss change at any monitored line of the system due to change in PV generation or load pattern. The complexity of the proposed method in terms of execution time is pretty much constant regardless of system size. This is one of the key strengths of the proposed approach. The following section derives an upper bound on the approximation error to ensure consistency of results obtained by the proposed analytical method.

4.1.2 Approximation error bound

This section further investigates the accuracy of the proposed approximation. First, the approximation error is computed and analytically upper-bounded. Thereafter, the bound on approximation error is verified using simulation scenarios tested on the IEEE 69 node test system.

Corollary 3. *For a single-phase distribution system, errors in approximating the changes in real and imaginary parts of line current flows (E^r_{MA} and E^i_{MA}, respectively) using (4.9) are upper bounded by,*

$$E^r \leq \sum_{A \in \mathcal{A}} \frac{\Delta P_A \Psi_{MA}}{V^r_A(1+\Phi_1)} + \frac{\Delta Q_A \Psi_{MA}}{V^i_A(1+\Phi_2)}, \tag{4.17}$$

$$E^i \leq \sum_{A \in \mathcal{A}} \frac{\Delta P_A \Psi_{MA}}{V^i_A(1+\Phi_2)} + \frac{\Delta Q_A \Psi_{MA}}{V^r_A(1+\Phi_1)}, \tag{4.18}$$

where, $\Phi_1 = \left(\frac{V^i_A}{V^r_A}\right)^2$ *and* $\Phi_2 = \Phi_1^{-1}$.

Proof. From Eq. (4.1), it can be seen that the voltage change compared to actual nodal voltage is small as in Eq. (4.6) and thus can be ignored, which yields the approximation

in Eq. (4.7). The error resulting from the assumption that ($\frac{\Delta V_A^r}{V_A^r}$ and $\frac{\Delta V_A^i}{V_A^i} \approx 0$) is upper bounded by Corollary 3. We can compute the approximation error (for real part of change in current) as follows,

$$E^r = \Delta I_e^r - \Delta \hat{I}_e^r, \tag{4.19}$$

where ΔI_e^r is the actual change in real part of current flow and $\Delta \hat{I}_e^r$ is the approximated change in real part of current flow. Therefore,

$$\begin{aligned} E^r &= \left[\frac{\Delta P_A (V_A^r + \Delta V_A^r)}{(V_A^r + \Delta V_A^r)^2 + (V_A^i + \Delta V_A^i)^2} - \frac{\Delta P_A V_A^r}{(V_A^r)^2 + (V_A^i)^2}\right] \\ &+ \left[\frac{\Delta Q_A (V_A^i + \Delta V_A^i)}{(V_A^r + \Delta V_A^r)^2 + (V_A^i + \Delta V_A^i)^2} - \frac{\Delta Q_A V_A^i}{(V_A^r)^2 + (V_A^i)^2}\right] \\ &= E_1^r + E_2^r \end{aligned}$$

E_1^r can be rewritten as,

$$E_1^r = \frac{\Delta P_A (1 + \frac{\Delta V_A^r}{V_A^r})}{V_A^r (1 + \frac{\Delta V_A^r}{V_A^r})^2 \left[1 + \frac{(V_A^i)^2}{(V_A^r)^2} \frac{(1 + \frac{\Delta V_A^i}{V_A^i})^2}{(1 + \frac{\Delta V_A^r}{V_A^r})^2}\right]} - \frac{\Delta P_A}{V_A^r \left[1 + \frac{(V_A^i)^2}{(V_A^r)^2}\right]}$$

Typically in distribution systems the change in nodal voltage compared to actual voltage is small, i.e., $\frac{\Delta V_A^r}{V_A^r} \approx 0$ and $\frac{\Delta V_A^i}{V_A^i} \approx 0$. Therefore, the previous equation can be rewritten as,

$$E_1^r = \frac{\Delta P_A}{V_A^r (1 + \Phi_1)} \left[\frac{1}{T^r} - 1\right]$$

where, $T^r = 1 + K^r$, $T^i = 1 + K^i$, $K^r = \frac{\Delta V_A^r}{V_A^r}$, $K^i = \frac{\Delta V_A^i}{V_A^i}$ and $\Phi_1 = \frac{(V_A^i)^2}{(V_A^r)^2}$. Considering the ratio of change in voltage to actual nodal voltage is small, the quantity $\frac{\Delta V_A^r}{V_A^r}$ will always be less than or equal to $1 - \frac{\Delta V_A^r}{V_A^r}$, i.e.,

$$K^r \leq 1 - K^r \Rightarrow \frac{K^r}{1 - K^r} \leq 1 \Rightarrow \frac{1}{T^r} - 1 \leq 1$$

$$\frac{\Delta P_A}{V_A^r(1+\Phi_1)}\left[\frac{1}{T^r}-1\right] \leq \frac{\Delta P_A}{V_A^r(1+\Phi_1)}$$
$$\Rightarrow E_1^r \leq \frac{\Delta P_A}{V_A^r(1+\Phi_1)} \tag{4.20}$$
$$\text{Similarly,} \quad E_2^r \leq \frac{\Delta Q_A}{V_A^i(1+\Phi_2)}.$$

Finally, by combining E_1^r and E_2^r, the error in approximating the real part of current change is upper bounded by,

$$E^r = E_1^r + E_2^r \leq \frac{\Delta P_A}{V_A^r(1+\Phi_1)} + \frac{\Delta Q_A}{V_A^i(1+\Phi_2)}. \tag{4.21}$$

Considering multiple actor nodes changing their complex power and repeating the same for imaginary part of current change yields,

$$E^r \leq \sum_{A\in\mathcal{A}} \frac{\Delta P_A \Psi_{MA}}{V_A^r(1+\Phi_1)} + \frac{\Delta Q_A \Psi_{MA}}{V_A^i(1+\Phi_2)}, \tag{4.22}$$

$$E^i \leq \sum_{A\in\mathcal{A}} \frac{\Delta P_A \Psi_{MA}}{V_A^i(1+\Phi_2)} + \frac{\Delta Q_A \Psi_{MA}}{V_A^r(1+\Phi_1)}, \tag{4.23}$$

which completes the proof of Corollary 3. □

The tightness of the upper bounds in Corollary 3 are validated via simulation on the IEEE 69 node test system. A simulation scenario is created where complex power varies at nodes 18 and 30 by $\Delta P = \Delta Q \in [-50, ..., 50]$ kW (and kVAr) and the change in current flow is monitored on line 5. The actual error is computed based on Eq. (4.19), i.e., the difference between numerical results using classical load flow and the proposed analytical approach. The error bound is computed based on the results provided by Corollary 3. Line 5 is randomly chosen to monitor line flow and compute the actual and approximation

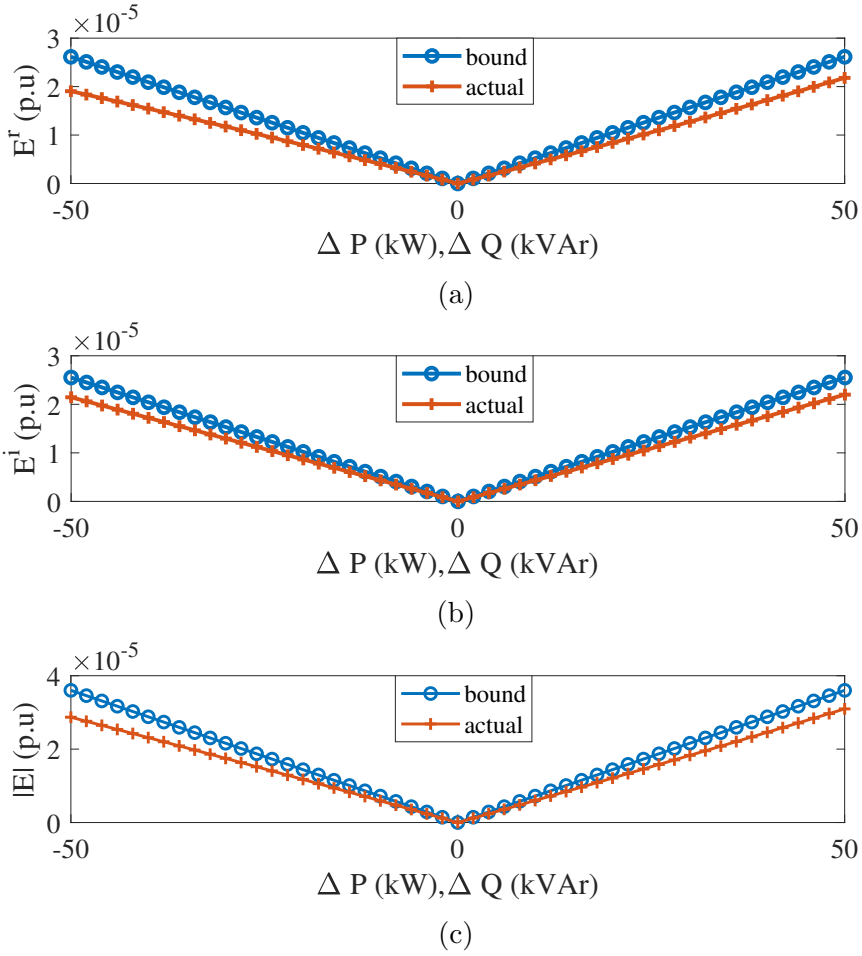

Figure 4.4: Approximation error bound using Corollary 3.

errors. However, the method is generic for any pair of actor nodes and monitored lines. Fig. 4.4 illustrates the actual error vs. the error bound for the aforementioned simulation scenario. The figure shows the errors in approximating real, imaginary and magnitude of current change. It can be seen from the figure that (4.17) and (4.18) present a tight upper bound for the actual error especially within the interval $[-20, ..., 20]$ kW (kVAr), which is consistent with real world power change scenarios. Therefore, the error bounds developed in Corollary 3 ensure the consistency and accuracy of the proposed analytical approach in approximating the change in line current. Next, this analytical framework is extended to account for variability associated with complex power injection (or withdrawal) at multiple active consumer sites in the system.

4.2 Probabilistic loss sensitivity analysis

Complex power at active consumer sites could vary randomly due to the variability associated with DER injections (such as rooftop PV units and wind turbines) or due to dynamic load patterns. These stochastic processes inevitably impact system losses, which in turn leads to economic losses. Therefore, modern distribution system operators require an accurate, yet computationally efficient, loss monitoring tool that accounts for power uncertainties. This helps to guide optimal asset management strategies to keep losses minimal in a real-time fashion during electric vehicle planning or DER control. In this section, Corollaries 1 and 2 are used as the starting point to compute the probability distributions of change in current and power losses at a particular monitored line, respectively. Specifically, Eq. (4.8) can be rewritten as follows,

$$\Delta I_{MA} = \Delta I^r_{MA} + j\Delta I^i_{MA},$$

where,

$$\begin{aligned} \Delta I^r_{MA} &\approx \frac{\Psi_{MA}(\Delta P_A \cos(\theta_A) - \Delta Q_A \sin(\theta_A))}{|V_A|} \\ \Delta I^i_{MA} &\approx \frac{\Psi_{MA}(-\Delta P_A \sin(\theta_A) - \Delta Q_A \cos(\theta_A))}{|V_A|}. \end{aligned} \tag{4.24}$$

Here, θ_A is the voltage angle of actor node A. Since multiple actor nodes impact the current flow at line M, using Corollaries 1 and 2, we conclude that

$$\Delta I_M = \sum_{A\in\mathcal{A}} \Delta I^r_{MA} + j \sum_{A\in\mathcal{A}} \Delta I^i_{MA}, \tag{4.25}$$

$$\begin{aligned} \Delta L_M = &\left[\Big| \sum_{A\in\mathcal{A}} \Delta I_{MA} \Big|^2 + 2\Re\Big(I^*_M \sum_{A\in\mathcal{A}} \Delta I_{MA} \Big) \right] R_M \\ &+ j \left[\Big| \sum_{A\in\mathcal{A}} \Delta I_{MA} \Big|^2 + 2\Re\Big(I^*_M \sum_{A\in\mathcal{A}} \Delta I_{MA} \Big) \right] X_M. \end{aligned} \tag{4.26}$$

DER injection or dynamic load patterns can be modeled as a probability distribution to account for the variability. In particular, complex power changes (withdrawal or injection) at active consumer sites can be modeled as a random vector $\boldsymbol{\Delta s} = [\Delta P_1, ..., \Delta P_N, \Delta Q_1, ..., \Delta Q_N]^T$ with mean $\boldsymbol{\mu} = \mathbf{0}$ and a covariance structure captured by the covariance matrix $\boldsymbol{\Sigma_{\Delta s}}$. The following subsections highlight the steps followed to derive the probability distribution of the squared magnitude of the change in current flow that is used in Eq. (4.26) to compute line losses.

4.2.1 Construct $\boldsymbol{\Sigma_{\Delta s}}$ and compute $\boldsymbol{k_r}$ and $\boldsymbol{k_i}$

$\boldsymbol{\Sigma_{\Delta s}}$ contains information about the variance of complex power change at active consumer locations that represents, for instance, the size of PV unit or the load pattern, etc. Off-diagonal elements of the covariance matrix capture the spatial correlation of complex power changes at different actor nodes. The spatial correlation is a byproduct of the geographical proximity of renewable energy sources. The covariance matrix depends on the size of the system and the number of active consumers changing their complex power as shown in Eq. (5.27) below. p_i and q_i are the active and reactive power injection or consumption at the i^{th} active consumer site, respectively, whereas $n \triangleq \mathcal{N}$ is the system size. The exact $\boldsymbol{\Sigma_{\Delta s}}$ of a particular system can be estimated based on historical data as discussed in [226], and is out of the scope of this work. If a node does not have DER units, the variance of complex power of that node can be set to zero and the standard kVA loading of that node will be used for the analysis. Additionally, the constant terms in (4.24) are arranged in $\boldsymbol{k_r}$ and $\boldsymbol{k_i}$ vectors. These vectors are functions of the magnitude of nodal base voltages and the nodal-line sensitivity relationships based system topology (defined by Ψ_{MA}). For each system, these vectors are fixed and can be readily computed using Eq. (4.27). It is important to note that the proposed analytical methodology to compute loss change is generic and is valid for any type of distribution system. However, steps to compute the intermediate values of the final loss expression could vary with the system topology. For instance, the procedure to determine Ψ_{MN} values of the weight vectors in (4.27) could vary with the system topology.

$$\boldsymbol{\Sigma}_{\boldsymbol{\Delta S}} = \begin{bmatrix} \sigma^2_{p_1} & \dots & cov(p_n, p_1) & cov(q_1, p_1) & \dots & cov(q_n, p_1) \\ \vdots & \ddots & \vdots & \vdots & \ddots & \vdots \\ cov(p_1, p_n) & \dots & \sigma^2_{p_n} & cov(q_1, p_n) & \dots & cov(q_n, q_n) \\ cov(p_1, q_1) & \dots & cov(p_n, q_1) & \sigma^2_{q_1} & \dots & cov(q_n, p_1) \\ \vdots & \ddots & \vdots & \vdots & \ddots & \vdots \\ cov(p_1, q_n) & \dots & cov(p_n, q_n) & cov(q_1, q_n) & \dots & \sigma^2_{q_n} \end{bmatrix}_{2\mathcal{N}\times 2\mathcal{N}} \tag{4.28}$$

The theoretical derivation of exact expressions for other system topology will be pursued as part of future work.

$$\boldsymbol{k}_r = \begin{bmatrix} \frac{\Psi_{M1}\cos\theta_1}{|V_1|} \\ \frac{\Psi_{M2}\cos\theta_1}{|V_2|} \\ \vdots \\ \frac{\Psi_{M\mathcal{N}}\cos\theta_{\mathcal{N}}}{|V_{\mathcal{N}}|} \\ -\frac{\Psi_{M1}\sin\theta_1}{|V_1|} \\ -\frac{\Psi_{M2}\sin\theta_1}{|V_2|} \\ \vdots \\ -\frac{\Psi_{M\mathcal{N}}\sin\theta_{\mathcal{N}}}{|V_{\mathcal{N}}|} \end{bmatrix}_{2\mathcal{N}\times 1} \quad \boldsymbol{k}_i = \begin{bmatrix} -\frac{\Psi_{M1}\sin\theta_1}{|V_1|} \\ -\frac{\Psi_{M2}\sin\theta_1}{|V_2|} \\ \vdots \\ -\frac{\Psi_{M\mathcal{N}}\sin\theta_{\mathcal{N}}}{|V_{\mathcal{N}}|} \\ -\frac{\Psi_{M1}\cos\theta_1}{|V_1|} \\ -\frac{\Psi_{M2}\cos\theta_1}{|V_2|} \\ \vdots \\ -\frac{\Psi_{M\mathcal{N}}\cos\theta_{\mathcal{N}}}{|V_{\mathcal{N}}|} \end{bmatrix}_{2\mathcal{N}\times 1} \tag{4.27}$$

Here, $\boldsymbol{\theta} = [\theta_1, ..., \theta_{\mathcal{N}}]^T$ represents the base voltage angles.

4.2.2 Probabilistic modeling of line current changes

It can be seen from Eq. (4.9) that the change in line current flows at a monitored line can be expressed as the aggregate changes in current flows caused by every actor node in the system. Now, consider random changes in complex power at actor nodes as given by the covariance matrix in Eq. (5.27). Using the Lindeberg-Feller central limit theorem, each of the probability distributions of ΔI^r_M and ΔI^i_M can be shown to converge to a Gaussian

distribution as,

$$\Delta I_M^r = \sum_{A \in \mathcal{A}} \Delta I_{MA}^r \approx \boldsymbol{k}_r^T \boldsymbol{\Delta s} \xrightarrow{D} \mathcal{N}(0, \boldsymbol{k}_r^T \boldsymbol{\Sigma}_{\boldsymbol{\Delta s}} \boldsymbol{k}_r), \tag{4.29}$$

$$\Delta I_M^i = \sum_{A \in \mathcal{A}} \Delta I_{MA}^i \approx \boldsymbol{k}_i^T \boldsymbol{\Delta s} \xrightarrow{D} \mathcal{N}(0, \boldsymbol{k}_i^T \boldsymbol{\Sigma}_{\boldsymbol{\Delta s}} \boldsymbol{k}_i). \tag{4.30}$$

Here, $\mathcal{A}$ is the set of actor nodes resulting in the change of current flow at line M. The terms $\boldsymbol{k}_r^T \boldsymbol{\Sigma}_{\boldsymbol{\Delta s}} \boldsymbol{k}_r \triangleq \sigma_r^2$ and $\boldsymbol{k}_i^T \boldsymbol{\Sigma}_{\boldsymbol{\Delta s}} \boldsymbol{k}_i \triangleq \sigma_i^2$ represent the variances of ΔI_M^r and ΔI_M^i, respectively.

4.2.3 Compute the distribution of $|\Delta I_M|^2$

The squared magnitude of current change at a monitored line M can be written as,

$$|\Delta I_M|^2 = (\Delta I_M^r)^2 + (\Delta I_M^i)^2. \tag{4.31}$$

Since the probability distributions of ΔI_M^r and ΔI_M^r converge to Gaussian distributions, the square of a Gaussian distribution, i.e., $(\Delta I_M^r)^2$ and $(\Delta I_M^i)^2$, follows a Gamma distribution with 0.5 as the shape parameter and scale parameter twice the variance of the Gaussian distribution [227]. That is,

$$(\Delta I_M^r)^2 \sim \Gamma(0.5, 2\sigma_r^2) \tag{4.32}$$

$$(\Delta I_M^i)^2 \sim \Gamma(0.5, 2\sigma_i^2) \tag{4.33}$$

Typically, in distribution systems the change in real and imaginary parts of current flow are correlated. In the proposed analytical method, this correlation is captured by Eq. (5.27) and (4.27). That is, the Gamma distributions in Eq. (4.32) and (4.33) are correlated by $K \triangleq \boldsymbol{k}_r^T \boldsymbol{\Sigma}_{\boldsymbol{\Delta s}} \boldsymbol{k}_i$. The sum of correlated Gamma distributions $\Gamma(0.5, 2\sigma_r^2)$ and $\Gamma(0.5, 2\sigma_i^2)$ also follows a Gamma distribution [228],

$$|\Delta I_M|^2 = (\Delta I_M^r)^2 + (\Delta I_M^i)^2 \sim \Gamma(k, \theta), \tag{4.34}$$

with scale and shape parameters $k = \frac{(\sigma_r^2+\sigma_i^2)}{\theta}$ and $\theta = \frac{2(\sigma_r^4+\sigma_i^4+2K^2)}{\sigma_r^2+\sigma_i^2}$, respectively.

4.2.4 Compute the distribution of ΔL_M^r and ΔL_M^i

This subsection derives the probability distribution of ΔL_M^r and ΔL_M^i based on the approximation in Corollary 2. The change in power loss at a monitored line M can be written in terms of real and imaginary parts as,

$$\begin{aligned}\Delta L_M &= \Delta L_M^r + j\Delta L_M^i \\ &= \Big[|\Delta I_M|^2 + 2\Re(I_M^* \Delta I_M)\Big] R_M \\ &\quad + j\Big[|\Delta I_M|^2 + 2\Re(I_M^* \Delta I_M)\Big] X_M\end{aligned}$$

From (4.34), $|\Delta I_M|^2 \sim \Gamma(k,\theta)$. Therefore,

$$\Delta L_M^r = \Big[\Gamma(k,\theta) + 2\Re(I_M^* \Delta I_M)\Big] R_M \text{ and,}$$

$$\Delta L_M^i = \Big[\Gamma(k,\theta) + 2\Re(I_M^* \Delta I_M)\Big] X_M.$$

If $X \sim \Gamma(k,\theta)$, then, $\forall a > 0, \quad aX \sim \Gamma(k, a\theta)$. Thus,

$$\Delta L_M^r = \Gamma(k, R_M\theta) + 2R_M\Re(I_M^* \Delta I_M), \tag{4.35}$$

$$\Delta L_M^i = \Gamma(k, X_M\theta) + 2X_M\Re(I_M^* \Delta I_M). \tag{4.36}$$

Fig. 6.6 shows a brief flowchart explaining the steps behind computing the probability distribution of change in active power losses using the proposed analytical approach.

4.2.5 Validation via simulation

This section validates the theoretical expressions derived earlier to compute the probability distributions of current and loss changes. For simplicity of demonstration, only the real

parts of both current and loss sensitivity analysis is shown. However, the proposed analytical approach is generic and can be applied to the imaginary parts as well. The proposed PLSA method is verified on the same IEEE 69 node test system. A scenario is created where complex power varies at a randomly selected set of actor nodes $A \in [5, 7, ..., 25]$ and the change in current and power losses are monitored on line $10 - 11$. It is assumed that actor nodes are integrated with PV units. To account for the variability in PV power outputs, complex power change ($\boldsymbol{\Delta s}$) among actor nodes is assumed to be random following a zero-mean Gaussian distribution with the covariance structure shown in Eq. (5.27). Although we assume a Gaussian distribution for power changes, the proposed method is generic to any choice of probability distribution. Additionally, PV power injection among actor nodes is correlated due to geographical proximity. Therefore, $\boldsymbol{\Sigma_{\Delta s}}$ captures those relationships by the off-diagonal covariance terms. For this particular case study, $\boldsymbol{\Sigma_{\Delta s}}$ is defined as follows. Active power variance on the diagonal is set to be 15 kW for nodes integrated with PV units. The reactive power variance for those nodes is set to 10 kVAr. For off-diagonal elements relating the change in active power among actor nodes, i.e., $cov(\Delta P_i, \Delta P_k) = 0.7$ where $i, j \in \boldsymbol{\mathcal{A}}$ and $i \neq j$. Furthermore, the covariance of change in reactive power $cov(\Delta Q_i, \Delta Q_k)$

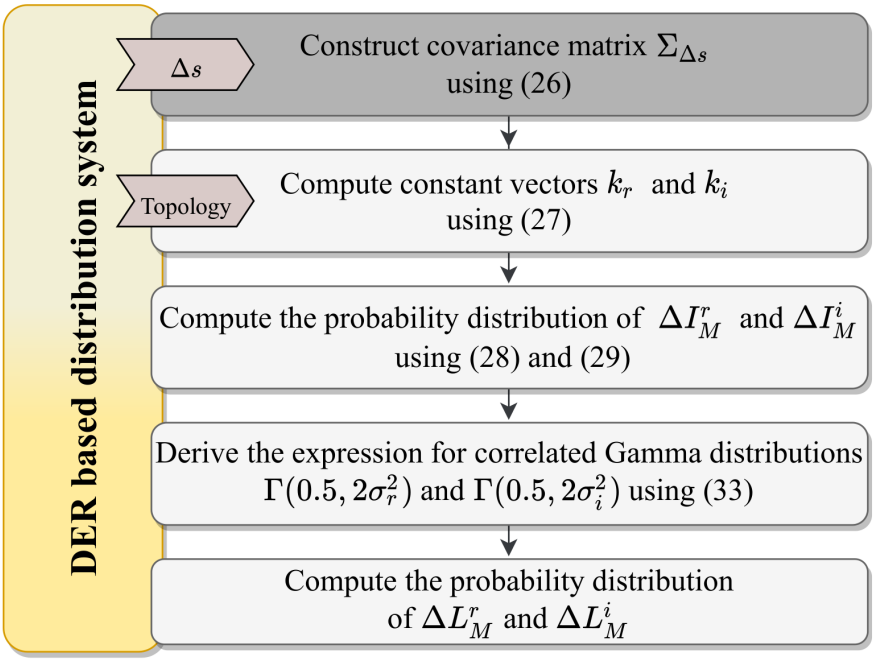

Figure 4.5: A flowchart of the proposed analytical PLSA approach.

is set to 0.6. Finally, the covariance between active and reactive power change $cov(\Delta P_i, \Delta Q_k)$ is set to 0.3. Variance and covariance of PV units in this scenario are kept the same for all actor nodes. However, the proposed approach is generic to accommodate various types of $\boldsymbol{\Sigma_{\Delta s}}$ structures.

The proposed analytical approach is compared to the benchmark results obtain by classical load flow-based sensitivity method. For the proposed analytical approach, firstly, the $\boldsymbol{k}_r$ and $\boldsymbol{k}_i$ are computed using Eq. (4.27), respectively. Then, the variance and covariance terms of change in real and imaginary parts of current are computed as,

$$\begin{aligned} \boldsymbol{\Sigma_{\Delta I_M}} &= \begin{bmatrix} \boldsymbol{k}_r^T \boldsymbol{\Sigma_{\Delta s}} \boldsymbol{k}_r & \boldsymbol{k}_i^T \boldsymbol{\Sigma_{\Delta s}} \boldsymbol{k}_r \\ \boldsymbol{k}_i^T \boldsymbol{\Sigma_{\Delta s}} \boldsymbol{k}_r & \boldsymbol{k}_i^T \boldsymbol{\Sigma_{\Delta s}} \boldsymbol{k}_i \end{bmatrix} \\ &= \begin{bmatrix} 0.8351 & -0.0354 \\ -0.0354 & 0.0787 \end{bmatrix} \times 10^{-3}. \end{aligned} \tag{4.37}$$

Thereafter, the distribution of change in real part of current is computed by sampling random variables using Eq. (4.29). For the benchmark results, load flow scenarios are created using the covariance matrix defined in (5.27). To illustrate the efficacy of the proposed approach, five different cases (namely case a, b, c, d, and e) are created by varying the number of load flow scenarios (as well as the number of random variables sampled with the proposed analytical approach). Specifically, we choose 100 simulations vs. 100 random variables, $1k$ simulations vs. $1k$ random variables, $10k$ simulations vs. $10k$ random variables, $100k$ simulations vs. $100k$ random variables, and $1m$ simulations vs. $1m$ random variables, for cases, a, b, c, d, and e, respectively. Fig. 4.6 shows the distribution of real part of current change on line 10-11 for all cases using the proposed analytical approach (red) compared to the simulation based method (blue). It can be inferred from the figure that the probability distributions shown in cases a, b, c, and d are less accurate than the distributions in case e. This is because the accuracy of the probability distribution improves with the increased number of scenarios (or number of random variables in the case of the proposed probabilistic approach). In order to make these comparisons objective, we use the Jensen-Shannon distance

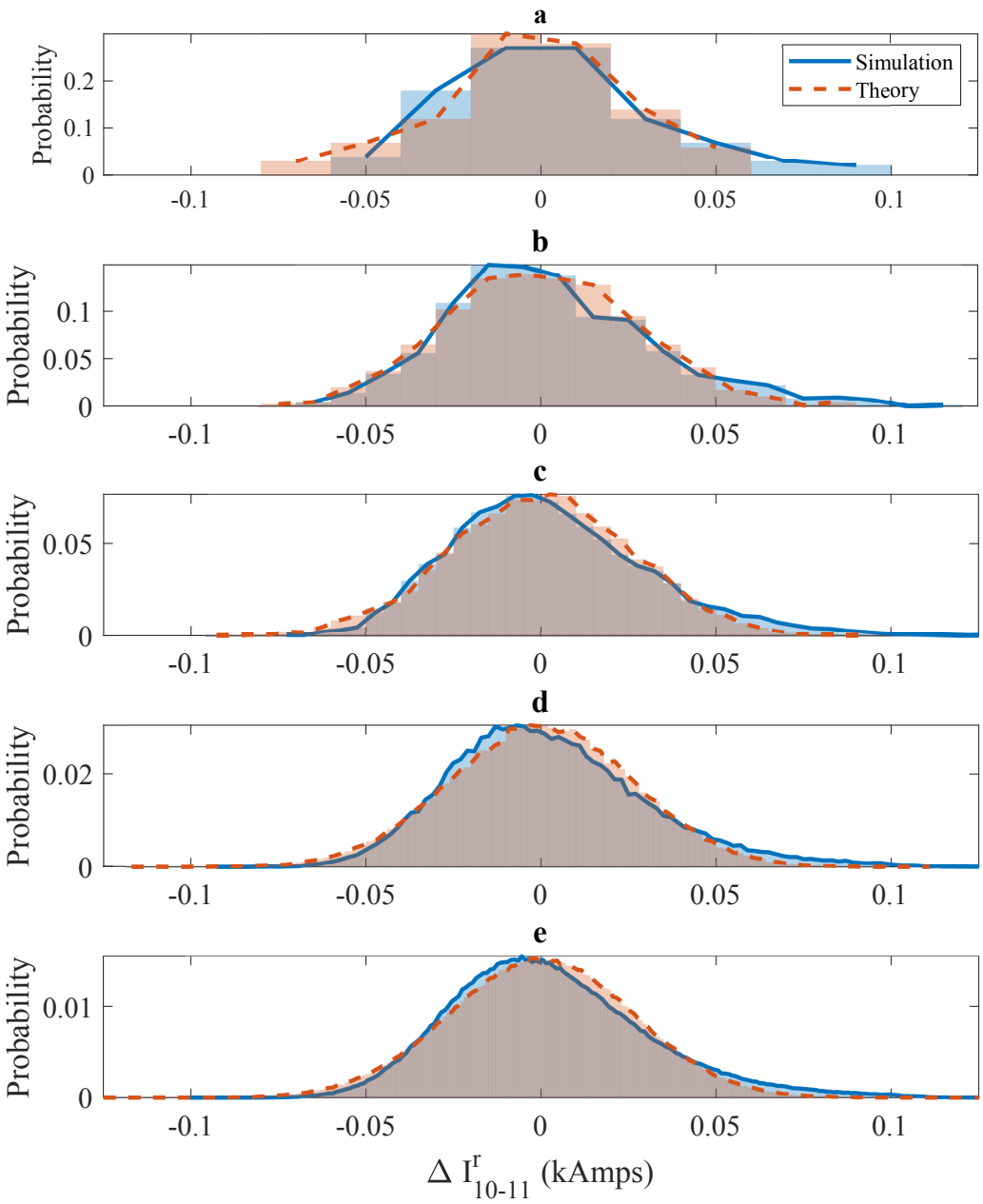

Figure 4.6: Probability distribution of change in real part of current flow ΔI_M^r for cases a, b, c, d and e.

(JSD), an information-theoretic similarity measure, to validate the accuracy of the proposed probabilistic approximation (compared to simulation-based classical load flow method) of both distributions of change in current flow as well as active power losses. The similarity (or

JSD) between simulations based and theoretical distributions can be computed as [229],

$$\text{JSD}(P||Q) = \frac{1}{2}D_{KL}(P||M) + \frac{1}{2}D_{KL}(Q||M), \tag{4.38}$$

where, $M = \frac{1}{2}(P+Q)$ and D_{KL} is the Kullback-Leibler (KL) divergence metric as a measure of the information lost when Q is used to approximate P evaluated at the support $x \in \mathcal{X}$ and can be written as,

$$D_{KL}(P||Q) = \sum_{x\in\mathcal{X}} P(x) \log\left(\frac{P(x)}{Q(x)}\right) \tag{4.39}$$

The JSD distance is used for validation instead of the KL divergence because the JSD is always symmetric, well defined, and bounded [230]. JSD can vary between 0 (meaning the two distributions are identical) and 1 (meaning the distributions are completely different). The JSD between actual simulation-based and theoretical distributions of change in current flow is in the order of 10^{-2}, which implies that the probabilistic approximation is accurate when compared to existing simulation-based method.

Subsequently, the shape and scale parameters of the Gamma distribution in Eq. (4.34) are computed as $k = 0.5913$ and $\theta = 0.0015$ to obtain the probability distribution of the change in active power loss on line $10-11$ using Eq. (4.35). The distribution of change in active power losses is computed for case e and illustrated in Fig. 4.7. The JSD between actual simulation-based and theoretical distribution of change in active power loss is found to be in the order of 10^{-2}. These results imply that it is possible to accurately evaluate the probability of line current flow or active power losses exceeding a certain threshold (γ). For instance, Table 4.2 shows the probability of real part of current change exceeding $\gamma_c = 0.002$ kAmps and active losses exceeding $\gamma_l = 0.5$ kW using classical method and the proposed analytical approach.

Table 4.2: Probability of exceeding the threshold γ.

Probability	Simulation	Theory
$\mathbb{P}(\lvert\Delta I^r_M\rvert > \gamma_c)$	0.8630	0.8561
$\mathbb{P}(\lvert\Delta L^r_M\rvert > \gamma_l)$	0.9404	0.9396

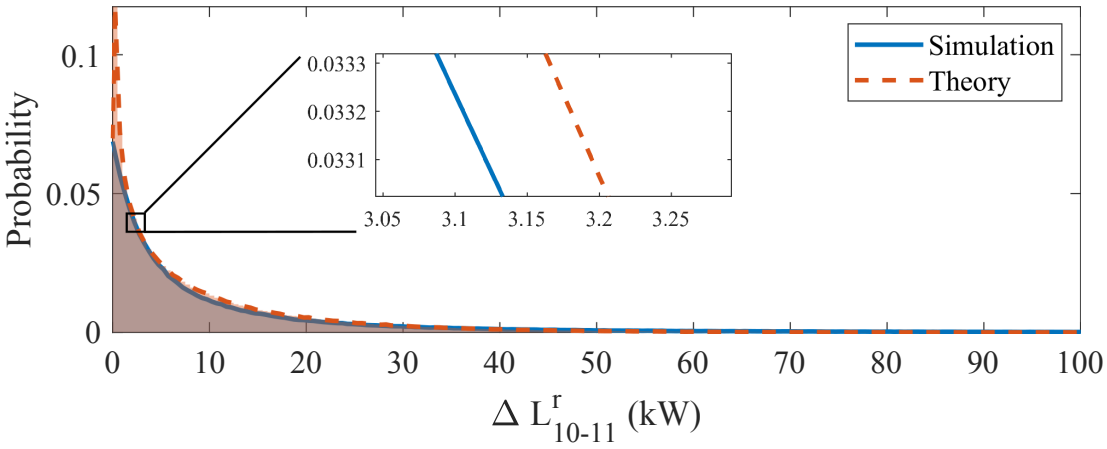

Figure 4.7: Probability distribution of change in active power losses ΔL_M^r.

Table 4.3: Execution time (s).

Case	Simulation	Theory
case a	0.2897	0.0472
case b	2.1852	0.0482
case c	19.1739	0.0694
case d	190.4614	0.0934
case e	1871.84421	0.2373

Finally, the computational complexity of the proposed method is compared via the execution time taken to compute the probability distributions of change in current and power loss for a given monitored line M, in this case, line $10-11$. The analysis is implemented with intel i-9 processor for all cases illustrated in Fig. 4.6 and the corresponding execution time taken by both approaches is reported in Table 4.3. The proposed analytical approach outperforms the classical simulation based method regardless of the number of simulations (or random variables in the case of the proposed approach) used to obtain the probability density curves. This is because sampling random variables from well-established probability distributions is faster compared the classical scenario-based analysis, which require simulating large number of scenarios to achieve the required accuracy. This implies that the proposed analytical framework accurately approximates the distribution of change in current flow and in line losses with significantly lower computational effort. It is important to note that the computational efficiency of the proposed approach is consistent regardless of

system size or choice of monitored lines. Therefore, with the proposed approach, it is possible to significantly simplify the process of loss monitoring in modern distribution systems, which enables various downstream applications such as EV and DER planning.

4.3 Summary

This chapter proposes a new probabilistic loss sensitivity analysis framework that builds off an analytical approximation of the change in power losses at a given line due to complex power changes at other nodes in the system. First, an analytical expression is derived to compute the change in line losses for deterministic power changes at one actor node. Then, the effect of random power changes at multiple active consumer sites is examined using the proposed approach. It is shown that the probability distribution of change in line power losses is well approximated by a Gamma distribution. The proposed analytical expressions are validated via simulations on the IEEE 69 node test system. Simulation results show that approximating the change in power loss at any line in the system is highly accurate with a JSD in the order of 10^{-2}. In addition, the proposed approach is computationally efficient when compared to traditional load flow-based sensitivity methods. In the next chapter, this probabilistic loss sensitivity framework is derived for 3-phase unbalanced distribution systems.

Chapter 5

Loss sensitivity analysis for three-phase unbalanced distribution systems

Despite their numerous benefits, the rapid onset of DERs and EVs introduces new technical challenges to distribution systems including (1) complex system operation due to reverse power flows [231], (2) voltage instability issues [232], (3) system imbalance due to high concentration of consumer activities on the three phases [24]; and (4) increased power losses due to poor DER and EV planning as well as their temporal uncertainty, caused by abrupt power changes [233]. Therefore, based on our preliminary results in Chapter 4, this chapter proposes a new stochastic framework that derives loss sensitivity for the general case, i.e., three-phase unbalanced distribution systems. As will be shown in this chapter, the extension to three phase unbalanced case is not trivial and is crucial for modern distribution system planning and operation given the variability in consumer activities on different phases of the system. The accuracy of the proposed approach is validated using the unbalanced IEEE 37 and IEEE 123-node test systems. It has been shown that the deterministic approximation offers over 98% accuracy via the mean absolute percentage error (MAPE) and the probability distributions can be estimated with very low Jensen-Shannon distances. The proposed

framework is used in Chapter 7 for EV charging station allocation in three-phase distribution systems.

5.1 Loss sensitivity for unbalanced systems

The proposed approach uses a three-phase unbalanced distribution system model with $\boldsymbol{\mathcal{N}}$ nodes connected by $\mathcal{L}$ distribution lines as shown in Fig. 5.1. Active and reactive power setpoints can change at any phase of any node in the system due to various consumer activities such as PV integration, EV charging, or load variability. This change induces variability in current flow at certain distribution lines, causing power losses to change. For example, an increase in local load at phase a of node $\boldsymbol{\mathcal{N}_e}$ increases the current flow at line e_a, which in turn increases losses. To distinguish nodes where complex power changes and lines where current flow is monitored, two terminologies are used: (1) *Actor node* (A) refers to the node where complex power changes happen; and (2) *Monitored line* (M) is the distribution line where current flow or power loss is monitored. Let $\Delta S_A^h = \Delta P_A^h + j\Delta Q_A^h$ be the change in active and reactive power at actor node A where $h \in \boldsymbol{\mathcal{H}} \triangleq \{a, b, c\}$ represents the phase sequence. Then, the current flow at the monitored line M changes from I_M^h to $I_M^{h'} \triangleq I_M^h + \Delta I_{MA}^h$, where ΔI_{MA}^h is change in current flow at phase h of line M due to complex power change ΔS_A^h at phase h of actor node A. Theorem 2 provides an analytical approximation of $\boldsymbol{\Delta I_{MA}^h}$ for unbalanced distribution systems.

Theorem 2. *For a three-phase unbalanced distribution system, the change in current flow at monitored line M (i.e., $\boldsymbol{\Delta I_{MA}^h} \triangleq [\Delta I_{MA}^a, \Delta I_{MA}^b, \Delta I_{MA}^c]^T$) due to complex power changes at the actor node A can be approximated as,*

$$\boldsymbol{\Delta I_{MA}^h} \approxeq \left[\frac{\Delta S_A^{a*} \Psi_{MA}^a}{V_A^{a*}}, \frac{\Delta S_A^{b*} \Psi_{MA}^b}{V_A^{b*}}, \frac{\Delta S_A^{c*} \Psi_{MA}^c}{V_A^{c*}} \right]^T, \tag{5.1}$$

where, $S_A^{h*} \forall h \in \boldsymbol{\mathcal{H}}$ is the complex conjugate of power change at actor node A, $V_A^{h*} \forall h \in \boldsymbol{\mathcal{H}}$ is the complex conjugate of actor node base voltage, and $\Psi_{MA}^h \forall h \in \boldsymbol{\mathcal{H}}$ is the influence indicator between the actor node and monitored line as derived in the proof below.

Proof. Consider the hypothetical three-phase unbalanced distribution system shown in Fig. 5.1. The three-phase current flow through line $\boldsymbol{e^h} \triangleq [e_a, e_b, e_c]^T \forall h \in \mathcal{H}$ can be written in terms of the nodal current flows (i.e., $\boldsymbol{I_e^h} \triangleq [I_e^a, I_e^b, I_e^c]^T$) as,

$$\boldsymbol{I_e^h} = \sum_{k \in \mathcal{N}_e} \left[I_k^a, I_k^b, I_k^c\right]^T = \sum_{k \in \mathcal{N}_e} \left[\frac{S_k^{a*}}{V_k^{a*}}, \frac{S_k^{b*}}{V_k^{b*}}, \frac{S_k^{c*}}{V_k^{c*}}\right]^T, \tag{5.2}$$

where, $k \in \mathcal{N}_e \in \mathcal{N}$, and S_k^{a*} and V_k^{a*} represent the complex conjugate of power and base voltage of actor node k, respectively. It is important to note that the following assumption is used throughout this chapter,

Assumption 3. *The source node operates at a unity voltage magnitude, i.e.,* $1\angle 0°$, $1\angle 120°$, *and* $1\angle -120°$ *for phases a, b, and c, respectively.*

When complex power changes at any of the phases of actor node $k \in \mathcal{N}_e$ by $\boldsymbol{\Delta S_e^h} \triangleq \left[\Delta S_k^a, \Delta S_k^b, \Delta S_k^c\right]^T$, the current flow through line $\boldsymbol{e^h}$ changes to,

$$\begin{aligned} \boldsymbol{I_e^{h'}} &= \sum_{k \in \mathcal{N}_e} \left[I_k^{a'}, I_k^{b'}, I_k^{c'}\right]^T \\ &= \sum_{k \in \mathcal{N}_e} \left[\frac{S_k^{a*} + \Delta S_k^a}{V_k^{a*} + \Delta V_k^{a*}}, \frac{S_k^{b*} + \Delta S_k^b}{V_k^{b*} + \Delta V_k^{b*}}, \frac{S_k^{c*} + \Delta S_k^c}{V_k^{c*} + \Delta V_k^{c*}}\right]^T. \end{aligned} \tag{5.3}$$

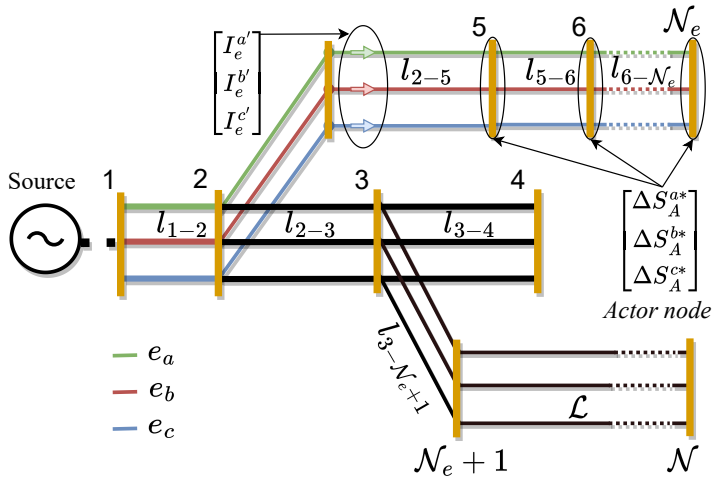

Figure 5.1: Illustration of a hypothetical three-phase unbalanced distribution system.

Here, $\boldsymbol{\Delta V_e^h} \triangleq \left[\Delta V_k^{a*}, \Delta V_k^{b*}, \Delta V_k^{c*}\right]^T$ represents the complex conjugate of voltage (e.g., $\Delta V_k^{a*} = \Delta V_k^{a,r} - j\Delta V_k^{a,i}$) at node k due to nodal complex power changes $\boldsymbol{\Delta S_e^h}$. Using equations (5.2) and (5.3), it is possible to compute the change in complex current flow ($\boldsymbol{\Delta I_e^h} \triangleq \boldsymbol{I_e^{h'}} - \boldsymbol{I_e^h}$) due to complex power changes as,

$$\begin{aligned}
\boldsymbol{\Delta I_e^h} =& \sum_{k\in\mathcal{N}_e} \left[\frac{S_k^{a*}+\Delta S_k^a}{V_k^{a*}+\Delta V_k^{a*}}, \frac{S_k^{b*}+\Delta S_k^b}{V_k^{b*}+\Delta V_k^{b*}}, \frac{S_k^{c*}+\Delta S_k^c}{V_k^{c*}+\Delta V_k^{c*}}\right]^T \\
&- \sum_{k\in\mathcal{N}_e} \left[\frac{S_k^{a*}}{V_k^{a*}}, \frac{S_k^{b*}}{V_k^{b*}}, \frac{S_k^{c*}}{V_k^{c*}}\right]^T \\
=& \sum_{k\in\mathcal{N}_e} \left[\frac{V_k^{a*}(S_k^{a*}+\Delta S_k^{a*}) - S_k^{a*}(V_k^{a*}+\Delta V_k^{a*})}{V_k^{a*}(V_k^{a*}+\Delta V_k^{a*})}, \right. \\
&\frac{V_k^{b*}(S_k^{b*}+\Delta S_k^{b*}) - S_k^{b*}(V_k^{b*}+\Delta V_k^{b*})}{V_k^{b*}(V_k^{b*}+\Delta V_k^{b*})}, \\
&\left.\frac{V_k^{c*}(S_k^{c*}+\Delta S_k^{c*}) - S_k^{c*}(V_k^{c*}+\Delta V_k^{c*})}{V_k^{c*}(V_k^{c*}+\Delta V_k^{c*})}\right]^T
\end{aligned} \tag{5.4}$$

Eq. (5.4) can be simplified further by considering the following assumption on voltage change [20],

Assumption 4. *The change in voltage compared to actual voltage states is small.*

Therefore, Eq. (5.4) reduces to,

$$\boldsymbol{\Delta I_e^h} \approxeq \sum_{k\in\mathcal{N}_e} \left[\frac{\Delta S_k^{a*}}{V_k^{a*}+\Delta V_k^{a*}}, \frac{\Delta S_k^{b*}}{V_k^{b*}+\Delta V_k^{b*}}, \frac{\Delta S_k^{c*}}{V_k^{c*}+\Delta V_k^{c*}}\right]^T. \tag{5.5}$$

Now assume that there is only on actor node ($k = A \in \boldsymbol{\mathcal{N}_e}$) where complex power varies, it is possible to write the change in current flow in terms of real and imaginary parts for different phases as,

$$\boldsymbol{\Delta I_e^h} \approxeq \left[\Delta I_e^{a,r} + j\Delta I_e^{a,i}, \Delta I_e^{b,r} + j\Delta I_e^{b,i}, \Delta I_e^{c,r} + j\Delta I_e^{c,i}\right]^T$$

where, for phase a, $\Delta I_e^{a,r}$ and $\Delta I_e^{a,r}$ can be written (without loss of generality) according to Lemma 1.

Lemma 1. *The current flow can be decomposed into terms of real and imaginary parts as follows,*

$$\Delta I_e^{a,r} + j\Delta I_e^{a,i} \triangleq \frac{\Delta P_A^a V_A^{a,r} + \Delta Q_A^a V_A^{a,i}}{(V_A^{a,r})^2 + (V_A^{a,i})^2} + j\frac{\Delta P_A V_A^{a,i} - \Delta Q_A V_A^{a,r}}{(V_A^{a,r})^2 + (V_A^{a,i})^2} = \frac{\Delta S_A^{a*}}{V_A^{a*}} \tag{5.6}$$

The complete proof of Lemma 1 is shown in Appendix A for phase a and similarly, $\boldsymbol{\Delta I_e^h}$ can be decomposed into real and imaginary parts for phases b and c. This concept can be generalized for cases where $A \notin \boldsymbol{\mathcal{N}_e}$ as shown in Fig. 5.1. Thus, for any line segment ($M \in \boldsymbol{e^h}$), if $A \notin \boldsymbol{\mathcal{N}_e}$, the influence indicator (Ψ_{MA}) between the actor node A and line M can be set to zero. This is because complex power changes at these nodes do not impact current flow at $M \in \boldsymbol{e^h}$. Otherwise (i.e., if $A \in \boldsymbol{\mathcal{N}_e}$), it can be set to 1. Therefore,

$$\boldsymbol{\Delta I_{MA}^h} \approx \left[\frac{\Delta S_A^{a*}\Psi_{MA}^a}{V_A^{a*}}, \frac{\Delta S_A^{b*}\Psi_{MA}^b}{V_A^{b*}}, \frac{\Delta S_A^{c*}\Psi_{MA}^c}{V_A^{c*}}\right]^T, \tag{5.7}$$

Hence, proved. □

Theorem 2 computes the change in current flow at M due to a single actor node A. However, there could be scenarios where multiple actor nodes (e.g., $\boldsymbol{\mathcal{A}}$) impact the current flow at M. This is because complex power may vary at different locations simultaneously. Hence, it is possible to extend Eq. (5.7) to the case of multiple actor nodes. Since there is a direct relation between every pair of actor-observation nodes, the change in current flow $\boldsymbol{\Delta I_M^h}$ can be written as the aggregate sum of individual changes induced by the different actor nodes, i.e.,

$$\boldsymbol{\Delta I_M^h} \approx \sum_{A \in \boldsymbol{\mathcal{A}}} \left[\frac{\Delta S_A^{a*}\Psi_{MA}^a}{V_A^{a*}}, \frac{\Delta S_A^{b*}\Psi_{MA}^b}{V_A^{b*}}, \frac{\Delta S_A^{c*}\Psi_{MA}^c}{V_A^{c*}}\right]^T. \tag{5.8}$$

Note that the subscript A in $\boldsymbol{\Delta I_M^h}$ has been dropped to note the impact of multiple actor nodes instead of one actor node. Using Eq. (5.8), it is possible to compute the change in power losses at line M due to the aggregate impact of multiple actor nodes as shown in

Theorem 3.

Theorem 3. *For a three-phase unbalanced distribution system, the change in power loss at any monitored line M due to the aggregate impact of complex power changes at multiple actor nodes $\mathcal{A}$ can be computed as,*

$$\mathbf{\Delta L^h_M} \sim \left[\left|\sum_{A\in\boldsymbol{\mathcal{A}}} \frac{\Delta S^{a*}_A \Psi^a_{MA}}{V^{a*}_A}\right|^2 + \epsilon^a, \left|\sum_{A\in\boldsymbol{\mathcal{A}}} \frac{\Delta S^{b*}_A \Psi^b_{MA}}{V^{b*}_A}\right|^2 + \epsilon^b, \left|\sum_{A\in\boldsymbol{\mathcal{A}}} \frac{\Delta S^{c*}_A \Psi^c_{MA}}{V^{c*}_A}\right|^2 + \epsilon^c\right] \mathbf{Z^h_M}, \quad (5.9)$$

where $\epsilon^h = 2\Re\left(I^{h*}_M \sum_{A\in\boldsymbol{\mathcal{A}}} \frac{\Delta S^{h*}_A \Psi^h_{MA}}{V^{h*}_A}\right) \forall h \in [a,b,c]$ *and* $\mathbf{Z^h_M}$ *is the impedance of line* M.

Proof. According to [224], power losses at any line M can be computed as,

$$\mathbf{L^h_M} = \left[|I^a_M|^2, |I^b_M|^2, |I^c_M|^2\right] \mathbf{Z^h_M} \tag{5.10}$$

where $\mathbf{Z^h_M}$ is the impedance matrix of line M and can be written in terms of the three phases a, b, and c as,

$$\mathbf{Z^h_M} = \begin{bmatrix} Z^{aa}_M, Z^{ab}_M, Z^{ac}_M \\ Z^{ba}_M, Z^{bb}_M, Z^{bc}_M \\ Z^{ca}_M, Z^{cb}_M, Z^{cc}_M \end{bmatrix} \tag{5.11}$$

when the current flow at line M changes from I^h_M to $I^h_M + \Delta I^h_M \forall h \in [a,b,c]$, power loss changes from $\mathbf{L^h_M}$ to $\mathbf{L^h_M} + \mathbf{\Delta L^h_M}$, i.e.,

$$\mathbf{\Delta L^h_M} = [|I^a_M + \Delta I^a_M|^2 - |I^a_M|^2, |I^b_M + \Delta I^b_M|^2 - |I^b_M|^2, |I^c_M + \Delta I^c_M|^2 - |I^c_M|^2]\mathbf{Z^h_M}. \tag{5.12}$$

Note that the terms $|I^h_M + \Delta I^h_M|^2 - |I^h_M|^2$ can be rewritten as $|\Delta I^h_M|^2 + 2\Re\left(I^{h*}_M \Delta I^h_M\right)$. Therefore, using Eq. (5.8), $\mathbf{\Delta L^h_M}$ can be written as,

$$\mathbf{\Delta L^h_M} \sim \left[\left|\sum_{A\in\boldsymbol{\mathcal{A}}} \frac{\Delta S^{a*}_A \Psi^a_{MA}}{V^{a*}_A}\right|^2 + \epsilon^a, \left|\sum_{A\in\boldsymbol{\mathcal{A}}} \frac{\Delta S^{b*}_A \Psi^b_{MA}}{V^{b*}_A}\right|^2 + \epsilon^b, \left|\sum_{A\in\boldsymbol{\mathcal{A}}} \frac{\Delta S^{c*}_A \Psi^c_{MA}}{V^{c*}_A}\right|^2 + \epsilon^c\right] \mathbf{Z^h_M}. \tag{5.13}$$

Hence, proved. □

The main analytical expressions derived in Eq. (5.8) and (5.13) are used in the next section to derive the stochastic sensitivity framework.

5.2 Analytical stochastic sensitivity framework

The increased integration of DERs and EVs as well as variable load patterns introduce high level of uncertainty that can impact system reliability. Fortunately, it is possible to characterize these uncertainties probabilistically and propagate the uncertainties to loss computations. Specifically, Fig. 5.2 shows the overall stochastic framework for loss sensitivity. Each of these steps are detailed below.

5.2.1 Derive the probability distribution of line flow

Given random variations of complex power changes, the parameters of the distribution of change in current flow is analytically derived Theorem 4.

Theorem 4. *For a three-phase unbalanced distribution system, the distribution of current change at any phase $h \in \mathcal{H} \triangleq \{a, b, c\}$ of any monitored line M due to the aggregate impact of random complex power changes at multiple actor nodes $\mathcal{A}$ converges to a multivariate Gaussian,*

$$\begin{bmatrix} \Delta I^h_{M,r} \\ \Delta I^h_{M,i} \end{bmatrix} \xrightarrow{Dist.} \mathcal{N}\left(\boldsymbol{\mu}_{ri} \triangleq \begin{bmatrix} \mu_r \\ \mu_i \end{bmatrix}, \boldsymbol{\Sigma}_{ri} \triangleq \begin{bmatrix} (\sigma^h_r)^2 & (\sigma^h_{ri})^2 \\ (\sigma^h_{ri})^2 & (\sigma^h_i)^2 \end{bmatrix} \right) \tag{5.14}$$

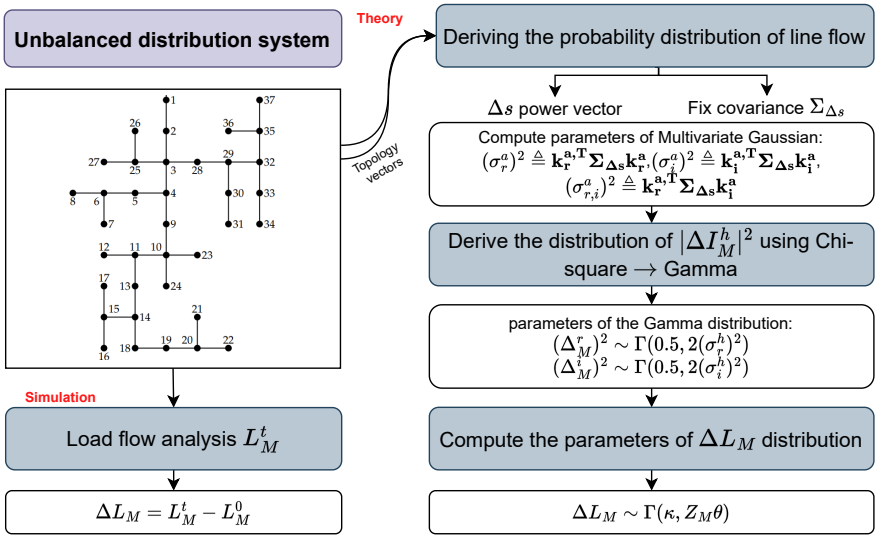

Figure 5.2: Flow chart of the proposed stochastic approach.

where, $\Delta I^h_{M,r}$ and $\Delta I^h_{M,i}$ are the changes in real and imaginary parts of current at phase h of node M.

Proof. Eq. (5.1) can be rewritten as,

$$\boldsymbol{\Delta I^h_{MA}} \approx \Psi^a_{MA}\left[\frac{\Delta P^a_A \cos\theta^a_A - \Delta Q^a_A \sin\theta^a_A}{|V^a_A|} + j\frac{-\Delta P^a_A \sin\theta^a_A - \Delta Q^a_A \cos\theta^a_A}{|V^a_A|}\right]. \quad (5.15)$$

Here, θ^a_A represents the voltage angle of $A \in \boldsymbol{\mathcal{A}}$. Note that the same expression can be written for phases b and c but omitted for brevity. Based on this expression, the terms Ψ_{MA} sin(.), cos(.), and $|V_A|$ can be aggregated in $\boldsymbol{k}^a_r$ and $\boldsymbol{k}^a_i$ for the active and reactive power changes, respectively as shown in Eq. (5.16) and (5.17).

$$\begin{aligned}\boldsymbol{k}^a_r = \Bigg[&\frac{\Psi^a_{M1}\cos\theta^a_1}{|V^a_1|}, \frac{\Psi^a_{M2}\cos\theta^a_1}{|V^a_2|}, \ldots, \frac{\Psi^a_{M\mathcal{N}}\cos\theta^a_{\mathcal{N}}}{|V^a_{\mathcal{N}}|},\\ &-\frac{\Psi^a_{M1}\sin\theta^a_1}{|V^a_1|}, -\frac{\Psi^a_{M2}\sin\theta^a_1}{|V^a_2|}, \ldots, -\frac{\Psi_{M\mathcal{N}^a}\sin\theta^a_{\mathcal{N}}}{|V^a_{\mathcal{N}}|}\Bigg]^T\end{aligned} \quad (5.16)$$

$$\begin{aligned}\boldsymbol{k}^a_i = \Bigg[&-\frac{\Psi^a_{M1}\sin\theta^a_1}{|V^a_1|}, -\frac{\Psi^a_{M2}\sin\theta^a_1}{|V^a_2|}, \ldots, -\frac{\Psi^a_{M\mathcal{N}}\sin\theta^a_{\mathcal{N}}}{|V^a_{\mathcal{N}}|},\\ &-\frac{\Psi^a_{M1}\cos\theta^a_1}{|V^a_1|}, -\frac{\Psi^a_{M2}\cos\theta^a_1}{|V^a_2|}, \ldots, -\frac{\Psi_{M\mathcal{N}^a}\cos\theta^a_{\mathcal{N}}}{|V^a_{\mathcal{N}}|}\Bigg]^T\end{aligned} \quad (5.17)$$

The complete definition of $\boldsymbol{k}_r$ and $\boldsymbol{k}_i$ vectors for phases b and c is listed in Appendix B. Note that complex power in Eq. (5.15) can vary randomly due to uncertainty associated with consumer activities. If $\boldsymbol{\Delta s} \triangleq [\Delta P_1, ..., \Delta P_{\mathcal{N}}, \Delta Q_1, ..., \Delta Q_{\mathcal{N}}]^T$ represents the vector of complex power change for any phase, it is possible to model the random behavior of consumer activities with mean $\boldsymbol{\mu} = 0$ and a covariance structure $\boldsymbol{\Sigma_{\Delta s}}$. Since power change can have correlation due to geographical proximity, this covariance matrix captures the variance (on the main diagonal) of power changes as well as the cross-correlation of power change on the off-diagonal terms. This matrix could be constructed using historical data or using sparsity-based state estimation techniques [145]. Having constructed the covariance matrix, it is possible to compute the probability distribution of real and imaginary parts of current change due to the impact of all actor nodes. Specifically, by invoking Lindeberg-Feller

Central Limit theorem, the terms $\boldsymbol{k}_r^{a,T}\boldsymbol{\Delta s}$ and $\boldsymbol{k}_i^{a,T}\boldsymbol{\Delta s}$ converge to a zero-mean Gaussian distribution, i.e.,

$$\begin{bmatrix} \Delta I_{M,r}^a \\ \Delta I_{M,i}^a \end{bmatrix} \approx \begin{bmatrix} \boldsymbol{k}_r^{a,T}\boldsymbol{\Delta s} \\ \boldsymbol{k}_i^{a,T}\boldsymbol{\Delta s} \end{bmatrix} \xrightarrow{\text{Dist.}} \begin{bmatrix} \mathcal{N}(0, \boldsymbol{k}_r^{a,T}\boldsymbol{\Sigma}_{\boldsymbol{\Delta s}}\boldsymbol{k}_r^a), \\ \mathcal{N}(0, \boldsymbol{k}_i^{a,T}\boldsymbol{\Sigma}_{\boldsymbol{\Delta s}}\boldsymbol{k}_i^a) \end{bmatrix} \tag{5.18}$$

Therefore, the distribution of real and imaginary parts of current flow for any phase can be computed as,

$$\boldsymbol{\Delta I_{M,r}^h} = \begin{bmatrix} \mathcal{N}(0, (\sigma_r^a)^2 \triangleq \boldsymbol{k}_r^{a,T}\boldsymbol{\Sigma}_{\boldsymbol{\Delta s}}\boldsymbol{k}_r^a) \\ \mathcal{N}(0, (\sigma_r^b)^2 \triangleq \boldsymbol{k}_r^{b,T}\boldsymbol{\Sigma}_{\boldsymbol{\Delta s}}\boldsymbol{k}_r^b) \\ \mathcal{N}(0, (\sigma_r^c)^2 \triangleq \boldsymbol{k}_r^{c,T}\boldsymbol{\Sigma}_{\boldsymbol{\Delta s}}\boldsymbol{k}_r^c) \end{bmatrix}, \tag{5.19}$$

$$\boldsymbol{\Delta I_{M,i}^h} = \begin{bmatrix} \mathcal{N}(0, (\sigma_i^a)^2 \triangleq \boldsymbol{k}_i^{a,T}\boldsymbol{\Sigma}_{\boldsymbol{\Delta s}}\boldsymbol{k}_i^a) \\ \mathcal{N}(0, (\sigma_i^b)^2 \triangleq \boldsymbol{k}_i^{b,T}\boldsymbol{\Sigma}_{\boldsymbol{\Delta s}}\boldsymbol{k}_i^b) \\ \mathcal{N}(0, (\sigma_i^c)^2 \triangleq \boldsymbol{k}_i^{c,T}\boldsymbol{\Sigma}_{\boldsymbol{\Delta s}}\boldsymbol{k}_i^c) \end{bmatrix} \tag{5.20}$$

In practical scenarios, there exists a correlation between the real and imaginary parts of current change. This relation is captured by the term $(\sigma_{ri}^a)^2 \triangleq \boldsymbol{k}_r^{a,T}\boldsymbol{\Sigma}_{\boldsymbol{\Delta s}}\boldsymbol{k}_i^a$. Therefore, the distribution of real and imaginary parts of current change converges to a multivariate Gaussian, i.e.,

$$\begin{bmatrix} \Delta I_{M,r}^a \\ \Delta I_{M,i}^a \end{bmatrix} \xrightarrow{\text{Dist.}} \boldsymbol{\mathcal{N}} \left(\boldsymbol{\mu}_{ri} \triangleq \begin{bmatrix} \mu_r \\ \mu_i \end{bmatrix}, \boldsymbol{\Sigma}_{ri} \triangleq \begin{bmatrix} (\sigma_r^a)^2 & (\sigma_{ri}^a)^2 \\ (\sigma_{ri}^a)^2 & (\sigma_i^a)^2 \end{bmatrix} \right) \tag{5.21}$$

For power changes about some base load value, it is reasonable to set the term $\boldsymbol{\mu}_{ri}$ to zero. Note that the bold notation $\boldsymbol{\mathcal{N}}$ is used for multivariate representation. Similarly, the procedure can be followed for phases b and c. Hence, Theorem 4 is proved. □

Next, the distribution of current flow is used to derive the probability distribution of losses at any monitored line M.

5.2.2 Derive the distribution of $|\Delta I_M^h|^2$

It can be seen from Eq. (5.9) that the distribution of losses at any line M is related to the change in current flow. Using distribution of change in current flow derived in Theorem 4, it is possible to compute the distribution of squared magnitude of current for any phase as $|\Delta I_M^h|^2 = \left(\Delta I_{M,r}^h\right)^2 + \left(\Delta I_{M,i}^h\right)^2 \forall h \in \boldsymbol{\mathcal{H}}$. The distribution of a squared Gaussian follows a Chi-square distribution and the sum of squared Gaussian distributions converges to a Gamma distribution [20, 227] with the following shape and scale parameters,

$$\begin{bmatrix} \left(\Delta I_{M,r}^h\right)^2 \\ \left(\Delta I_{M,i}^h\right)^2 \end{bmatrix} \xrightarrow{\text{Dist.}} \begin{bmatrix} \Gamma\left(0.5, 2(\sigma_r^h)^2\right) \\ \Gamma\left(0.5, 2(\sigma_i^h)^2\right) \end{bmatrix}. \tag{5.22}$$

The sum of Gamma random variables in Eq. (5.22) also follows a Gamma random variable with shape and scale parameters κ_h and θ_h, respectively [228],

$$|\Delta I_M^h|^2 \xrightarrow{\text{Dist.}} \Gamma\left(\kappa_h, \theta_h\right), \tag{5.23}$$

where, $\kappa_h \triangleq \frac{\left((\sigma_r^h)^2+(\sigma_i^h)^2\right)}{\theta_h}$ and $\theta_h \triangleq \frac{2\left((\sigma_r^h)^4+(\sigma_i^h)^4+2K^2\right)}{(\sigma_r^h)^2+(\sigma_i^h)^2}$. Note that the correlation of the multivariate random variables in Eq. (5.14) is reflected in the Gamma distribution by the correlation parameter K.

5.2.3 Parameters of ΔL_M^h considering three phase mutual coupling

To derive the distribution of losses at line M, the effect of the base current must be considered. Specifically, the equivalent of the term ϵ^h in Eq. (5.9) can be computed by taking the mean of the term $2\Re\left(I_M^{h,*}\Delta I_M^h\right)$, which results in a shifted Gamma distribution by the constant c_h. Therefore, the probability distribution of losses $\mathbf{\Delta L_M^h}$ follows a shifted Gamma distribution with shape and scale parameters κ_h and θ_h, respectively, denoted by $\hat{\Gamma}$. Finally, by considering the effect of the mutual impedance across different phases in Eq. (5.11), the

distribution of $\mathbf{\Delta L_M^h}$ can be computed as,

$$\mathbf{\Delta L_M^h} \xrightarrow{\text{Dist.}} \left[\hat{\Gamma}\left(\kappa_a, \theta_a\right), \hat{\Gamma}\left(\kappa_b, \theta_b\right), \hat{\Gamma}\left(\kappa_c, \theta_c\right)\right] \mathbf{Z_M^h} \tag{5.24}$$

where, $\mathbf{Z_M^h}$ is defined according to Eq. (5.11). Eq. (5.24) can be simplified further in cases where complex power varies simultaneously at the three phases, which results in equal scale parameters across the three phases, i.e., $\theta_a = \theta_b = \theta_c = \theta$ [234]. That is,

$$\mathbf{\Delta L_M^h} \xrightarrow{\text{Dist.}} \begin{bmatrix} \hat{\Gamma}\left(\kappa_a + \kappa_b + \kappa_c, \theta\right)\left(Z_{aa} + Z_{ab} + Z_{ac} \triangleq Z_a^{'}\right) \\ \hat{\Gamma}\left(\kappa_a + \kappa_b + \kappa_c, \theta\right)\left(Z_{ba} + Z_{bb} + Z_{bc} \triangleq Z_b^{'}\right) \\ \hat{\Gamma}\left(\kappa_a + \kappa_b + \kappa_c, \theta\right)\left(Z_{ca} + Z_{cb} + Z_{cc} \triangleq Z_c^{'}\right) \end{bmatrix} \tag{5.25}$$

Eq. (5.25) can be used to compute the distribution change in real losses by considering the real part of the line impedance $[Z_a^{'}, Z_b^{'}, Z_c^{'}]$. Finally, for any Gamma distributed random variable, $y \sim \Gamma(\kappa, \theta) \rightarrow ay \sim \Gamma(\kappa, a\theta) \forall a > 0$. Therefore,

$$\mathbf{\Delta L_M^h} \xrightarrow{\text{Dist.}} \begin{bmatrix} \hat{\Gamma}\left(\kappa^{'}, Z_a^{'}\theta\right) \\ \hat{\Gamma}\left(\kappa^{'}, Z_b^{'}\theta\right) \\ \hat{\Gamma}\left(\kappa^{'}, Z_c^{'}\theta\right) \end{bmatrix} \tag{5.26}$$

where, $\kappa^{'} = \kappa_a + \kappa_b + \kappa_c$. Next section validates the effectiveness of the proposed approach for three-phase unbalanced distribution systems.

5.3 Verification via simulation

The efficacy of the proposed approach is verified via simulations on the IEEE 37 and IEEE 123-node test systems [235]. For brevity of demonstration, only the real part of change in current flow and losses are reported and the method is generic and can be used to compute the change in imaginary parts as well. First, a scenario is simulated where complex power changes deterministically across randomly selected actor nodes. Table 5.1 shows these actor nodes,

phases, and the power change values. The choice of power change trends at different phases is different and that is to reflect practical scenarios as there could be different consumer activities impacting losses simultaneously. For example, negative power change can result from increased PV injection whereas a positive power change could mean an increase in EV charging load. It is important to note that the power profile for nodes with no complex power change is kept according to the standard specifications of the system [235]. Next, we use the proposed approach to compute the change in current flow as well as the change in losses across the three phases. To validate the proposed approach, we use the actual changes computed via simulation-based load flow method. Fig. 5.3 and 5.4 show the change in real part of current flow at all three phases of the monitored lines for the IEEE 37 and IEEE 123-node test systems due to the complex power changes tabulated in Table 5.1. Theory refers to the proposed approach whereas simulation is the classical load flow based method. It can be seen from the figures that the proposed approach approximates the change in current with high accuracy compared to the actual load flow method. Note that lines closer to the source node, e.g., node 2,3,...,etc., experience higher changes compared to other lines, which is expected due to the radial structure of these systems. In addition, note that for the IEEE 123-phase c, no change in current flow is experienced for lines 20,...,50. This is because the destination nodes of these lines are not among the actor node list in Table 5.1. Having computed the change in line current flow, it is now possible to compute the change in line losses. Therefore, the aggregate change in line losses due to multiple actor nodes is computed via the proposed approach (Eq. 5.9) and shown in Fig. 5.5. It is clear from the figure that, for all cases, the proposed approach approximates actual changes in power losses with high accuracy.

To show the advantage of the proposed approach in terms of accounting for uncertainties associated with consumer activities, we simulate a scenario where power changes randomly at different nodes. In particular, we model the stochastic nature of consumer activities as a trend component along with a zero mean multivariate Gaussian with covariance structure $\mathbf{\Sigma_{\Delta s}}$ as shown in Eq. (5.27). The diagonal terms represent the variance in active and reactive power change. In this particular case, we assume 25 kW and 4 kVAr for simplicity.

Table 5.1: Complex power changes (in kVA) for randomly selected actor nodes.

System details		Phase a	Phase b	Phase c
IEEE 37	Node	[2,5,10,20, 28,30]	[7,11,17,25, 27,29,31,35]	[4,6,8,10, ...,36]
	ΔS	60-j15	40+j5	30+j0
IEEE 123	Node	[2,4,6, 8,10..,30]	[20,22,24, 26,28,...,65]	[70,72,74, ...,110]
	ΔS	20-j15	40+j5	-30-j3

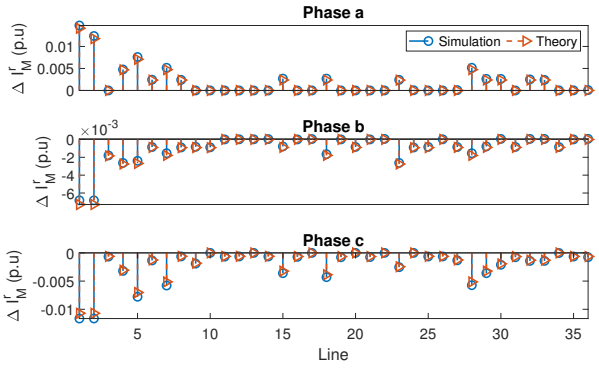

Figure 5.3: $\boldsymbol{\Delta I^h_{M,r}}$ for IEEE 37-node test system.

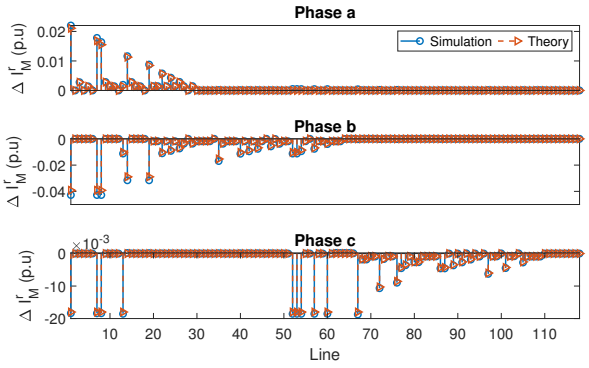

Figure 5.4: $\boldsymbol{\Delta I^h_{M,r}}$ for IEEE 123-node test system.

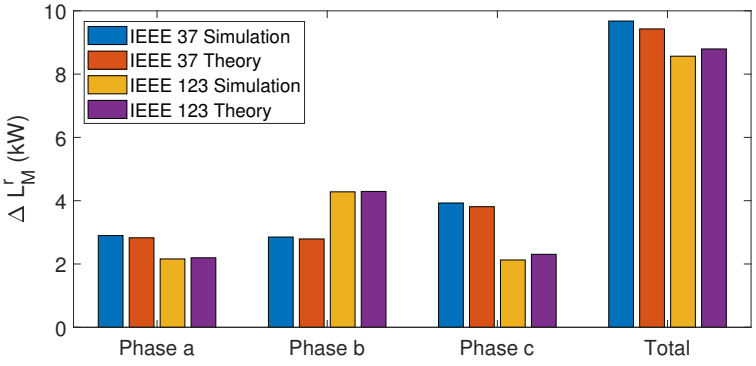

Figure 5.5: Change in $\boldsymbol{\Delta L^h_{M,r}}$ due to aggregate impact of multiple actor nodes.

However, the approach can be applied with different active and reactive power variance. It is important to note that, the change in active and reactive power at different actor nodes can be correlated due to geographical proximity. This is reflected in the covariance structure by the off-diagonal terms of $\boldsymbol{\Sigma_{\Delta s}}$. The covariance matrix in Eq. (5.27) is defined for the IEEE 37-node test system as,

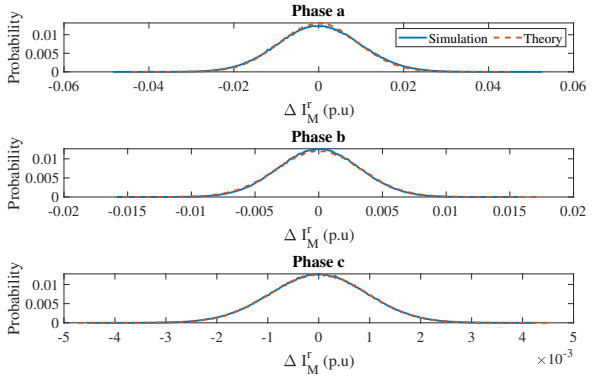

Figure 5.6: Distribution of $\boldsymbol{\Delta I^h_{M,r}}$ for IEEE 37-node test system.

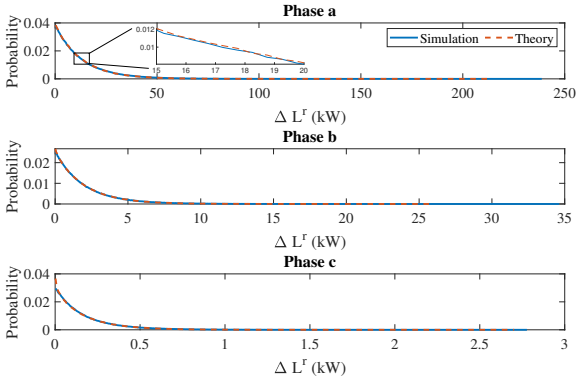

Figure 5.7: Distribution of $\boldsymbol{\Delta L^h_{M,r}}$ for IEEE 37-node test system.

$$\begin{bmatrix} 5 & & 1 & \dots & & 0.001 \\ & \ddots & & & & \\ 1 & & 5 & & 0.001 & \\ \vdots & & & \ddots & & \vdots \\ & 0.001 & & & 2 & 1 \\ & & & & \ddots & \\ 0.001 & & & \dots & 1 & 2 \end{bmatrix} \tag{5.27}$$

where actor nodes are chosen randomly for the three phases according to Eq. (5.28),

$$\begin{aligned} &\boldsymbol{\mathcal{A}}^a \triangleq [2,3,4,...,36] \quad \boldsymbol{\mathcal{A}}^b \triangleq [2,4,6,...,36] \\ &\boldsymbol{\mathcal{A}}^c \triangleq [2,7,12,...,36]. \end{aligned} \tag{5.28}$$

It is important to note that the proposed approach and the theoretical derivations will also work for other distribution models for power change. With this covariance structure, the parameters of the multivariate Gaussian in Eq. (5.21) can be computed for any phase given any monitored line. In this scenario, we compute the parameters of the distribution for monitored line number 2 as shown in Eq. (5.29),

$$\begin{bmatrix} (\sigma_r^a)^2 & (\sigma_{ri}^a)^2 \\ (\sigma_{ri}^a)^2 & (\sigma_i^a)^2 \end{bmatrix} = \begin{bmatrix} 0.7671 & -0.0058 \\ -0.0058 & 0.6542 \end{bmatrix}. \tag{5.29}$$

The resulting distribution of change in current flow for the three phases of this monitored line are illustrated in Fig. 5.6. The proposed approach (in red) uses the multivariate Gaussian in Eq. (5.21) whereas the simulation method (blue) samples random variables by running multiple load flow-based scenarios. For fair comparison, the number random variables sampled with the proposed approach and the number of scenarios for load flow-based method are kept the same, i.e., 1 million. This is also done to ensure high statistical-inference accuracy where the probability density function of change in current flow stabilizes. As can be seen from the figure, the proposed stochastic approach estimates the actual distribution with high accuracy. Note that the highest change in current flow is exhibited at phase a of the monitored line and that is because a larger number of actor nodes change their complex power (Eq. (5.28)) at phase a relative to phases b and c. This allows computing shape and scale parameters of the Gamma distribution to determine the change in power losses at the monitored line (Eq. (5.24)). For this case, the shape and scale parameters turn out to be $[0.99, 0.97, 0.91]$ and $[13.00, 2.01, 0.18]$ for phases a, b, and c, respectively. The resulting Gamma distributions are depicted in Fig. (5.7), where consumer activities at phase a result in higher losses. The same procedure is repeated for the IEEE 123-node test system but with different active and reactive power variance (i.e., 25kW and 12kVAr) at $[50, 25, 26]$ randomly selected actor nodes for phases a, b, and c, respectively. For brevity of demonstration, only the resulting distribution of change in losses is reported as illustrated in Fig. 5.8.

Next, the accuracy of the proposed approach compared to actual results (obtained via classical load flow-based method) is evaluated. First, we use the mean absolute percentage error

Table 5.2: Accuracy evaluation of the proposed approach.

System	**Deterministic measure (%)**			**Stochastic measure**
	Mean	Min	Max	$0 \leq \text{JSD} \leq 1$
IEEE 37	0.7526	0.0004	3.4133	0.0030
IEEE 123	1.1669	0.0032	3.5655	0.0048

(MAPE) to test the accuracy of the deterministic approximation of change in line losses. Specifically, we run multiple Monte-Carlo simulations using the spatial distribution of actor nodes (Table 5.1) while changing their active power with in the range $[-\Delta S_b, +\Delta S_b]$ with a step of 1 kW. In this case, ΔS_b is chosen to be the maximum base load (across the three phases) to test the approach under scenarios of abrupt power changes. Finally, the MAPE is recorded for every scenario for both IEEE 37 and IEEE 123-node test systems and is summarized in the deterministic part of Table 5.2. The table shows that the proposed approach offers over $\sim 96\%$ approximation accuracy (i.e., $\sim 4\%$ maximum MAPE) for very large power changes while the approximation accuracy is well over 98% when considering mean MAPE. Note that these values include errors obtained for all phases in both systems. In addition, to evaluate the accuracy of approximating the probability distribution of change in line losses, we use Jensen–Shannon distance (JSD), a standard statistical-distance measure that is used to quantify the similarity between two probability distributions. JSD ranges between 0 and

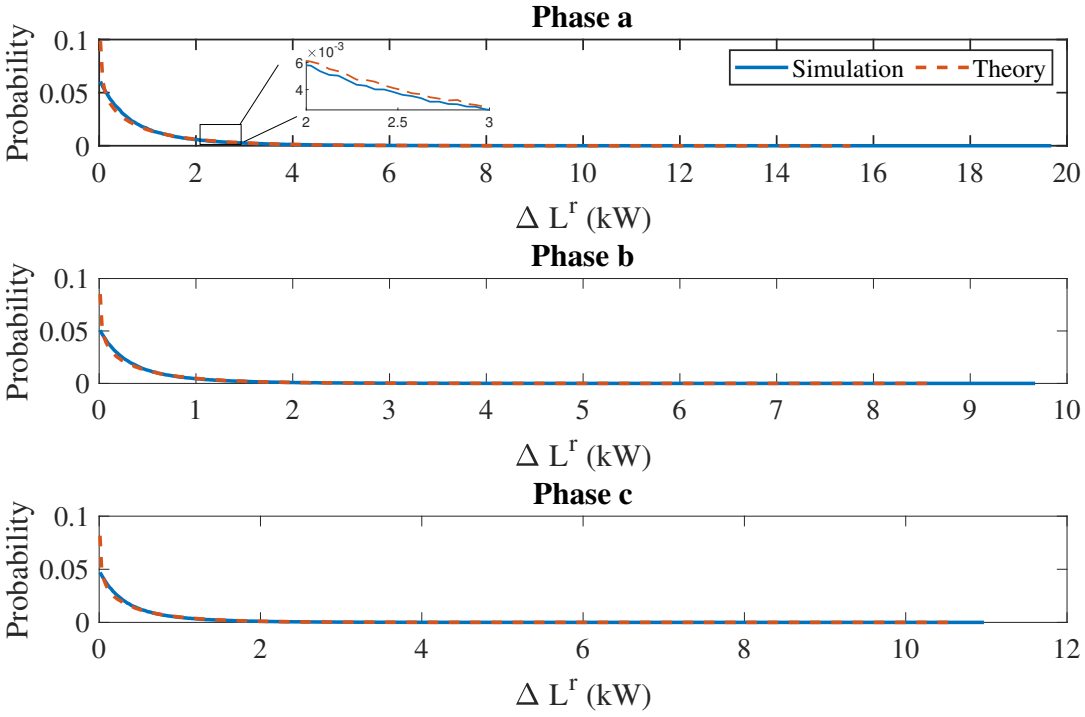

Figure 5.8: Distribution of $\boldsymbol{\Delta L^{h}_{M,r}}$ for IEEE 123-node test system.

Table 5.3: Computational complexity analysis.

Method	**IEEE 37**	**IEEE 123**
Proposed (s)	0.6361	0.6762
Simulation-based (s)	1490	7630

1 with 0 representing identical distributions and 1 representing completely different distributions. We evaluate the JSD measures for the probability distributions shown in Fig. 5.7 and 5.8 and report the average JSDs (over the three phases) in Table 5.2. It can be seen from the table that the JSD is in the order of 10^{-3}, which implies that the probability distribution computed with the proposed approach estimates the actual distribution (obtained via classical load flow approach) with high accuracy.

Finally, the computational efficiency of the proposed approach is analyzed by comparing the execution time taken by the proposed approach and simulation-based method to compute the distribution of change in current flow and line losses. It is important to note that all cases have been analyzed with an Intel i-9 based processor running at 3.60GHz. The proposed approach computes the parameters of standard probability distributions while the classical simulation-based method uses multiple Monte-Carlo simulations to account for the randomness introduced by power changes. In this case, 1 million random variables are sampled with the proposed approach and 1 million Monte-Carlo simulations are performed with the classical simulation-based method. The execution time (in seconds) taken by both approaches is reported in Table 5.3. It is found that the proposed approach computes the distribution of change in line losses for the IEEE 37-node test system within a second, compared to 1490 seconds in the classical simulation-based method. In addition, the proposed approach computes the distribution of line losses within a second for the IEEE 123-node test system whereas it takes the simulation-based approach 7630 seconds to compute the same distribution. It can also be seen how the gap in computational complexity increases for larger systems with the classical simulation-based approach whereas the computational efficiency is constant (i.e., within 1 second) with the proposed approach.

5.4 Summary

This chapter proposes a new generic framework that analytically derives probabilistic expressions that quantify the impact of consumer technologies on line losses in three-phase unbalanced distribution systems. First, the proposed approach starts with a deterministic approximation of change in line current flow and losses due to the effect of power change at multiple consumer sites. Then, these approximations are used to derive the probability distribution of losses. One of the strengths of the proposed approach is the ability to systematically incorporate the randomness that results from abrupt power changes at any phase due to grid-edge technologies. The performance of the proposed approach is validated via simulations on the IEEE 37 and IEEE 123-node test systems. It has been found that the proposed approach offers a consistent computational efficiency, i.e., an execution time within a second, regardless of the test system used. However, with the classical load flow-based approach, the computational complexity has significantly increased as the size of the test system increased. In addition to this computational efficiency, the proposed approach offers high approximation accuracy. For example, it has been found that the average MAPE errors are $< 2\%$ with a JSD in the order of 10^{-3} for the probability distribution of change in power losses. In Chapter 7, the proposed approach will be used for EV charging station allocation.

Chapter 6

Sensitivity-based voltage monitoring

Many recent research efforts have explored the possibility of using reactive power capabilities of PV generators through smart inverters in either a centralized [60], [61] or decentralized [62] scheme. The efficacy of these control methods is dependent on the ability to accurately predict voltage violations in the system so that operational setpoints of the PV inverters can be appropriately set in advance. Load flow based look-ahead prediction approaches are cumbersome, computationally complex and not scalable. Therefore, the development of a computationally efficient, yet accurate voltage-violation prediction approach that predicts future violations as well as their uncertainty bounds is critically important for control and management of distribution systems. After developing a tool for monitoring losses in unbalanced distribution systems in Chapter 5, this chapter aims at developing and testing a computationally efficient voltage violation prediction scheme while considering different penetration levels of PV generation. In contrast with probabilistic voltage sensitivity analysis (PVSA) [56, 236], the present research focuses on identifying nodes with high probability of violating voltage limits at different time instances. Leveraging existing knowledge of voltage states along with uncertain forecasts of power generation/consumption, probabilistic voltage sensitivity analysis is used to reveal impending voltage issues at any location in the system. The development of voltage violation prediction rule is crucial as it enables applying hosting capacity analysis (7) and efficient voltage control algorithms 8.

6.1 Preemptive voltage monitoring

6.1.1 Background: Voltage Sensitivity Analysis

For a given three-phase distribution system, analytical voltage sensitivity analysis estimates the complex voltage change at a particular node (observation node O) as a result of complex power change at another node (actor node A) in the system [236]. The usefulness of this approach is seen in the reduced computational complexity in comparison with Newton-Raphson based power flow methods. The change of power consumption at an actor node A from S_A to $S_A + \Delta S_A$ results in voltage change at observation node O from V_O to $V_O + \Delta V_O$. The voltage sensitivity for a given observation node O can be calculated using Theorem 5 [236].

Theorem 5. *For a given three phase distribution network, the change in voltage at an observation node ($\boldsymbol{\Delta V_O}$) due to change in power consumption at an actor node (ΔS_A) is approximated by:*

$$\boldsymbol{\Delta V_O} \approx -\begin{bmatrix} \frac{\Delta S_A^a Z_{OA}^{aa}}{V_A^{a*}} + \frac{\Delta S_A^b Z_{OA}^{ab}}{V_A^{b*}} + \frac{\Delta S_A^c Z_{OA}^{ac}}{V_A^{c*}} \\ \frac{\Delta S_A^b Z_{OA}^{ba}}{V_A^{a*}} + \frac{\Delta S_A^b Z_{OA}^{bb}}{V_A^{b*}} + \frac{\Delta S_A^c Z_{OA}^{bc}}{V_A^{c*}} \\ \frac{\Delta S_A^a Z_{OA}^{ca}}{V_A^{a*}} + \frac{\Delta S_A^b Z_{OA}^{cb}}{V_A^{b*}} + \frac{\Delta S_A^c Z_{OA}^{cc}}{V_A^{c*}} \end{bmatrix} \tag{6.1}$$

where $\boldsymbol{\Delta V_O}$ is a vector consisting of the voltage change in phases a, b, and c at an observation node O given by ΔV_O^a, ΔV_O^b and ΔV_O^c. V_A^* and ΔS_A represent the complex conjugate of voltage and complex power change at actor node A, respectively. The superscripts a, b, and c represent different phases and Z corresponds to the self and mutual impedance of the shared line between the actor and observation node.

The voltage change due to multiple actor nodes $A \in \mathcal{A}$ can be formulated as the cumulative effect of all actor nodes on a particular observation node as given in corollary 4 [57].

Corollary 4. *For a given three phase distribution network, the cumulative change in complex voltage at an observation node O due to the change in complex power at multiple actor nodes*

can be formulated as:

$$\boldsymbol{\Delta V_O} \approx -\sum_{A\in\mathcal{A}} \begin{bmatrix} \frac{\Delta S_A^a Z_{OA}^{aa}}{V_A^{a*}} + \frac{\Delta S_A^b Z_{OA}^{ab}}{V_A^{b*}} + \frac{\Delta S_A^c Z_{OA}^{ac}}{V_A^{c*}} \\ \frac{\Delta S_A^b Z_{OA}^{ba}}{V_A^{a*}} + \frac{\Delta S_A^b Z_{OA}^{bb}}{V_A^{b*}} + \frac{\Delta S_A^c Z_{OA}^{bc}}{V_A^{c*}} \\ \frac{\Delta S_A^a Z_{OA}^{ca}}{V_A^{a*}} + \frac{\Delta S_A^b Z_{OA}^{cb}}{V_A^{b*}} + \frac{\Delta S_A^c Z_{OA}^{cc}}{V_A^{c*}} \end{bmatrix} \tag{6.2}$$

where, $\mathcal{A}$ represents the set of all actor nodes resulting in the complex voltage change at node O.

The analytical method presented in corollary 4 gives us a computationally efficient method for computing the probability of voltage change at any given observation node O due to change in complex power at multiple actor nodes $A \in \mathcal{A}$. Further, the execution time of the method to calculate the voltage sensitivity for a single observation node is an order faster (e.g., with an intel i7 processor based PC, it is 0.00871s, compared to 0.0537s in classical load flow method for the modified IEEE 37 bus system). This clearly shows that the proposed approach has an edge over traditional methods in terms of computational efficiency and the difference further increases with the size of the network. The analysis in this chapter is based on the probabilistic extension of corollary 1.

6.1.2 Voltage violation prediction rule

The voltage sensitivity analysis derived in section II is extended to predict the probability distribution of voltage at an observation node due to complex power change at multiple actor nodes. The analytical approach in this work assumes that based on measurements of complex power and voltages at a subset of locations, it is possible to estimate voltage states across the entire network, similar to the approaches presented in [56] [52]. The variability in complex power injection or consumption at actor nodes results in random voltage fluctuations at observation nodes. In this case, actor nodes represent active consumers integrated with distributed PV generation. Subsequently, if $\boldsymbol{V_O^p}$ is the present three phase voltage at an observation node O that is obtained from system measurements, then $\boldsymbol{V_O^f}$ represents the future predicted complex voltage vector at that particular observation node. $\boldsymbol{V_O^f}$ is expected

to be random due to the uncertainty introduced by the distributed PV generation and corresponds to,

$$\boldsymbol{V_O^f} = \boldsymbol{V_O^p} + \boldsymbol{\Delta V_O}. \tag{6.3}$$

Here, $\boldsymbol{\Delta V_O}$ represents the change in voltage at an observation node due to random complex power changes at actor nodes. Considering a single phase for simplicity, the voltage change at an observation node O due to single actor node A can be expressed in terms of real and imaginary part of voltage change as follows:

$$\Delta V_{OA}^{a} = \Delta V_{OA}^{a,r} + j\Delta V_{OA}^{a,i} \tag{6.4}$$

where,

$$\begin{aligned}
\Delta V_{OA}^{a,r} &= -\frac{1}{|V_A^a|}(\Delta P_A^a(R_{OA}^u \cos\theta_A - X_{OA}^u \sin\theta_A) - \Delta Q_A^a(R_{OA}^u \sin\theta_A + X_{OA}^u \cos\theta_A)) \\
\Delta V_{OA}^{a,i} &= -\frac{1}{|V_A^a|}(\Delta Q_A^a(R_{OA}^u \cos\theta_A - X_{OA}^u \sin\theta_A) + \Delta P_A^a(R_{OA}^u \sin\theta_A + X_{OA}^u \cos\theta_A))
\end{aligned} \tag{6.5}$$

where, u represents different phase sequences, i.e., aa, ab, ac in phase a. ΔP_A^a and ΔQ_A^a represent the active and reactive power changes at phase a of actor node A, R_{OA}^u and X_{OA}^u are the real and imaginary parts of the impedance of the shared line between the observation O and actor node A, and θ_A is the phase angle of the voltage at the actor node A.

Similar to corollary 1, (6.4) can be extended to accommodate the impact of multiple actor nodes. Therefore, the cumulative voltage change at a single phase in an observation node O due to multiple actor nodes $A \in \mathcal{A}$ can be written as:

$$\Delta V_O = \sum_{A\in\mathcal{A}} \Delta V_{OA}^{a} = \sum_{A\in\mathcal{A}} \Delta V_{OA}^{a,r} + j \sum_{A\in\mathcal{A}} \Delta V_{OA}^{a,i} \tag{6.6}$$

At each time instant, the active and reactive power injections in the system can be modeled as random variables based on the variability of distributed PV generation at active consumer sites. Therefore, it is natural to model ΔV_O as a random variable as well. The derivation of

the distribution of $|\Delta V_O|$ is the focus of the next subsection.

6.1.3 Probability distribution of predicted voltage

Theorem 2 provides the probability distribution of the magnitude of predicted voltage at an observation node O due to complex power change at multiple actor nodes $A \in \mathcal{A}$ for a single phase.

Theorem 2. For a given unbalanced distribution network, the predicted voltage magnitude ($|V_O^f|$) at an observation node O due to complex power changes at multiple actor nodes $A \in \mathcal{A}$ follows a *Rician* distribution, i.e.,

$$|V_O^f| \sim Rician(\kappa, \sigma) \tag{6.7}$$

where, $\kappa = \sqrt{w}$ and $\sigma = \sqrt{\lambda}$ with,

$$\lambda = \frac{\sigma_r^4(1+2\mu_r^2) + \sigma_i^4(1+2\mu_i^2)}{\sigma_r^2(1+2\mu_r^2) + \sigma_i^2(1+2\mu_i^2)} \tag{6.8}$$

and,

$$w = \frac{(\sigma_r^2\mu_r^2 + \sigma_i^2\mu_i^2)(\sigma_r^2 + \sigma_i^2 + 2\sigma_r^2\mu_r^2 + 2\sigma_i^2\mu_i^2)}{\sigma_r^4 + \sigma_i^4 + 2\sigma_r^4\mu_r^2 + 2\sigma_r^4\mu_i^2} \tag{6.9}$$

here, $\sigma_r^2 = \boldsymbol{c_r}^T \Sigma_{\Delta S} \boldsymbol{c_r}$, $\sigma_i^2 = \boldsymbol{c_i^T} \Sigma_{\Delta S} \boldsymbol{c_i}$, $\mu_r = V_O^{r,p} + \boldsymbol{c_r^T \mu_{\Delta S}}$, and $\mu_i = V_O^{i,p} + \boldsymbol{c_i^T \mu_{\Delta S}}$. In this context, $V_O^{r,p}$ and $V_O^{i,p}$ are the present estimated values of real and imaginary parts of voltage. $\boldsymbol{c_r}$ and $\boldsymbol{c_i}$ are based on system topology and $\boldsymbol{\mu_{\Delta S}}$ and $\Sigma_{\Delta S}$ are related to variability in power change as will be discussed in the proof.

Proof. The variability of PV generation randomizes the associated power output. In this case, the forecast of power change is modeled as a non-zero mean random vector with mean $\boldsymbol{\mu_{\Delta S}}$ and covariance $\Sigma_{\Delta S}$. This model captures a nominal forecast ($\boldsymbol{\mu_{\Delta S}}$) and the associated error in forecast characterized by $\Sigma_{\Delta S}$. The real and reactive power represent the net nodal load changes given the presence of distributed PV generation at active consumer sites. Accordingly, $\boldsymbol{\Delta S}$ can be represented as shown in (8.16) with n representing the number of

nodes in the system.

$$\boldsymbol{\Delta S} = [\Delta P_1^a, ..., \Delta P_n^a, \Delta Q_1^a, ..., \Delta Q_n^a] \tag{6.10}$$

The following steps detail the steps involved in the derivation of the distribution of $|V_O^f|$.

Computation of covariance matrix $\Sigma_{\Delta S}$

The covariance matrix $\Sigma_{\Delta S}$ captures the relationship between complex power changes at multiple actor nodes and can be determined based on historical measurements. For a given system, the diagonal elements of the covariance matrix (i.e., variance) depend on the size of distributed PV generation and the uncertainty in the forecast. The off diagonal elements of the covariance matrix are based on the future net-load forecasts given a particular spatial PV generation and load profile. If a particular node in the network is not integrated with distributed PV generation, then the mean and variance term of the respective node is equivalent to their typical load variability. Accordingly, the covariance matrix $\Sigma_{\Delta S}$ can be formulated as shown in Appendix D. In this matrix, n represents the number of nodes in the desired network and p_i and q_i are the active and reactive power injection or demand at the i^{th} active consumer site, respectively. $\sigma_{p_i}^2$ and $\sigma_{q_i}^2$ capture the variance of active and reactive power generation across different actor nodes, respectively, and the off diagonal elements capture the correlation between various generators due to geographical proximity.

Computation of $\boldsymbol{c_r}$ and $\boldsymbol{c_i}$ vectors

The present work assumes prior knowledge of the system parameters. To begin with, define $\boldsymbol{c_r}$ and $\boldsymbol{c_i}$ as follows:

$$\boldsymbol{c_r} = [\boldsymbol{c_r^{aa}}, \boldsymbol{c_r^{ab}}, \boldsymbol{c_r^{ac}}]^T, \boldsymbol{c_i} = [\boldsymbol{c_i^{aa}}, \boldsymbol{c_i^{ab}}, \boldsymbol{c_i^{ac}}]^T \tag{6.11}$$

For simplicity, the vectors are shown for single phase, i.e., phase a, where each vector is composed of three sub-vectors corresponding to self and mutual phases. $\boldsymbol{c_r}$and $\boldsymbol{c_i}$ for a

single phase can be computed as,

$$\boldsymbol{c_r^{aa}} = \begin{bmatrix} \frac{-(R_{O1}^{aa}\cos(\theta_1) - X_{O1}^{aa}\sin(\theta_1))}{|V_1^a|} \\ \vdots \\ \frac{-(R_{On}^{aa}\cos(\theta_n) - X_{On}^{aa}\sin(\theta_n))}{|V_n^a|} \\ \frac{(R_{O1}^{aa}\sin(\theta_1) + X_{O1}^{aa}\cos(\theta_1))}{|V_1^a|} \\ \vdots \\ \frac{(R_{On}^{aa}\sin(\theta_n) + X_{On}^{aa}\cos(\theta_n))}{|V_n^a|} \end{bmatrix} \tag{6.12}$$

$$\boldsymbol{c_i^{aa}} = \begin{bmatrix} \frac{-(R_{O1}^{aa}\sin(\theta_1) + X_{O1}^{aa}\cos(\theta_1))}{|V_1^a|} \\ \vdots \\ \frac{-(R_{On}^{aa}\sin(\theta_n) + X_{On}^{aa}\cos(\theta_n))}{|V_n^a|} \\ \frac{-(R_{O1}^{aa}\cos(\theta_1) - X_{O1}^{aa}\sin(\theta_1))}{|V_1^a|} \\ \vdots \\ \frac{-(R_{On}^{aa}\cos(\theta_n) - X_{On}^{aa}\sin(\theta_n))}{|V_n^a|} \end{bmatrix} \tag{6.13}$$

The aforementioned vectors are constant for a given system with a particular set of active consumer (actor) nodes integrated with distributed PV generation. The elements of $\boldsymbol{c_r}$ and $\boldsymbol{c_i}$ vectors consist of the ratio of the impedance of shared path (between the observation and actor node) to the rated voltage of the associated phase, (e.g., in this case, it would be phase a). When the system topology changes, the $\boldsymbol{c_r}$ and $\boldsymbol{c_i}$ vectors are expected to change as well.

Probability distribution of ΔV_o^r and ΔV_o^i

This subsection provides an expression for the real and imaginary parts of voltage change at an observation node due to complex power change at multiple actor nodes. The change in voltage at an observation node is expressed as the sum of voltage changes induced by each actor node as shown by corollary 1 in section II. Thus, the probability distribution of real

and imaginary part of voltage change are formulated as follows:

$$\Delta V_O^{a,r} = \sum_{A \in \mathcal{A}} \Delta V_{OA}^r = \boldsymbol{c_r^T \Delta S} \xrightarrow{D} \mathcal{N}(\boldsymbol{c_r^T \mu_{\Delta S}}, \boldsymbol{c_r^T} \Sigma_{\Delta S} \boldsymbol{c_r}) \tag{6.14}$$

$$\Delta V_O^{a,i} = \sum_{A \in \mathcal{A}} \Delta V_{OA}^i = \boldsymbol{c_i^T \Delta S} \xrightarrow{D} \mathcal{N}(\boldsymbol{c_i^T \mu_{\Delta S}}, \boldsymbol{c_i^T} \Sigma_{\Delta S} \boldsymbol{c_i}) \tag{6.15}$$

where $\mathcal{A}$ represents the set of actor nodes resulting in voltage change at the observation node O. Using Lindeberg-Feller CLT, (6.14) and (6.15) indicate that $\Delta V_O^{a,r}$ and $\Delta V_O^{a,i}$ converge in distribution to a Gaussian random variable.

The covariance between real ΔV_O^r and imaginary ΔV_O^i parts of voltage change corresponds to $cov(\Delta V_O^r, \Delta V_O^i) = \boldsymbol{c_r^T} \Sigma_{\Delta S} \boldsymbol{c_i}$. Thus, the real and imaginary parts of voltage change at an observation node can be rewritten as a multi-variate normal vector corresponding to,

$$\boldsymbol{\Delta V_O} \triangleq \begin{bmatrix} \Delta V_O^r \\ \Delta V_O^i \end{bmatrix} \sim \mathcal{N}(\boldsymbol{\mu_1}, \Sigma_1) \tag{6.16}$$

where,

$$\boldsymbol{\mu_1} = \begin{bmatrix} \boldsymbol{c_r^T \mu_{\Delta S}} \\ \boldsymbol{c_i^T \mu_{\Delta S}} \end{bmatrix} \tag{6.17}$$

$$\Sigma_1 = \begin{bmatrix} \boldsymbol{c_r^T} \Sigma_{\Delta S} \boldsymbol{c_r} & \boldsymbol{c_r^T} \Sigma_{\Delta S} \boldsymbol{c_i} \\ \boldsymbol{c_r^T} \Sigma_{\Delta S} \boldsymbol{c_i} & \boldsymbol{c_i^T} \Sigma_{\Delta S} \boldsymbol{c_i} \end{bmatrix} \tag{6.18}$$

Recall the expression of $\boldsymbol{V_O^f}$ and $\boldsymbol{V_O^p}$ from section II. The real and imaginary parts of predicted voltage can be written as:

$$\boldsymbol{V_O^f} \triangleq \begin{bmatrix} V_O^{r,f} \\ V_O^{i,f} \end{bmatrix} = \begin{bmatrix} V_O^{r,p} \\ V_O^{i,p} \end{bmatrix} + \begin{bmatrix} \Delta V_O^r \\ \Delta V_O^i \end{bmatrix} \tag{6.19}$$

$$\boldsymbol{V_O^f} \sim \mathcal{N}(\begin{bmatrix} V_O^{r,p} + \boldsymbol{c_r^T \mu_{\Delta S}} \\ V_O^{i,p} + \boldsymbol{c_i^T \mu_{\Delta S}} \end{bmatrix}, \Sigma_1) \tag{6.20}$$

$$|V_O^f|^2 = (V_O^{r,f})^2 + (V_O^{i,f})^2 \tag{6.21}$$

The distribution of the squared magnitude of V_O^f is a sum of dependent non-central chi-square distributions. Each real and imaginary part of the predicted voltage follows non zero mean Gaussian distribution and thus their squares will have a non central chi square distribution [234],

$$|V_O^f|^2 \sim \sigma_r^2 \chi_1^2(\mu_r^2) + \sigma_i^2 \chi_1^2(\mu_i^2) \tag{6.22}$$

where, σ and μ are the weight and non centrality parameter of non central chi square distribution with one degree of freedom, respectively. The sum of weighted non-central chi-square distributions can then be approximated with a scaled non-central chi-square with weight λ, non-centrality parameter w, and v degrees of freedom as[234]:

$$|V_O^f|^2 \sim \lambda \chi_v^2(w) \tag{6.23}$$

where,

$$\lambda = \frac{\sigma_r^4(1+2\mu_r^2) + \sigma_i^4(1+2\mu_i^2)}{\sigma_r^2(1+2\mu_r^2) + \sigma_i^2(1+2\mu_i^2)} \tag{6.24}$$

$$w = \frac{(\sigma_r^2\mu_r^2 + \sigma_i^2\mu_i^2)(\sigma_r^2 + \sigma_i^2 + 2\sigma_r^2\mu_r^2 + 2\sigma_i^2\mu_i^2)}{\sigma_r^4 + \sigma_i^4 + 2\sigma_r^4\mu_r^2 + 2\sigma_r^4\mu_i^2} \tag{6.25}$$

$$v = \frac{(\sigma_r^2 + \sigma_i^2)(\sigma_r^2 + \sigma_i^2 + 2\sigma_r^2\mu_r^2 + 2\sigma_i^2\mu_i^2)}{\sigma_r^2 + \sigma_i^2 + 2(\sigma_r^4\mu_r^2) + 2(\sigma_i^4\mu_i^2)} \tag{6.26}$$

Since the square root of a non-central chi-square random variables follows a Rician distribution [234], the magnitude of predicted voltage change will follow a Rician distribution:

$$|V_O^f| \sim Rician(\kappa, \sigma) \tag{6.27}$$

where, $\kappa = \sqrt{w}$ and $\sigma = \sqrt{\lambda}$, which is consistent with (6.66). This expression is first validated

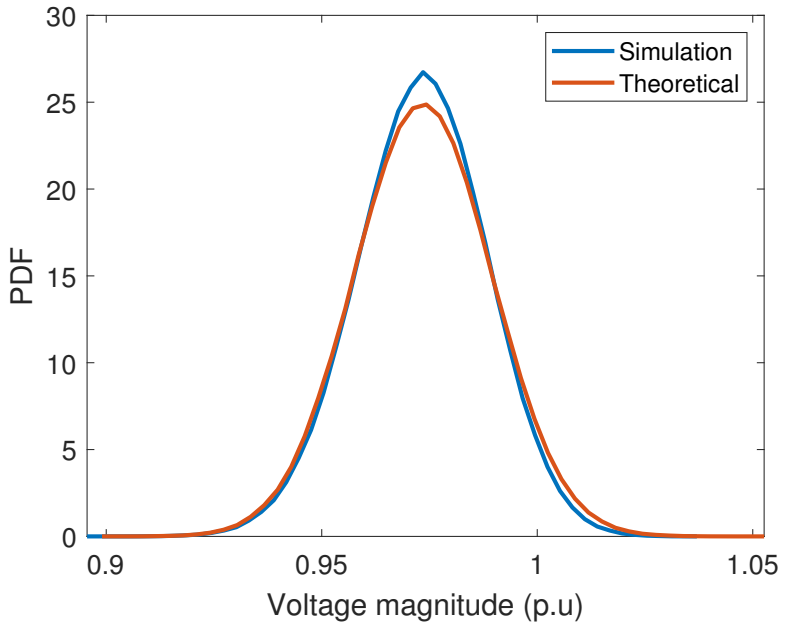

Figure 6.1: Predicted voltage using (6.27) vs. load flow.

on the modified IEEE 37 bus system. Figure 6.1 shows the predicted voltage at observation node 22 using the expression derived in (6.27) vs. the values calculated using the load flow method. For the current setup, four arbitrary actor nodes are chosen for the validation test, namely, 2, 11, 20, and 29. The Jensen-Shannon distance between the theoretical and simulated distribution is in the order of 10^{-2}. Jensen-Shannon distance ranges from 0 to 1 indicating exact distribution match and mismatch, respectively. Thus, the proposed method is highly accurate in predicting the distribution of voltage at a particular observation node.

6.1.4 Assessment of node vulnerability to voltage violation

The aim of this work is to identify nodes with high probability of voltage violation. The expression derived in (6.27) shows that the predicted voltage magnitude $|V_O^f|$ follows a Rician distribution. $P_v(t)$, the probability of node voltage violation at a given time instant corresponds to

$$P_v(t) = 1 - P(0.95 < |V_O^f| < 1.05). \tag{6.28}$$

(6.28) can be used to identify vulnerable nodes by comparing $P_v(t)$ with a particular threshold. The threshold used in this chapter is 0.5, i.e., nodes with voltage-violation probabilities higher than 0.5 are considered vulnerable. The method is generic and can be implemented on all observation nodes in the network. This assessment provides an insight into the voltage status of the network at a future time instant. The assessment criterion is computationally efficient and the outcome can be used as an input for voltage control.

6.1.5 Verification via simulation

This section summarizes the simulation results and findings related to PVSA based preemptive voltage monitoring strategy. First, the violation prediction method is tested on the IEEE 37 node test system. Next, a catastrophic scenario is presented where the system experiences a complete loss of generation at a particular actor node and the efficacy of the proposed voltage violation prediction is evaluated. Actual voltage violations in the system are extracted using power flow solutions for the purpose of validating the proposed approach. Among the 37 system nodes, a subset of nodes is considered to be active consumers with integrated distributed PV generation and voltage status is monitored on all system (observation) nodes. For the first case, A hypothetical solar PV generation scenario is considered from noon to 18:00 with power and voltage measurement availability every 15 minutes. The solar PV generation in this work is modeled as a random process with a component of uncertainty to illustrate a profile that follows real world scenarios as follows:

$$G_{PV}(t) = S(t) + R_s(t). \tag{6.29}$$

Here, $S(t)$ is the mean forecast trend of the solar PV generation and $R_s(t)$ represents a zero mean uncorrelated Gaussian random process illustrating the uncertainty in PV generation. Figure 6.2 shows the solar PV generation model used ($S(t)$) as well as the net-power curve used for simulation in this chapter. Time instances where the net-power is negative indicates reversed power flow in the grid due to surplus solar PV generation. Although this particular

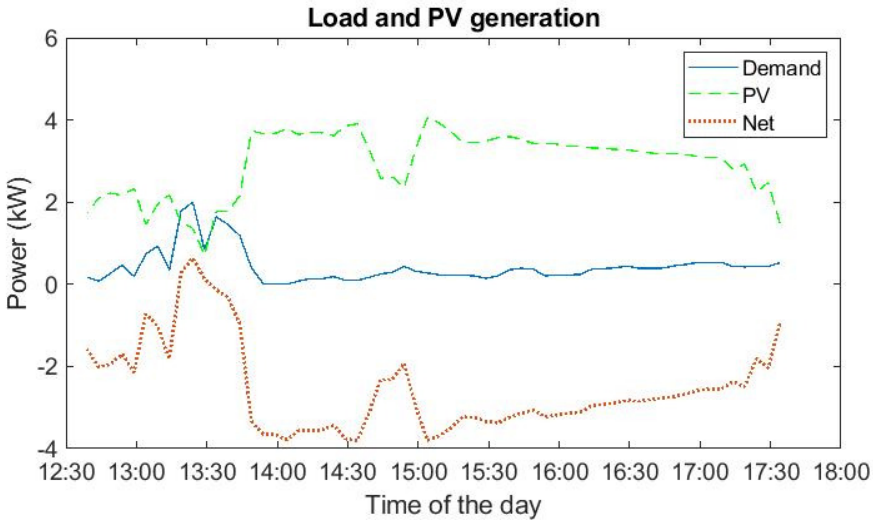

Figure 6.2: Solar PV generation profile for each unit.

scenario is considered, the proposed method is generic and applicable to different scenarios. Initially, net-power injections, system data such as node locations and line impedances are used to compute the cumulative effect of actor nodes on all observation nodes in the network. The analytical expressions presented in section 6.1.1 are the basis for estimating the mean and variance of voltage at all nodes as discussed in section 6.1.2. The covariance matrix $\Sigma_{\Delta S}$ is computed relying on estimates of historical data. The network topology is used to compute vectors $\boldsymbol{c_r}$ and $\boldsymbol{c_i}$ as formulated in (6.11). Finally, node voltage state estimates as well as the analytical voltage change probability distribution are utilized to compute the probability of node voltage violation according to the threshold given in section 6.1.4. In the first case study, a hypothetical 30% Penetration Level (PL) of distributed PV generation is randomly allocated among 14 actor nodes and voltage state is monitored across all observation nodes in the network. Figure 6.3 shows the number of violations in the system using the proposed method in (6.27) vs. load flow method. From figure 6.3, it can be inferred that the proposed method accurately predicts voltage violations in the system compared to actual violations calculated using load flow method.

In the next case study, a scenario with complete loss of PV generation at a certain time instant is investigated. In this case, actor nodes are assigned to three different 24 hour PV generation profiles contributing to a 70 % PL for demonstrating the generality of the

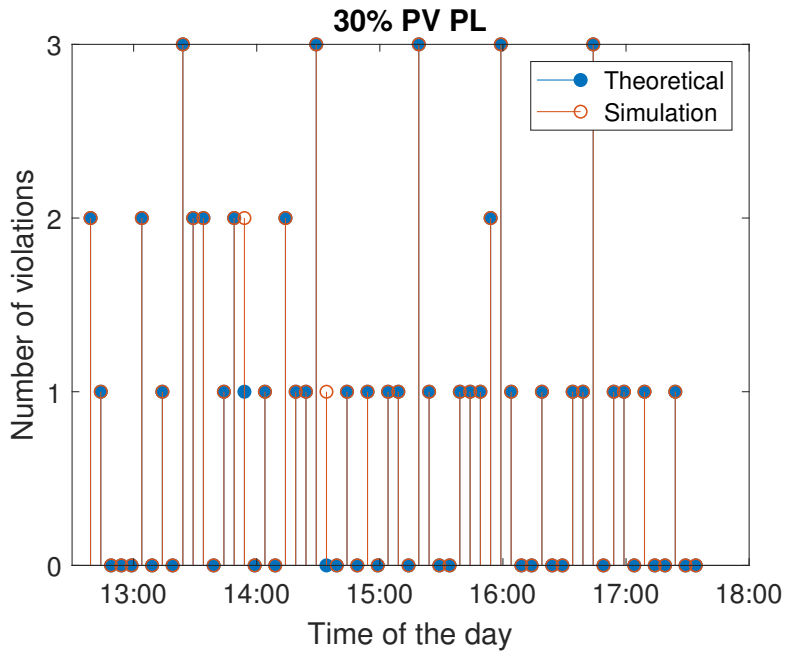

Figure 6.3: Voltage violation prediction using (6.27) vs. load flow.

proposed method. The system in this case consists of 20 arbitrary active consumer nodes integrated with distributed PV generation. Similar to the first case study, voltage state is monitored across all nodes in the network. Figure 6.4 shows the number of voltage violations in the system using the proposed analytical method in (6.27) vs. load flow method with a PV generation loss scenario occurring at time 16:32 of the day. It can be inferred that the proposed method effectively predicts voltage violations not only under normal operation conditions but also under generation loss scenarios. Finally, the accuracy of the proposed method is quantified via multiple Monte-Carlo simulations. Two cases are considered for investigating the accuracy of the proposed method, namely, 30% and 70% PLs. For both cases, 20 arbitrary actor nodes are integrated with distributed PV generation and voltage state is monitored across all nodes in the network. Both scenarios are simulated for 100 Monte-Carlo simulations and the mean prediction error is obtained. Table 6.1 shows the prediction error for both cases, which demonstrates that the effectiveness of the proposed method in predicting voltage violations in the system is higher than 95%. Therefore, the proposed method can provide effective foresight on voltage violations to system operators, which can then be utilized to implement an appropriate optimal voltage control strategy.

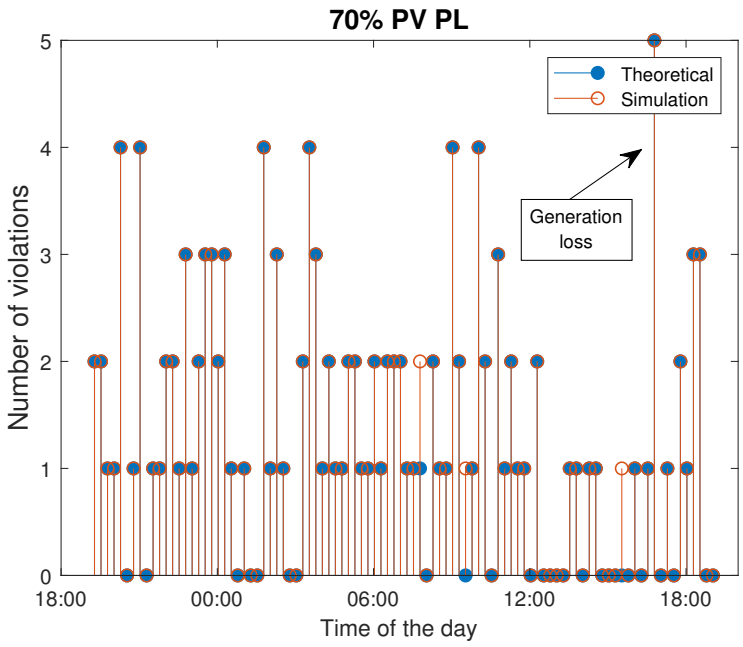

Figure 6.4: Voltage violation prediction using (6.27) vs. load flow (70% PL).

Table 6.1: Theoretical vs. actual voltage violations.

PL	Prediction error (%)
30%	4.31
70%	4.43

6.2 PVSA with uncertainty in state estimates

If we assume uncertainty in the voltage state estimates, then, the present voltage V_O^p in Eq. (6.20) can be rewritten as,

$$\boldsymbol{V_O^p} \triangleq \begin{bmatrix} V_O^{r,p} \\ V_O^{i,p} \end{bmatrix} \sim \mathcal{N}(\mu_2, \Sigma_2) \tag{6.30}$$

Where,

$$\mu_2 = \begin{bmatrix} V_O^{r,p} \\ V_O^{i,p} \end{bmatrix} \tag{6.31}$$

$$\Sigma_2 = \begin{bmatrix} \sigma_{r,p}^2 & cov(V_O^{r,p}, V_O^{i,p}) \\ cov(V_O^{i,p}, V_O^{r,p}) & \sigma_{i,p}^2 \end{bmatrix} \tag{6.32}$$

The expression of V_O^f is based on the present voltage. Thus, the real and imaginary parts of predicted voltage can be rewritten as,

$$\boldsymbol{V_O^f} \triangleq \begin{bmatrix} V_O^{r,f} \\ V_O^{i,f} \end{bmatrix} = \begin{bmatrix} V_O^{r,p} \\ V_O^{i,p} \end{bmatrix} + \begin{bmatrix} \Delta V_O^r \\ \Delta V_O^i \end{bmatrix}, \tag{6.33}$$

$$\boldsymbol{V_O^f} \sim \mathcal{N}\left(\begin{bmatrix} V_O^{r,p} \\ V_O^{i,p} \end{bmatrix}, \begin{bmatrix} \sigma_{r,p}^2 & cov(V_O^{r,p}, V_O^{i,p}) \\ cov(V_O^{i,p}, V_O^{r,p}) & \sigma_{i,p}^2 \end{bmatrix} \right) + \mathcal{N}\left(\begin{bmatrix} C_r^T \mu_{\Delta S} \\ C_i^T \mu_{\Delta S} \end{bmatrix}, \begin{bmatrix} C_r^T \Sigma C_r & C_r^T \Sigma C_i \\ C_r^T \Sigma C_i & C_i^T \Sigma C_i \end{bmatrix} \right) \tag{6.34}$$

The sum of two independent Gaussian distributions is also Gaussian. Therefore,

$$\boldsymbol{V_O^f} \sim \mathcal{N}(\mu_3, \Sigma_3) \tag{6.35}$$

Where,

$$\mu_3 = \begin{bmatrix} V_O^{r,p} + C_r^T \mu_{\Delta S} \\ V_O^{i,p} + C_i^T \mu_{\Delta S} \end{bmatrix} \tag{6.36}$$

$$\mu_3 = \begin{bmatrix} \sigma_{r,p}^2 + C_r^T \Sigma C_r & cov(V_O^{r,p}, V_O^{i,p}) + C_r^T \Sigma C_i \\ cov(V_O^{i,p}, V_O^{r,p}) + C_r^T \Sigma C_i & \sigma_{i,p}^2 + C_i^T \Sigma C_i \end{bmatrix}. \tag{6.37}$$

The magnitude of predicted voltage can be written as,

$$|V_O^f|^2 = (V_O^{r,f})^2 + (V_O^{i,f})^2 \tag{6.38}$$

The distribution of the squared magnitude of V_O^f is a sum of dependent non-central chi-square distributions. Each real and imaginary part of the predicted voltage follows non zero

Gaussian distribution and thus their squares show non central chi square distribution,

$$|V_O^f|^2 \sim \sigma_r^2 \chi_1^2(\mu_r^2) + \sigma_i^2 \chi_1^2(\mu_i^2) \tag{6.39}$$

where, σ and μ are the weight and non centrality parameters of non central chi square distribution with one degree of freedom, respectively. The sum of weighted non-central chi-square distributions can then be approximated with a scaled non-central chi-square with weight α, non-centrality parameter β, and ρ degrees of freedom as,

$$|V_O^f|^2 \sim \alpha \chi_\rho^2(\beta) \tag{6.40}$$

where,

$$\alpha = \frac{\sigma_r^4(1+2\mu_r^2) + \sigma_i^4(1+2\mu_i^2)}{\sigma_r^2(1+2\mu_r^2) + \sigma_i^2(1+2\mu_i^2)} \tag{6.41}$$

$$\beta = \frac{(\sigma_r^2\mu_r^2 + \sigma_i^2\mu_i^2)(\sigma_r^2 + \sigma_i^2 + 2\sigma_r^2\mu_r^2 + 2\sigma_i^2\mu_i^2)}{\sigma_r^4 + \sigma_i^4 + 2\sigma_r^4\mu_r^2 + 2\sigma_r^4\mu_i^2} \tag{6.42}$$

$$\rho = \frac{(\sigma_r^2 + \sigma_i^2)(\sigma_r^2 + \sigma_i^2 + 2\sigma_r^2\mu_r^2 + 2\sigma_i^2\mu_i^2)}{\sigma_r^2 + \sigma_i^2 + 2(\sigma_r^4\mu_r^2) + 2(\sigma_i^4\mu_i^2)} \tag{6.43}$$

Since the square root of a non-central chi-square random variables follows a Rician distribution, the magnitude of predicted voltage change will follow a Rician distribution,

$$|V_O^f| \sim Rician(\kappa, \sigma) \tag{6.44}$$

where, $\kappa = \sqrt{\beta}$ and $\sigma = \sqrt{\alpha}$. To test the performance of the modified PVSA rule, a scenario is simulated using the setup presented in section 6.1.5 and the voltage violation prediction error is recorded for the regular and the modified PVSA rules.This slide provides a simulation scenario to show the performance of the updated PVSA rule. Fig. 6.5 shows the prediction error against variance in voltage magnitude. It can be seen that the regular PVSA rule results in higher prediction error and that is because it assumes that present voltage measurements are correct, while in reality they are erroneous. The modified PVSA

rule on the other hand captures measurement errors, which is why the performance of the modified PVSA rule is consistently better compared to the regular one.

6.3 Voltage violation prediction with Bayesian Matrix Completion

The proposed VVP technique is summarized in Fig. 6.6 and the functional blocks are detailed in this section. It is assumed that measurements come from SCADA system carrying information about active and reactive power as well as real and imaginary parts of nodal voltages. SCADA measurements are collected through sensor data aggregation system and sent for DSSE. It is important to mention that SCADA measurements are available only at a subset of nodes as highlighted by the bold circles in Fig. 6.6. To estimate the states at all nodes, BMC based DSSE is used and the corresponding estimation variance is derived. Finally, state estimates, their variance, and available measurements are used within the PVSA framework to derive the probability distribution of future nodal voltage states ($\mathbf{V}_O^f$) in real-time. This allows for the computation of probability of voltage violation induced by complex power fluctuations at any location in the system. It is assumed that complex power

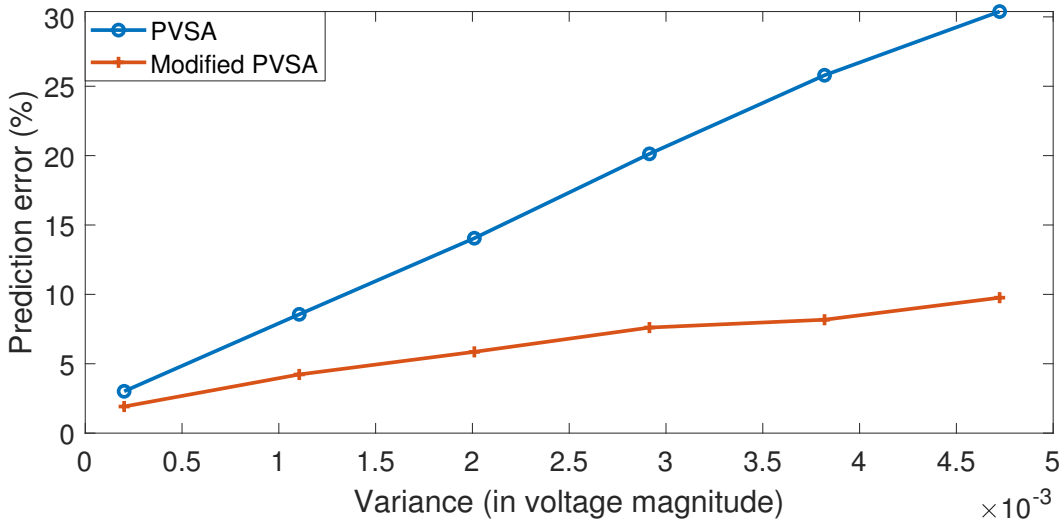

Figure 6.5: Prediction error using: (a) PVSA-Eq. (6.27); and (b) Modified PVSA-Eq. (6.44).

changes occur due to time-varying PV injections and variable load patterns.

6.3.1 BMC-based system observability

DSSE task is difficult due to the lack of sufficient measurements making the system unobservable [237]. Consider an unbalanced distribution system with $\mathcal{N}$ nodes. Let $\mathbf{X}$ denote a matrix that contains information on nodal complex power values, real and imaginary parts of voltage, and voltage magnitudes for all nodes $\mathcal{N}$ in the system. In practice, due to limited number of measurements in the distribution system, only some elements of the matrix $\mathbf{X}$ are known (i.e., $\mathbf{X}$ is incomplete). BMC aims to complete this matrix $\mathbf{X}$ by estimating the unobserved states based on a suitable low rank approximation [238]. The low rank property in the matrix $\mathbf{X}$ results due to: (1) spatial correlation between measurements at different locations; and (2) the correlation between different types of measurements via power-flow equations. If we assume that the measurements at the slack bus are known, it is possible to use the measurements at the non-slack buses to construct the data matrix.

Let $m \in \mathcal{N}$ denote the set of phases at all the non-slack buses. The measurement matrix $\mathbf{Z}$ is constructed such that each row represents a phase and each column represents the measurement associated with the phase of each bus. For each $b \in m$, each row of the matrix

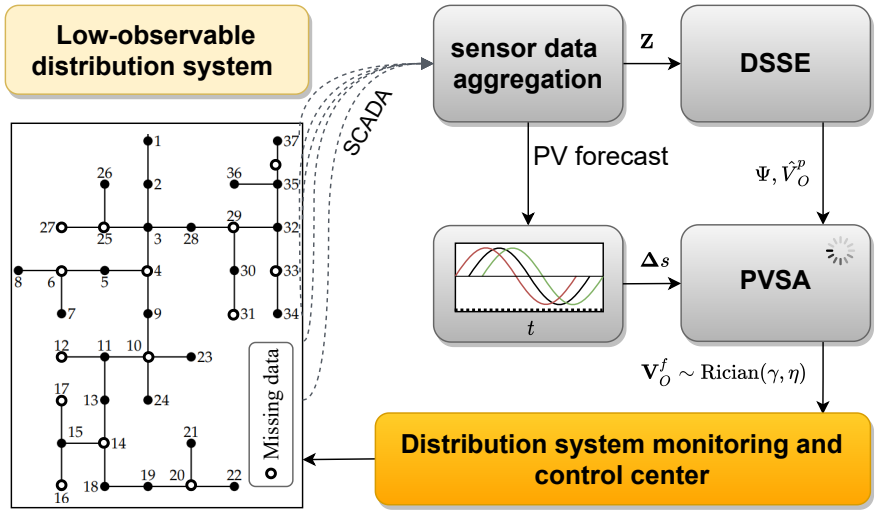

Figure 6.6: VVP flowchart.

$\mathbf{Z} \in \mathbb{R}^{m \times n}$ with $n = 5$ is structured as,

$$[\mathbf{P}_b, \mathbf{Q}_b, \Re(\mathbf{v}_b), \Im(\mathbf{v}_b), |\mathbf{v}_b|], \tag{6.45}$$

where, $\mathbf{P}_b$ and $\mathbf{Q}_b$ represent the active power and reactive power injections at each phase of non-slack bus b respectively. The terms $\Re(\mathbf{v}_b)$ and $\Im(\mathbf{v}_b)$ represent the real and imaginary parts of voltage phasors at each phase of non-slack buses, respectively. Let $\Omega \subseteq \{1, ..., m\} \times \{1, ..., n\}$ describe the known entries in $\mathbf{Z}$. The known entries can also be written as,

$$\mathbf{Z}_{lj} = \mathbf{X}_{lj} + \mathbf{N}_{lj}, \;\; (l, j) \in \Omega \tag{6.46}$$

where, $\mathbf{X}_{lj}$ and $\mathbf{N}_{lj}$ refers to the row entry l and column entry j in the matrix $\mathbf{X}$ and $\mathbf{N}$, respectively. The unknown low rank matrix $\mathbf{X}$ is factorized into two matrices as $\mathbf{X} = \mathbf{A}\mathbf{B}^\intercal$. Here, $\mathbf{A}$ is an $m \times r$ matrix and $\mathbf{B}$ is an $n \times r$ matrix such that $\text{rank}(\mathbf{X}) = r$. The matrix $\mathbf{X}$ is the sum of the outer-products of the columns of $\mathbf{A}$ and $\mathbf{B}$ such that,

$$\mathbf{X} = \sum_{l=1}^{k} \mathbf{a}_{.l} \mathbf{b}_{.l}^\intercal \tag{6.47}$$

where, $k \geq r$, $\mathbf{a}_{.l}$ and $\mathbf{b}_{.l}$ denote the l^{th} column of matrix $\mathbf{A}$ and $\mathbf{B}$ respectively. The l^{th} row of matrix $\mathbf{A}$ and $\mathbf{B}$ is represented by $\mathbf{a}_{l.}$ and $\mathbf{b}_{l.}$ respectively. The low rank matrix is obtained by setting most of the columns in $\mathbf{A}$ and $\mathbf{B}$ to zero. To achieve this condition, the columns of $\mathbf{A}$ and $\mathbf{B}$ are associated with Gaussian priors of precisions γ_l, that is

$$\mathbf{p}(\mathbf{A}|\boldsymbol{\gamma}) = \prod_{l=1}^{k} \mathcal{N}(\mathbf{a}_{.l}|\mathbf{0}, \gamma_l^{-1}\mathbf{I}_m) \tag{6.48}$$

$$\mathbf{p}(\mathbf{B}|\boldsymbol{\gamma}) = \prod_{l=1}^{k} \mathcal{N}(\mathbf{b}_{.l}|\mathbf{0}, \gamma_l^{-1}\mathbf{I}_n) \tag{6.49}$$

During inference, most of the γ_l's take large values, thus forcing the columns of $\mathbf{A}$ and $\mathbf{B}$ to go to zero. The columns of $\mathbf{A}$ and $\mathbf{B}$ have the same sparsity profile enforced by the common

precisions γ_l. These sparsity priors on the factorized matrix encourages low-rank solutions. The precision γ_l are assumed to have a Gamma hyperprior given as,

$$\mathbf{p}(\gamma_l) = Gamma(c, \frac{1}{d}) \tag{6.50}$$

The parameters c and d are set to small values to obtain broad hyperpriors. Using the model (6.46) and factorized matrices $\mathbf{A}$ and $\mathbf{B}$, the conditional distribution of the observations are obtained as,

$$\mathbf{p}(\mathbf{Z}|\mathbf{A}, \mathbf{B}) = \prod_{(l,j)\in\Omega} \mathcal{N}(Z_{lj}|X_{lj}, \beta^{-1}) \tag{6.51}$$

where β is the noise precision of each measurement. The joint distribution is therefore given as,

$$\mathbf{p}(\mathbf{Z}, \mathbf{A}, \mathbf{B}, \boldsymbol{\gamma}) = \mathbf{p}(\mathbf{Z}|\mathbf{A}, \mathbf{B})\mathbf{p}(\mathbf{A}|\boldsymbol{\gamma})\mathbf{p}(\mathbf{B}|\boldsymbol{\gamma})\mathbf{p}(\boldsymbol{\gamma}) \tag{6.52}$$

The evaluation of posterior distributions is obtained by mean field variational Bayes [238]. The posterior distribution of $\mathbf{A}$ and $\mathbf{B}$ decompose as independent distributions of their rows. The approximate posterior distributions of the latent variables are updated as,

$$\mathbf{q}(\mathbf{a}_{l\cdot}) = \mathcal{N}\left(\mathbf{a}_{l\cdot}|\langle \mathbf{a}_{l\cdot}\rangle, \boldsymbol{\Sigma}_l^a\right) \tag{6.53}$$

where the mean and covariance are defined as,

$$\langle \mathbf{a}_{l\cdot}\rangle^\intercal = \langle\beta\rangle \boldsymbol{\Sigma}_l^a \langle \mathbf{B}_l\rangle^\intercal \mathbf{z}_{l\cdot}^\intercal \tag{6.54}$$

$$\boldsymbol{\Sigma}_l^a = \left(\langle\beta\rangle \langle \mathbf{B}_l^\intercal \mathbf{B}_l\rangle + \boldsymbol{\Gamma}\right)^{-1} \tag{6.55}$$

Here,

$$\langle \mathbf{B}_l^\intercal \mathbf{B}_l\rangle = \sum_{j:(l,j)\in\Omega} \left(\langle \mathbf{b}_{j\cdot}^\intercal\rangle\langle \mathbf{b}_{j\cdot}\rangle + \boldsymbol{\Sigma}_j^b\right) \tag{6.56}$$

and $\mathbf{\Gamma} = diag(\boldsymbol{\gamma})$. Similarly, the posterior density of j^{th} row of $\mathbf{B}$ is found as,

$$\mathbf{q}(\mathbf{b}_{j\cdot}) = \mathcal{N}\left(\mathbf{b}_{j\cdot}|\langle\mathbf{b}_{j\cdot}\rangle, \mathbf{\Sigma}_j^b\right) \tag{6.57}$$

where the mean and covariance are defined as,

$$\langle\mathbf{b}_{j\cdot}\rangle^\intercal = \langle\beta\rangle\, \mathbf{\Sigma}_j^b \langle\mathbf{A}_j\rangle^\intercal \mathbf{z}_{\cdot j}^\intercal \tag{6.58}$$

$$\mathbf{\Sigma}_j^b = \left(\langle\beta\rangle \left\langle\mathbf{A}_j^\intercal\mathbf{A}_j\right\rangle + \mathbf{\Gamma}\right)^{-1} \tag{6.59}$$

The posterior density of γ_l becomes a gamma distribution

$$\mathbf{q}(\gamma_l) \propto \gamma_l^{\left(c-1+\frac{m+n}{2}\right)} \exp\left(-\gamma_l \frac{2d + \langle\mathbf{a}_{\cdot l}^\intercal\mathbf{a}_{\cdot l}\rangle + \langle\mathbf{b}_{\cdot l}^\intercal\mathbf{b}_{\cdot l}\rangle}{2}\right) \tag{6.60}$$

with mean,

$$\langle\gamma_l\rangle = \frac{2c + m + n}{2d + \langle\mathbf{a}_{\cdot l}^\intercal\mathbf{a}_{\cdot l}\rangle + \langle\mathbf{b}_{\cdot l}^\intercal\mathbf{b}_{\cdot l}\rangle} \tag{6.61}$$

The required expectations are given by

$$\langle\mathbf{a}_{\cdot l}^\intercal\mathbf{a}_{\cdot l}\rangle = \langle\mathbf{a}_{\cdot l}\rangle^\intercal\langle\mathbf{a}_{\cdot l}\rangle + \sum_j \left(\mathbf{\Sigma}_l^a\right)_{ll}, \tag{6.62}$$

$$\langle\mathbf{b}_{\cdot l}^\intercal\mathbf{b}_{\cdot l}\rangle = \langle\mathbf{b}_{\cdot l}\rangle^\intercal\langle\mathbf{b}_{\cdot l}\rangle + \sum_j \left(\mathbf{\Sigma}_l^b\right)_{ll} \tag{6.63}$$

The approximate posterior distribution of β is given as,

$$\langle\beta\rangle = \frac{(FAD) \times m \times n}{\langle\|\mathbf{Z} - P_\Omega(\mathbf{A}\mathbf{B}^\intercal)\|\rangle_F^2} \tag{6.64}$$

The variance of estimated elements in the complete matrix $\mathbf{X}$ is given as,

$$\mathbf{\Psi}_{l,j} = tr(\mathbf{b}_{j\cdot}\mathbf{\Sigma}_l^a\mathbf{b}_{j\cdot}^\intercal) + tr(\mathbf{a}_{l\cdot}\mathbf{\Sigma}_j^b\mathbf{a}_{l\cdot}^\intercal) + tr(\mathbf{\Sigma}_j^b\mathbf{\Sigma}_l^a) \tag{6.65}$$

where, $tr(\cdot)$ is the trace. The next subsection describes VVP in low-observable distribution systems. Specifically, the estimated complete matrix $\mathbf{X}$ as well as the variance of estimates computed in $\mathbf{\Psi}$ will be used in a probabilistic sensitivity analysis framework for VVP.

6.3.2 Sensitivity based violation prediction

Voltage can fluctuate at any node (*observation node* O) in the system due to complex power changes at another node (*actor node* A). Nodal voltages may exceed safe operational limits (i.e., $0.95 < |V| < 1.05$ p.u) due to abrupt complex power changes at actor nodes, which is undesired for distribution system operation. Recent research [10] has shown that it is possible to predict such nodal voltage violations using PVSA. That is, if complex power at a particular actor node A changes from S_A to $S_A + \Delta S_A$, the voltage changes at any observation node O from V_O to $V_O + \Delta V_O$. In this process, the change in voltage ΔV_O can be linearly approximated with a tight upper bound that guarantees accuracy [72]. This approximation can then used to systematically incorporate uncertainty associated with complex power changes at actor nodes, which results in a unique probability distribution of the predicted voltage magnitude at observation nodes [10]. However, in actual distribution systems, voltage state measurements are not available at every node. Therefore, Theorem 6 provides the probability distribution of predicted voltage magnitude at observation nodes in low-observable distribution systems.

Theorem 6. *For a given unbalanced distribution system, the predicted voltage magnitude* ($|V_O^f|$) *at an observation node* O *due to complex power changes at multiple actor nodes* $A \in \mathcal{A}$ *in low-observable distribution systems follows a Rician distribution, i.e.,*

$$|V_O^f| \sim Rician(\upsilon, \eta) \tag{6.66}$$

where, $\upsilon = \sqrt{\tau}$ *and* $\eta = \sqrt{\xi}$ *with,*

$$\xi = \frac{\sigma_r^4(1 + 2\mu_r^2) + \sigma_i^4(1 + 2\mu_i^2)}{\sigma_r^2(1 + 2\mu_r^2) + \sigma_i^2(1 + 2\mu_i^2)} \tag{6.67}$$

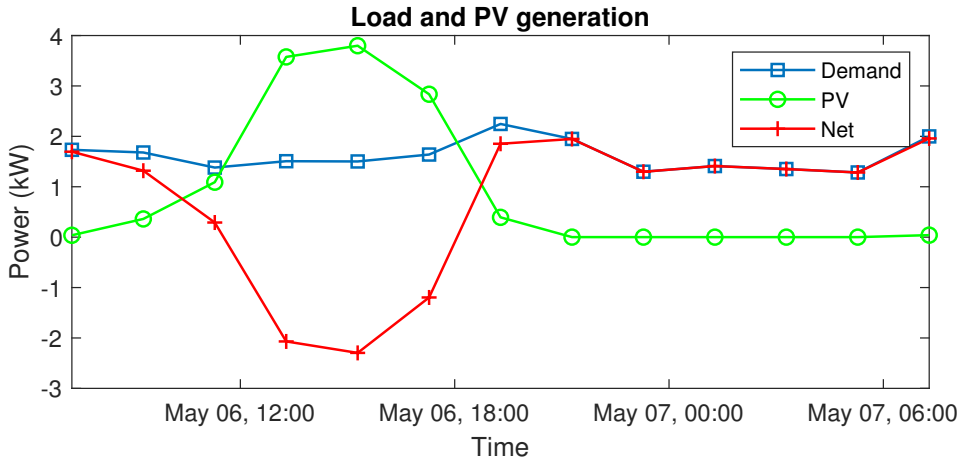

Figure 6.7: PV generation and load profile.

and,

$$\tau = \frac{(\sigma_r^2\mu_r^2 + \sigma_i^2\mu_i^2)(\sigma_r^2 + \sigma_i^2 + 2\sigma_r^2\mu_r^2 + 2\sigma_i^2\mu_i^2)}{\sigma_r^4 + \sigma_i^4 + 2\sigma_r^4\mu_r^2 + 2\sigma_r^4\mu_i^2}. \tag{6.68}$$

Here, $\sigma_r^2 = \mathbf{\Psi}_{O,3} + \mathbf{c_r}^\intercal \mathbf{\Sigma_{\Delta S}} \mathbf{c_r}$, $\sigma_i^2 = \mathbf{\Psi}_{O,4} + \mathbf{c_i}^\intercal \mathbf{\Sigma_{\Delta S}} \mathbf{c_i}$, $\mu_r = \mathbf{X}_{O,3} + \mathbf{c_r^T} \boldsymbol{\mu}_{\boldsymbol{\Delta S}}$, *and* $\mu_i = \mathbf{X}_{O,4} + \mathbf{c_i^T} \boldsymbol{\mu}_{\boldsymbol{\Delta S}}$. $\mathbf{\Psi}_{O,3}$ *and* $\mathbf{\Psi}_{O,4}$ *represent the variance of real and imaginary parts of voltage estimates according to (6.65) whereas* $\mathbf{X}_{O,3}$ *and* $\mathbf{X}_{O,4}$ *are the present estimates of real and imaginary parts of voltage (6.47), respectively.* $\mathbf{c_r}$ *and* $\mathbf{c_i}$ *are based on system topology.* $\boldsymbol{\mu}_{\boldsymbol{\Delta S}}$ *is the mean of change in voltage states with* $\boldsymbol{\Delta S} = [\Delta P_1^a, ..., \Delta P_n^a, \Delta Q_1^a, ..., \Delta Q_n^a]^\intercal$ *is the vector of complex power changes and* $\mathbf{\Sigma_{\Delta S}}$ *is a the covariance matrix that contains the variance and cross-covariance terms of complex power change across different actor nodes as shown in Eq. (12) of [10].*

Proof. Let $\hat{\mathbf{V}}_\mathbf{O}^\mathbf{p}$ be the present voltage state at observation node O. It is possible to write the predicted future voltage state $\mathbf{V}_O^f$ in terms of the voltage change introduced by the DERs at actor nodes, i.e.,

$$\mathbf{V_O^f} = \hat{\mathbf{V}}_\mathbf{O}^\mathbf{p} + \mathbf{\Delta V_O}, \tag{6.69}$$

where $\mathbf{\Delta V_O}$ is the change in voltage states at observation nodes that is caused by complex power changes at DERs. More details on how to compute this voltage change can be found in [72]. To account for system unobservability, we use the real and imaginary parts of voltage estimates $\mathbf{X}_{O,3}$ and $\mathbf{X}_{O,4}$ as well as their estimation variance, i.e., $\mathbf{\Psi}_{O,3}$ and $\mathbf{\Psi}_{O,4}$, respectively.

Therefore, the present voltage estimates $\hat{\mathbf{V}}_O^p$ can be written as,

$$\hat{\mathbf{V}}_{\mathbf{O}}^{\mathbf{p}} = [\hat{V}_O^{r,p}, \hat{V}_O^{i,p}]^\intercal \triangleq [\mathbf{X}_{O,3}, \mathbf{X}_{O,4}]^\intercal. \tag{6.70}$$

Follows from (6.64), the distribution of present voltage states follows a Gaussian distribution,

$$\hat{\mathbf{V}}_{\mathbf{O}}^{\mathbf{p}} \sim \mathcal{N}(\boldsymbol{\mu}_p, \boldsymbol{\Sigma}_p), \text{ with } \boldsymbol{\mu}_p = [\mathbf{X}_{O,3}, \mathbf{X}_{O,4}]^\intercal \tag{6.71}$$

and

$$\boldsymbol{\Sigma}_p = \begin{bmatrix} \boldsymbol{\Psi}_{O,3} & cov(\mathbf{X}_{O,3}, \mathbf{X}_{O,4}) \\ cov(\mathbf{X}_{O,4}, \mathbf{X}_{O,3}) & \boldsymbol{\Psi}_{O,4} \end{bmatrix} \forall O \in m \tag{6.72}$$

The distribution of $\mathbf{V}_{\mathbf{O}}^{\mathbf{f}}$ is based on the present voltage. Thus, the real and imaginary parts of $\mathbf{V}_{\mathbf{O}}^{\mathbf{f}} \triangleq [V_O^{r,f},\ V_O^{i,f}]^\intercal$ can be rewritten as $\mathbf{V}_{\mathbf{O}}^{\mathbf{f}} = [\mathbf{X}_{O,3},\ \mathbf{X}_{O,4}]^\intercal + [\Delta V_O^r,\ \Delta V_O^i]^\intercal$. Thus,

$$\mathbf{V}_{\mathbf{O}}^{\mathbf{f}} \sim \mathcal{N}\left(\begin{bmatrix} \mathbf{X}_{O,3} \\ \mathbf{X}_{O,4} \end{bmatrix} + \begin{bmatrix} \mathbf{c}_r^\intercal \boldsymbol{\mu}_{\boldsymbol{\Delta S}} \\ \mathbf{c}_i^\intercal \boldsymbol{\mu}_{\boldsymbol{\Delta S}} \end{bmatrix}, \begin{bmatrix} \lambda_r & \delta_f \\ \delta_f & \lambda_i \end{bmatrix} \right) \tag{6.73}$$

where, $\lambda_r = \boldsymbol{\Psi}_{O,3} + \mathbf{c}_r^\intercal \boldsymbol{\Sigma}_{\boldsymbol{\Delta S}} \mathbf{c}_r$, $\lambda_i = \boldsymbol{\Psi}_{O,4} + \mathbf{c}_i^\intercal \boldsymbol{\Sigma}_{\boldsymbol{\Delta S}} \mathbf{c}_i$, $\delta_f = cov(\mathbf{X}_{O,3}, \mathbf{X}_{O,4}) + \mathbf{c}_r^\intercal \boldsymbol{\Sigma}_{\boldsymbol{\Delta S}} \mathbf{c}_i$. The terms $\mathbf{c}^\intercal \boldsymbol{\mu}_{\boldsymbol{\Delta S}}$ and $\mathbf{c}^\intercal \boldsymbol{\Sigma}_{\boldsymbol{\Delta S}} \mathbf{c}$ are the mean and variance of real and imaginary voltage change caused by complex power changes at all actor nodes denoted by the subscripts r or i, respectively. The distribution of $|V_O^f|^2 = (V_O^{r,f})^2 + (V_O^{r,f})^2$ follows a scaled non-central chi-square with weight ξ, non-centrality parameter τ and $\rho = 1$ degrees of freedom as [10],

$$|V_O^f|^2 \sim \xi \chi_\rho^2(\tau) \tag{6.74}$$

where, ξ and τ are given in (6.67) and (6.68), respectively. $\sigma_r^2 = \boldsymbol{\Psi}_{O,3} + \mathbf{c}_r^\intercal \boldsymbol{\Sigma}_{\boldsymbol{\Delta S}} \mathbf{c}_r$, $\sigma_i^2 = \boldsymbol{\Psi}_{O,4} + \mathbf{c}_i^\intercal \boldsymbol{\Sigma}_{\boldsymbol{\Delta S}} \mathbf{c}_i$, $\mu_r = \mathbf{X}_{O,3} + \mathbf{c}_r^\intercal \boldsymbol{\mu}_{\boldsymbol{\Delta S}}$ and $\mu_r = \mathbf{X}_{O,4} + \mathbf{c}_i^\intercal \boldsymbol{\mu}_{\boldsymbol{\Delta S}}$. Since the square root of non-central chi-square random variables follows a Rician distribution, the magnitude of predicted

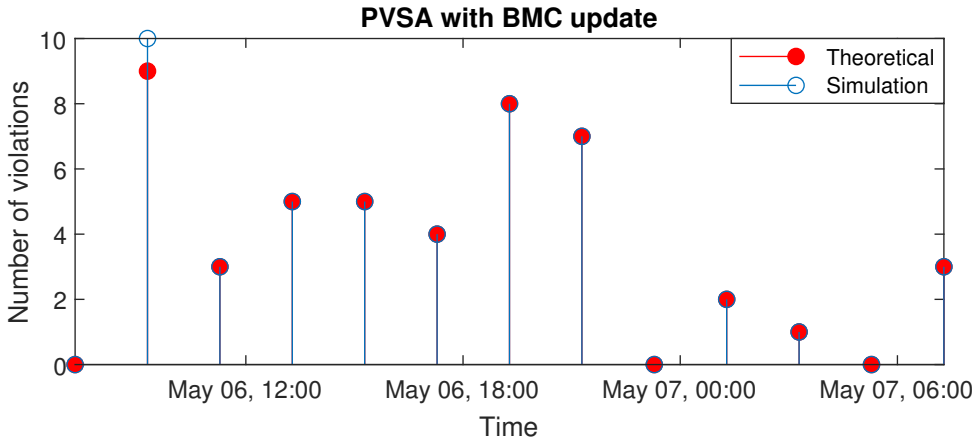

Figure 6.8: Predicted vs. actual voltage violations.

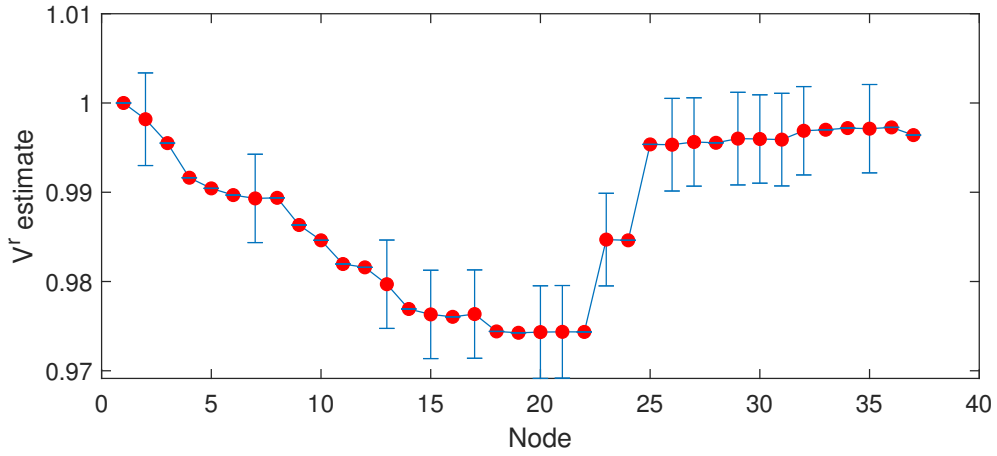

Figure 6.9: Mean and variance of $\hat{\mathbf{V}}_O^{r,p}$ at phase a.

voltage change will follow a Rician distribution,

$$|V_O^f| \sim \text{Rician}(\upsilon, \eta) \tag{6.75}$$

where, $\upsilon = \sqrt{\tau}$ and $\eta = \sqrt{\xi}$. □

6.3.3 Verification via simulation

This section validates the proposed VVP rule in low observable distribution systems. The method is verified on the unbalanced 37 node test system [235]. It is assumed that the system is unobservable with 50% as a fraction of available data as highlighted by the dark

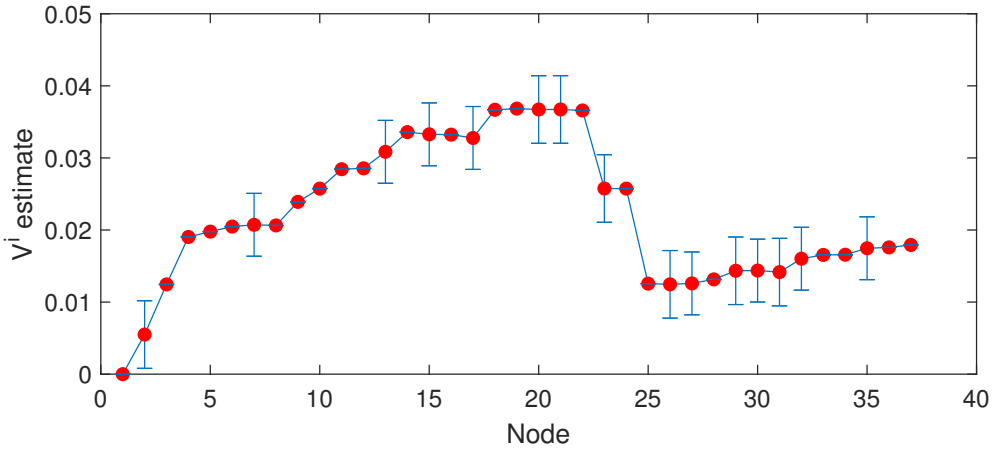

Figure 6.10: Mean and variance of $\hat{\mathbf{V}}_O^{i,p}$ at phase a.

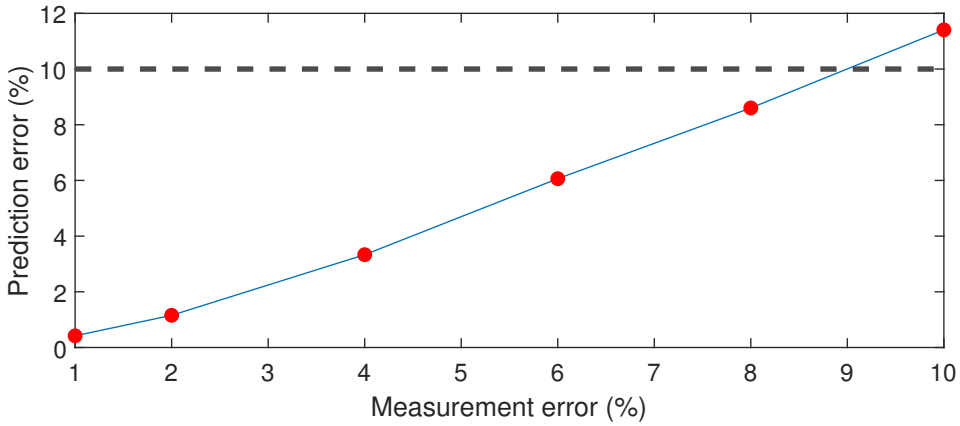

Figure 6.11: Prediction accuracy with erroneous voltage states.

circles in Fig. 6.6. 14 actor nodes ($\mathcal{A} = [5, ..., 18]$) are randomly selected and integrated with PV units at phase a. PV active power injection is modeled as a random process with uncertainty component as,

$$\Delta P_{pv} = S(t) + r(t) \tag{6.76}$$

where, $S(t)$ is the mean forecast trend of PV active power injection and $r(t) \sim \mathcal{N}(0, \sigma_{pv}^2)$ is a zero mean Gaussian that incorporates injection variability with variance σ_{pv}^2. It is important to note that PVSA approach is also applicable where $r(t)$ is non-Gaussian [72]. Fig. 8.7 shows $S(t)$ as well as the load pattern of one actor node. The VVP is computed based on Theorem 6 over the entire time period and $\mathbf{V_O^P}$ for all nodes where state measurements are unavailable is

estimated using BMC. Two scenarios are analyzed to show the effectiveness of the proposed method. For the first scenario, it is assumed that the state estimates ($[\mathbf{X}_{O,3}, \mathbf{X}_{O,4}]^\intercal$) are perfect, i.e., no process noise is injected in (6.71). The resulting violation prediction for this scenario is plotted in Fig. 6.8. This figure shows VVP using Theorem 6 compared to actual violation count computed by classical load flow method (simulation). It can be seen that using state estimates of the BMC, the prediction rule is accurate in preemptively identifying nodal voltage violations. Next, we assume that the knowledge of present voltage states at observation nodes ($\mathbf{V}_{\mathbf{O}}^{\mathbf{p}}$) is erroneous with covariance structure (6.72) based on the matrix $\mathbf{\Psi}$ in (6.65). Figures 6.9 and 6.10 show the mean and variance of real and imaginary parts of present voltage estimates. It can be seen that the variance of nodes where measurements are unavailable is higher than that of nodes where measurements are available. This variance is used together with errors in state measurements to validate the accuracy of the proposed approach. For validation, the simulation setup is repeated for 50 Monte Carlo simulations over different values of measurement errors and the prediction error is computed based on the different between the proposed approach and classical load flow method. It can be seen from Fig. 6.11 that it is possible to obtain low prediction errors as measurement error increases. For typical real world values of measurement errors (e.g., at most 5-6% of actual values), the prediction accuracy is over 90%. This demonstrates the effectiveness of the proposed method against errors in the knowledge of present voltage states, which makes it suitable for proactive control applications.

6.4 Summary

This chapter proposes a new preemptive voltage monitoring method that provides useful foresight on violations in the system. The proposed approach is based on probabilistic voltage sensitivity analysis where the probability of voltage violation is computed for all system nodes given changes in power injections at different system nodes. Simulation results demonstrate that the proposed voltage violation prediction method is extremely accurate with a low prediction error of approximately 4 %. In addition, the voltage violation prediction

rule is updated to account for increased errors in voltage magnitude measurement, resulting in additional accuracy gains compare to the regular rule. In cases where present voltage measurements are missing, the developed approach is integrated with BMC-based state estimation approach. It has been shown through simulation that the proposed approach is accurate in predicting voltage violations when compared to actual load flow solution with as low as 50% fraction of available voltage state measurements. In addition, the prediction error is found be consistently below 10% for different ranges of variance in measurement errors. The proposed approach helps simplify hosting capacity analysis (Chapter 7) and develop proactive voltage control strategies in power distribution systems as shown in Chapter 8.

Chapter 7

System planning with high penetration levels of DERs and EVs

The developed probabilistic sensitivity approaches in Chapters 5 and 6 consider only temporal uncertainties of power changes at the grid-edge. For example, the probabilistic loss sensitivity analysis in Chapter 5 considers the impact of temporal uncertainty of power changes on line losses. Similarly, the performance of the voltage violation prediction rule in Chapter 6 is tested with a hypothetical PV and load profile over six hour-period. However, there could also be spatial uncertainty in the distribution of consumers with PV generation across the system. Given the accuracy-complexity trade-offs with existing planning approaches, deriving an analytical relationship that also accounts for the spatial randomness helps improve the efficacy of existing distribution system planning frameworks. Therefore, this chapter proposes an analytical derivation for Spatio-temporal probabilistic voltage sensitivity analysis (ST-PVSA) to account for random distribution of PVs. The ST-PVSA approach is validated against actual load-flow results for computing PV hosting capacity using the IEEE 37 and IEEE 123-node test systems. Additionally, this chapter derives the probability distribution of total system losses as well as total voltage changes for efficient EV charging station allocation applications. Results show that it is possible to find locations that minimize total losses and voltage deviations with EV charging station placement.

7.1 Spatio-temporal sensitivity framework

7.1.1 Hosting capacity analysis with simulation-based approach

This section describes a typical load flow-based approach of determining the HC of the system. Here, the net power injection is increased in steps by allocating power to PVs located at random locations of the network. Then, load flow is executed for each penetration levels to track the number of node voltage violations throughout the network. This process is repeated for increasing penetration levels until the number of violations exceeds the threshold. The corresponding power (penetration level) is the HC for a particular PV deployment scenario. Thereafter, the complete process is repeated multiple times to cover all possible spatial distribution of the PV installations and the minimum capacity across all such scenarios is the final HC of the network. The scenario based analysis presents a huge computational burden due to the requirement of multiple load flow runs. Fig. 7.1 depicts the flow chart of the existing load flow-based approach of computing HC [81]. Alternatively, this chapter attempts to develop a probabilistic VSA approach that determines the HC in a computationally efficient manner. As mentioned in [80], a comprehensive analysis of PV distribution needs to monitor voltage, protection, power quality and control limits. However, voltage is the primary concern for many utilities [81, 239]. So, similar to [79, 81], this work only considers voltage limits to determine the PV HC. The first step towards the probabilistic VSA approach for HC is to derive an analytical expression of voltage sensitivity due to random power change at random locations in the network, as presented in the next section.

7.1.2 ST-PVSA for random distribution of PVs

This section details the steps involved in the derivation of the probability distribution of voltage change at network nodes due to random power changes at random locations of the network. Throughout this chapter, observation nodes are referred to those nodes where voltage change is observed and actor nodes are those where power changes. The change in complex voltage at any phase (say phase a) of observation node O due to change in complex

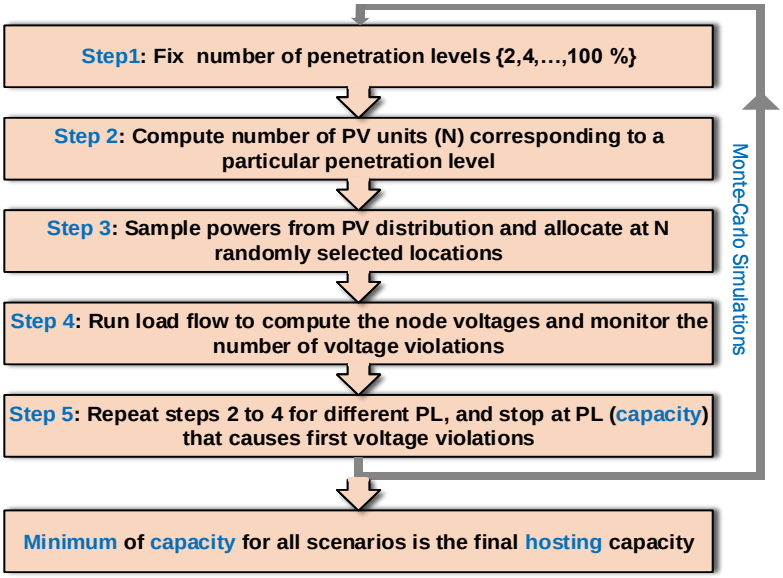

Figure 7.1: Flowchart of Load flow based HC method

power at any phase of a single actor node A is given by [57],

$$\Delta V_{OA}^{a} \approx -\left[\frac{\Delta S_A^{a\star} Z_{OA}^{aa}}{V_A^{a\star}} + \frac{\Delta S_A^{b\star} Z_{OA}^{ab}}{V_A^{b\star}} + \frac{\Delta S_A^{c\star} Z_{OA}^{ac}}{V_A^{c\star}}\right], \tag{7.1}$$

where, superscript a, b and c represent the three phases; this notation is used throughout the chapter. $V_A^{a\star}$ and ΔS_A^{a} represent complex conjugate of voltage at phase a and complex power change at actor node A, respectively; Z_{OA} denotes the impedance matrix including self and mutual line impedance of the shared path between observation node and actor node from the source node. The subscript A represents the actor node where power is varying. In [57], the authors use the eqn. (7.1) to derive the distribution of voltage change. However, the distribution only incorporates the temporal uncertainty associated with power change, thereby prevents its uses in hosting capacity analysis. Therefore, here, we leverage eqn. (7.1) to derive a generic probability distribution of voltage change, considering both temporal and spatial randomness in a three phase unbalanced network. In this regard, the complex voltage change in (7.1) is decomposed into real and imaginary parts as,

$$\Delta V_{OA}^{a} = \Delta V_{OA}^{a,r} + j\Delta V_{OA}^{a,i}. \tag{7.2}$$

For simplicity, the voltage change expression throughout the derivation is shown for a single phase (phase a). However, similar form and approach is applicable to other phases as well. On expanding power change ($\Delta S_A^{a\star} = \Delta P - j\Delta Q$) and impedance ($Z_{OA} = R + jX$) components in (7.1), the real ($\Delta V_{OA}^{a,r}$) and imaginary parts ($\Delta V_{OA}^{a,i}$) of voltage change at phase a of the observation node O can be written as,

$$\Delta V_{OA}^{a,r} = \sum_{h,u} \frac{-1}{|V_A^h|}[\Delta P_A^h(R_{OA}^u cos(\omega_A) - X_{OA}^u sin(\omega_A)) + \Delta Q_A^h(R_{OA}^u sin(\omega_A) + X_{OA}^u cos(\omega_A))]$$
$$\Delta V_{OA}^{a,i} = \sum_{h,u} \frac{-1}{|V_A^h|}[\Delta P_A^h(R_{OA}^u sin(\omega_A) + X_{OA}^u cos(\omega_A)) + \Delta Q_A^h(X_{OA}^u sin(\omega_A) - R_{OA}^u cos(\omega_A))] \tag{7.3}$$

where $h \,\epsilon\, \tilde{H}$ and $u \,\epsilon\, \tilde{U}$. The set $\tilde{H} = \{a, b, c\}$ denotes different phases and the set $\tilde{U} = \{aa, ab, ac\}$ represents phase sequence for the corresponding phase. ΔP_A^h and ΔQ_A^h are the active and reactive power changes, respectively. R_{OA}^h and X_{OA}^h are the resistance and reactance of shared path between the observation node O and actor node A from the source node. V_A^h denotes the complex rated voltage of actor node A. The magnitude and angle of voltage at a particular phase, say phase a, of node A are given by $|V_A^a|$ and θ_A^a, respectively with reference to the slack bus. ω_A denotes the rated voltage angle of the actor node A. The detailed steps to obtain equation (7.3) from equation (7.2) are described in Appendix C. Line voltage of the network is always kept within permissible limits, and thus it is reasonable to assume the phase difference of 120° between the voltage angles of different phases with the same angle for all the node voltages of each phase. Based on this assumption, $\Delta V_{OA}^{a,r}, \Delta V_{OA}^{a,i}$ can be rewritten as,

$$\begin{aligned}\Delta V_{OA}^{a,r} = \frac{-\Delta P_A^a R_{OA}^{aa}}{|V_A^a|} + \frac{\Delta P_A^b}{|V_A^b|}\left(\frac{R_{OA}^{ab}}{2} - \frac{\sqrt{3}X_{OA}^{ab}}{2}\right) + \\ \frac{\Delta P_A^c}{|V_A^c|}\left(\frac{R_{OA}^{ac}}{2} + \frac{\sqrt{3}X_{OA}^{ac}}{2}\right) - \frac{\Delta Q_A^a X_{OA}^{aa}}{|V_A^a|} + \\ \frac{\Delta Q_A^b}{|V_A^b|}\left(\frac{\sqrt{3}R_{OA}^{ab}}{2} + \frac{X_{OA}^{ab}}{2}\right) + \frac{\Delta Q_A^c}{|V_A^c|}\left(\frac{-\sqrt{3}R_{OA}^{ac}}{2} + \frac{X_{OA}^{ac}}{2}\right)\end{aligned} \tag{7.4}$$

$$\Delta V_{OA}^{a,i} = \frac{-\Delta P_A^a X_{OA}^{aa}}{|V_A^a|} + \frac{\Delta P_A^b}{|V_A^b|}\left(\frac{\sqrt{3}R_{OA}^{ab}}{2} + \frac{X_{OA}^{ab}}{2}\right) + \frac{\Delta P_A^c}{|V_A^c|}\left(\frac{-\sqrt{3}R_{OA}^{ac}}{2} + \frac{X_{OA}^{ac}}{2}\right) + \frac{\Delta Q_A^a R_{OA}^{aa}}{|V_A^a|} + \frac{\Delta Q_A^b}{|V_A^b|}\left(-\frac{R_{OA}^{ab}}{2} + \frac{\sqrt{3}X_{OA}^{ab}}{2}\right) + \frac{\Delta Q_A^c}{|V_A^c|}\left(-\frac{R_{OA}^{ac}}{2} - \frac{\sqrt{3}X_{OA}^{ac}}{2}\right) \tag{7.5}$$

The real (7.4) and imaginary (7.5) parts of the voltage change can further be represented in a simplified form as,

$$\Delta V_{OA}^{a,r} = (\mathbf{Z^{a,r}})^{\mathbf{T}}\mathbf{\Delta S}, \qquad \Delta V_{OA}^{a,i} = (\mathbf{Z^{a,i}})^{\mathbf{T}}\mathbf{\Delta S} \tag{7.6}$$

$$\mathbf{Z^{a,r}} = \begin{bmatrix} -R_{OA}^{aa} \\ \frac{R_{OA}^{ab}}{2} - \frac{\sqrt{3}X_{OA}^{ab}}{2} \\ \frac{R_{OA}^{ac}}{2} + \frac{\sqrt{3}X_{OA}^{ac}}{2} \\ -X_{OA}^{aa} \\ [1pt]\frac{\sqrt{3}R_{OA}^{ab}}{2} + \frac{X_{OA}^{ab}}{2} \\ \frac{-\sqrt{3}R_{OA}^{ac}}{2} + \frac{X_{OA}^{ac}}{2} \end{bmatrix}, \mathbf{Z^{a,i}} = \begin{bmatrix} -X_{OA}^{aa} \\ \frac{\sqrt{3}R_{OA}^{ab}}{2} + \frac{X_{OA}^{ab}}{2} \\ \frac{-\sqrt{3}R_{OA}^{ac}}{2} + \frac{X_{OA}^{ac}}{2} \\ R_{OA}^{aa} \\ \frac{-R_{OA}^{ab}}{2} + \frac{\sqrt{3}X_{OA}^{ab}}{2} \\ \frac{-R_{OA}^{ac}}{2} - \frac{\sqrt{3}X_{OA}^{ac}}{2} \end{bmatrix}, \qquad \mathbf{\Delta S} = \begin{bmatrix} \frac{\Delta P_A^a}{|V_A^a|} \\ \frac{\Delta P_A^b}{|V_A^b|} \\ \frac{\Delta P_A^c}{|V_A^c|} \\ \frac{\Delta Q_A^a}{|V_A^a|} \\ \frac{\Delta Q_A^b}{|V_A^b|} \\ \frac{\Delta Q_A^c}{|V_A^c|} \end{bmatrix}$$

where $\mathbf{Z^{a,r}}$ and $\mathbf{Z^{a,i}}$ are the vectors incorporating shared path impedance terms corresponding to real and imaginary parts of voltage change, respectively. To represent the random variation of PV generation, the real and reactive power change is modeled as a random variable. Consistent with the prior efforts in modeling PV generation as a time series with a trend component and Gaussian noise [52, 240], the power variation is assumed to be Gaussian. It is important to note that the framework is quite general to account for any arbitrary random variable with finite mean and variance. Therefore, the vector $\mathbf{\Delta S}$, which incorporate the terms corresponding to the ratio of power change and constant base voltages, can be expressed as Gaussian random vector $\mathbf{\Delta S} \sim \mathcal{N}(\mu_{\Delta S}, \sum_{\Delta S})$ with $\boldsymbol{\mu_{\Delta S}}$ being mean vector, and

covariance matrix $\sum_{\Delta S}$ as,

$$\begin{bmatrix} \sigma^2_{\frac{P^a}{|V^a_A|}} & \dots & cov(\Delta P^a_A/|V^a_A|, \Delta Q^c_A/|V^c_A|) \\ \vdots & \ddots & \vdots \\ cov(\Delta P^a_A/|V^a_A|, \Delta Q^c_A/|V^c_A|) & \dots & \sigma^2_{\frac{Q^c}{|V^c_A|}} \end{bmatrix} \tag{7.7}$$

Here, the diagonal and off-diagonal elements indicate variance and covariance among the terms that are ratio of power changes and base voltages across different phases of actor nodes, respectively. The impedance of the shared line between a given observation node (O) and a random actor node can be modeled as a correlated random variable. The mean, variance and covariance of resistance R_{OA} and reactance X_{OA} corresponding to a given observation node O can be estimated based on actual line impedance data. In addition, let $\boldsymbol{\mu_{Z^r}}$ and $\boldsymbol{\mu_{Z^i}}$ represent the mean of real ($\boldsymbol{Z^{a,r}}$) and imaginary ($\boldsymbol{Z^{a,i}}$) parts of impedance vector, respectively. The average is taken over all the nodes of the network with respect to the observation node. Similarly, $\sum_{Z^r}$ and $\sum_{Z^i}$ denote the covariance matrices of $\boldsymbol{Z^{a,r}}$ and $\boldsymbol{Z^{a,i}}$, respectively. The correlation coefficient between the shared path impedances for various actor nodes is computed based on network parameters. Particularly, the objective of this work is to derive the probability distribution of the magnitude of voltage change at an observation node due to random power variation of PVs located at random nodes, which will further be used to estimate the system HC. The probability distribution of real $\Delta V^{a,r}_{OA}$ and imaginary components $\Delta V^{a,i}_{OA}$ of the voltage change due to random spatial distribution of multiple PV units can be derived using the following steps:

Step 1: *Compute mean and variance of* $\Delta V^{a,r}_{OA}$ *and* $\Delta V^{a,i}_{OA}$ *due to a single actor node*: Using (7.6), the mean of the voltage change can be expressed as the expectation of product of two terms, i.e., the shared path impedance vector ($\boldsymbol{Z^{a,r}}$ for real and $\boldsymbol{Z^{a,i}}$ for imaginary part) and power change vector $\boldsymbol{\Delta S}$. As the terms in the product are mutually independent, the expectation of their product can be applied to individual terms separately yielding the mean

of real (μ_r) and imaginary (μ_i) parts as,

$$\begin{aligned} \mu_r &= E[Z_o^{(a,r)^T} \Delta S] = \boldsymbol{\mu_{Z_o^{a,r}} \mu_{\Delta S}} \\ \mu_i &= E[Z^{(a,i)^T} \Delta S] = \boldsymbol{\mu_{Z_o^{a,i}} \mu_{\Delta S}} \end{aligned} \tag{7.8}$$

Furthermore, the variance of real and imaginary parts of the voltage change can be computed as shown below,

$$\begin{aligned} \text{Var}(\Delta V_{OA}^{a,r}) &= E[(Z^{(a,r)^T} \Delta S)^2] - E[(Z^{(a,r)^T} \Delta S)]^2 \\ \text{Var}(\Delta V_{OA}^{a,i}) &= E[(Z^{(a,i)^T} \Delta S)^2] - E[(Z^{(a,i)^T} \Delta S)]^2. \end{aligned} \tag{7.9}$$

Since Z_r^T and ΔS are independent, the expectation of their product can be written in terms of product of their individual expectation as,

$$E[Z^{(a,r)^T} \Delta S \Delta S^T Z^{a,r}] - (E[Z^{(a,r)^T}] E[\Delta S])^2. \tag{7.10}$$

For simplicity, the equation for variance is shown for the real part of voltage change and a similar form exists for imaginary part. Now, using the properties of matrix trace, the variance of the real part can be rewritten as,

$$\begin{aligned} E[Tr(Z_r Z_r^T \Delta S \Delta S^T)] - (\mu_{Z^r} \mu_{\Delta S})^2 &= Tr(E[Z_r Z_r^T] E[\Delta S \Delta S^T]) - (\mu_{Z^r} \mu_{\Delta S})^2 \\ &= Tr[(\mu_{Z^r} \mu_{Z^r}^T + \textstyle\sum_{Z^r})(\mu_{\Delta S} \mu_{\Delta S}^T + \textstyle\sum_{\Delta S})] - (\mu_{Z^r} \mu_{\Delta S})^2 \\ = Tr(\mu_{Z^r} \mu_{Z^r}^T \mu_{\Delta S} \mu_{\Delta S}^T) + Tr(\mu_{Z^r} \mu_{Z^r}^T \textstyle\sum_{\Delta S}) + Tr(\textstyle\sum_{Z^r} \mu_{\Delta S} \mu_{\Delta S}^T) + Tr(\textstyle\sum_{Z^r} \textstyle\sum_{\Delta S}) - (\mu_{Z^r}^T \mu_{\Delta S})^2 \end{aligned} \tag{7.11}$$

Now, the term $Tr(\mu_{Z^r} \mu_{Z^r}^T \mu_{\Delta S} \mu_{\Delta S}^T)$ is rearranged to $(\mu_{Z^r} \mu_{\Delta S})^2$, that cancels the last term of (7.11). After applying trace operator, the variance of real part can be expressed as,

$$\boldsymbol{\mu_{Z^r}^T \Sigma_{\Delta S} \mu_{Z^r} + \mu_{\Delta S}^T \Sigma_{Z^r} \mu_{\Delta S} + Tr(\Sigma_{Z^r} \Sigma_{\Delta S})} \tag{7.12}$$

Following the same steps from equations (7.10- 7.12), the variance of imaginary part of voltage change can be written as,

$$\boldsymbol{\mu}_{\boldsymbol{Z}^i}^{\boldsymbol{T}}\boldsymbol{\Sigma}_{\boldsymbol{\Delta S}}\boldsymbol{\mu}_{\boldsymbol{Z}^i} + \boldsymbol{\mu}_{\boldsymbol{\Delta S}}^{\boldsymbol{T}}\boldsymbol{\Sigma}_{\boldsymbol{Z}^i}\boldsymbol{\mu}_{\boldsymbol{\Delta S}} + Tr(\boldsymbol{\Sigma}_{\boldsymbol{Z}^i}\boldsymbol{\Sigma}_{\boldsymbol{\Delta S}}) \tag{7.13}$$

Step 2: *Compute covariance between real* $\Delta V_{OA}^{a,r}$ *and imaginary* $\Delta V_{OA}^{a,i}$ *parts of voltage change*:

The covariance between the real and imaginary parts of voltage change can be expressed as:

$$\begin{aligned} Cov(\Delta V_{OA}^{a,r}, \Delta V_{OA}^{a,i}) &= E(\Delta V_{OA}^{a,r}\Delta V_{OA}^{a,i}) - E(\Delta V_{OA}^{a,r})E(\Delta V_{OA}^{a,i}) \\ &= E[Z_A^{(a,r)^T}\Delta S_A Z_A^{(a,i)^T}\Delta S_A] \end{aligned} \tag{7.14}$$

$\boldsymbol{Z^{(a,r)^T}\Delta S}$ and $\boldsymbol{Z^{(a,i)^T}\Delta S}$ are expanded using eqn. (7.4) and (7.5) to express covariance as the expectation of following term,

$$E[A \times B]$$

where,

$$\begin{aligned} A = &\frac{\Delta P_A^a}{|V_A^a|}(-R_{OA}^{aa}) + \frac{\Delta P_A^b}{|V_A^b|}\left(\frac{R_{OA}^{ab}}{2} - \frac{\sqrt{3}X_{OA}^{ab}}{2}\right) + \frac{\Delta P_A^c}{|V_A^c|}\left(\frac{R_{OA}^{ac}}{2} + \frac{\sqrt{3}X_{OA}^{ac}}{2}\right) \\ &-\frac{\Delta Q_A^a}{|V_A^a|}X_{OA}^{aa} + \frac{\Delta Q_A^b}{|V_A^b|}\left(\frac{\sqrt{3}R_{OA}^{ab}}{2} + \frac{X_{OA}^{ab}}{2}\right) + \frac{\Delta Q_A^c}{|V_A^c|}\left(-\frac{\sqrt{3}R_{O1}^{ac}}{2} + \frac{X_{O1}^{ac}}{2}\right) \end{aligned}$$

and,

$$\begin{aligned} B = &\frac{\Delta P_A^a}{|V_A^a|}(-X_{OA}^{aa}) + \frac{\Delta P_A^b}{|V_A^b|}\left(\frac{\sqrt{3}R_{OA}^{ab}}{2} + \frac{X_{OA}^{ab}}{2}\right) + \frac{\Delta P_A^c}{|V_A^c|}\left(\frac{-\sqrt{3}R_{OA}^{ac}}{2} + \frac{X_{OA}^{ac}}{2}\right) \\ &+\frac{\Delta Q_A^a}{|V_A^a|}R_{OA}^{aa} + \frac{\Delta Q_A^b}{|V_A^b|}\left(-\frac{R_{OA}^{ab}}{2} + \frac{\sqrt{3}X_{OA}^{ab}}{2}\right) + \frac{\Delta Q_A^c}{|V_A^c|}\left(-\frac{R_{OA}^{ac}}{2} - \frac{\sqrt{3}X_{OA}^{ac}}{2}\right) \end{aligned}$$

Terms inside the expectation operator are cross multiplied as,

$$\begin{aligned}
&\frac{\rho_{p^a}\sigma^2_{p^a}}{|V^a_A|^2}\mu_{R^{aa}}\mu_{X^{aa}} - \frac{\rho_{q^a}}{|V^a_A|^2}\sigma^2_{q^a}\mu_{R^{aa}}\mu_{X^{aa}} + \\
&\frac{\rho_{p^b}}{|V^b_A|^2}\sigma^2_{p^b}\left(0.43\mu^2_{R^{ab}} - 0.5\mu_{R^{ab}}\mu_{X^{ab}} - 0.43\mu^2_{X^{ab}}\right) + \\
&\frac{\rho_{p^c}}{|V^c_A|^2}\sigma^2_{p^c}\left(-0.43\mu^2_{R^{ac}} - 0.5\mu_{R^{ac}}\mu_{X^{ac}} + 0.43\mu^2_{X^{ac}}\right) + \\
&\frac{\rho_{q^b}}{|V^b_A|^2}\sigma^2_{q^b}\left(-0.43\mu^2_{R^{ab}} + 0.5\mu_{R^{ab}}\mu_{X^{ab}} + 0.43\mu^2_{X^{ab}}\right) + \\
&\frac{\rho_{q^c}}{|V^c_A|^2}\sigma^2_{q^c}\left(0.43\mu^2_{R^{ac}} + 0.5\mu_{R^{ac}}\mu_{X^{ac}} - 0.43\mu^2_{X^{ac}}\right) + \\
&\frac{\rho_{p^aq^a}}{|V_A|^2}\sigma_{p^a}\sigma_{q^a}\left(-\mu^2_{R^{aa}} + \mu^2_{X^{aa}}\right) + \\
&\frac{\rho_{p^bq^b}}{|V^b_A|^2}\sigma_{p^b}\sigma_{q^b}\left(0.5\mu^2_{R^{ab}} + \sqrt{3}\mu_{R^{ab}}\mu_{X^{ab}} - 0.5\mu^2_{X^{ab}}\right) + \\
&\frac{\rho_{p^cq^c}}{|V^a_c|^2}\sigma_{p^c}\sigma_{q^c}\left(0.5\mu^2_{R^{ac}} - \sqrt{3}\mu_{R^{ac}}\mu_{X^{ac}} - 0.5\mu^2_{X^{ac}}\right)
\end{aligned} \tag{7.15}$$

where, ρ_{p^h} and ρ_{q^h} denote the correlation coefficients of active power and reactive power change among the same phase of different actor nodes with h representing the corresponding phase term ($h = \{a, b, c\}$), respectively. $\rho_{p^hq^h}$ denotes the correlation coefficient between the active and reactive power within the same phase. Similarly, $\sigma^2_{p^h}$ and $\sigma^2_{q^h}$ depict the variance of active power and reactive power change, respectively. For random impedance part, μ_{R^k} and μ_{X^k} denote the mean of shared path resistance and reactance between all the nodes and a certain observation node, respectively, with k representing the corresponding self/mutual impedance terms ($k = aa, ab, ac, ba, bb, bc, ca, cb, cc$). It is important to note that all the defined parameters with respect to power change are user defined and usually set based on historical data, whereas, the parameters corresponding to shared path impedance are computed based on the network specifications.

Step 3: *Compute covariance between* $\Delta V^{a,(r,i)}_{OA1}$ *and* $\Delta V^{a,(r,i)}_{OA2}$:

The covariance between the real component of complex voltage change caused by two differ-

ent PVs located at actor nodes $A1$ and $A2$ can be calculated as:

$$\begin{aligned} Cov(\Delta V_{OA1}^{a,r}, \Delta V_{OA2}^{a,r}) &= E(\Delta V_{OA1}^{a,r} \Delta V_{OA2}^{a,r}) - E(\Delta V_{OA1}^{a,r}) E(\Delta V_{OA2}^{a,r}) \\ &= E[\boldsymbol{Z_{A1}^{(a,r)^T}} \boldsymbol{\Delta S_{A1}} \boldsymbol{Z_{A2}^{(a,r)^T}} \boldsymbol{\Delta S_{A2}}] \end{aligned} \tag{7.16}$$

Using equation (7.4), $\boldsymbol{Z^{(a,r)^T}} \boldsymbol{\Delta S}$ can be expanded for both the actor nodes in the following way,

$$\left[\frac{\Delta P_1^a}{|V_1^a|}(-R_{O1}^{aa}) + \frac{\Delta P_1^b}{|V_1^b|}\left(\frac{R_{O1}^{ab}}{2} - \frac{\sqrt{3}X_{O1}^{ab}}{2}\right) + \frac{\Delta P_1^c}{|V_1^c|}\left(\frac{R_{O1}^{ac}}{2} + \frac{\sqrt{3}X_{O1}^{ac}}{2}\right) - \frac{\Delta Q_1^a}{|V_1^a|}X_{O1}^{aa} + \frac{\Delta Q_1^b}{|V_1^b|}\left(\frac{\sqrt{3}R_{O1}^{ab}}{2} + \frac{X_{O1}^{ab}}{2}\right) + \frac{\Delta Q_1^c}{|V_1^c|}\left(-\frac{\sqrt{3}R_{O1}^{ac}}{2} + \frac{X_{O1}^{ac}}{2}\right)\right] \times$$

$$\left[\frac{\Delta P_2^a}{|V_2^a|}(-R_{O2}^{aa}) + \frac{\Delta P_2^b}{|V_2^b|}\left(\frac{R_{O2}^{ab}}{2} - \frac{\sqrt{3}X_{O2}^{ab}}{2}\right) + \frac{\Delta P_2^c}{|V_2^c|}\left(\frac{R_{O2}^{ac}}{2} + \frac{\sqrt{3}X_{O2}^{ac}}{2}\right) - \frac{\Delta Q_2^a}{|V_2^a|}X_{O2}^{aa} + \frac{\Delta Q_2^b}{|V_2^b|}\left(\frac{\sqrt{3}R_{O2}^{ab}}{2} + \frac{X_{O2}^{ab}}{2}\right) + \frac{\Delta Q_2^c}{|V_2^c|}\left(-\frac{\sqrt{3}R_{O2}^{ac}}{2} + \frac{X_{O2}^{ac}}{2}\right)\right]$$

For simplicity, actor nodes $A1$ and $A2$ are denoted by subscript 1 and 2, respectively. Like (7.15), the terms inside the expectation operator is cross multiplied to express covariance,

$$\begin{aligned} &\frac{\rho_{p^a}}{|V_A^a|^2}\sigma_{p^a}^2\mu_{R^{aa}}^2 + \frac{\rho_{q^a}}{|V_A^a|^2}\sigma_{q^a}^2\mu_{X^{aa}}^2 + \\ &\frac{\rho_{p^b}}{|V_A^b|^2}\sigma_{p^b}^2\left(0.25\mu_{R^{ab}}^2 - 0.86\mu_{R^{ab}}\mu_{X^{ab}} + 0.75\mu_{X^{ab}}^2\right) + \\ &\frac{\rho_{p^c}}{|V_A^c|^2}\sigma_{p^c}^2\left(0.25\mu_{R^{ac}}^2 + 0.86\mu_{R^{ac}}\mu_{X^{ac}} + 0.75\mu_{X^{ac}}^2\right) + \\ &\frac{\rho_{q^b}}{|V_A^b|^2}\sigma_{q^b}^2\left(0.75\mu_{R^{ab}}^2 + 0.86\mu_{R^{ab}}\mu_{X^{ab}} + 0.25\mu_{X^{ab}}^2\right) + \\ &\frac{\rho_{q^c}}{|V_A^c|^2}\sigma_{q^c}^2\left(0.75\mu_{R^{ac}}^2 - 0.86\mu_{R^{ac}}\mu_{X^{ac}} + 0.25\mu_{X^{ac}}^2\right) - \\ &\frac{\rho_{p^aq^a}}{|V_A^a|}\sigma_{p^a}\sigma_{q^a}\left(2\mu_{R^{aa}}\mu_{X^{aa}}\right) - \\ &\frac{\rho_{p^bq^b}}{|V_A^b|^2}\sigma_{p^b}\sigma_{q^b}\left(0.86\mu_{R^{ab}}^2 - \mu_{R^{ab}}\mu_{X^{ab}} - 0.86\mu_{X^{ab}}^2\right) + \\ &\frac{\rho_{p^cq^c}}{|V_c^c|^2}\sigma_{p^c}\sigma_{q^c}\left(-0.86\mu_{R^{ac}}^2 - \mu_{R^{ac}}\mu_{X^{ac}} + 0.86\mu_{X^{ac}}^2\right) \end{aligned} \tag{7.17}$$

The correlation coefficients and variances are same as defined in equation (7.15). Now, following the same steps from (7.16) to (7.17), yields corresponding covariance for the imaginary part of voltage change.

Step 4: *Compute mean and variance of* $\Delta V_{OA}^{a,r}$ *and* $\Delta V_{OA}^{a,i}$ *due to randomly distributed multiple actor nodes*:

The mean value of real and imaginary parts of voltage change due to randomly distributed multiple actor nodes are :

$$E[\Delta V_O^{a,r}] = \mu_r = E\sum_{A=1}^{N} \Delta V_{OA}^{a,r} = N\boldsymbol{\mu_{Z_o^r}\mu_{\Delta S}}$$
$$E[\Delta V_O^{a,i}] = \mu_i = E\sum_{A=1}^{N} \Delta V_{OA}^{a,i} = N\boldsymbol{\mu_{Z_o^i}\mu_{\Delta S}} \tag{7.18}$$

Further, the variance of real and imaginary parts of the net voltage change can be expressed as,

$$\mathrm{Var}[\Delta V_O^{a,r}] = \sigma_r^2 = Var\sum_{A=1}^{N}(Z_A^{(a,r)^T}\Delta S) = NVar(\boldsymbol{Z^{(a,r)^T}\Delta S}) + 2\sum_{I<J} Cov(\Delta V_{OI}^{a,r}, \Delta V_{OJ}^{a,r})$$
$$\mathrm{Var}[\Delta V_O^{a,i}] = \sigma_i^2 = Var\sum_{A=1}^{N}(Z_A^{(a,i)^T}\Delta S) = NVar(\boldsymbol{Z^{(a,i)^T}\Delta S}) + 2\sum_{I<J} Cov(\Delta V_{OI}^{a,i}, \Delta V_{OJ}^{a,i}) \tag{7.19}$$

Now, by invoking Lindeberg-Feller central limit theorem, it can be shown that the real and imaginary parts of voltage change follow non zero mean Gaussian distribution with mean and variance as stated in equations (7.18) and (7.19), respectively. As the square of non zero mean Gaussian variable follows non-central chi-square distribution [234], the distribution of the squared magnitude of ΔV_O^a is the sum of dependent non-central chi-square variables.

$$|\Delta V_O^a|^2 \sim \sigma_r^2\chi_1^2(\mu_r^2) + \sigma_i^2\chi_1^2(\mu_i^2) \tag{7.20}$$

where σ^2 and μ^2 are the weight and non centrality parameters of non central chi square distribution with one degree of freedom corresponding to both real and imaginary parts of the voltage change. The sum of weighted non-central chi-square distributions can then be approximated with a scaled non-central chi-square with weight λ, non-centrality parameter

w, and v degrees of freedom as shown below [234]:

$$|\Delta V_O^a|^2 \sim \lambda \chi_v^2(w), \tag{7.21}$$

$$\begin{aligned} \lambda &= \frac{\sigma_r^4\,(1+2\mu_r^2)+\sigma_i^4\,(1+2\mu_i^2)}{\sigma_r^2\,(1+2\mu_r^2)+\sigma_i^2\,(1+2\mu_i^2)} \\ w &= \frac{(\sigma_r^2\mu_r^2+\sigma_i^2\mu_i^2)\,(\sigma_r^2+\sigma_i^2+2\sigma_r^2\mu_r^2+2\sigma_i^2\mu_i^2)}{\sigma_r^4+\sigma_i^4+2\sigma_r^4\mu_r^2+2\sigma_r^4\mu_i^2} \\ v &= \frac{(\sigma_r^2+\sigma_i^2)\,(\sigma_r^2+\sigma_i^2+2\sigma_r^2\mu_r^2+2\sigma_i^2\mu_i^2)}{\sigma_r^2+\sigma_i^2+2\,(\sigma_r^4\mu_r^2)+2\,(\sigma_i^4\mu_i^2)} \end{aligned} \tag{7.22}$$

Since the square root of a non-central chi-square random variables follows a Rician distribution [234], the magnitude of voltage change will follow a Rician distribution:

$$|\Delta V_O^a| \sim Rician(k,\sigma) \tag{7.23}$$

where $k = \sqrt{w}$ and $\sigma = \sqrt{\lambda}$. The magnitudes of voltage changes for other phases follow a similar expression with the respective phase values. If the power variation is assumed to follow a zero-mean Gaussian distribution, which is a typical assumption used in many prior works [52, 240], $\boldsymbol{\mu_{\Delta S}}$ vanishes from the mean (eqn. 7.8) and variance (eqn. 7.12-7.13) equations of voltage change. This eventually leads to zero value for μ_r and μ_i. Again, by invoking Lindeberg-Feller central limit theorem, one can show that the real and imaginary parts of the voltage change follow zero-mean normal distributions as,

$$\Delta V_O^{a,r} \overset{D}{\sim} \mathcal{N}(0,\sigma_r^2), \qquad \Delta V_O^{a,i} \overset{D}{\sim} \mathcal{N}(0,\sigma_i^2) \tag{7.24}$$

The square of the magnitude of voltage change follows a gamma distribution [228], and subsequently, the magnitude of voltage change follows a Nakagami distribution [241],

$$|\Delta V_O^a| \sim Nakagami(m,\omega), \tag{7.25}$$

where parameter $\theta = 2(\sigma_r^4 + \sigma_i^4 + 2c^2)/(\sigma_r^2 + \sigma_i^2)$, shape parameter $m = (\sigma_r^2 + \sigma_i^2)/\theta$, scale parameter $\omega = \sqrt{m\theta}$, and c being the covariance between the real and imaginary parts of voltage change. In the next sections, the proposed ST-PVSA method is first validated using simulations, and then it is employed to estimate PV HC in a efficient manner.

7.1.3 Validation of ST-PVSA

The proposed probability distribution of the voltage change is validated on the modified IEEE 37-node test system. The nominal voltage of the test system is 4.8 kV. The actual distribution of the magnitude of the voltage change is obtained using Newton-Raphson based sensitivity analysis method, and the theoretical distribution is obtained using the proposed method of ST-PVSA. A scenario is considered for simulation where 9 PV units are located at random locations in the distribution system. The power at the actor nodes, i.e., the nodes injected with PVs, varies randomly due to fluctuations in PV generation. For illustration, 9 actor nodes are chosen where change in PV generation at a particular time instant is modeled as a zero mean Gaussian random variable. However, ST-PVSA is valid for any number of actor nodes with any arbitrary distribution of power variation. Typically, unbalance in the distribution system is caused by single phase loads. Therefore, unbalance in our experiments is achieved by employing single-phase and two-phase loads in the standard three-phase test networks. The base loads are the same as provided in the distribution system analysis sub-committee report [242]. Unbalance can also be induced by unequal power change across different phases of the system. However, the magnitude of power change needs to be strong enough which also depend on the base loads. The covariance matrix $\sum_{\Delta S}$ captures the spatial correlation of PV generation, which exists because of geographical proximity as PVs in the same region typically exhibit same generation profile. The diagonal elements of the covariance matrix contain variances that depend on the size of PV units and the off-diagonal elements capture the effect of geographical proximity of these PV units. In our simulation, the variance of change in real power (ΔP) is set to 5 kW and the variance of change in reactive power (ΔQ) is set to 0.5 kVar. The values of the correlation coefficients ρ_{p^h}, ρ_{q^h} and

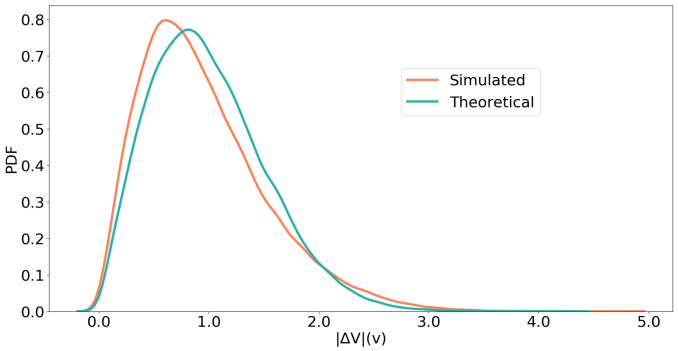

Figure 7.2: Distribution of voltage change at node 9

$\rho_{p^h q^h}$ are set to 0.2, 0.2, and -0.5, respectively for all the phases. Variance can be set to zero for nodes with no PVs. Now, for random impedance part, the mean and variance of resistance and reactance between random actor node and observation node 9 is calculated from data of the IEEE 37-node test system. The value of correlation coefficient between resistance and reactance is 0.99. Fig. 7.2 compares the actual distribution of the magnitude of voltage change with the proposed ST-PVSA case. The actual distribution of ΔV_9 is obtained by randomly varying powers of all actor nodes at phase-a and subsequently, voltage change at node 9 is computed by using Newton-Raphson based method. Further, Monte-Carlo simulations (MCS) are incorporated to capture the uncertainties associated with the power changes. Here, voltage changes are computed for one million MCS. The scaled histogram of $|\Delta V_9|$ is depicted through the orange curve in the Fig. 7.2. The theoretical distribution computed with equations (7.18) and (7.19) is shown by blue curve in Fig. 7.2. It can be observed that the probability distribution computed using the proposed method is very close to the actual simulated distribution with 0.18 as Jensen-Shannon distance. Further, the execution time of our method to calculate the voltage change distribution in both the 37-node and 123-node networks are within 1 min, whereas the time exceeds 120 min in the classical load flow based method. Thus, ST-PVSA is order 2 faster compared to the conventional approach. This experiment demonstrates the effectiveness of the proposed ST-PVSA approach.

7.1.4 ST-PVSA for PV hosting capacity

This section presents the methodology for computing HC with the proposed ST-PVSA approach. As ST-PVSA provides the probability distribution of voltage change at a node due to random power changes at random locations of the network, it suffices to identify voltage violations for different PV penetration levels. The procedure to determine HC begins with fixing the number of penetration levels say from 1% to 100% level at an increment of 1%. Then, the number of PV units (N_k) that need to be integrated for each penetration level is computed using eqn. (7.26). N_k is determined statistically based on the distribution of real PV sizes. The size of actual PV installations in the state of California, USA is collected from the California dataset [243]. Figure 7.3 depicts the scaled histogram of PV sizes which approximately follows a gamma distribution. The penetration level is divided into various bands based on the percentage of total demand. For instance, k varies from 1 to 5 for 5 bands, i.e., $(0-20\%), (21-40\%)$ ... $(81-100\%)$. A unique N_k is defined for each band such that the same number of PV units is used for all penetration levels in that particular band. In each band k, the power injection increases with the increasing penetration levels at N_k random locations. This is logical in a sense that it is not necessary to increase the number of PV units for simulating increasing penetration level rather it can be achieved by increasing the power injection in the existing PVs. However, the power injections cannot be increased beyond a certain limit due to the restriction of PV size. Therefore, N_k increases as we move to the higher penetration band. N_k for a particular penetration band k is computed as following:

$$N_k = \frac{\text{Mean penetration level for band } k}{\text{Max PV size}} \tag{7.26}$$

where "Max PV size" comes from the PV size distribution and the mean penetration level is the average power injection for band k. In the third step, N_k is used to obtain the mean ($\mu^l_{\Delta S}$) of power change vector ΔS (eqn. 7.4) for each penetration level l, such that $\mu^l_{\Delta S} N^l \approx P_l$. Here, P_l and N^l are the net power injection and PV units for penetration level l, respectively. The complex voltage change due to power injection is added to the base voltage to get the future voltage. Following the same arguments as mentioned in Theorem

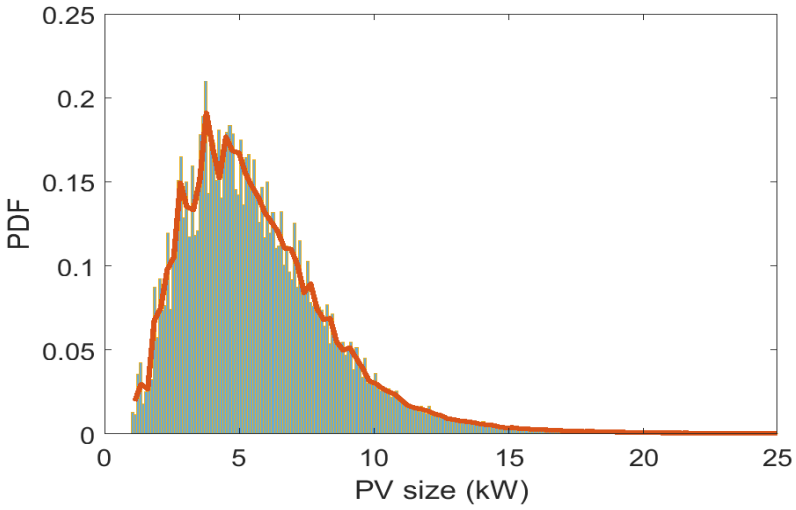

Figure 7.3: Distribution of PV sizes from california dataset

2 of [10], the distribution of future voltage is shown to follow Rician with the parameters as defined in equation (7.22). The mean of real (μ_r) and imaginary (μ_i) parts of voltage change (7.18) are added to the corresponding parts of base voltage to get the mean value of the future voltage. The mean future voltage is then plugged in the derived eqn. (7.23) to find the distribution of future voltage at all nodes of the network. Nodes that have a probability of voltage violation greater than the threshold are classified as highly vulnerable nodes, and violations are reported. For illustration, a violation is recorded when the probability of voltage violations is more than 0.5. 0.5 is unbiased and gives equal preference to both detection and non-detection of violations. The complete process is repeated for increasing penetration levels until the algorithm encounters the first violation. The corresponding penetration level is the HC of the system. "First voltage violation" refers to the situation when we observe voltage violations in the system for the very first time while increasing the PV penetration level. In this work, the minimum penetration level for which the violation is observed for the first time is considered as the hosting capacity. Algorithm 1 provides the pseudo-code of ST-PVSA approach to compute HC.

To evaluate the performance of ST-PVSA in determining the HC, load flow based HC is used as a benchmark. Similar to the ST-PVSA approach, the PV penetration level is fixed from 1% to 100% level at 1% increment. For each penetration level, Monte Carlo

Algorithm 1 Proposed ST-PVSA method to compute Hosting capacity

1: Fix number of penetration levels $(1, 2, ...100\%)$
2: Calculate number of PVs for a particular penetration level using equation (7.26).
3: Compute mean and variance of power change vector corresponding to a particular penetration level.
4: Use ST-PVSA to compute node voltages and track total number of voltage violations.
5: Repeat steps 2 to 4 for different penetration levels.
6: The penetration level that causes first voltage violations is the hosting capacity.

simulations are repeated $10k$ times thereby creating one million different PV deployment scenarios. For illustration purposes, the loads on the test network are chosen as reported in the IEEE PES distribution system analysis subcommittee report [242] . However, the proposed method is generic enough to accommodate other loading scenarios such as daytime (10 am-2 pm) maximum load and daytime minimum. Finally, for each penetration level, N_k locations are selected randomly to allocate PV units and load flow is executed to track the voltage violations. For IEEE 37-node network, the number of PV units for each of the five penetration level bands are $5, 10, 20, 25$ and 30. The power is increased from 10 kW (1% penetration level) to 1100 kW (100% level) in steps of 11 kW. Fig. 7.4 depicts the variation of violations count with increasing penetration levels. It can be observed that the proposed STPVSA approach is 100% accurate in estimating HC of IEEE 37-node test network. In other words, the penetration level predicted by ST-PVSA aligns well with those computed from the load flow based approach (i.e., lies within the range of load flow based HC values). Further, to demonstrate the scalability of the proposed method, the HC analysis is also validated on the IEEE 123-node system.

Table 7.1 presents the HC values computed with the proposed ST-PVSA based approach and existing load flow-based method for a various number of scenarios. It is worth noting that for each PV penetration level, ST-PVSA needs to be run once (independent of scenarios), whereas multiple simulations are required for convergence in the load flow-based approach. For the IEEE-37 node network, ST-PVSA yields a HC of 33% which lies in the range of values computed with load flow based approach. Similarly, for the IEEE-123 test network, the ST-PVSA based HC value is 39%, which again intersects with that of load flow's approach.

Furthermore, the proposed approach is also evaluated for a balanced load case in the IEEE 37-node test system. The estimated value of HC turns out to be 41%, whereas 42% is obtained with 30k simulations in the conventional approach. This demonstrates the generalizability of our method. Additionally, HC seems to decrease for an unbalanced case compared to a balanced one although all the factors (power change and network parameters) remain unchanged. This is because of non-uniformity in voltages across the buses which increases the probability of extreme voltages leading to violations in a relatively earlier stage compared to a balanced load scenario.

Along with the high estimation accuracy, ST-PVSA offers a significant advantage in terms of computational complexity. Table 7.2 represents the execution time of scenarios simulated in 7.1 for the two test networks. All experiments are conducted in a machine with an Intel-i7 processor and 16 Gb RAM. It can be inferred from Table 7.2 that in IEEE 123-node test network, the ST-PVSA is three orders faster than the load flow-based approach, and the gap will further increase as the network size grows.

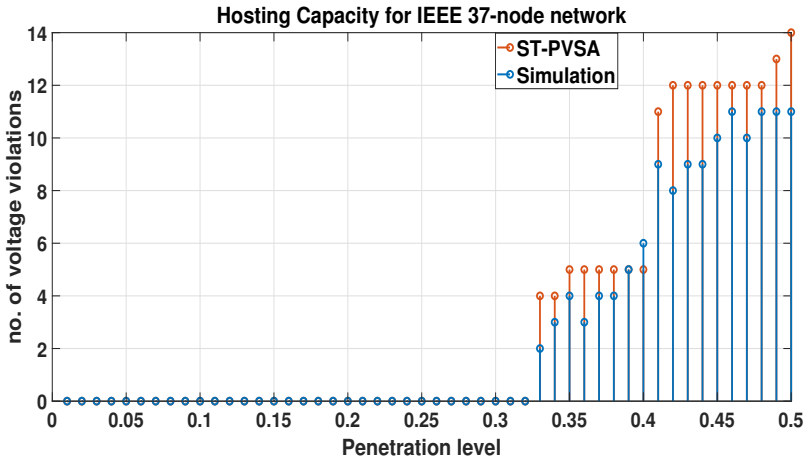

Figure 7.4: Variation of violations count with Penetration levels

The above-discussed experiments demonstrate the efficacy of ST-PVSA for a typical snapshot type HC. Further, it will be more effective for a dynamic HC, which is relatively a new way of analyzing HC of distribution systems. Dynamic HC is not based on worst-case snapshot power flows. It requires probabilistic screens that consider the uncertainty around the time-series input variables, like hourly PV productions and building loads. Power flow

Table 7.1: Hosting capacity with Load flow and ST-PVSA

Test Network	Scenarios*	1k (%)	10k (%)	30k (%)	40k %	50k %	60k%
IEEE 37	Load Flow	33	32	31	31	31	31
	ST-PVSA	33					
IEEE 123	Load Flow	44	43	42	41	40	40
	ST-PVSA	39					

Table 7.2: Execution time with Load flow and ST-PVSA

Test Network	Scenarios*	1k (min)	10k (min)	30k (min)
IEEE 37	LF	1.93	18.8	55.7
	ST-PVSA	1.13		
IEEE 123	LF	43.93	400.2	1195.6
	ST-PVSA	3.91		

analysis is conducted on large time-series data of load and PV on an hourly basis. For a real distribution model with thousands of nodes and one-second resolution data, simulations could take a few days [79]. Furthermore, the PV and load uncertainties have significant influences on hosting capacity values. Under this type of dynamic analysis, the proposed approach could work very efficiently by accurately capturing voltage violations in an acceptable amount of time. The performance of ST-PVSA in dynamic HC will be investigated as part of our future work.

7.2 Probabilistic EV charging station planning

The proposed EV charging station planning technique is summarized in this section. First, the system model is described then the theoretical formulation of the probabilistic allocation (considering power losses and voltage deviation) is presented. A flowchart of the proposed approach is shown in Fig. 7.6. As can be seem from the figure, it is assumed that topology information, e.g., voltage profiles, nodal complex power changes, and line parameters, is available, which is then used within the probabilistic allocation framework. Though, if measurements are not available, one can use sparsity-based state estimation techniques to approximate system states. Additionally, it is assumed that charging stations can be integrated at any node in the system with equal probability. Based on the allocation results,

EV charging station size is optimized via a quadratic optimization framework to ensure all EV demand is met.

7.2.1 System model

Consider a hypothetical three-phase unbalanced distribution system with $\mathcal{N}$ nodes and $\mathcal{L}$ lines as shown in Fig. 7.5. The increase in active power demand due to EV charging station placement at any node in the system causes increase in current flow and drop in voltage magnitude. To quantify this impact, one can use analytical sensitivity approximations given their computational efficiency and high accuracy compared to classical sensitivity methods [20, 26]. Specifically, a change in complex power at any node $A \in \mathcal{N}$ from S_A to $S_A + \Delta S_A$ results in voltage and current flow changes, i.e., ΔV_O and ΔI_M. Here, $O \in \mathcal{N}$ and $M \in \mathcal{L}$ are nodes and lines where the change in voltage and loss are monitored, respectively. For example, integrating a charging station at node 2 with a rating of ΔP_2 leads to a positive increase in the current flow to the destination by ΔI_{3-2} as highlighted in green color in Fig. 7.5, which causes an increase in line losses (ΔL_{0-2}). Additionally, voltage at the destination node changes by ΔV_2. Note that due to the radial structure of the system, current flow at other lines, e.g., ΔI_{0-3}, and ΔI_{3-2}, change due to ΔP_2 at node 2 and similarly the voltage changes at other nodes, e.g., ΔV_3, ΔV_4 as highlighted by the red lines in Fig. 7.5. Power change due to EV activity is uncertain, which can lead to abrupt fluctuations in voltage profiles and power losses. Therefore, to account for this random behavior, we adopt a probabilistic framework to capture the change in losses and voltage profiles.

7.2.2 Allocation via probabilistic sensitivity analysis

Based on the proposed system model, the main objective in this section is to find EV charging station location that results in the least active power losses and voltage deviations. Specifically, let ΔL_t^r be the change in system active losses and $|\Delta V_t|$ the magnitude of aggregate voltage change across all nodes, then the γ is the location that minimizes ΔL_t^r

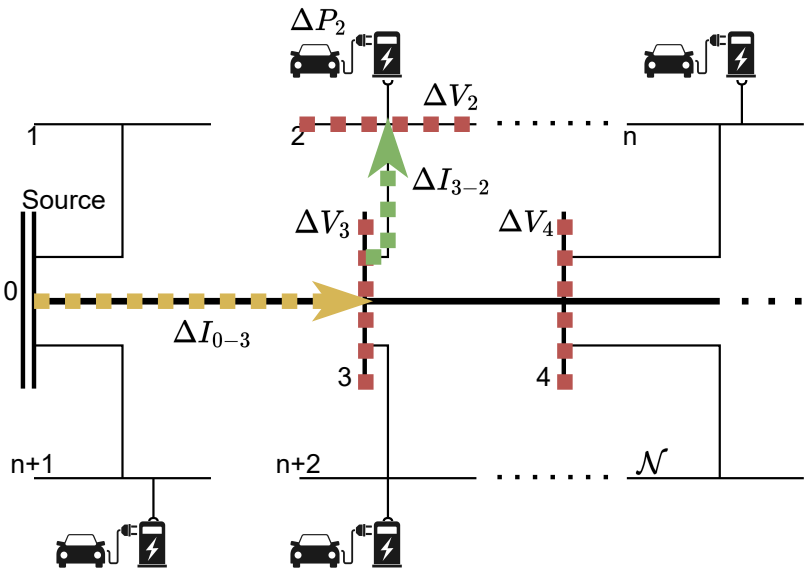

Figure 7.5: Illustration of a hypothetical power distribution system.

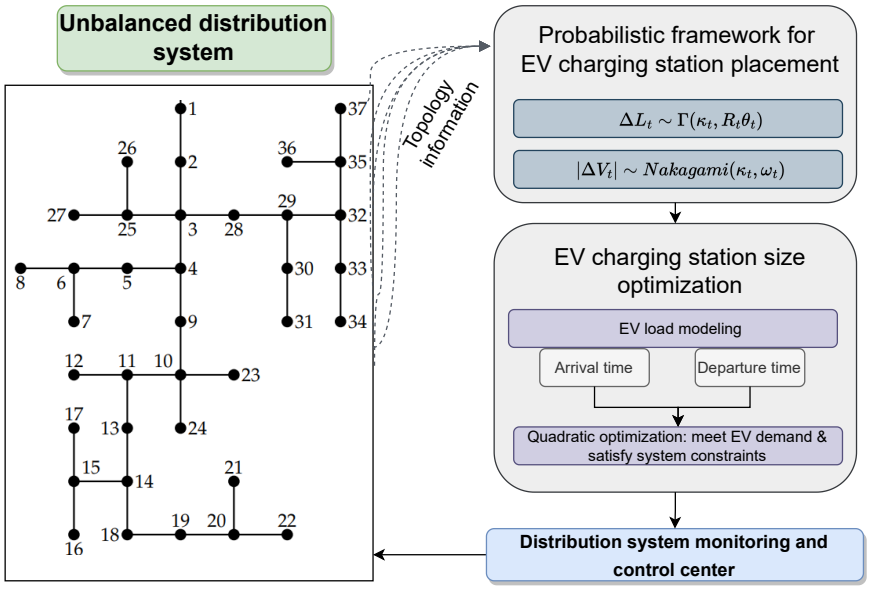

Figure 7.6: Flowchart of the proposed approach.

and $|\Delta V_t|$, i.e.,

$$\gamma \triangleq \underset{n}{argmin}(\Delta L_t^n, |\Delta V_t^n|) \; \forall n \in \mathcal{N} \tag{7.27}$$

$$\text{s.t.} \quad \Delta P_n \sim \textbf{Unif}\,[P_{min}, P_{max}\text{kW}] \tag{7.27a}$$

For every possible location $n \in \mathcal{N}$, EV charging station is integrated and the resulting probability distributions of change in voltage and active power losses are evaluated. P_{min} and P_{max} represent the minimum and maximum kW rating of the desired charger, e.g., 1-5 kW for level-1 charger or 5-20 kW for a level-2 charger. This probabilistic framework models EV load as a random variable and derives the resulting probability distribution of change in line losses as well as the magnitude of voltage change. Specifically, for any unbalanced distribution system, the vector of change in active and reactive power at all nodes, i.e., $\boldsymbol{\Delta S} \triangleq [\Delta P_1, \Delta P_2, ..., \Delta P_{\mathcal{N}}, \Delta Q_1, \Delta Q_2, ..., \Delta Q_{\mathcal{N}}]^T$, can be modeled as a random vector with zero mean and a covariance structure $\boldsymbol{\Sigma_{\Delta S}}$. The elements of $\boldsymbol{\Sigma_{\Delta S}}$ contain variance and cross covaraince of active and reactive power changes at different nodes in the system. Elements where nodes are not integrated with a charging station can be set to zero. This covariance matrix can be computed based on historical data or using hypothetical measurements [20]. Given this random power change, the probability distribution of voltage deviation at any node (O) in the system follows a Nakagami distribution [72],

$$|\Delta V_O| \sim Nakagami(k, \omega) \tag{7.28}$$

with shape and spread parameters $k \triangleq (\sigma_r^2 + \sigma_i^2)/\theta$ and $\omega \triangleq \sqrt{k\theta}$, respectively. Here, $\theta \triangleq 2(\sigma_r^4 + \sigma_i^4 + 2c^2)/(\sigma_r^2 + \sigma_i^2)$. Note that the terms σ_r^2, σ_i^2, and c are related to the covariance matrix $\boldsymbol{\Sigma_{\Delta S}}$ and topology information vectors $\mathbf{C_r}$ and $\mathbf{C_i}$, e.g., $\sigma_r^2 \triangleq \mathbf{C_r}^T \boldsymbol{\Sigma_{\Delta S}} \mathbf{C_r}$, $\sigma_i^2 \triangleq \mathbf{C_i}^T \boldsymbol{\Sigma_{\Delta S}} \mathbf{C_i}$, and $c^2 \triangleq \mathbf{C_r}^T \boldsymbol{\Sigma_{\Delta S}} \mathbf{C_i}$. Further details on proof and on topology information vectors can be found in [72]. Similarly, given the covariance structure $\boldsymbol{\Sigma_{\Delta S}}$, it is possible to compute the distribution of change in active power losses (ΔL_M^r) at line M, which is shown to follow a Gamma distribution in [20],

$$\Delta L_M \sim \Gamma(k, R_M\theta) + 2R_M(I_M^* \Delta I_M). \tag{7.29}$$

With shape and scale parameters k and θ, respectively. R_m represents the resistance of line M, I_M^* is the complex conjugate of current flow through line M, and ΔI_M is the change in

current passing through line M. Note that the topology information vectors used to derive Eq. (7.29) are different from Eq. (7.28) as shown in [20]-Eq. (27). Since I_M is a deterministic quantity whereas ΔI_M is random. Therefore, by taking the mean of th term $2R_M(I_M^* \Delta I_M)$, Eq. (7.29) can be rewritten as,

$$\Delta L_M \sim \Gamma^{'}(k, R_M \theta) \tag{7.30}$$

where, $\Gamma^{'}$ is the shifted Gamma distribution. However, Eq. (7.30) provides the distribution of change in losses for a particular line M. To quantify the impact of EVCS placement on total system losses, the aggregate distribution of change in losses caused by all line segments ($\mathcal{L}$) must be added. This can be computed by deriving the distribution of total change in current flow through the system. Thus, considering all line segments $l \in \mathcal{L}$, the aggregate variance of change in real and imaginary parts of current flow $(\sigma_{r,t}^2, \sigma_{i,t}^2)$ as well as their correlation (c_t) can be computed as the sum of variances of individual line segments, i.e.,

$$\sigma_{r,t}^2 = \sum_{l \in \mathcal{L}} \sigma_{r,l}^2, \sigma_{i,t}^2 = \sum_{l \in \mathcal{L}} \sigma_{i,l}^2, \text{ and}, c_t = \sum_{l \in \mathcal{L}} c_l. \tag{7.31}$$

By invoking Lindeberg-Feller central limit theorem, the distribution of total change in real and imaginary parts of current flow converges to a multivariate Gaussian,

$$\begin{bmatrix} \Delta I_{r,t} \\ \Delta I_{r,i} \end{bmatrix} \sim \mathcal{N}\left(\mathbf{0}, \begin{bmatrix} \sigma_{r,t}^2 & c_t \\ c_t & \sigma_{i,t}^2 \end{bmatrix} \right) \tag{7.32}$$

By computing the distribution of squared magnitude of change in current $|\Delta I_t|^2 \triangleq \Delta I_{r,t}^2 + \Delta I_{i,t}^2$, the distribution of change in system loss converges to a Gamma distribution,

$$\Delta L_t \sim \Gamma^{'}(k_t, R_t \theta_t). \tag{7.33}$$

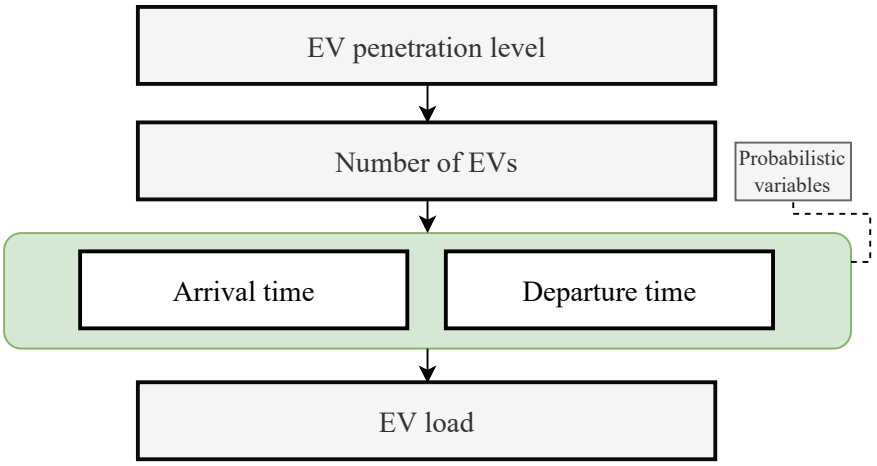

Figure 7.7: EV load modeling.

Here, $k_t \triangleq (\sigma_{r,t}^2 + \sigma_{i,t}^2)/\theta_t$ and $\theta_t \triangleq 2(\sigma_{r,t}^4 + \sigma_{i,t}^4 + 2c_t^2)/(\sigma_{r,t}^2 + \sigma_{i,t}^2)$. Similarly, one can compute the distribution of total change in voltage for all nodes as,

$$|\Delta V_t| \sim Nakagami(k_t, \omega_t) \tag{7.34}$$

where, $\omega_t \triangleq \sqrt{k_t \theta_t}$. Notice that the support set of both Gamma and Nakagami distributions is $x > 0$. The allocation results obtained via Eq. (7.27) are used in the next section to optimize the size of charging stations.

7.2.3 Size optimization of charging stations

The EV load in this section is based on a probabilistic EV arrival and departure model over a time period of 24 hours as shown in Fig. 7.7. First, the EV penetration level and number of EVs are specified. In this section, the type of EV charger is chosen as a 240-volt standard level-2 charger with a power output rating of 5-20 kW. Then, the number of present EVs at every hour is estimated based on their arrival and departure probabilities. It is assumed that EVs are plugged-in over the entire time period between arrival and departure times, which approximates the vector of EV loads at every time step, $\mathbf{d}_{ev}$. Based on this setup, it is possible to construct a quadratic formulation that computes the optimal sizes of charging

stations while satisfying system constraints,

$$\min_{\mathbf{\Delta p}} \; ||\mathbf{\Delta p} - \mathbf{d}_{ev}||_2 \tag{7.35}$$

$$\text{s.t.} \quad \mathbf{v}_{min} \leq \mathbf{v}_0 + \mathbf{B}\mathbf{\Delta p} \leq \mathbf{v}_{max} \tag{7.35a}$$

$$\mathbf{P} + \mathbf{\Delta p}_{min} \leq \mathbf{\Delta p} \leq \mathbf{P} + \mathbf{\Delta p}_{max} \tag{7.35b}$$

$$|\mathbf{C}\mathbf{\Delta p}| \leq \mathbf{I}_{max} \tag{7.35c}$$

Here, $\mathbf{v}_0$ is the vector of initial voltage magnitude of all nodes and $\mathbf{v}_{min}$ and $\mathbf{v}_{max}$ are the vectors of upper and lower bounds on voltage, respectively. $\mathbf{B}$ is the voltage sensitivity matrix with respect to active power changes and $\mathbf{\Delta p}_{min}$ and $\mathbf{\Delta p}_{max}$ are the limits on nodal active power changes. This constraint is kept to prevent abrupt power changes while taking into account the base active power demand vector $\mathbf{P}$. Constraint 7.35c prevents line overloading where $\mathbf{C}$ is the current flow sensitivity matrix with respective to active power changes and $\mathbf{I}_{max}$ is the vector of maximum current flow.

7.2.4 Simulation results

This section validates the proposed probabilistic approach for EV charging station planning. The effectiveness of the probabilistic method is verified via simulation on the unbalanced IEEE 123-node test system. The test system is divided into multiple service regions according to the Thiessen polygons theorem [94]. This theorem divides the network into multiple regions where EVs are within a reachable distance to the charging station in every region as shown in Fig. 7.8. Next, we use Eq. (7.27) to determine nodes with least contribution to

Table 7.3: Distribution parameters for select nodes.

Node	**Nakagami parameters**		**Gamma parameters**	
	Shape	Spread	Shape	Scale
35	0.9781	5.0485e-6	0.7187	0.1675
36	0.9008	8.1120e-6	0.7187	0.1955
37	0.9659	9.1895e-6	0.7187	0.2236

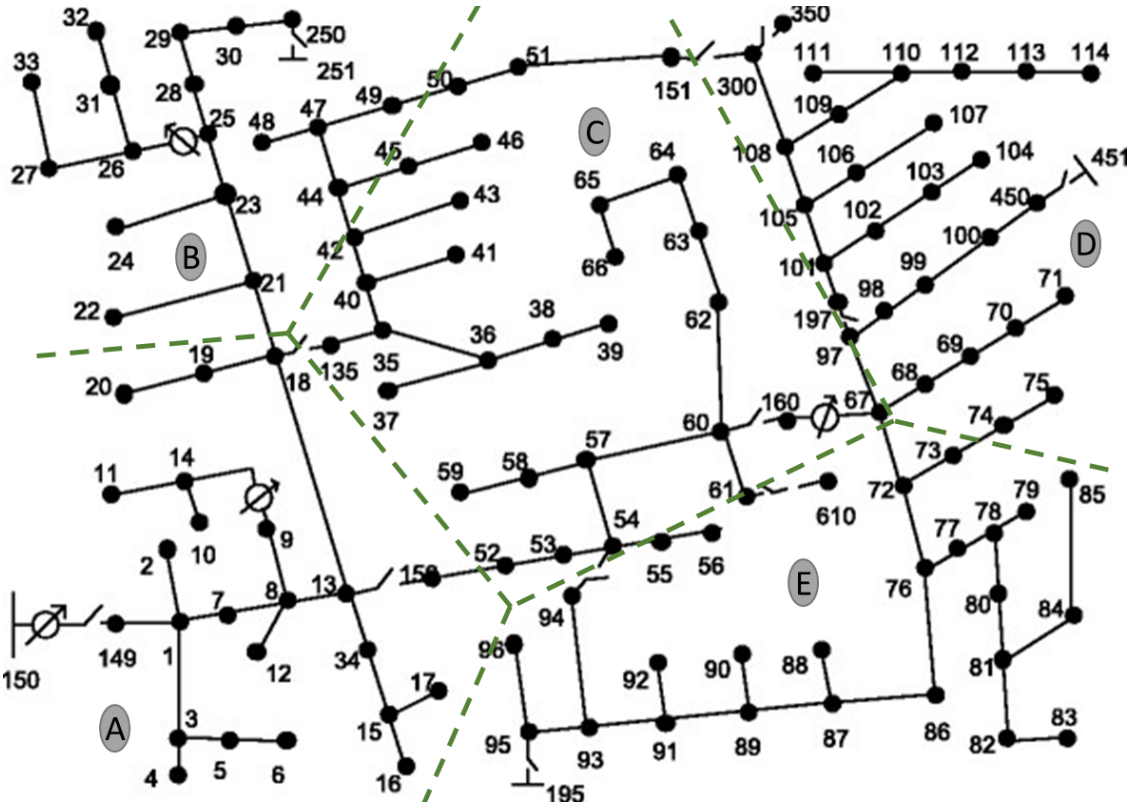

Figure 7.8: Modified IEEE 123-node test system indicating service regions.

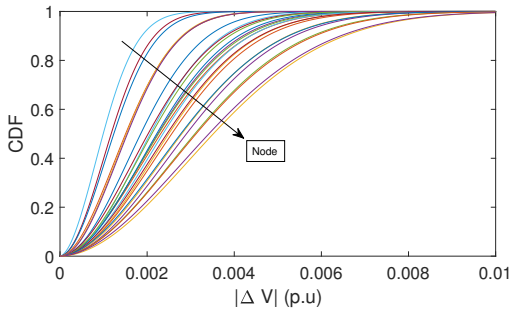

Figure 7.9: Cumulative density function for voltage change due to different nodes.

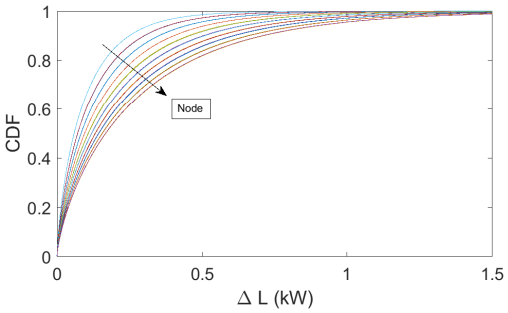

Figure 7.10: Cumulative density function for loss change due to different nodes.

total system losses and voltage deviations. For this, the parameters of Nakagami and Gamma distributions are computed for every candidate location of EV charging station for all regions. For example, Table 7.3 shows the parameters of the Nakagami and Gamma distributions for 3 different nodes in region C. Note that the shape parameters of the Gamma distribution are same for the three nodes and that is because the size of EV charging, i.e., 10 kW, is set to be equal for all the analyzed nodes within every service region, which is done to ensure

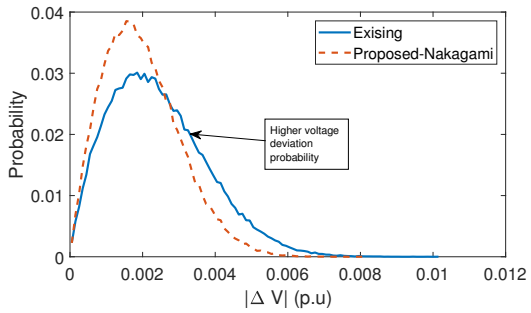

Figure 7.11: Probability distribution of change in voltage.

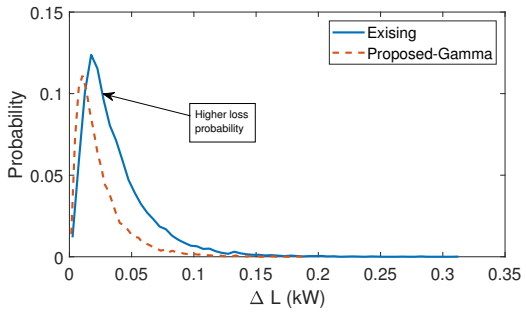

Figure 7.12: Probability distribution of total system losses.

fair comparative analysis. Since the impact of each node is analyzed individually using these parameters, the shape parameters will be equal for all nodes. On the other hand, the scale parameters are different for all nodes as can be seen from Table 7.3, which determines the influence of each node on total system losses. This trend is different with the distribution of voltage deviation, i.e., the shape parameter of Nakagami distribution in Table 7.3. It can be seen that the shape parameters are different, which is due to the difference in mutual path impedance of the analyzed nodes despite having equal size of EV charging station. More information on these topology parameters can be found in [20] and [72]. It is possible to evaluate the CDF for every individual node and examine its impacts on the change in losses and voltage deviation. To evaluate the CDF for different nodes, we choose a support set of

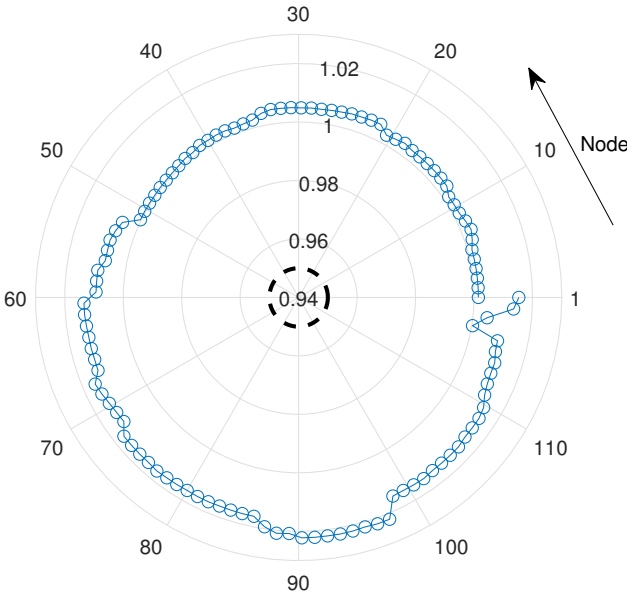

Figure 7.13: Voltage profiles with optimized EV charging station sizes.

[0 0.1] p.u with 0.001 steps for the distribution of voltage deviation whereas a support set of [0 1.5] kW has been used for the distribution of change in losses. Figures 7.9 and 7.10 show the CDF plots of the change in losses and voltage deviation for all nodes in service region C. It turns out that node 35 (whose CDF is shown in blue color for both cases) is the node that contributes the least to power loss and voltage deviation. This result is consistent with the radial structure of the distribution system where the closer the node to the substation, the less impact it will have on voltage deviation, hence resulting in less losses. While this can be trivial for small systems, the analysis can be complex for practical systems with a very large number of nodes, especially when there is a high penetration levels of DERs such as PV that counteract the effect of increased EV load. The procedure is repeated for all service regions and the optimal locations are found to be $[1, 21, 35, 68, 55]$. Next, we compare the performance of the proposed approach in terms of reducing the impacts on system parameters. Specifically, we compare the distribution of power loss and voltage deviation resulting from the proposed approach compared to the case when EV charging stations are placed in the center of service regions, i.e., $[2, 31, 39, 107, 87]$. Figures 7.11 and 7.12 show a comparison of the resulting probability distributions. It can be seen that using the proposed approach results in lower losses as well as voltage deviations.

Finally, the size of the charging stations is optimized using the quadratic formulation in Eq. (7.35). It is assumed that there are $[500, 200, 600, 500, 300]$ EVs at each service region, respectively. The arrival and departure times of EVs are modeled according to the generalized extreme value distribution with parameters, $\zeta = 0.0629, \sigma = 0.5492, \mu = 8.9068$ and $\zeta = -0.2821, \sigma = 1.1106, \mu = 16.4070$, respectively [99]. The upper and lower voltage limits in Eq. (7.35) are kept as [0.95 1.05] p.u whereas $\mathbf{I}_{max}$ and $\mathbf{\Delta p}_{min,max}$ kept as 10 Amps and [0 5000] kW, respectively. After solving the quadratic formulation in *Eq.*(7.35), the corresponding sizes of EV charging stations turns out to be [2377.0 950.8 2775.8 2085.7 830.7] kW. It is important to note that line current flows and nodal voltages are kept within the specified operational limits. For example, Fig. 7.13 shows the voltage magnitude of all system nodes after the charging stating sizing procedure. It can be seen that the voltage magnitudes are all above 0.95 p.u, which ensures safe operation of the system. Therefore,

the proposed approach can be used for efficient planning of EV charging stations without sacrificing system reliability.

7.3 Summary

This chapter presents an analytical approach to compute the probability distribution of voltage change at a particular node due to Spatio-temporal uncertainties. The proposed approach is validated with a conventional load flow based approach in two different test systems namely the IEEE 37 and IEEE 123. The estimated probability distribution matches with the baseline to a high degree of accuracy (as demonstrated with a low Jensen-Shannon distance of 0.18). Our method is fairly accurate in identifying the hosting capacity and offers huge advantage in terms of computational efficiency. In the IEEE 123-node test system, the proposed method is two orders faster compared to conventional load flow based approach and this gap will further increase as the network size grows. In addition, this chapter analyses the impact of Spatio-temporal uncertainties of EV charging station placement on total system losses and voltage deviations. The proposed approach approximates the change in total system losses due to charging station placement as a Gamma distribution, with well defined shape and scale parameters, and the distribution of total voltage deviation as a Nakagami distribution. With this information, the IEEE 123-node test system is divided into multiple service area whose impact on system's performance can be analyzed separately. Next, the arrival and departure times of EVs for each area is modeled using the generalized extreme value distribution, which allows computing the expected EV demand. Finally, the size of charging stations is computed based on a quadratic optimization framework that ensures safe operational limits of system constraints. Results show that the proposed approach helps significantly reduce power losses and voltage deviations compared to the case when charging stations are randomly placed in the service areas. The developed Spatio-temporal analysis in this chapter serves as a key enabler of identifying the maximum allowable limit of DERs/EV integration at which the system requires control algorithms to mitigate voltage violations as discussed in Chapter 8.

Chapter 8

Inverter-based DER control for improved voltage stability margin

The variability in DER injection (e.g., fluctuations in PV power outputs due to climate conditions) and the randomness associated with EV user charging patterns may cause voltage violations that are difficult to eliminate using classical voltage control devices such as tap changers and capacitor banks [120]. Given predicted voltage violations using the probabilistic framework in Chapter 6, it is possible to prevent these violations by adjusting the setpoints of inverter-based DERs in the system. For example, several research efforts attempt to address the possibility of real-time voltage control with the via inverter-based DERs within a model predictive control (MPC) setup [111, 244, 245]. However, these MPC based methods assume full availablility of system measurements, which may not hold promise in practical setups due to the lack of measurements. This issue can be solved by installing measurement devices at all nodes in the system. Nevertheless, this solution creates additional stress on the communication infrastructure and will also require huge installation costs, especially for large systems [145]. Therefore, the aim of the first part of this chapter is to address these limitations by proposing a new MPC based method for optimal voltage control in low-observable distribution systems with the presence of PV injections. Unlike existing literature, this work does not assume full availability of state measurements at all nodes and uses matrix

completion (MC)-based approach to estimate missing states. Another challenge that faces system operators is that the rapid growth in DER integration makes it difficult to identify the most suitable locations to include in their voltage control programs. This is because using a large number of control points is not practical [246]. Additionally, using large number of DERs for control increases the communication requirements between utility and field controllers, which in turn can increase their vulnerability to cyber intrusions [12]. Therefore, to fully harness the potential of inverter-based DERs in voltage control programs, there is a need for new frameworks that identifies strategic control locations while ensuring safe voltage margins. Thus, the aim of the second part of this chapter is to address these research gaps by providing a general framework that utilizes the control participation factors (CPFs) of nodes integrated with inverter-based DERs to identify the optimal set of nodes that participate in the control program, which we refer to in this dissertation as the *system voltage influencer* set (SVI). Inspired by the DIVF approach [32], the SVI set in this paper contains the most dominant nodes that influence voltage fluctuations across the entire system. We show in this paper that, using the SVI set for voltage control applications via inverter-based DERs provides, (1) faster execution time than using all DERs for control, (2) significantly lower control cost compared to the same number of non-SVI controllers; and (3) high robustness against uncertainty of complex power changes, which can be due to loads or DER injections.

8.1 Voltage control in low-observable systems

The proposed control technique is summarized in Fig. 8.1 whose functional blocks are detailed in this section. This section is organised as follows: First, the formulation for MC based state estimation (SE) is presented. In the second subsection, it is shown how the estimated states are utilised in the MPC for voltage regulation across the network. The final part of this section details the voltage sensitivity analysis (VSA) which is utilised in the control algorithm for the prediction process. For developing the proposed technique, it is assumed that measurements of the distribution system are available at a small subset of nodes with the help of supervisory control and data acquisition (SCADA) system, PV units

with available active power injection forecasts (p^f) and a set of Var compensators at PV locations. Additionally, PV inverters are assumed to operate at a maximum power point tracking mode.

8.1.1 Matrix completion based state estimation

Consider an N-node three phase unbalanced distribution system where the measurements are only available at the nodes given by set ψ. It is considered that with the measurements taken at the nodes ψ, the system is not observable. In the measured nodes, the three phase values of voltage magnitudes, active and reactive power values are measured. Hence in total, 9 measurements are taken in each measurement node. To illustrate the MC technique, $\mathbf{X} \in \mathbb{R}^{(N-1)\times 15}$ is considered as the complete matrix to be computed for the nodes other than slack bus. For this complete matrix $\mathbf{X}$, its elements corresponding to row j is defined as

$$\mathbf{X}_j = \begin{bmatrix} \mathbf{e}_j^{abc} & \mathbf{f}_j^{abc} & |\mathbf{v}|_j^{abc^2} & \mathbf{c}_j^{abc} & \mathbf{d}_j^{abc} \end{bmatrix} \tag{8.1}$$

The superscript abc indicate the defined variables are accounted for all the three phases of the network. The variables $\mathbf{e}_j$, $\mathbf{f}_j$ and $|\mathbf{v}|_j$ denote the real, imaginary and the absolute

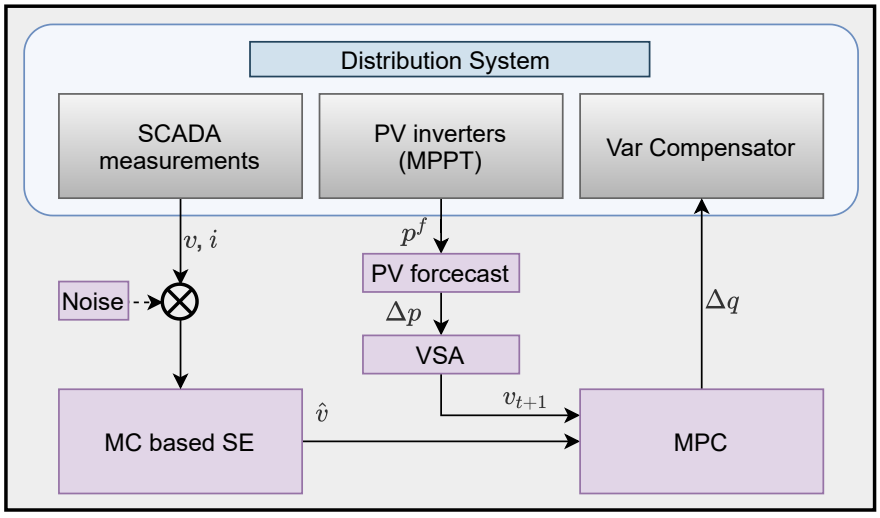

Figure 8.1: Flowchart of the proposed method.

value of the voltage phasor corresponding to node index j; $\mathbf{c}_j$ and $\mathbf{d}_j$ indicate the real and imaginary parts of current injections at node index j which can be obtained from the linear formulation (8.2) that employs the measured values of real power injection $\mathbf{p}_j$ and reactive power injection $\mathbf{q}_j$, i.e.,

$$\mathbf{c}_j + \mathrm{i}\mathbf{d}_j \approx \frac{\mathbf{p}_j - \mathrm{i}\mathbf{q}_j}{|\mathbf{v}|_j} \tag{8.2}$$

This linear structure is obtained under the assumption that that the voltage angle differences between the incident nodes are typically closer to zero in distribution systems. With this definition, the elements of the partial matrix $\mathbf{M} \in \mathbb{R}^{(N-1)\times 15}$ with respect to row j is filled as

$$\mathbf{M}_j = \begin{cases} \begin{bmatrix} \mathbf{0} & \mathbf{0} & |\mathbf{v}|_j^{abc^2} & \mathbf{c}_j^{abc} & \mathbf{d}_j^{abc} \end{bmatrix} & \text{if } j \in \psi \\ \\ \begin{bmatrix} \mathbf{0} & \mathbf{0} & \mathbf{0} & \mathbf{0} & \mathbf{0} \end{bmatrix} & \text{if } j \notin \psi \end{cases} \tag{8.3}$$

It is easy to notice that the available measurements enter the partial matrix at its respective positions. On the other hand, the unavailable values are filled with zeros. To obtain the completed matrix, $\mathbf{X}$, its low rank property is exploited by using its nuclear norm as a part of cost function in the MC problem [145]. Such a formulation for the MC problem should account for the system constraints, which can be written as

$$\begin{bmatrix} \mathbf{e}_j^{abc} - \mathrm{e}_s^{abc} \\ \mathbf{f}_j^{abc} - \mathrm{f}_s^{abc} \end{bmatrix} = \sum_{k=1}^{N-1} \begin{bmatrix} R_{jk}^{abc} & -X_{jk}^{abc} \\ X_{jk}^{abc} & R_{jk}^{abc} \end{bmatrix} \begin{bmatrix} c_k^{abc} \\ d_k^{abc} \end{bmatrix} \tag{8.4}$$

where, $\mathbf{e}_j^{abc}$ and $\mathbf{f}_j^{abc}$ are the real and imaginary parts of voltage for the three phases at node j and R_{jk}^{abc} and X_{jk}^{abc} are the real and imaginary parts of the three phase bus impedance

matrix element corresponding to node indices j and k. Here, the subscript s denotes the index of slack bus. Similarly the constraints for voltage magnitude measurements can be written in linear form as,

$$\mathbf{e}_j^0 \cdot \mathbf{e}_j^{abc} + \mathbf{f}_j^0 \cdot \mathbf{f}_j^{abc} \approx \mathbf{v}_j^{abc^2} \tag{8.5}$$

where $\mathbf{e}_j^0$ and $\mathbf{f}_j^0$ are the real and imaginary parts of voltage phasor estimated at the previous batch of measurements at all the phases in relation to node j. Due to the presence of noise in the measurements, these system constrains are enforced in a relaxed approach so that the problem is feasible. Such a formulation for MC problem is given as [247],

$$\arg \min_{\mathbf{X},\boldsymbol{\epsilon},\boldsymbol{\zeta}} \|\mathbf{X}\|_* + \mathbf{w}_1^T \boldsymbol{\epsilon} + \mathbf{w}_2^T \boldsymbol{\zeta} \tag{8.6a}$$

such that

$$\|\mathbf{X}_\psi - \mathbf{M}_\psi\|_F \leq \delta \tag{8.6b}$$

$$\begin{bmatrix} \mathbf{e}_j^{abc} & \mathbf{f}_j^{abc} & |\mathbf{v}|_j^{abc^2} & \mathbf{c}_j^{abc} & \mathbf{d}_j^{abc} \end{bmatrix} = \mathbf{X}_j,\ \forall j \in \Omega \tag{8.6c}$$

$$\left| \sum_{k=1}^{N-1} \begin{bmatrix} R_{jk}^{abc} & -X_{jk}^{abc} \\ X_{jk}^{abc} & R_{jk}^{abc} \end{bmatrix} \begin{bmatrix} \mathbf{c}_k^{abc} \\ \mathbf{d}_k^{abc} \end{bmatrix} - \begin{bmatrix} \mathbf{e}_j^{abc} - \mathrm{e}_s^{abc} \\ \mathbf{f}_j^{abc} - \mathrm{f}_s^{abc} \end{bmatrix} \right| \leq \boldsymbol{\epsilon}_j,\ \forall j \in \Omega \tag{8.6d}$$

$$\left| \begin{bmatrix} \mathbf{e}_j^0 & \mathbf{f}_j^0 \end{bmatrix} \begin{bmatrix} \mathbf{e}_j^{abc} \\ \mathbf{f}_j^{abc} \end{bmatrix} - \mathbf{v}_j^{abc^2} \right| \leq \boldsymbol{\zeta}_j,\ \forall j \in \Omega \tag{8.6e}$$

$$\begin{bmatrix} \boldsymbol{\epsilon}_j \\ \boldsymbol{\zeta}_j \end{bmatrix} \geq \mathbf{0},\ \forall j \in \Omega \tag{8.6f}$$

for some tolerance values δ, $\boldsymbol{\epsilon}_j$, and $\boldsymbol{\zeta}_j$. Here, Ω is the set of all node indices in the given distribution system except the slack bus. The formulation given in (8.6) is different from the

technique given in [247] as the values of power injection measurements are transformed into equivalent current phasors which are used in the MC process. In this manner, the values of voltage phasors at the nodes without measurement devices can be imputed used in MPC for voltage control. In our implementation, the weights, $\mathbf{w}_1^T$ and $\mathbf{w}_2^T$ are set to 1 so that each of the governing equation defined in the constraints (8.6d) and (8.6e) are equally important in relative to each other. δ is set to the value of noise variance of the available measurements as suggested in [247].

8.1.2 Non-linear model predictive control

The control objective in this section is to maintain nodal voltage magnitudes within the predefined limits $0.95 < |\mathbf{v}| < 1.05$ p.u. In cases where any of the nodal voltages fall outside the safe operational limits, the proposed controller will apply the minimum control policies to regulate these voltages. To find the optimal control policies, a finite-horizon ($[l, \mathcal{N}_c - 1]$) MPC is used. The MPC controller uses the latest available forecast of DER power output to predict voltage states during the prediction horizon $\mathcal{N}_p$ and find a cost-minimizing control policy. However, only the control policy corresponding to the first voltage state is implemented. Then, the voltage states are predicted again and the procedure is repeated from the current new voltage states, resulting in a new control policy [248]. In this section, it is assumed that $\mathcal{N}_p < \mathcal{N}_c - 1$. This prediction horizon is shifted forward until step $\mathcal{N}_c - 1$, which results in

the following quadratic program,

$$\min_{\mathbf{u}} \quad \sum_{l=1}^{\mathcal{N}_c-1} \mathbf{u}_{t+l|t}^T \mathbf{R} \mathbf{u}_{t+l|t} \tag{8.7a}$$

$$\text{s.t. } \mathbf{x}_{t+l|t} = \mathbf{A}\mathbf{x}_{t+l-1|t} + \mathbf{B}\mathbf{u}_{t+l-1|t} + \mathbf{D}\mathbf{w}_{t+l-1|t}, \; \forall l \in [1, \mathcal{N}_c - 1] \tag{8.7b}$$

$$\mathbf{c}_{t+l|t} = \mathbf{c}_{t+l-1|t} + \mathbf{u}_{t+l-1|t}, \; \forall l \in [1, \mathcal{N}_c - 1] \tag{8.7c}$$

$$\mathbf{v}_{min}^2 \leq \mathbf{G}_x \mathbf{x}_{t+l|t} \leq \mathbf{v}_{max}^2, \; \forall l \in [1, \mathcal{N}_c - 1] \tag{8.7d}$$

$$\mathbf{c}_{min} \leq \mathbf{c}_{t+l|t} \leq \mathbf{c}_{max}, \; \forall l \in [1, \mathcal{N}_c - 1] \tag{8.7e}$$

$$\mathbf{u}_{min} \leq \mathbf{u}_{t+l|t} \leq \mathbf{u}_{max}, \; \forall l \in [1, \mathcal{N}_c - 1] \tag{8.7f}$$

Here, $\mathbf{u}_{t+l|t}$ represents the optimal control policies, i.e., optimal changes in complex power at different nodes that regulate nodal voltages. $\mathbf{c}_{t+l|t}$ is the total change in nodal complex power where $\mathbf{c}_{t+l-1|t}$ is the change in base loadings at time instant $l-1$. The constraint (8.7d) brings voltage states within safe operational limits in the control horizon. The matrix $\mathbf{R} \triangleq \mathbf{R}^T \succ 0$ is a weight matrix that penalizes control actions. A dynamical prediction model has to be specified to predict the trajectories to be controlled over the horizon $\mathcal{N}_c - 1$, i.e., nodal voltage states. For unbalanced distribution systems, the voltage dynamical model can be written as [249]

$$\mathbf{x}_{t+l|t} = \mathbf{A}\mathbf{x}_{t+l-1|t} + \Delta\mathbf{x}_{t+l-1|t}. \tag{8.8}$$

Here, $\mathbf{x}_{t+l|t} \triangleq [\mathbf{e}_{t+l|t}, \mathbf{f}_{t+l|t}]^T \in \mathbb{R}^{2N \times 1}$ is a vector containing the real ($\mathbf{e}$) and imaginary ($\mathbf{f}$) parts of voltage states at step l and $\mathbf{A}$ is an identity matrix of size $2N \times 2N$. $\Delta\mathbf{x}_{t+l-1|t} \triangleq \mathbf{B}\mathbf{u}_{t+l-1|t} + \mathbf{D}\mathbf{v}_{t+l-1|t}$ represents nodal voltage changes due to PV power injections at actor nodes, where $\mathbf{u}_{t+l-1|t}$ and $\mathbf{w}_{t+l-1|t}$ are vectors containing the change in reactive and active power at actor nodes, respectively. $\mathbf{G}_x$ is a linear approximation matrix that relates the real valued state vector $\mathbf{x}_{t+l|t}$ which contains the real and imaginary parts of voltage phasor to the squared voltage magnitude value. The linear approximation is same as the approximation made in (8.6e). $\mathbf{B}$ and $\mathbf{D}$ are sensitivity matrices that relate the nodal complex power changes to the change in real and imaginary parts of voltage and can be computed based

on the analytical voltage sensitivity framework introduced in our previous work [10] and summarized below. It can be noticed that the voltage magnitude limits in (8.7d) are enforced as hard constraints and hence this formulation can be applied when the VAr compensators have necessary capacity to carry out voltage regulation under the prescribed load condition and PV forecast values.

8.1.3 Analytical voltage sensitivity

When complex power changes at an actor node A from $\mathbf{s}_A$ to $\mathbf{s}_A + \mathbf{\Delta s}_A$ the voltage state at an observation node O changes from $\mathbf{v}_O$ to $\mathbf{v}_O + \mathbf{\Delta v}_O$. $\mathbf{v}_O$, $\mathbf{\Delta v}_O$, $\mathbf{s}_A$ and $\mathbf{\Delta s}_A$ are vectors that contain voltage states, the change in voltage, complex power states and the change in complex power at observation node O and actor node A for phases, a, b and c, respectively. Using analytical voltage sensitivity, the voltage change for any observation node O can be approximated for multiple actor nodes as,

Theorem 7. *For a given three phase distribution system, the cumulative change in complex voltage at an observation node O due to the change in complex power at multiple actor nodes can be formulated as,*

$$\mathbf{\Delta v_O} \approx -\sum_{A\in\dagger} \begin{bmatrix} \frac{\Delta s_A^a Z_{OA}^{aa}}{v_A^{a*}} + \frac{\Delta s_A^b Z_{OA}^{ab}}{v_A^{b*}} + \frac{\Delta s_A^c Z_{OA}^{ac}}{v_A^{c*}} \\ \frac{\Delta s_A^b Z_{OA}^{ba}}{v_A^{a*}} + \frac{\Delta s_A^b Z_{OA}^{bb}}{v_A^{b*}} + \frac{\Delta s_A^c Z_{OA}^{bc}}{v_A^{c*}} \\ \frac{\Delta s_A^a Z_{OA}^{ca}}{v_A^{a*}} + \frac{\Delta s_A^b Z_{OA}^{cb}}{v_A^{b*}} + \frac{\Delta s_A^c Z_{OA}^{cc}}{v_A^{c*}} \end{bmatrix} \tag{8.9}$$

v_A^* and Δs_A represent the complex conjugate of voltage and complex power change at actor node A, respectively. The superscripts a, b, and c represent different phases and Z corresponds to the self and mutual impedance of the shared line between the actor and observation node. Here, $\dagger$ represents the set of all actor nodes resulting in the complex voltage change at node O. Proof can be found in [10].

The analytical method presented in Theorem 1 can be extended to compute the voltage

Table 8.1: Performance of voltage estimation.

	Mean	Min	Max	σ
MAPE (%)	0.1677	0.0958	0.2767	0.0382
MAE (°)	0.0950	0.0557	0.1604	0.0239

sensitivity at all observation nodes, i.e., (8.9) can be written as,

$$\Delta \mathbf{v} = -(\mathbf{Z}\boldsymbol{\mathcal{V}}^b)\Delta \mathbf{s}^* \tag{8.10}$$

where $\boldsymbol{\mathcal{V}}^b = \text{diag}(\mathbf{v}_b^*)^{-1}$ and $\mathbf{v}_b$ is a vector containing the nodal base voltages assuming no complex power changes. Here, $\mathbf{Z}$ is the bus impedance matrix and $\Delta \mathbf{s}^* = [\Delta \mathbf{p} + \boldsymbol{i}\Delta \mathbf{q}]$ is vector of the complex conjugate of change in apparent power at all nodes of the system. Note that $\Delta \mathbf{v}$ is the vector of complex voltage change at all nodes and can be written in terms of real and imaginary parts as,

$$\Delta \mathbf{x}_{t+l-1|t} \triangleq [\Delta \mathbf{e}_{t+l-1|t} \Delta \mathbf{f}_{t+l|t-1}]^T \tag{8.11}$$

$$\begin{aligned} &= [\Re(\mathbf{Z}\boldsymbol{\mathcal{V}}^b)\Delta \mathbf{q}_{t+l|t-1}, \Im(\mathbf{Z}\boldsymbol{\mathcal{V}}^b)\Delta \mathbf{q}_{t+l-1|t}]^T \\ &-[\Re(\mathbf{Z}\boldsymbol{\mathcal{V}}^b)\Delta \mathbf{p}_{t+l-1|t}, \Im(\mathbf{Z}\boldsymbol{\mathcal{V}}^b)\Delta \mathbf{p}_{t+l-1|t}]^T \end{aligned}. \tag{8.12}$$

Here, $\Delta \mathbf{p}_{t+l-1|t} \triangleq \mathbf{w}_{t+l-1|t}$ is based on available PV forecasts and $\Delta \mathbf{q}_{t+l-1|t} \triangleq \mathbf{u}_{t+l-1|t}$ is the control variable. $\Delta \mathbf{p}$ for nodes that do not change complex power (e.g., does not have PV units) can be set to zero. The main advantage of analytical voltage sensitivity framework is the computational efficiency [10] when compared to classical sensitivity methods.

8.1.4 Simulation results

This section validates the proposed voltage control approach. The method is verified on the unbalanced 37 node test system. A scenario is created where SCADA measurements are available at 50% of system nodes. These nodes are highlighted in blue circles whereas nodes with no available measurements are highlighted in red circles in Fig. 8.2. 5 PV units are

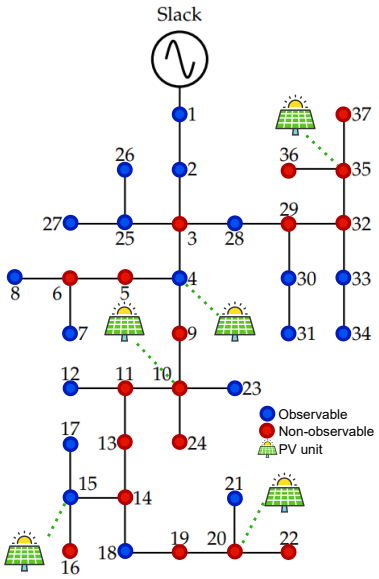

Figure 8.2: Modified IEEE 37-node unbalanced distribution system.

installed at phases a, b and c of nodes 4, 10, 15, 20 and 35. The maximum PV penetration by the PV units is set to supply 30% of total demand according to the daily PV profile shown in Fig. 8.3. SCADA measurements and PV forecasts are assumed to be available every half

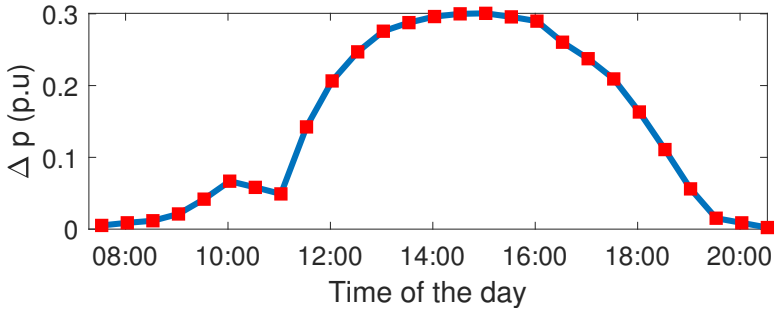

Figure 8.3: PV profile.

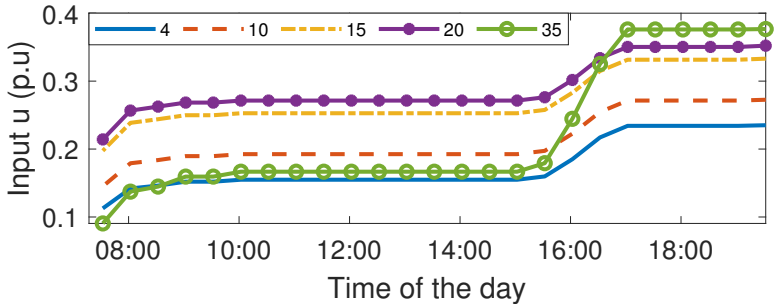

Figure 8.4: $3-\phi$ Aggregate optimal control actions at VCs.

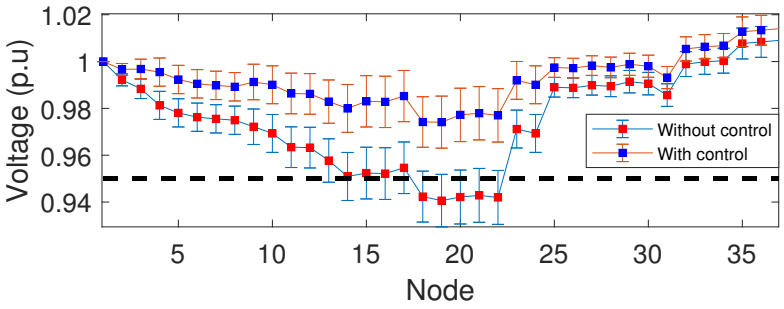

Figure 8.5: Voltage profile at all observation nodes.

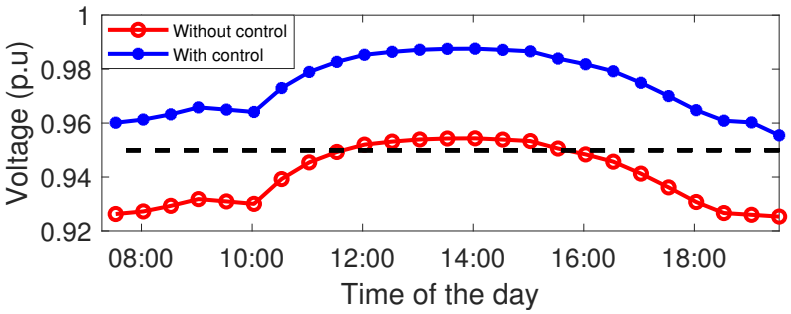

Figure 8.6: Voltage profile at phase a of node 19.

an hour starting from 07:30:00 until 19:30:00, which results in $\mathcal{N}_c = 25$ control steps. First, voltage states are estimated based on the available SCADA measurements using MC. The performance of SE over the control horizon is examined using mean absolute percentage error (MAPE) for voltage magnitudes and mean absolute error (MAE) for voltage angles. Table 8.1 shows the mean, minimum, maximum and standard deviation (σ) of MAPE and MAE of voltage estimates. The table indicates that the estimation errors are very low with 50% observable nodes, which shows the accuracy of voltage estimates. Thereafter, voltage estimates are passed together with PV forecasts to the MPC plant. It is important to note that (8.7d) considers the squared magnitude of lower and upper limits of voltage profiles to ensure convexity of the inequality constraint. The penalty matrix $\mathbf{R}$ is chosen to be identity matrix, i.e., control actions at all VCs are equally penalized. The proposed method, however, is generic to any choice of penalty matrix. In cases where VCs have different penalties, control actions will be higher on nodes with lower penalties. Finally, the MPC is implemented to obtain optimal control actions, which are shown in Fig. 8.4 as the $3-\phi$

aggregate $\Delta\mathbf{q}$ at actor nodes. It can be seen from the figure that the control action at node 35 is higher than that of node 4 and that is due to the inequality constraints imposed on nodal reactive power injections as in Eq. (8.7e). Fig. 8.5 shows an error bar plot of voltage profiles of at phase a of all nodes with and without control actions. The Figure shows the mean value of each nodal voltage as well as its relative standard deviation over the entire control horizon $\mathcal{N}_c$. It can be seen that nodes 18, 19, 20, 21, and 22 violate the safe operational limits without implementing control. This is because these nodes lie within the farthest region from the slack bus. After applying the proposed control method, all violations are eliminated. In addition, the variance of the lowest violation, i.e., node 19, does not exceed the violation limit after applying control. Fig. 8.6 illustrates the worst case scenario that occurs at node 19. It can be seen that voltage profile at node 19 is maintained within safe operational limits across the entire control horizon. This demonstrates the effectiveness of the proposed method in controlling voltage violations in low-observable distribution systems with the presence of DER injections.

8.2 Dominant influencer-based voltage control

8.2.1 System model

Consider a three-phase unbalanced power distribution system with n nodes connected by distribution lines. It is assumed that m inverter-based DER units are integrated in the system to supply local loads. It is also assumed that the source node operates at $1\angle 0°$ p.u [27]. In this section, the set of *actor nodes* ($\mathcal{A}$) refers to nodes where complex power varies due to either PV power injection or local load consumption. The set of *observation nodes* ($\mathcal{O}$) is the set of nodes where voltage state is monitored. Voltage at observation nodes changes due to complex power changes at actor nodes. Let Δe_O and Δf_O represent the change in real and imaginary parts of voltage at observation node O, respectively, and let the complex power change at any phase of actor node $A \in \mathcal{A}$ be $\Delta S_A = \Delta p_A + j\Delta q_A$. Then, the vector ($\mathbf{\Delta x}_O \triangleq [\Delta e_O \quad \Delta f_O]^\intercal$) of change in real and imaginary parts of voltage at any phase of

observation node $O \in \mathcal{O}$ can be analytically computed using [72],

$$\mathbf{\Delta x}_O = \begin{bmatrix} \Re(Z_{OA}\mathcal{V}) \\ \Im(Z_{OA}\mathcal{V}) \end{bmatrix} \Delta p_A + \begin{bmatrix} \Im(Z_{OA}\mathcal{V}) \\ -\Re(Z_{OA}\mathcal{V}) \end{bmatrix} \Delta q_A \tag{8.13}$$

where, Z_{OA} is the mutual path impedance between nodes A and O from the substation node and $\mathcal{V} = (V_A^*)^{-1}$. Here, V_A^* is the complex conjugate of initial voltage at node A. Equation (8.13) can be written in a vectorial form for all observation nodes $\mathcal{O}$ as,

$$\mathbf{\Delta x} = \mathbf{D\Delta p} + \mathbf{B\Delta q} \tag{8.14}$$

where $\mathbf{\Delta x} \triangleq [\mathbf{\Delta e}(1), ..., \mathbf{\Delta e}(n), \mathbf{\Delta f}(1), ..., \mathbf{\Delta f}(n)]^T \in \mathbb{R}^{2n\times 1}$ is a column vector that consists of the change in real ($\mathbf{\Delta e}$) and imaginary ($\mathbf{\Delta f}$) parts of voltage at all observation nodes. Note that the set of observation nodes contains all n nodes, i.e., the change in voltage is monitored across all system nodes. $\mathbf{\Delta p} \in \mathbb{R}^m$ and $\mathbf{\Delta q} \in \mathbb{R}^{m\times 1}$ are vectors that capture the change in active and reactive power at all actor nodes $\mathcal{A}$, respectively. Matrices $\mathbf{D} \in \mathbb{R}^{2n\times m}$ and $\mathbf{B} \in \mathbb{R}^{2n\times m}$ are sensitivity matrices that relate the change in real and imaginary parts of voltage at all observation nodes with respect to the change in active and reactive power at actor nodes, respectively. This analytical approximation can be used to quickly compute the change in real and imaginary parts of voltage due to complex power changes. It has been shown that this analytical framework is computationally efficient and highly accurate when validated against classical load flow method. The approximation error introduced by this approximation is very small (e.g., in the order of 10^{-4}) and tightly upper bounded [72], which guarantees the performance while computing the change in voltage states [27]. Let $t = 0$ be the time step when system state is measured using sensors, it is possible to use the analytical approach to compute the vector of real and imaginary parts of nodal voltage states $\mathbf{x} \triangleq [\mathbf{e} \quad \mathbf{f}]^T$ at all observation nodes as,

$$\mathbf{x} = \mathbf{A}\mathbf{x}_0 + \mathbf{\Delta x}_0 \tag{8.15}$$

where $\mathbf{x}_0 \triangleq [\mathbf{e}_0 \quad \mathbf{f}_0]^\intercal$ is the vector of the real and imaginary parts of initial voltage states, $\mathbf{A} \in \mathbb{R}^{2n \times 2n}$ is an identity matrix and $\mathbf{\Delta x}_0$ is the vector of change in voltage as computed using (8.14). Using this system model, next section details the proposed analytical approach for computing SVI nodes.

8.2.2 System voltage influencer paradigm

The set of DIVF nodes $\mathfrak{D}_{\boldsymbol{O}} \in \mathcal{A} \subset n$ of a particular observation node $O \in \mathcal{O} \subset n$ are the nodes with the highest impact on nodal voltage fluctuations at that observation node [32]. The use of DIVF nodes allows us to identify the most effective actor nodes to control distribution system voltage, thus reducing the dimension of the control problem and minimizing the computational time with minimal to no impact on optimality [32]. Two factors impact the rank of actor nodes within the DIVF set: (1) the spatial distribution and phase of actor nodes within the distribution system; and (2) the variance of complex power changes at that actor node. Thus, it is possible to use well-known probability distributions with information-theoretical distance measures to compute these dominant nodes.

Information-theoretical approach

The information-theoretical approach is based on novel probabilistic voltage sensitivity analysis [32] that computes the change in real and imaginary parts of voltage based on random complex power changes at actor nodes $\mathcal{A} \in n$. Let the power change vector $\mathbf{\Delta s}$ be defined as,

$$\begin{aligned}\mathbf{\Delta s} \triangleq &[\Delta p_1^a, \Delta q_1^a, \Delta p_1^b, \Delta q_1^b, \Delta p_1^c, \Delta q_1^c, ..., \\ &\Delta p_A^a, \Delta q_A^a, \Delta p_A^b, \Delta q_A^b, \Delta p_A^c, \Delta q_A^c]^\intercal \forall A \in \mathcal{A}\end{aligned} \tag{8.16}$$

where the super scripts a, b, and c represent different phases. Then, the complex power changes at actor nodes can be modeled as a random vector $\mathbf{\Delta s}$ with mean $\boldsymbol{\mu}_{\mathbf{\Delta s}}$ and covariance matrix $\mathbf{\Sigma}_{\mathbf{\Delta s}}$. The covariance matrix captures the correlation of complex power changes due

to geographical proximity. For completeness, we list the exact definition of the covariance matrix $\mathbf{\Sigma_{\Delta s}}$ in Appendix D. Consider phase a for simplicity and let $\Delta x^a_{O.1}$ and $\Delta x^a_{O.2}$ be the real and imaginary parts of voltage change at node O due to complex power change at multiple actor nodes within the set $\mathcal{A}$, respectively. Note that the numbers in the subscripts $O.1$ and $O.2$ denote the real and imaginary parts, respectively. By invoking the Lindeberg-Feller central limit theorem, it is possible to show that the distribution of change in real and imaginary parts of voltage in (8.14) due to multiple actor nodes $\mathcal{A}$ converge to Gaussian distributions, i.e.,

$$\Delta x^a_{O.1} \xrightarrow{D} \mathcal{N}(\mu_{O.1} \triangleq \mathbf{c}^{a\intercal}_{O.1}\boldsymbol{\mu}_{\mathbf{\Delta s}}, \sigma^2_{O.1} \triangleq \mathbf{c}^{a\intercal}_{O.1}\mathbf{\Sigma}_{\mathbf{\Delta s}}\mathbf{c}^a_{O.1}) \tag{8.17}$$

$$\Delta x^a_{O.2} \xrightarrow{D} \mathcal{N}(\mu_{O.2} \triangleq \mathbf{c}^{a\intercal}_{O.2}\boldsymbol{\mu}_{\mathbf{\Delta s}}, \sigma^2_{O.2} \triangleq \mathbf{c}^{a\intercal}_{O.2}\mathbf{\Sigma}_{\mathbf{\Delta s}}\mathbf{c}^a_{O.2}) \tag{8.18}$$

where vectors $\mathbf{c}^a_{O.1}$ and $\mathbf{c}^a_{O.1}$ are constant vectors that can be computed based on system topology (see [32] for proof and more details). Note that the correlation between real and imaginary parts of change in voltage at node O can be captured by $c \triangleq \mathbf{c}^{a\intercal}_{O.1}\mathbf{\Sigma}_{\mathbf{\Delta s}}\mathbf{c}^a_{O.2}$. Following the procedure in [32], it is possible to show that the distribution of change in voltage magnitude $\Delta x^a_{O.\mathfrak{M}} \triangleq |\Delta x^a_{O.1} + j\Delta x^a_{O.2}|$ follows a Nakagami distribution with well-defined shape and scale parameters where $O.\mathfrak{M}$ denotes the magnitude of voltage change. The next step is to compute the distribution of voltage change due to a single actor node $A \in \mathcal{A}$ using,

$$\begin{aligned}\Delta x^{a,A}_{O.1} &\xrightarrow{D} \mathcal{N}(\mu_{O.1} \triangleq \mathbf{c}^{a\intercal}_{O.1}\boldsymbol{\mu}^A_{\mathbf{\Delta s}}, \sigma^2_{O.1} \triangleq \mathbf{c}^{a\intercal}_{O.1}\mathbf{\Sigma}^A_{\mathbf{\Delta s}}\mathbf{c}^a_{O.1}) \\ \Delta x^{a,A}_{O.2} &\xrightarrow{D} \mathcal{N}(\mu_{O.2} \triangleq \mathbf{c}^{a\intercal}_{O.2}\boldsymbol{\mu}^A_{\mathbf{\Delta s}}, \sigma^2_{O.2} \triangleq \mathbf{c}^{a\intercal}_{O.2}\mathbf{\Sigma}^A_{\mathbf{\Delta s}}\mathbf{c}^a_{O.2}).\end{aligned} \tag{8.19}$$

Here, $\boldsymbol{\mu}^A_{\mathbf{\Delta s}}$ and $\mathbf{\Sigma}^A_{\mathbf{\Delta s}}$ can be computed by setting all entries to zeros except for that of actor node A. The resulting change in voltage magnitude can be computed as $\Delta x^{a,A}_{O.\mathfrak{M}} \triangleq |\Delta x^{a,A}_{O.1} + j\Delta x^{a,A}_{O.2}|$. After computing the distribution of change in voltage magnitude due to all actor nodes ($\Delta x^a_{O.m}$) and due to actor node A only ($\Delta x^{a,A}_{O.m}$), one can use the Kullback-

Liebler (KL) divergence to compute the influence scores of each actor node, i.e.,

$$D_{KL}(\Delta x^{a}_{O.\mathfrak{M}}||\Delta x^{a,A}_{O.\mathfrak{M}}) = \frac{1}{2}\Bigg[\mathrm{Tr}\Big(\mathbf{\Sigma}^{-1}_{\Delta x^{a}_{O.\mathfrak{M}}}\mathbf{\Sigma}_{\Delta x^{a,A}_{O.\mathfrak{M}}}\Big) + (\mu_{\Delta x^{a}_{O.\mathfrak{M}}} - \mu_{\Delta x^{a,A}_{O.\mathfrak{M}}})^{\intercal}\mathbf{\Sigma}^{-1}_{\Delta x^{a}_{O.\mathfrak{M}}}(\mu_{\Delta x^{a}_{O.\mathfrak{M}}} - \mu_{\Delta x^{a,A}_{O.\mathfrak{M}}}) - 2 + \ln\frac{\|\mathbf{\Sigma}^{-1}_{\Delta x^{a}_{O.\mathfrak{M}}}\|}{\|\mathbf{\Sigma}^{-1}_{\Delta x^{a,A}_{O.\mathfrak{M}}}\|}\Bigg]. \tag{8.20}$$

The distance $D_{KL}(\Delta x^{a}_{O.m}||\Delta x^{a,i}_{O.m})\forall i \in \mathcal{A}$ can be computed for all actor nodes, which results in a unique ranking of actor nodes based on their influence on the magnitude of voltage change at observation node O. The divergence metric in (8.20) can also be computed using other measures such as Bhattacharyya or Jensen-Shannon distances. For simplicity of demonstration, we only use the KL divergence since Bhattacharyya and Jensen-Shannon distances provide identical ranking of nodes that is very accurate when compared to classical load flow-based method. Notice that (8.20) ranks actor nodes based on their influence on each individual observation node. In distribution systems, there might be multiple nodes that experience voltage violations [27]. In addition, there can be scenarios where certain nodes are high in rank for some observation nodes but low in rank for others. Therefore, it is important to use a set whose nodes are dominant for all observation nodes. Next section explains in details the steps behind computing the SVI set of dominant nodes ($\mathfrak{D}^{*}_{O}$) for voltage control applications.

SVI for voltage control applications

Let $\check{\mathcal{O}} \triangleq [O_1, O_2, ..., O_{\check{n}}]^{\intercal}$ be the set of observation nodes for any $\check{n} \subset n$. Then for each observation node $O_i \forall i \in \check{\mathcal{O}}$, the DIVF set ($\mathfrak{D}_{O_i}$) for each observation node can be computed and sorted using (8.20), i.e.,

$$\begin{aligned}
\mathfrak{D}_{O_1} &= \{d^1_{O_1}, d^2_{O_1}, ..., d^{m-1}_{O_1}, d^m_{O_1}\} \forall m \in n \\
&\vdots \qquad\qquad\qquad \vdots \\
\mathfrak{D}_{O_{\check{n}}} &= \{d^1_{O_{\check{n}}}, d^2_{O_{\check{n}}}, ..., d^{m-1}_{O_{\check{n}}}, d^m_{O_{\check{n}}}\} \forall m \in n
\end{aligned} \tag{8.21}$$

where, $d^j_{O_i}$ is the j^{th} most dominant node of voltage fluctuations for observation node O_i. In other words, the lower the superscript the higher the impact of the respective actor node on the change in voltage of that observation node will be. Notice that a natural way to find the SVI set of nodes would be the union of DIVF sets of individual observation nodes in (8.21), i.e.,

$$\begin{aligned}
\mathfrak{D}_{\check{\mathcal{O}}} &= \bigcup_{i=1}^{\check{n}} \mathfrak{D}_{O_i} = \mathfrak{D}_{O_1} \cup \mathfrak{D}_{O_2} \cup .... \cup \mathfrak{D}_{O_{\check{n}}} \\
&= \{d^1_{O_1}, d^2_{O_1}, ..., d^m_{O_1}\} \cup \{d^1_{O_2}, d^2_{O_2}, ..., d^m_{O_2}\} \cup ... \\
&\quad \cup \{d^1_{O_{\check{n}}}, d^2_{O_{\check{n}}}, ..., d^{m-1}_{O_{\check{n}}}, d^m_{O_{\check{n}}}\} \\
&= \{d^1_{\check{\mathcal{O}}}, d^2_{\check{\mathcal{O}}}, ..., d^{m-1}_{\check{\mathcal{O}}}, d^m_{\check{\mathcal{O}}}\}.
\end{aligned} \tag{8.22}$$

According to (8.20) and (8.21), it can be seen that there can be nodes with minimal impact on voltage services at any observation node. Therefore, in the final step of selecting the SVI set, the control participation factor (CPF) is used to rank the actor nodes within the set. For any node $i \in \mathfrak{D}_{\check{\mathcal{O}}}$ the CPF can be computed as,

$$\begin{aligned}
\text{CPF}_i = |\mathbf{x}^\intercal_{O_1}\mathbf{x}_{O_1} - 1|||\mathbf{B}(\mathbf{x}_{O_1}, d^i_{\check{\mathcal{O}}})|| \\
+|\mathbf{x}^\intercal_{O_2}\mathbf{x}_{O_2} - 1|||\mathbf{B}(\mathbf{x}_{O_2}, d^i_{\check{\mathcal{O}}})||+... \\
+ |\mathbf{x}^\intercal_{O_{\check{n}}}\mathbf{x}_{O_{\check{n}}} - 1|||\mathbf{B}(\mathbf{x}_{O_{\check{n}}}, d^i_{\check{\mathcal{O}}})||.
\end{aligned} \tag{8.23}$$

Here, the term $|\mathbf{x}_{O_j}^{\intercal}\mathbf{x}_{O_j} - 1|$ is the absolute deviation of squared magnitude of voltage at node j from 1 p.u whereas $\mathbf{B}(\mathbf{x}_{O_j}, d_{\check{\mathcal{O}}}^{i})$ is a vector that contains the sensitivity of the change in real and imaginary parts of voltage at node j with respect to reactive power injections at dominant node $d_{\check{\mathcal{O}}}^{i} \in \mathfrak{D}_{\check{\mathcal{O}}}$. Finally, the nodes can be ranked in a descending order depending on their CPFs as,

$$\begin{aligned} \text{Rank } 1 &\triangleq \arg\max_{d_{\check{\mathcal{O}}}^{i}} \ \text{CPF}_i \\ \text{Rank } m &\triangleq \arg\min_{d_{\check{\mathcal{O}}}^{i}} \ \text{CPF}_i. \end{aligned} \tag{8.24}$$

Note that the minimum rank that can be obtained is m since there are m actor nodes in (8.21). The rank of all other actor nodes falls between 1 and m, depending on their CPFs. This framework is generic and allows distribution system operators to choose any arbitrary number ($\check{m}$) of dominant nodes to participate in the voltage control framework, which yields the optimal SVI set,

$$\mathfrak{D}_{\check{\mathcal{O}}}^{*} = \{d_{\check{\mathcal{O}}}^{1*}, d_{\check{\mathcal{O}}}^{2*}, ..., d_{\check{\mathcal{O}}}^{(\check{m}-1)*}, d_{\check{\mathcal{O}}}^{\check{m}*}\}. \tag{8.25}$$

Two key properties of the SVI set and its application to Problem 1 are highlighted in the following propositions.

Proposition 1. *Let $\check{m}$ be the cardinality of SVI set whose nodes participate in the voltage control program with $\check{n}$ critical locations that experience voltage violations. Then, it is possible to reduce the computational complexity of Problem 1 (below) by at least a factor of $(m - \check{m})$ for any SVI set with $1 < \check{m} \leq m$.*

Proposition 2. *Assume that Problem 1 is feasible for any $k \in [0, N-1] \in \mathbb{Z}_{>1}$. Let $\mathfrak{D}_{\check{\mathcal{O}}}^{*} \triangleq \{d_{\check{\mathcal{O}}}^{1*}, d_{\check{\mathcal{O}}}^{2*}, ..., d_{\check{\mathcal{O}}}^{(\check{m}-1)*}, d_{\check{\mathcal{O}}}^{\check{m}*}\}$ be the SVI set. Then, for any $\hat{\mathfrak{D}}_{\check{\mathcal{O}}}^{*} \triangleq \mathfrak{D}_{\check{\mathcal{O}}} \backslash \{\mathfrak{D}_{\check{\mathcal{O}}}^{*}\}$ with cardinality $|\hat{\mathfrak{D}}_{\check{\mathcal{O}}}^{*}| = m - \check{m}$,*

$$\begin{aligned} &(V(\mathbf{x}_0, \boldsymbol{\Delta}\mathbf{q}_k^{*}) \mid \boldsymbol{\Delta}\mathbf{q}_k^{*} \in \mathfrak{D}_{\check{\mathcal{O}}}^{*}) \\ &\qquad < (V(\mathbf{x}_0, \boldsymbol{\Delta}\mathbf{q}_k^{*}) \mid \boldsymbol{\Delta}\mathbf{q}_k^{*} \in \hat{\mathfrak{D}}_{\check{\mathcal{O}}}^{*}) \ \forall k \end{aligned} \tag{8.26}$$

where $\mathbf{\Delta q}_k^*$ *is the optimal control sequence.*

The complete proof of Proposition 1 and 2 can be found in Appendix E and F, respectively. Next section discusses voltage control via inverter-based DERs as the potential application of SVI nodes.

Use case: Efficient voltage control

Based on the proposed system model in Eq. (8.15), it is possible to formulate a quadratic program to control voltage profiles by adjusting the reactive power outputs of inverter-based DER resources. This framework is illustrated in Problem 1. To implement SVI-based voltage control, it is possible to use the approximation of change in voltage shown in Eq. (8.14) in a predictive control setup where voltage violations can be predicted [27]. This is done by computing the future voltage state vector based on the latest available measurements of change in PV injections or local load patterns [250]. For this, we develop a finite-horizon model predictive control approach that finds an optimal control sequence $\mathbf{\Delta q}$ whenever a voltage violation is predicted over a given prediction horizon N_p. At every prediction window, only the control sequence that corresponds to the first prediction of voltage states is implemented [248]. The prediction window is shifted again by N_p steps, resulting in a new optimal control sequence for every time instance in the control horizon $[0, ..., N_c - 1]$. This dynamical setup in terms of the control horizon is shown in Problem 1,

Problem 1. *For a fixed* $N \in \mathbb{Z}_{>1}$*, let* $\mathbf{\Delta x}_k \in [\mathbf{\Delta x}_0, ..., \mathbf{\Delta x}_{N_c-1}]$ *be the vector of change in real and imaginary parts of voltages over the control horizon and let* $\mathbf{x}_k \in [\mathbf{x}_1, ..., \mathbf{x}_{N_c}]$ *be the voltage state vector computed using (8.15) with initial voltage vector* $\mathbf{x}_0$*. Then, find an optimal control sequence* $\mathbf{\Delta q}_k \in [\mathbf{\Delta q}_0, ..., \mathbf{\Delta q}_{N_c-1}]$ *that minimizes the cost function* V*,*

$$V(\mathbf{\Delta q}_k|\mathbf{x}_0) = \min_{\mathbf{\Delta q}_k} \sum_{k=0}^{N_c-1} L(\mathbf{\Delta q}_k) \tag{8.27}$$

$$s.t. \quad \mathbf{x}_{k+1} = \mathbf{A}\mathbf{x}_k + \mathbf{D}\mathbf{\Delta p}_k + \mathbf{B}\mathbf{\Delta q}_k \forall l \in [0, N_c - 1] \tag{8.27a}$$

$$\mathbf{H}\mathbf{x}_k + \mathbf{G}\mathbf{\Delta q}_k \leq \mathbf{h}_k \forall l \in [0, N_c - 1] \tag{8.27b}$$

where $\mathbf{h}_k = [-\boldsymbol{\Delta}\underline{\mathbf{q}}, \boldsymbol{\Delta}\overline{\mathbf{q}}, -\underline{\mathbf{v}}, \overline{\mathbf{v}}]^\intercal$ *is a vector that represents the lower and upper bounds on control sequence and voltage magnitudes, respectively.* $\mathbf{G} \triangleq \mathbf{C}_x\boldsymbol{\Gamma}$ *with* $\mathbf{C}_x \in \mathbb{R}^{(2m+2n)\times n}$ *and* $\mathbf{H} \in \mathbb{R}^{(2m+2n)\times 2m}$ *are rotation matrices of appropriate dimension to maintain consistent constraints. Note that the matrix* $\boldsymbol{\Gamma} \in \mathbb{R}^{n\times 2n}$ *is used to transform the vector of real and imaginary parts of nodal voltage states into a of vector voltage magnitudes form [31],*

$$\boldsymbol{\Gamma} \triangleq \begin{bmatrix} \Re(\mathbf{t}(1)) & \dots & 0 & -\Im(\mathbf{t}(1)) & \dots & 0 \\ \vdots & \ddots & \vdots & \vdots & \ddots & \vdots \\ 0 & \dots & \Re(\mathbf{t}(n)) & 0 & \dots & -\Im(\mathbf{t}(n)) \end{bmatrix} \tag{8.28}$$

Here, $\mathbf{t}$ *is a vector that contains the nominal voltage of all nodes* $\mathbf{t} \in \mathbb{R}^n$ *(i.e.,* $1\angle 0°, 1\angle 120°$ *and* $1\angle -120°$*) for phases a, b, and c, respectively.*

The function $L(.)$ is used to penalize control actions, which prevents abrupt changes in system dynamics and minimize interference with the existing voltage regulation devices in the system[120]. Throughout this section, it is assumed that $L(\boldsymbol{\Delta}\mathbf{q}) \triangleq \boldsymbol{\Delta}\mathbf{q}^\intercal\mathbf{R}\boldsymbol{\Delta}\mathbf{q}$ where $\mathbf{R} \succ 0 \in \mathbb{R}^{m\times m}$ is a positive-definite matrix. The available reactive power support in the system varies depending on individual constraints of control nodes as well as system overall capabilities. This variability occurs due to the reactive power injected by the PV inverter or the existing load reactive power demand. Therefore, the vectors of lower and upper bounds in inequality constraint (8.27b) can be defined dynamically across the entire control horizon to represent changes the available reactive power support by each controller. To solve Problem 1, we use the interior point method [251, 252] as it has been shown in [253] that this method is highly accurate with significant computational efficiency compared to other approaches such as active set method. Though what we propose in this chapter is mainly based on the SVI paradigm, and thus our goal is not to compete with other models for solving Problem 1. For completeness, we include the details on this implementation in Appendix G. The voltage state vector ($\mathbf{x}$) can vary randomly due to uncertainty of DER power outputs, variability in load patterns, or inaccurate state estimates (or measurements). These stochastic processes can heavily impact the accuracy of voltage control algorithms

[31]. Specifically, nodal voltage magnitudes under uncertainty scenarios can still violate the permissible stability margins even when the control algorithm is active [254]. Therefore, utilities and distribution system operators require robust control algorithms that guarantee voltage stability under such scenarios. In this section, equation (8.27a) in Problem 1 is used to derive a stochastic control approach. Specifically, (8.27a) can be rewritten as,

$$\mathbf{x}_{k+1} = \mathbf{A}\mathbf{x}_k + \mathbf{D}\boldsymbol{\Delta}\mathbf{p}_k + \mathbf{B}\boldsymbol{\Delta}\mathbf{q}_k + \mathbf{w}_k \forall l \in [0, N_c - 1] \tag{8.29}$$

where, $\mathbf{w}_k \sim \mathcal{N}(\boldsymbol{\mu}_w, \boldsymbol{\Sigma}_w)$ is a Gaussian uncertainty with a mean vector $\boldsymbol{\mu}_w$ and a covariance structure $\boldsymbol{\Sigma}_w$. The diagonal elements of $\boldsymbol{\Sigma}_w$ represent the variance of voltage change due to random power changes or inaccurate state measurements. This covariance matrix can be constructed based on historical data [254] or using sparsity-based Bayesian state estimation techniques [255]. Assuming that we use (8.29) to solve Problem 1, the algorithm will not capture the uncertainty introduced by $\boldsymbol{\Sigma}_w$ and the deterministic inequality constraint (8.27a) might be violated. Therefore, the equivalent stochastic formulation in Problem 2 is used to capture this uncertainty.

Problem 2. *For a fixed $N \in \mathbb{Z}_{>1}$, let $\boldsymbol{\Delta}\mathbf{x}_k \in [\boldsymbol{\Delta}\mathbf{x}_0, ..., \boldsymbol{\Delta}\mathbf{x}_{N_c-1}]$ be the vector of change in real and imaginary parts of voltages over the control horizon and let $\mathbf{x}_k \in [\mathbf{x}_1, ..., \mathbf{x}_{N_c}]$ be the voltage state vector with uncertainty component as given in (8.29). Then, find an optimal control sequence $\boldsymbol{\Delta}\mathbf{q}_k \in [\boldsymbol{\Delta}\mathbf{q}_0, ..., \boldsymbol{\Delta}\mathbf{q}_{N_c-1}]$ that minimizes the expected value of the cost function V,*

$$V(\mathbf{x}_0, \boldsymbol{\Delta}\mathbf{q}_k) = \min_{\boldsymbol{\Delta}\mathbf{q}_k} \mathbb{E}\left(\sum_{k=0}^{N-1} \boldsymbol{\Delta}\mathbf{q}_k^{\mathrm{T}} \mathbf{R} \boldsymbol{\Delta}\mathbf{q}_k \right) \tag{8.30}$$

$$s.t. \quad \mathbf{x}_{k+1} = \mathbf{A}\mathbf{x}_k + \mathbf{D}\boldsymbol{\Delta}\mathbf{p}_k + \mathbf{B}\boldsymbol{\Delta}\mathbf{q}_k + \mathbf{w}_k \forall k \in [0, N_c - 1] \tag{8.30a}$$

$$\mathbb{P}(\mathbf{H}\mathbf{x}_k + \mathbf{G}\boldsymbol{\Delta}\mathbf{q}_k \leq \mathbf{h}_k) \geq \boldsymbol{\alpha} \forall k \in [0, N_c - 1] \tag{8.30b}$$

where, $\{\mathbf{0} \leq \boldsymbol{\alpha} \leq \mathbf{1}\}$ is a vector whose elements are predefined tightening (or risk) parameters. A higher risk parameter reduces the risk of violating the inequality constraint in

(8.30b).

Note that the stochastic formulation in Problem 2 can be efficiently solved by computing the stage-wise error matrix caused by the uncertainty vector $\mathbf{w}_k$ and converting the chance constraint eq. (8.30b) to its deterministic equivalent [256].

8.2.3 Simulation results

This section validates the efficacy of the proposed voltage control approach using the IEEE 37 and IEEE 123-node test systems. First, the approach is validated via simulations on the unbalanced IEEE 37 node test system. The nominal voltage of this test system is 4.8 kV. A scenario is created where inverter-based PV units are integrated at 15 randomly selected actor nodes. These actor nodes are $[7, 8, 9, 12, 14, 17, 18, 22, 26, 27, 28, 30, 31, 34, 36]$. To determine the set of SVI nodes for observation nodes, we use the probabilistic approach in Eq. (8.20). In particular, we model complex power changes at the 15 actor nodes as a zero-mean Gaussian vector Eq. (8.16) with a covariance structure that captures the geographical proximity between different actor nodes. Although it is assumed that complex power variations follow a Gaussian distribution, the proposed approach is generic to other probability distributions. The mean and variance of the complex power change at actor nodes is chosen as follows, The

Table 8.2: Ranked DIVF set of observation nodes.

Observation Node	R 1	R 2	R 3	R 4	R 5
5	7	9	12	14	22
11	12	14	22	9	7
21	17	22	18	14	12
31	31	30	8	18	36

Table 8.3: CPF of different actor nodes.

Node	CPF	Node	CPF	Node	CPF
7	0.0078↓	17	0.0187↑	28	0.0049↓
8	0.0107↓	18	0.0194↑	30	0.0049↓
9	0.0117↑	22	0.0117↓	31	0.0049↓
12	0.0148↑	26	0.0049↓	34	0.0049↓
14	0.0181↑	27	0.0049↓	36	0.0049↓

variance of active and reactive power change at actor nodes according to the exact phase sequence is chosen as follows [32],

$$\begin{aligned}
\boldsymbol{\Delta S_A} &\sim \mathcal{N}\left(\begin{bmatrix} 0 \\ 0 \end{bmatrix}, \begin{bmatrix} 1.5 & -0.05 \\ -0.05 & 0.25 \end{bmatrix} \right), \\
\boldsymbol{A} &\epsilon \{7^c, 8^a, 12^c, 27^b, 28^c\} \\
\boldsymbol{\Delta S_A} &\sim \mathcal{N}\left(\begin{bmatrix} 0 \\ 0 \end{bmatrix}, \begin{bmatrix} 3 & -0.1 \\ -0.1 & 0.5 \end{bmatrix} \right), \\
\boldsymbol{A} &\epsilon \{7^b, 18^a, 22^c, 34^b, 36^b\} \\
\boldsymbol{\Delta S_A} &\sim \mathcal{N}\left(\begin{bmatrix} 0 \\ 0 \end{bmatrix}, \begin{bmatrix} 4.5 & -0.2 \\ -0.2 & 0.75 \end{bmatrix} \right), \\
\boldsymbol{A} &\epsilon \{9^c, 14^c, 26^c, 30^a, 31^a\}
\end{aligned} \tag{8.31}$$

where superscript over actor nodes, i.e., $\{a, b, c\}$ represent respective phases of actor nodes at which power is varying. Table 8.2 shows the ranked top 5 DIVF nodes for randomly selected observation nodes at phase 'a' computed using eq. (8.20). For example, it can be seen that node 7 is the most dominant node that impacts voltage fluctuations at node 5. The is because the KL divergence of node 7 is higher than that of other actor nodes when node 5 is the observation node. Notice that when an observation node is an actor node, this observation node will have the highest impact on its own voltage profile (e.g., node 31), which is expected since the voltage profile is impacted more significantly by its local VAR signal compared to that of other nodes [120]. However, there can be scenarios where some nodes are highly dominant (in terms of voltage fluctuations) for some observation nodes but less dominant for others. For example, although node 12 is the most dominant actor node for observation node 11, it is ranked as the 5th most dominant node for observation node 21. Therefore, we use the CPF score in eq. (8.35) to compute the impact of complex power changes at each actor node on the voltage profiles of all observation nodes. Table 8.3 shows the CPF score for all actor nodes in the system. It can be seen from the table that the most

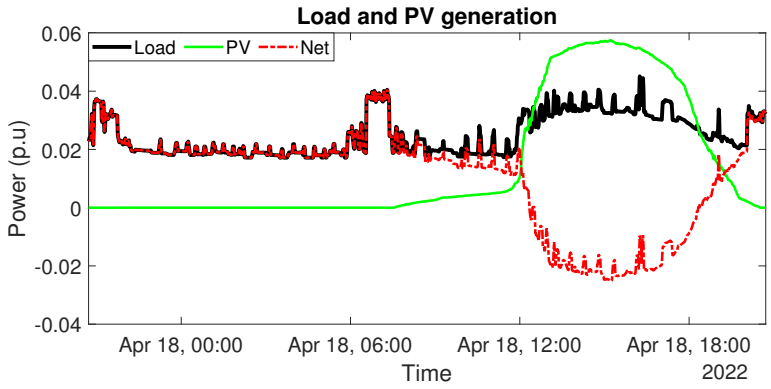

Figure 8.7: Variable PV and load profile.

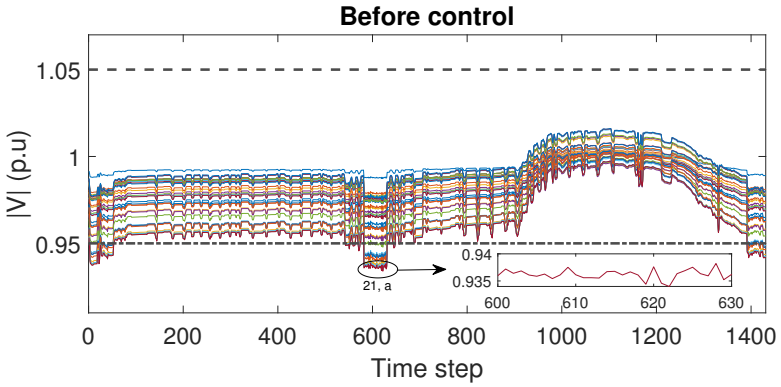

Figure 8.8: Uncontrolled voltage magnitudes of all nodes.

dominant node that impacts voltage fluctuations at all observation nodes is node 18 followed by nodes 17, 14, etc. Now it is possible to compute the SVI set of dominant nodes ($\mathfrak{D}^*_{\check{\mathcal{O}}}$) that participate in the voltage control program. We use the top five dominant nodes (shown by upward arrows in Table 8.3) in the SVI set for this scenario. However, the proposed approach is generic for any choice of nodes and this case is chosen merely to demonstrate the efficacy of the proposed approach. In this case, the SVI set of dominant nodes turns out to be $\mathfrak{D}^*_{\check{\mathcal{O}}} = \{18, 17, 14, 12, 9\}$

To test the effectiveness of the SVI set, it is assumed that actor nodes are integrated with PV units. PV active power injection is modeled as a random process with an uncertainty component as, $\Delta P_{pv} = S(t) + r(t)$ where, $S(t)$ is the mean forecast trend of the active power injection at actor nodes and $r(t) \sim \mathcal{N}(0, \sigma^2_{pv})$ is a zero mean Gaussian that captures PV uncertainty with variance of σ^2_{pv}. In addition to variable PV injections, we assume that the

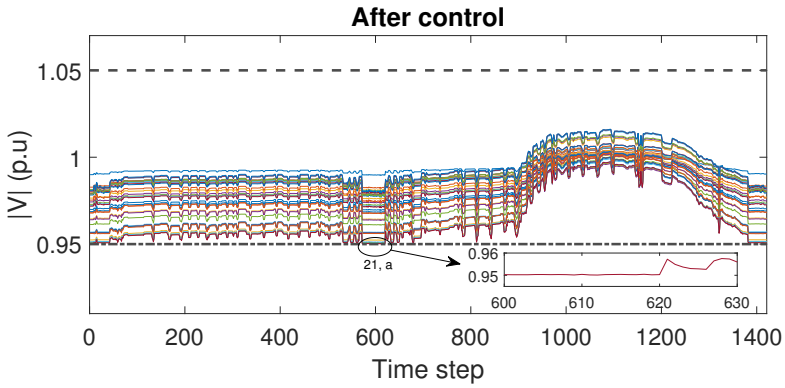

Figure 8.9: Controlled voltage magnitudes of all nodes.

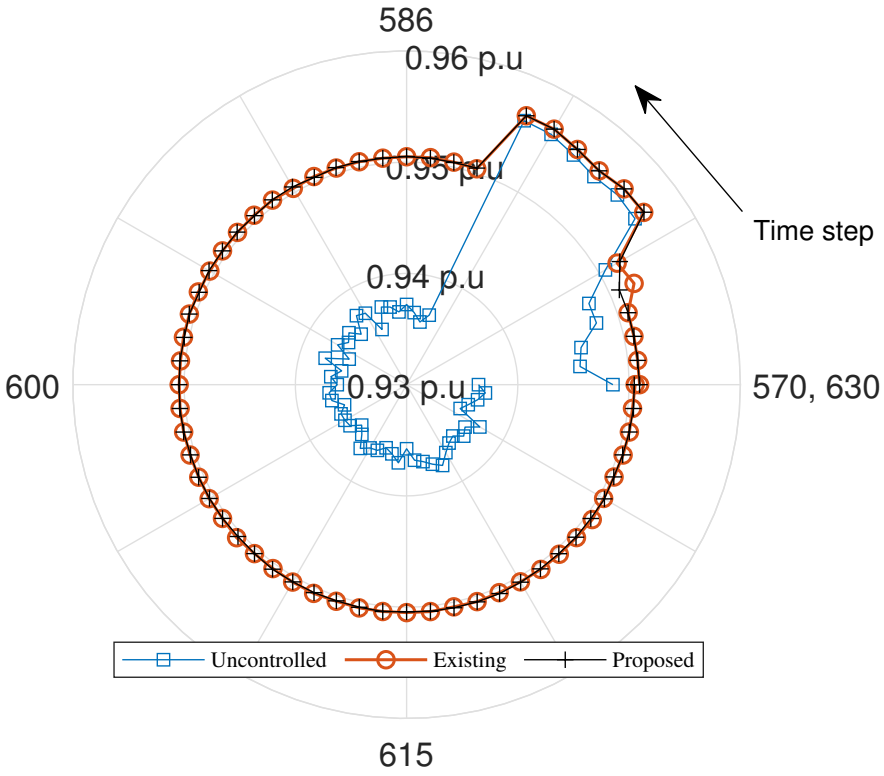

Figure 8.10: Voltage magnitude of node with most significant violation (IEEE 37).

local load is also variable. Fig. 8.7 shows the mean forecast trend of PV injection as well as the variable load pattern, which are based on actual data obtained via eGauge home energy monitoring system [257]. This data is available for one day every minute starting from 20:43:00 until 20:43:00 as shown in the figure.

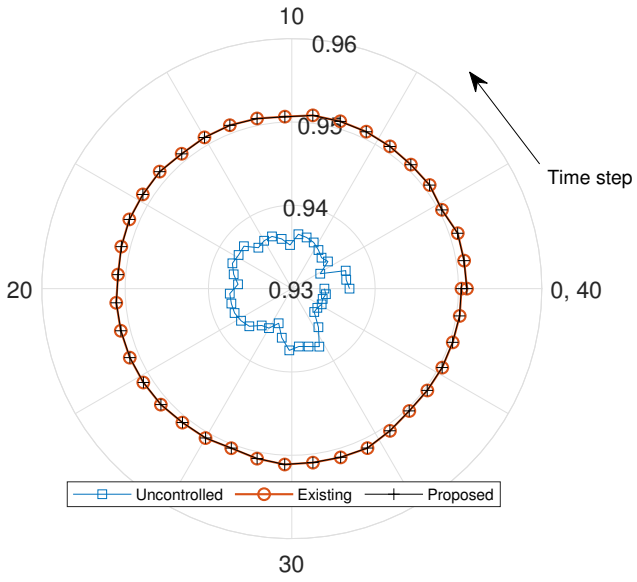

Figure 8.11: Voltage magnitude of node with most significant violation (IEEE 123).

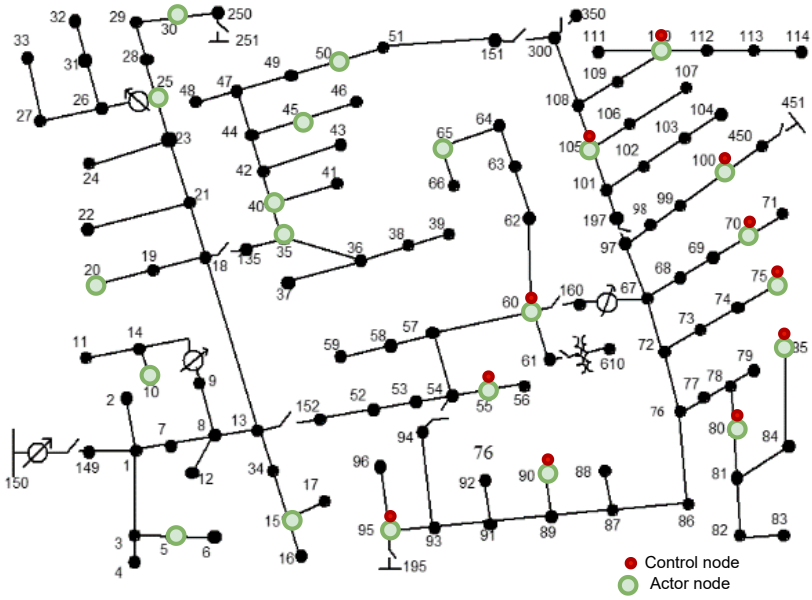

Figure 8.12: Modified IEEE 123-node test system.

Effectiveness of mitigating voltage violations

First, we test the effectiveness of the proposed approach in eliminating all voltage violations given this time horizon. The voltage safe operational limits are set according to the ANSI C84.1 standard, i.e., $0.95 \leq \mathbf{\Gamma x} \leq 1.05$ p.u. Fig. 8.8 shows the voltage magnitudes of all nodes as a result of the complex power changes at actor nodes. It can be seen that the

system experiences multiple under-voltage violations at three different time intervals. The most significant violation is experienced at node 21 phase 'a' as shown in the figure between the interval $[590 - 640]$. The proposed predictive control approach is implemented using the SVI set $\mathfrak{D}^*_{\mathcal{O}}$ to obtain the optimal control sequence, i.e., kVAr adjustments. Fig. 8.9 shows the controlled voltage magnitudes. It can be seen that the proposed approach is able to eliminate all voltage violations across the entire control horizon, which demonstrates the effectiveness of the proposed approach in eliminating all voltage violations. In addition, Fig. 8.10 shows the uncontrolled and controlled voltage magnitude of node 21 over the time period 570-630 (most significant violation) using (1) the proposed approach; and (2) the case when all nodes are chosen to participate in the control program. It can be seen that the proposed approach offers voltage control efficiency (within the 0.95 p.u threshold) similar to the case where all nodes are chosen, which further guarantees the efficiency of the proposed approach. To test the effectiveness of the proposed approach on large systems, a scenario is created with the IEEE 123-node test system where 22 nodes are integrated with inverter-based PV units as shown in Fig. 8.12 with the SVI nodes highlighted in red circles. For simplicity of illustration, the same PV profile has been used from the previous scenario as shown in Fig. 8.7 with time interval of $[0, 40]$. Fig. 8.11 shows the voltage magnitude of the node with the most significant violation as well as the controlled voltage state using the proposed approach and the case where all actor nodes are used in the control program. It can be seen that the proposed approach offers an identical voltage control performance compared to the case when all nodes participate in the control program, which also guarantees the performance of the proposed approach for large systems.

Capturing uncertainty

Next, the effectiveness of the proposed approach is tested against noise in the knowledge of voltage state vector. It is assumed that the voltage state vector varies randomly due to the uncertainty vector $\mathbf{w}_k$ in (8.29). The mean of model uncertainty vector $\mathbf{w}_k$ is chosen to be 0.001 p.u and the variance is set to 10^{-5}. Although the same parameters of the distribution

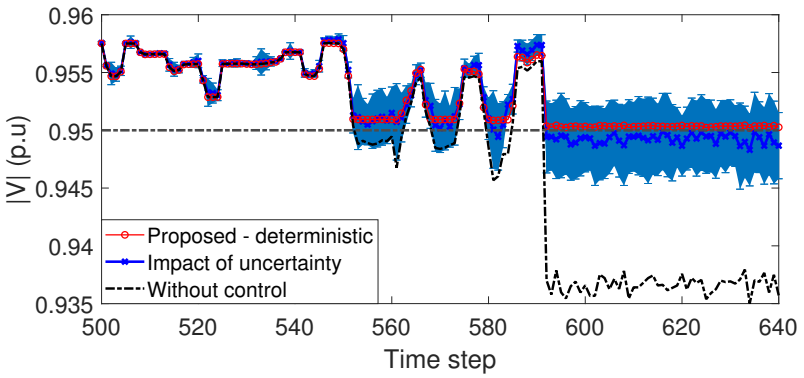

Figure 8.13: Control performance without accounting for uncertainty.

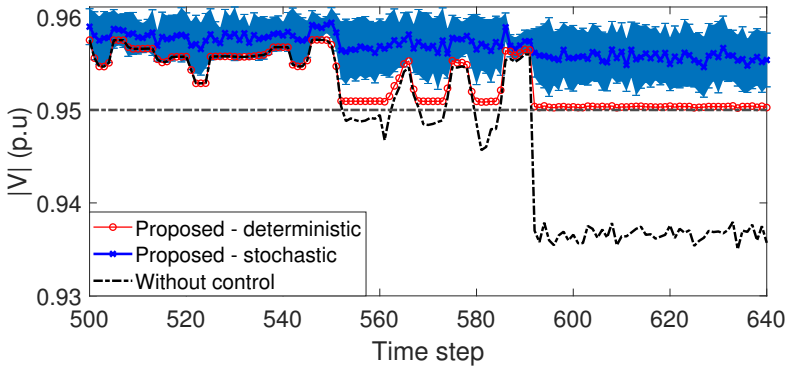

Figure 8.14: Control performance with the proposed stochastic framework.

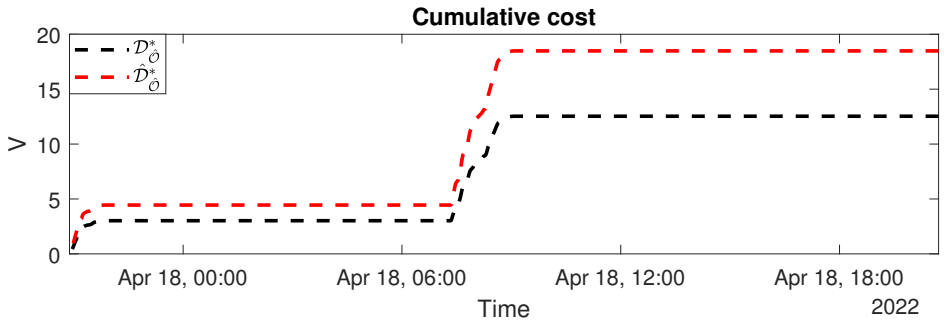

Figure 8.15: Cumulative cost comparison (IEEE 37).

are used to reflect uncertainty at all nodes, the proposed approach is generic and can be applied to the case of different uncertainty parameters for different nodes. Fig. 8.13 shows the voltage profile of node 21 over the time step $500 - 640$ where the most significant violation is experienced. The dark dotted line shows the uncontrolled voltage state. The red line represents the controlled voltage sate with the proposed approach assuming no uncertainty

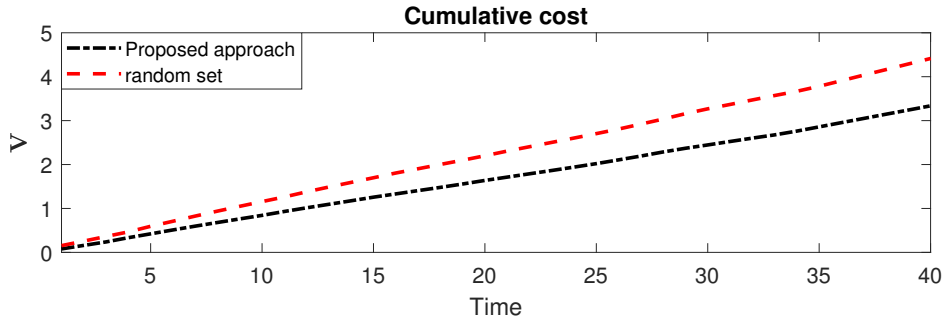

Figure 8.16: Cumulative cost comparison (IEEE 123).

whereas the blue error bar illustrates the impact of injected uncertainty ($\mathbf{w}_k$) on the performance of the control algorithm, i.e., controlled voltage states with uncertainty. To obtain reasonable accuracy, the impact of uncertainty shown in the figure is computed by running 100 simulations. It can be seen from the figure that the introduced uncertainty causes the voltage states to fall outside the safe operational limits even when the control algorithm is active. This is because the controllers assume that the estimated voltage state vector is accurate while in reality it is noisy. Therefore, the controllers' output is less compared to the case when the voltage state vector is deterministic, causing unanticipated violations. To eliminate the unanticipated violations caused by uncertainty, the stochastic control framework in Problem 2 is used. The tightening vector $\boldsymbol{\alpha}$ is set to $0.97\overrightarrow{\mathbf{1}}$ where $\overrightarrow{\mathbf{1}}$ is a vector of ones. This tightening parameter is chosen to ensure the chance constraint in (8.30b) is satisfied with high probability. Fig. 8.14 shows the controlled voltage states using the stochastic approach to account for state uncertainty. Specifically, the blue error bar shows the performance of the proposed approach when the state uncertainty is captured by the chance constraint. It can be seen from the figure that the proposed stochastic approach, compared to the case shown in Fig. 8.13, eliminates all unanticipated violations over the entire control window $500 - 640$, which illustrates the robustness of the proposed approach against practical uncertainty scenarios.

Comparative analysis of cumulative cost

Along with the effectiveness in eliminating voltage violations, the proposed approach provides lower control cost compared to cases where the control set is not optimally chosen. For this, we compare the absolute cumulative cost incurred by using the proposed SVI set ($\mathfrak{D}^*_{\check{\mathcal{O}}}$) against the case when a random set ($\hat{\mathfrak{D}}^*_{\check{\mathcal{O}}}$) of the same size is chosen to participate in the control program. The cumulative cost for the random set is computed by averaging the cumulative stage-wise cost over 100 Monte-Carlo realizations to obtain a reasonable accuracy. Fig. 8.15 illustrates the cumulative cost of the these cases over the entire control horizon, i.e., $k \in [0, N_c - 1]$. It can be seen from the figure that the cumulative cost of both cases increases around the time of the day when voltage violations are experienced in the system, which is expected as the controllers adjust their output to overcome these violations. However, the cumulative cost incurred by the proposed approach (shown in dark dotted line) is significantly lower than the random case (shown in red color), which highlights the efficiency of the proposed approach. Similarly, the proposed approach offers a significant efficiency improvement in terms of control cost for large systems as shown in Fig. 8.16 for the IEEE123-node test system. It is important to note that this efficiency is necessary for modern distribution system control applications given the limited control resources across different nodes [120].

Computational complexity analysis

To further test the efficacy of the proposed approach, we compare the execution time taken by the control algorithm when the proposed SVI set ($\mathfrak{D}^*_{\check{\mathcal{O}}}$) is used against the case where all controllable resources ($\boldsymbol{\mathcal{A}}$) are utilized. The analysis for all cases is implemented using an inter i-9 processor and the corresponding execution time taken by both approaches is reported in Table 8.4. It is important to note that, for both control cases, the convergence is achieved and all voltage states are maintained within safe operational limits. It can be seen from the table that the time taken to successfully control voltage violations is at least an order faster compared to the standard case when all nodes are used in the control algorithm for both

Table 8.4: Comparison of the computational complexity in terms of execution time.

Method	**IEEE 37**	**IEEE 123**
Proposed	0.0136	0.4304
Existing	0.1578	7.4735

test systems (i.e., the IEEE 37 and IEEE 123). Note that with the inclusion of time taken to compute the SVI set, the proposed approach is significantly faster (i.e., multiple orders faster) compared to classical load-flow based approach. Thus, the proposed approach offers a significant improvement in the computational time in terms of computing the dominant nodes and providing voltage support. With this computational advantage, it is possible to leverage the proposed approach to simplify voltage control processes in modern distribution systems considering high levels of consumer edge technologies.

8.3 Dynamic system voltage influencer paradigm

The SVI for any power distribution system is the set of nodes that has the highest impact on all voltage states in the system. Determining the SVI nodes depends on two major factors: (1) the location of node in the system; and (2) the amount of complex power change at this location [32]. Leveraging the strategic location and the power variability of the SVI nodes can potentially improve the efficiency of voltage support programs in terms of reactive power utilization cost [246]. Fig. 8.17 shows an illustration of the dynamic SVI concept across the control horizon $k \in [0, ..., N_c - 1]$. At every time step, complex power changes, base voltages, and topology information are used in the control center, e.g., DSO, to find the SVI nodes that will be used for reactive power support. It can be seen from the figure that the control points (highlighted in red circles) change over time, which improves the efficiency of the voltage control program in terms of reactive power utilization cost. The following subsections discuss the exact steps behind determining the SVI nodes dynamically.

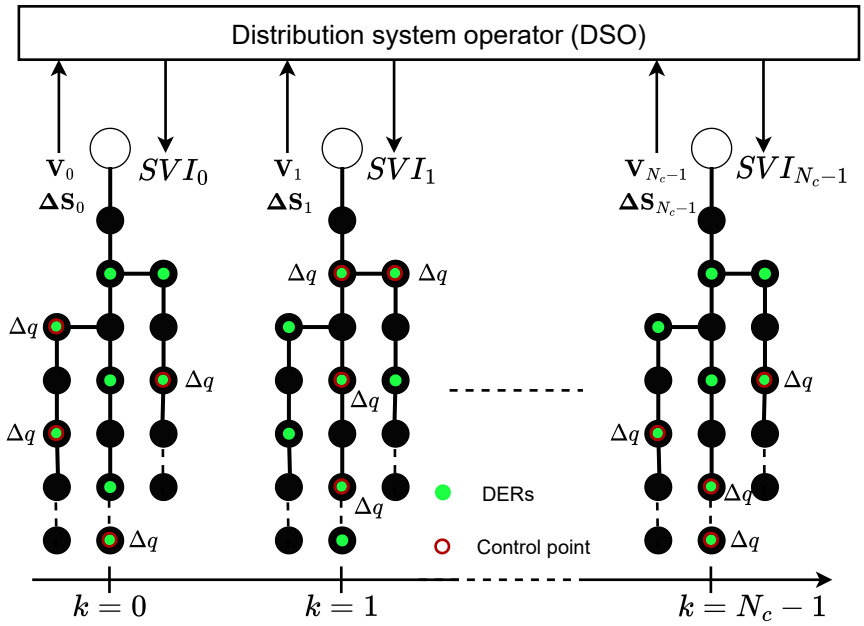

Figure 8.17: Illustration of the dynamic SVI paradigm.

8.3.1 Compute the distribution of voltage magnitude

Uncertainty in complex power changes at actor node causes random changes in voltage magnitudes of observation nodes [250]. The distribution of voltage magnitude at any observation node due to complex power changes at all actor nodes in the system has been shown to follow a Rician distribution with noncentrality and scale parameters κ and σ, respectively [27],

$$|V_O^f| \sim Rician(\kappa, \sigma), \tag{8.32}$$

where, $\kappa = \sqrt{w}$ and $\sigma = \sqrt{\lambda}$ are based on system topology and complex power changes at actor nodes. See [27] for proof of eq. (8.32) and more details. Next, the distribution of voltage magnitude can be used to determine the dominant influencers for each observation node, which can then be used to obtain the SVI nodes.

8.3.2 Obtain and rank nodal dominant influencers

To determine the ranked set of dominant influencers for each observation node, two probability distributions must be computed at every time step $k \in [0, ..., N_c - 1]$,

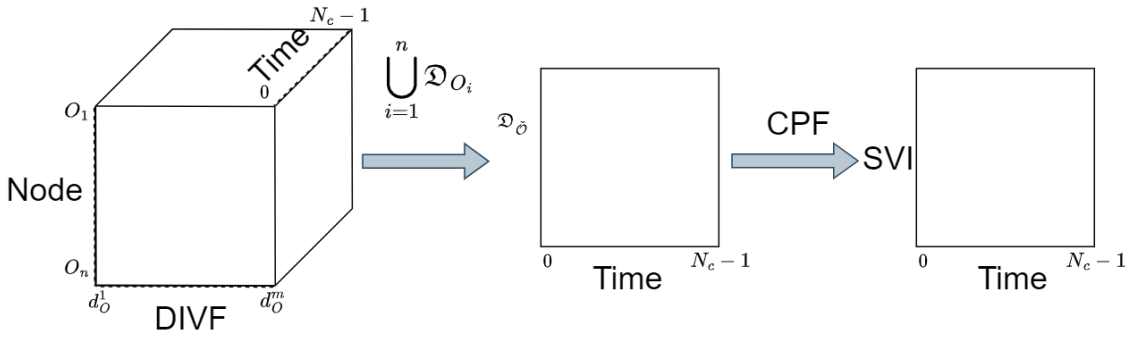

Figure 8.18: Summary of the proposed dynamic SVI paradigm.

- The distribution of voltage magnitude due to the effect of all actor nodes: $|V_O^f|_k$.
- The distribution of voltage magnitude due to the effect of a single actor node (A): $|V_O^{f,A}|_k$.

For a given observation node O, the most domiant influencer node is the node that minimizes the statistical distance between the two distributions. To quantify the statistical distance between the probability distributions, we use the Kullback–Leibler (KL) divergence as it is multiple orders faster in terms of execution time [32] compared to classical load-flow based approaches. This process can be repeated for every pair of actor and observation nodes, which can then be used to rank the actor nodes in terms of there influence on the voltage profile of each observation node. As shown in our prior work [32], this computation is very efficient as it relies on analytical approximations. Thus, for every observation node $j \in n$ at every time step $k \in [0, ..., N_c - 1]$ there is a unique set of DIVF nodes ($\mathfrak{D}_{O_{j,k}}$) that impact its voltage profile, i.e.,

$$\mathfrak{D}_{O_{j,k}} = \{d^1_{O_{j,k}}, d^2_{O_{j,k}}, ..., d^m_{O_{j,k}}\}, \tag{8.33}$$

where, $d^1_{O_{j,k}}$ and $d^m_{O_{j,k}}$ are the most and least dominant nodes, respectively.

8.3.3 Compute the system voltage influencer set

A natural way to compute the SVI nodes is to dynamically ($\forall k \in [0, ..., N_c - 1]$) compute the union of DIVF sets considering all observation nodes as follows,

$$\begin{aligned}\mathfrak{D}_{\check{\mathcal{O}},k} &= \bigcup_{j=1}^{n} \mathfrak{D}_{O_{j,k}} = \mathfrak{D}_{O_{1,k}} \cup \mathfrak{D}_{O_{2,k}} \cup .... \cup \mathfrak{D}_{O_{n,k}} \\ &= \{d^1_{\check{\mathcal{O}},k}, d^2_{\check{\mathcal{O}},k}, ..., d^m_{\check{\mathcal{O}},k}\}. \end{aligned} \tag{8.34}$$

However, there might be cases where some actor nodes are high in rank for certain observation nodes but low in rank for others. To prevent such cases, a control participation factor (CPF) is developed to assign weights to the nodes within the union set in eq. (8.34). For any actor node $i \in \mathfrak{D}_{\check{\mathcal{O}},k}$ at any time step k, CPF^i_k can be computed as,

$$\begin{aligned}\text{CPF}^i_k &= |\mathbf{x}^T_{O_{1,k}} \mathbf{x}_{O_{1,k}} - 1|||\mathbf{B}(\mathbf{x}_{O_{1,k}}, d^i_{\check{\mathcal{O}},k})||+... \\ &+|\mathbf{x}^\intercal_{O_{n,k}} \mathbf{x}_{O_{n,k}} - 1|||\mathbf{B}(\mathbf{x}_{O_{n,k}}, d^i_{\check{\mathcal{O}},k})||. \end{aligned} \tag{8.35}$$

Here, the term $|\mathbf{x}^T_{O_{1,k}} \mathbf{x}_{O_{1,k}} - 1|$ contains the voltage deviation from the nominal value (i.e., 1 p.u) and $||\mathbf{B}(\mathbf{x}_{O_{1,k}}, d^i_{\check{\mathcal{O}},k})||$ represents the sensitivity between actor and observation nodes obtained using eq. (**??**). Finally, the actor nodes can be ranked in a descending order to obtain the SVI set ($\mathfrak{D}^*_{\check{\mathcal{O}}}$) that have the maximum influence on system voltage profiles where the utility can choose the top $\check{m} \in m$ nodes to provide reactive power support,

$$\mathfrak{D}^*_{\check{\mathcal{O}}} = \{d^{1*}_{\check{\mathcal{O}},k}, d^{2*}_{\check{\mathcal{O}},k}, ..., d^{(\check{m}-1)*}_{\check{\mathcal{O}},k}, d^{\check{m}*}_{\check{\mathcal{O}},k}\}. \tag{8.36}$$

Fig. 8.18 shows a summary of the proposed approach. Note that the DIVF sets of individual nodes at the initial step are computed sequentially for each node, which then can be used to compute the SVI nodes.

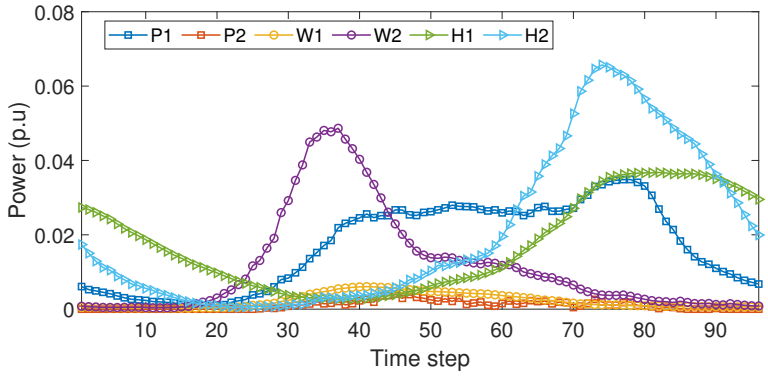

Figure 8.19: EV charging behavior for different charger types.

8.3.4 Simulation results

The proposed dynamic SVI approach is verified via simulations on the unbalanced IEEE 37 node test system with base voltage of 4.8 kV. 15 nodes are randomly chosen to be integrated with PV assets. To account for PV power output variability, it is assumed that the PV profile varies randomly according to a mean forecast trend ($S(t)$) with an uncertainty component

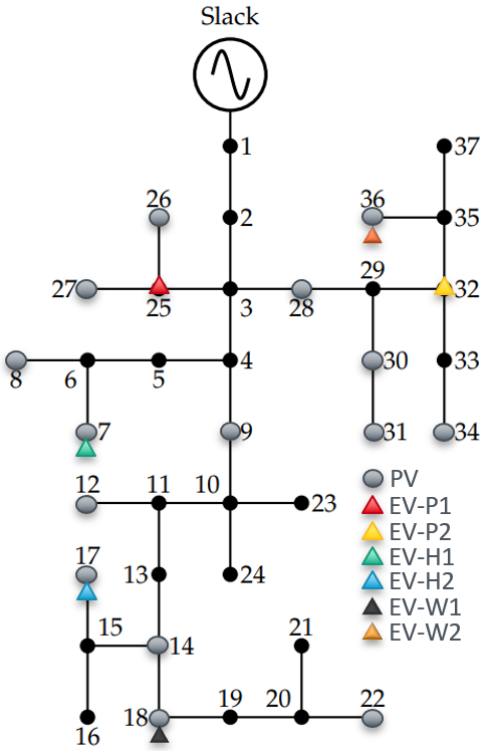

Figure 8.20: Modified IEEE 37 node test system.

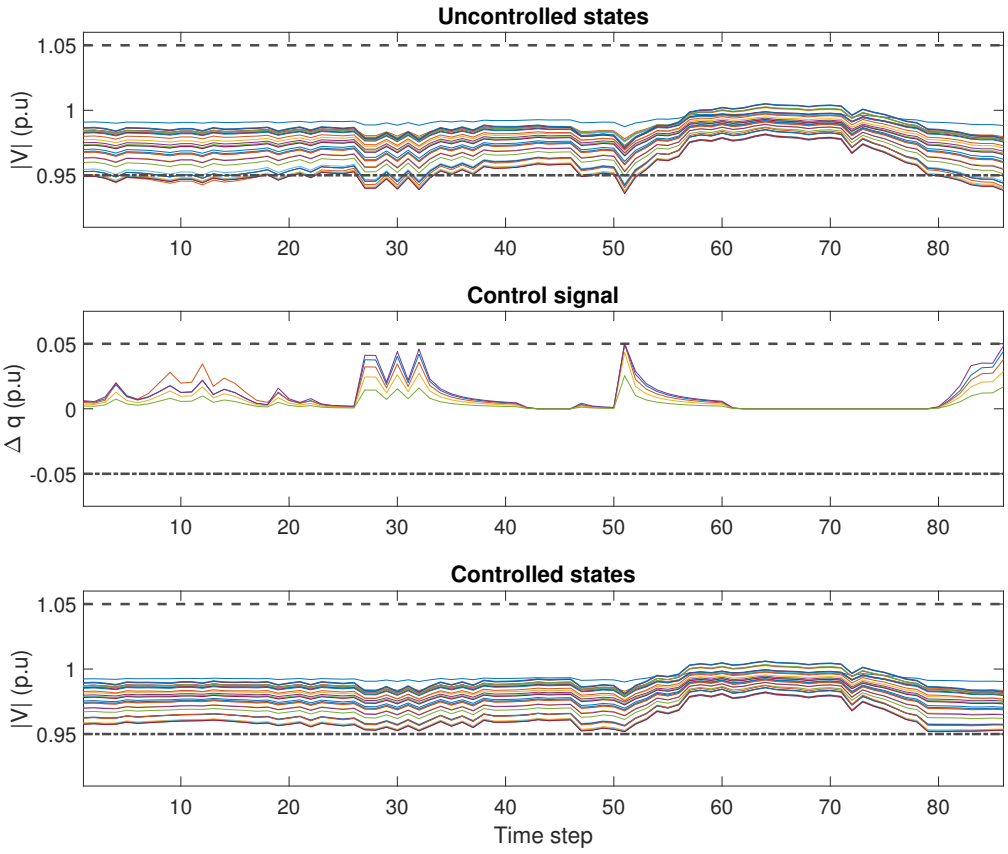

Figure 8.21: Voltage control performance for all nodes.

$(r(t))$, i.e., $\Delta P_{PV}(t) = S(t) + r(t)$. The PV data is obtained via eGauge monitoring system for one day at 15 minute intervals [257]. In addition to the PV profile, we assume that 6 different EV charging stations are also integrated into the system at 6 randomly selected locations. The EV profiles include public, work, and home charging stations with two charger types, i.e., level 1 and level 2 chargers. The daily EV charging station profiles with 15 minute intervals (shown in Fig. 8.19) are obtained through EVI-Pro tool that contains EV charging load estimates, which is developed by National Renewable Energy Laboratory and the California Energy Commission [**?**]. The spatial distribution of PV assets and EV charging stations is illustrated in Fig. 8.20. Using this scenario, the DIVF nodes are computed for all nodes in the system at all time steps using eq. (8.33). For example, the top dominant influencer node for node 5 is found to be 7 for time steps 1 and 15 whereas it is 8

for time step 30. This is due to the difference in PV injection, load, and EV consumption at these nodes for the different time steps. It is important to note that these ranks can differ for observation nodes and time steps. Therefore, the accuracy of the proposed approach is evaluated against actual load flow-based method by averaging the identification error over all possible observation nodes (36 nodes excluding the source node) and time steps (96 steps for a 24-hour profile with 15 minutes intervals). It is found that the accuracy of identifying top dominant node and top-5 dominant nodes is 97.29% and 95.10%, respectively. Note that the proposed approach is multiple orders faster compared to classical load flow-based method since sampling random variables from standard probability distributions, e.g., eq. (8.32), removes the need to simulate large number of scenarios [20].

Next, the top five DIVF nodes are used to compute SVI nodes for all time steps according to eq. 8.36. The resulting dynamic SVI nodes are computed and ranked in a descending order (R1 to R5) as shown for selected time steps in Table 8.5. The SVI nodes are then used to implement reactive power support at any time voltage violation is predicted at any node in the system. The voltage control performance using the SVI nodes is shown in Fig. 8.21. It can be seen from Fig. 8.21-(a) that multiple voltage violations are experienced at different time instances due to increased load or EV consumption. To prevent such violations, the SVI nodes are used within the voltage control problem in eq. (8.27). The corresponding reactive power setpoints for different SVI nodes are shown in Fig. 8.21-(b) and the controlled voltage states are illustrated in Fig. 8.21-(c). It can be seen from the figure that it is possible to eliminate all voltage violations using the dynamic SVI paradigm. Moreover, the proposed SVI approach helps to reduce the cumulative control cost compared to the cases when the SVI set is static or is randomly chosen. Fig. 8.22 shows the cost-effectiveness of the proposed approach compared to the other cases. The static SVI approach uses the initial SVI nodes (i.e., at time step 0) for the entire control horizon whereas the dynamic random case chooses any random set of control nodes without incorporating their influence on system voltage profiles. The cost of the lateral case is computed by averaging the cumulative cost of 100 random scenarios where nodes are randomly chosen. It can be seen that the proposed dynamic SVI approach offers a significant cost reduction compared to other cases and that

Table 8.5: Dynamic SVI nodes for voltage control applications.

Node	SVI-1	SVI-14	SVI-16	SVI-30	SVI-60	SVI-90
R1	18	18	18	18	18	18
R2	17	17	17	17	17	17
R3	12	12	14	14	12	12
R4	22	22	12	12	22	22
R5	8	9	22	22	8	8

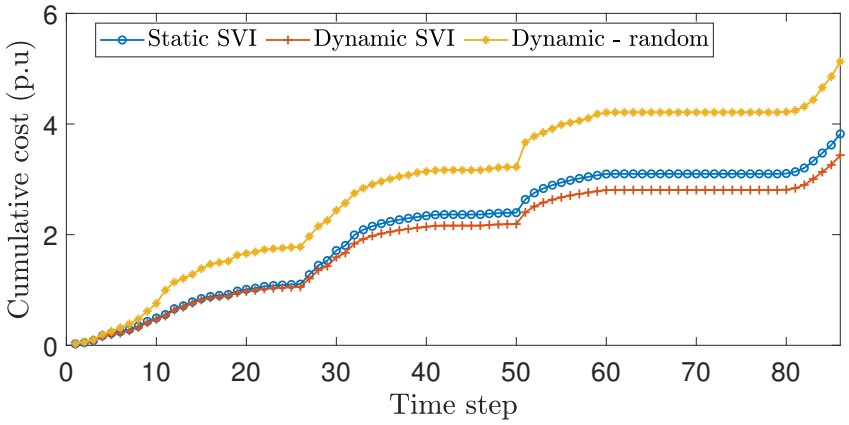

Figure 8.22: Cumulative control cost.

is because the influence of actor nodes on system voltage profiles is incorporated at every time step of the control horizon. Therefore, identifying dynamic SVI nodes helps utilities to implement cost-effective voltage control programs especially in cases where reactive power supply is limited in the system.

8.4 Summary

This chapter proposes a new SE based voltage control framework that helps to efficiently eliminate voltage violations in distribution systems via inverter-based DERs. First, voltage states are estimated using MC based method and then voltage estimates with PV forecasts are utilized by a finite-horizon MPC to regulate nodal voltages while satisfying system constraints. Additionally, the proposed framework uses an analytical voltage sensitivity framework to predict voltage states for a given PV injection profile. Simulation results demonstrate that the proposed framework works well for applications where voltage measurements are

not available across all nodes in the system. Additionally, this chapter identifies strategic locations to implement inverter-based DER control. In this regard, the CPF factor is used to rank nodes with DERs based on their voltage influence, which then can be used to identify the SVI set that can be used in the control program. Results show that the proposed approach offers at least an order faster execution time and reduces the overall control cost when compared to existing methods while taking into account uncertainty related to complex power changes of DERs or load variability. The advantages of the proposed approach make it a suitable tool for real-time voltage control applications in modern distribution systems. Additionally, the proposed approach is generic and can be applied with any control architecture, which can scale up these advantages.

Chapter 9

Conclusions and future work

This chapter concludes the dissertation by summarizing the major contributions and highlighting future research directions.

9.1 Conclusion

In the light of increased integrated of grid-edge technologies, e.g., DERs and EVs, in modern power distribution systems, impact analysis studies have garnered a huge attention. This dissertation addresses fundamental research questions related to efficient modern distribution system planning, operation, and control with the presence on high penetration levels of these technologies. Specifically, this dissertation develops simple, yet accurate, analytical impact-assessment frameworks that can be utilized for various downstream applications. First, a foundational sensitivity analysis framework is developed to quantify the impact of grid-edge technologies on line losses and voltage magnitudes. Then, by leveraging existing knowledge of state measurements along with uncertain forecasts of power generation/demand, a probabilistic sensitivity framework is used to reveal impending voltage issues and excessive power losses at any node/line in the system at different time instances. The main goals across all of the proposed frameworks in this dissertation center around: (1) capturing uncertainties of power changes, (2) alleviating the computational burden of existing methods, (3) providing

foresight to reduce the reliance on reactionary approaches; and (4) mitigating modeling inefficiencies to remove accuracy-complexity trade-offs. The development of these frameworks helps system operators quickly quantify detrimental impacts of grid-edge technologies, plan their integration, and identify strategic locations to participate in voltage control programs, which is a key achievement that improves system efficiency and ensures its reliability. The major contributions of this dissertation are summarized below:

Over the past few decades, power loss minimization in distribution systems has gained popularity and the need for LSA frameworks has become a necessity for its successful implementation. Existing work on LSA mostly focuses on system planning aspects through DER optimal placement and sizing. However, enabling LSA-based system operational applications is a vital step toward the successful transition to modern distribution systems. In Chapter 3, a comprehensive overview analysis of LSA applications in modern distribution systems is presented. First, the theoretical formulations of existing LSA methods are summarized. Then, based on the analysis of literature, open research gaps and future research pathways are discussed.

Chapter 4 develops a computationally efficient probabilistic loss sensitivity framework for approximating the impact of random power changes on power losses. First, an analytical expression is derived to approximate the change in line losses for any given deterministic power changes. Then, the analytical expression is extended to a probabilistic framework that accommodates variability related to power changes. The proposed approach is validated via simulation against the traditional load flow-based sensitivity method using the IEEE 69 node test system. Simulation results demonstrate that the proposed approach is accurate and computationally efficient. The proposed framework is useful for real-time loss monitoring and EV charging station allocation studies as shown in Chapter 7. Chapter 5 generalizes the concept developed in Chapter 4 and proposes a novel sensitivity framework that quantifies the impact of grid-edge technologies on line losses for three-phase unbalanced distribution systems. The effectiveness of the proposed approach is illustrated via simulations using the IEEE 37 and IEEE 123-node test systems. Results show that the proposed approach offers over $\sim 98\%$ approximation accuracy with four-orders faster execution time when compared to

classical approaches, resulting in a unique tool that enables efficient planning in unbalanced distribution systems, where the amount of power changes may differ at different phases.

Chapter 6 proposes a novel voltage monitoring approach based on low-complexity, analytical probabilistic voltage sensitivity analysis. Using system data and forecasts, the proposed approach predicts the probability distribution of node voltage magnitudes, which is then used to identify nodes that may violate the nominal operational limits, e.g., $0.95 < |v| < 1.05$ p.u with high probability. The method is tested on the unbalanced IEEE 37-node test system considering integrated distributed solar energy sources. The method is validated against the classic load flow-based method and offers over 95% accuracy in predicting voltage violations. The usefulness of this work is not only in predicting voltage violations in unbalanced distribution grids, but also in opening up the door for optimal voltage control applications. The developed prediction rule is also updated to account for voltage measurement error or missing values. The usefulness of this approach is not only in predicting voltage violations in unbalanced systems, but also in opening up the door for proactive voltage control applications.

In Chapter 7, a new Spatio-temporal sensitivity approach is based on probabilistic voltage sensitivity analysis that exploits both spatial and temporal uncertainties associated with PV injections. The derived distribution is used to quantify voltage violations for various PV penetration levels and subsequently determine the hosting capacity of the system without the need to examine a large number of load-flow scenarios. Similarly, the Spatio-temporal uncertainties are evaluated tp identify nodes with least contribution to losses and voltage deviations used as candidate nodes for charging station placement. The proposed frameworks are validated via conventional load flow-based simulation approach on the IEEE 37 and IEEE 123 node test systems. Results show that using the proposed Spatio-temporal sensitivity analysis helps remove the accuracy-complexity trade-off associated with classical load flow-based methods.

Finally, Chapter 8 proposes sensitivity-based voltage control frameworks by leveraging the capabilities of inverter-based DERs. Specifically, a new system voltage influencer (SVI) paradigm is derived based on analytical voltage sensitivity analysis to identify the most

suitable inverter-based DER assets that must be engaged in the voltage control program. SVI nodes are based on existing system topology and temporal changes in local load, DER, or EV patterns. Therefore, the proposed approach ranks the SVI nodes and uses the most influential nodes for voltage control applications. The proposed approach is verified via simulations on the IEEE 37 and IEEE 123-node test systems. In cases where voltage measurements are not available, a matrix completion-based state estimation approach is used to estimate missing voltage states. In addition to eliminating voltage violations, results show that the proposed approach helps reduce the cumulative control cost.

9.2 Future work

This section presents possible future research directions in the areas of impact assessment, and sensitivity-based planning and operation of modern power distribution systems. The following lists possible extensions to the work presented in this dissertation:

- The proposed probabilistic loss sensitivity analysis framework in Chapters 4 and 5 uses existing topology information to guide the approximation. However, there could be scenarios where this information is variable due to system reconfiguration, or is inaccessible to system operators, especially at the secondary level. Therefore, extending the proposed frameworks to different system topologies can be pursued in the future.

- The voltage violation prediction rule in Chapter 6 uses present voltage states to predict voltage violations based on anticipated power changes. It would be useful to investigate the performance of data-driven approaches in this regard. By leveraging historical power data within a machine learning approach, it is possible to estimate voltage sensitivity coefficients without the need to rely on present voltage states, especially in low-observable systems.

- One of the major strengths of the proposed hosting capacity analysis framework in Chapter 7 is the computational efficiency. One could leverage this advantage to develop a dynamic hosting capacity evaluation that involves continuous time series data of

power demand, PV injection, and EV load. Additionally, it is possible to develop a generic hosting capacity analysis framework that analyzes not only voltage violations but also current flow limits and power losses. In the presence of high EV penetration levels, a dynamic evaluation of individual feeders/nodes' hosting capacity becomes crucial in order to avoid network congestion and improve consumer experience.

- The EV charging station planning presented in Chapter 7 analyses the performance solely from a distribution system operator perspective. In addition to distribution system indicators, it would be useful to generalize the analysis to include traffic network constraints such as EV flows and congested areas. Moreover, customer-oriented metrics such as distance to charging stations and dynamic pricing can be analyzed as part of future work.

- The proposed SVI paradigm in Chapter 8, although tested with a centralized control architecture, it is generic and can be applied with any existing control architecture. Therefore, future research can focus on testing the developed approach with a decentralized control architecture for additional computational benefits, especially for large systems. In addition, it is possible to use reinforcement learning to guide the control architecture to simplify the iterations of interior point method. Moreover, the proposed model can be extended to include adjusting active power setpoints with incentivized customer participation in the voltage control program.

- The analytical sensitivity metrics developed in Chapters 4 to 8 are validated on distribution systems. Given the generalizibility of these metrics, it would be useful to develop similar analytical approaches for transmission system. This extension enables system operators to study the impact of power/voltage changes in both domains, i.e., distribution and transmission systems, on each other, resulting in a holistic impact-analysis tool that reveals impending issues in both entities.

Bibliography

[1] A. Ehsan and Q. Yang, "Optimal integration and planning of renewable distributed generation in the power distribution networks: A review of analytical techniques," *Applied Energy*, vol. 210, pp. 44–59, 2018.

[2] M. H. Amini, M. P. Moghaddam, and O. Karabasoglu, "Simultaneous allocation of electric vehicles' parking lots and distributed renewable resources in smart power distribution networks," *Sustainable cities and society*, vol. 28, pp. 332–342, 2017.

[3] F. Al-Turjman and M. Abujubbeh, "Iot-enabled smart grid via sm: An overview," *Future Generation Computer Systems*, vol. 96, pp. 579–590, 2019.

[4] K. Jhala, B. Natarajan, and A. Pahwa, "Prospect theory-based active consumer behavior under variable electricity pricing," *IEEE Transactions on Smart Grid*, vol. 10, no. 3, pp. 2809–2819, 2018.

[5] J. Ebrahimi, M. Abedini, and M. M. Rezaei, "Optimal scheduling of distributed generations in microgrids for reducing system peak load based on load shifting," *Sustainable Energy, Grids and Networks*, vol. 23, p. 100368, 2020.

[6] N. Stringer, N. Haghdadi, A. Bruce, and I. MacGill, "Fair consumer outcomes in the balance: Data driven analysis of distributed pv curtailment," *Renewable Energy*, vol. 173, pp. 972–986, 2021.

[7] H. Mortazavi, H. Mehrjerdi, M. Saad, S. Lefebvre, D. Asber, and L. Lenoir, "A monitoring technique for reversed power flow detection with high pv penetration level," *IEEE Transactions on Smart Grid*, vol. 6, no. 5, pp. 2221–2232, 2015.

[8] C. Zhang and Y. Xu, "Hierarchically-coordinated voltage/var control of distribution networks using pv inverters," *IEEE Transactions on Smart Grid*, vol. 11, no. 4, pp. 2942–2953, 2020.

[9] K. E. Adetunji, I. W. Hofsajer, A. M. Abu-Mahfouz, and L. Cheng, "Category-based multiobjective approach for optimal integration of distributed generation and energy storage systems in distribution networks," *IEEE Access*, vol. 9, pp. 28237–28250, 2021.

[10] M. Abujubbeh, S. Munikoti, and B. Natarajan, "Probabilistic voltage sensitivity based preemptive voltage monitoring in unbalanced distribution networks," *arXiv preprint arXiv:2008.10814*, pp. 1–6, 2020.

[11] P. Jahangiri and D. C. Aliprantis, "Distributed volt/var control by pv inverters," *IEEE Transactions on power systems*, vol. 28, no. 3, pp. 3429–3439, 2013.

[12] S. Xu, Y. Xue, and L. Chang, "Review of power system support functions for inverter-based distributed energy resources-standards, control algorithms, and trends," *IEEE open journal of Power electronics*, vol. 2, pp. 88–105, 2021.

[13] D. G. Photovoltaics and E. Storage, "Ieee standard for interconnection and interoperability of distributed energy resources with associated electric power systems interfaces," *IEEE Std*, pp. 1547–2018, 2018.

[14] S. Munikoti, M. Abujubbeh, K. Jhala, and B. Natarajan, "A novel framework for hosting capacity analysis with spatio-temporal probabilistic voltage sensitivity analysis," *International Journal of Electrical Power & Energy Systems*, vol. 134, p. 107426, 2022.

[15] W. Sheng, K.-Y. Liu, Y. Liu, X. Meng, and Y. Li, "Optimal placement and sizing of distributed generation via an improved nondominated sorting genetic algorithm ii," *IEEE Transactions on Power Delivery*, vol. 30, no. 2, pp. 569–578, 2014.

[16] C. Wang and M. H. Nehrir, "Analytical approaches for optimal placement of distributed generation sources in power systems," *IEEE Transactions on Power systems*, vol. 19, no. 4, pp. 2068–2076, 2004.

[17] P. Díaz, M. Pérez-Cisneros, E. Cuevas, O. Camarena, F. A. F. Martinez, and A. González, "A swarm approach for improving voltage profiles and reduce power loss on electrical distribution networks," *IEEE Access*, vol. 6, pp. 49498–49512, 2018.

[18] E. R. Ramos, A. G. Expósito, J. R. Santos, and F. L. Iborra, "Path-based distribution network modeling: application to reconfiguration for loss reduction," *IEEE Transactions on power systems*, vol. 20, no. 2, pp. 556–564, 2005.

[19] B. Mirafzal and A. Adib, "On grid-interactive smart inverters: features and advancements," *IEEE Access*, vol. 8, pp. 160526–160536, 2020.

[20] M. Abujubbeh, S. Munikoti, A. Pahwa, and B. Natarajan, "Probabilistic loss sensitivity analysis in power distribution systems," *IEEE Transactions on Power Systems*, 2022.

[21] M. Abujubbeh and B. Natarajan, "Overview of loss sensitivity analysis in modern distribution systems," *IEEE Access*, vol. 10, pp. 16037–16051, 2022.

[22] M. Abujubbeh, S. Munikoti, and B. Natarajan, "Analytical power loss sensitivity analysis in distribution systems," in *2021 IEEE Power & Energy Society General Meeting (PESGM)*, pp. 1–5, IEEE, 2021.

[23] Y. Liu, Z. Li, and Y. Zhou, "Data-driven-aided linear three-phase power flow model for distribution power systems," *IEEE Transactions on Power Systems*, 2021.

[24] L. Huang, D. Chen, C. S. Lai, Z. Huang, A. F. Zobaa, and L. L. Lai, "A distributed optimization model for mitigating three-phase power imbalance with electric vehicles and grid battery," *Electric Power Systems Research*, vol. 210, p. 108080, 2022.

[25] M. Abujubbeh and B. Natarajan, "A novel stochastic framework to quantify losses in unbalanced distribution systems," *IEEE Transactions on Power Systems*, 2023.

[26] M. Abujubbeh, S. Dahale, and B. Natarajan, "Voltage violation prediction in unobservable distribution systems," in *2022 IEEE Power & Energy Society General Meeting (PESGM)*, pp. 1–5, IEEE, 2022.

[27] M. Abujubbeh, S. Munikoti, and B. Natarajan, "Probabilistic voltage sensitivity based preemptive voltage monitoring in unbalanced distribution networks," in *2020 52nd North American Power Symposium (NAPS)*, pp. 1–6, IEEE, 2021.

[28] M. Abujubbeh and B. Natarajan, "A new probabilistic framework for ev charging station planning in distribution systems considering spatio-temporal uncertainties," in *IEEE Kansas Power and Energy Conference (KPEC)*, Under Review, 2023.

[29] M. Abujubbeh, M. Sai, K. Jhala, and B. Natarajan, "A new analytical voltage influencer paradigm for voltage control in power distribution systems," *International Journal of Electrical Power & Energy Systems*, 2023.

[30] M. Abujubbeh and B. Natarajan, "A novel dynamic voltage influencing metric for cost-effective voltage control in unbalanced distribution systems," in *2023 IEEE PES GTD, Istanbul*, Accepted, 2023.

[31] M. Abujubbeh, R. K. James, A. Pahwa, B. Natarajan, *et al.*, "Optimal voltage control in low-observable unbalanced distribution systems," in *2022 IEEE Power & Energy Society Innovative Smart Grid Technologies Conference (ISGT)*, pp. 1–5, IEEE, 2022.

[32] S. Munikoti, M. Abujubbeh, K. Jhala, and B. Natarajan, "An information theoretic approach to identify dominant voltage influencers for unbalanced distribution systems," *IEEE Transactions on Power Systems*, 2022.

[33] J. Guerrero, A. C. Chapman, and G. Verbic, "Decentralized p2p energy trading under network constraints in a low-voltage network," *IEEE Transactions on Smart Grid*, vol. 10, no. 5, pp. 5163–5173, 2018.

[34] B. Singh and D. K. Mishra, "A survey on enhancement of power system performances

by optimally placed dg in distribution networks," *Energy Reports*, vol. 4, pp. 129–158, 2018.

[35] R. S. Rao, K. Ravindra, K. Satish, and S. Narasimham, "Power loss minimization in distribution system using network reconfiguration in the presence of distributed generation," *IEEE transactions on power systems*, vol. 28, no. 1, pp. 317–325, 2012.

[36] Y. Li, B. Feng, G. Li, J. Qi, D. Zhao, and Y. Mu, "Optimal distributed generation planning in active distribution networks considering integration of energy storage," *Applied energy*, vol. 210, pp. 1073–1081, 2018.

[37] C. Wang and M. Nehrir, "Analytical approaches for optimal placement of distributed generation sources in power systems," in *IEEE Power Engineering Society General Meeting, 2005*, pp. 2393–Vol, IEEE, 2005.

[38] H. Hedayati, S. A. Nabaviniaki, and A. Akbarimajd, "A method for placement of dg units in distribution networks," *IEEE transactions on power delivery*, vol. 23, no. 3, pp. 1620–1628, 2008.

[39] M. Kashem, A. D. Le, M. Negnevitsky, and G. Ledwich, "Distributed generation for minimization of power losses in distribution systems," in *2006 IEEE Power Engineering Society General Meeting*, pp. 8–pp, IEEE, 2006.

[40] V. M. Quezada, J. R. Abbad, and T. G. S. Roman, "Assessment of energy distribution losses for increasing penetration of distributed generation," *IEEE Transactions on power systems*, vol. 21, no. 2, pp. 533–540, 2006.

[41] D. Kirschen, R. Allan, and G. Strbac, "Contributions of individual generators to loads and flows," *IEEE Transactions on power systems*, vol. 12, no. 1, pp. 52–60, 1997.

[42] A. J. Conejo, F. D. Galiana, and I. Kockar, "Z-bus loss allocation," *IEEE Transactions on Power Systems*, vol. 16, no. 1, pp. 105–110, 2001.

[43] J. Bialek, "Tracing the flow of electricity," *IEE Proceedings-Generation, Transmission and Distribution*, vol. 143, no. 4, pp. 313–320, 1996.

[44] F. Tamp and P. Ciufo, "A sensitivity analysis toolkit for the simplification of mv distribution network voltage management," *IEEE Transactions on Smart Grid*, vol. 5, no. 2, pp. 559–568, 2014.

[45] F. Rotaru, G. Chicco, G. Grigoras, and G. Cartina, "Two-stage distributed generation optimal sizing with clustering-based node selection," *International journal of electrical power & energy systems*, vol. 40, no. 1, pp. 120–129, 2012.

[46] A. Koirala, T. Van Acker, D. Van Hertem, J. Camargo, and R. D'hulst, "General polynomial chaos vs crude monte carlo for probabilistic evaluation of distribution systems," in *2020 International Conference on Probabilistic Methods Applied to Power Systems (PMAPS)*, pp. 1–6, IEEE, 2020.

[47] J. Laowanitwattana and S. Uatrongjit, "Probabilistic power flow analysis based on arbitrary polynomial chaos expansion for networks with uncertain renewable sources," *IEEJ transactions on Electrical and Electronic Engineering*, vol. 13, no. 12, pp. 1754–1759, 2018.

[48] J. Lu, L. L. Zhang, D. Y. Shi, T. Li, J. C. Tang, and D. Cui, "On-line data splicing power flow analysis method based on sensitivity," *Energy Reports*, vol. 7, pp. 326–333, 2021.

[49] J. Dancker, C. Klabunde, and M. Wolter, "Sensitivity factors in electricity-heating integrated energy systems," *Energy*, vol. 229, p. 120600, 2021.

[50] W. Wu and B. Lin, "Benefits of electric vehicles integrating into power grid," *Energy*, vol. 224, p. 120108, 2021.

[51] M. Abujubbeh and M. Fahrioglu, "Determining maximum allowable pv penetration level in transmission networks: Case analysis-northern cyprus power system," in *2019*

1st Global Power, Energy and Communication Conference (GPECOM), pp. 292–297, IEEE, 2019.

[52] K. Jhala, V. Krishnan, B. Natarajan, and Y. Zhang, "Data-driven preemptive voltage monitoring and control using probabilistic voltage sensitivities," in *2019 IEEE Power & Energy Society General Meeting (PESGM)*, pp. 1–5, IEEE, 2019.

[53] K. Jhala, B. Natarajan, and A. Pahwa, "Probabilistic voltage sensitivity analysis (pvsa) for random spatial distribution of active consumers," in *2018 IEEE Power & Energy Society Innovative Smart Grid Technologies Conference (ISGT)*, pp. 1–5, IEEE, 2018.

[54] E. P. Madruga and L. N. Canha, "Allocation and integrated configuration of capacitor banks and voltage regulators considering multi-objective variables in smart grid distribution system," in *2010 9th IEEE/IAS International Conference on Industry Applications-INDUSCON 2010*, pp. 1–6, IEEE, 2010.

[55] B. B. Zad, J. Lobry, and F. Vallee, "Coordinated control of on-load tap changer and d-statcom for voltage regulation of radial distribution systems with dg units," in *2013 3rd International Conference on Electric Power and Energy Conversion Systems*, pp. 1–5, IEEE, 2013.

[56] K. Jhala, B. Natarajan, and A. Pahwa, "Probabilistic voltage sensitivity analysis (pvsa)—a novel approach to quantify impact of active consumers," *IEEE Transactions on Power Systems*, vol. 33, no. 3, pp. 2518–2527, 2017.

[57] S. Munikoti, B. Natarajan, K. Jhala, and K. Lai, "Probabilistic voltage sensitivity analysis to quantify impact of high pv penetration on unbalanced distribution system," *IEEE Transactions on Power Systems*, pp. 1–1, 2021.

[58] K. Jhala, B. Natarajan, and A. Pahwa, "The dominant influencer of voltage fluctuation (divf) for power distribution system," *IEEE Transactions on Power Systems*, vol. 34, no. 6, pp. 4847–4856, 2019.

[59] R. Seguin, J. Woyak, D. Costyk, J. Hambrick, and B. Mather, "High-penetration pv integration handbook for distribution engineers," tech. rep., National Renewable Energy Lab.(NREL), Golden, CO (United States), 2016.

[60] S. Deshmukh, B. Natarajan, and A. Pahwa, "Voltage/var control in distribution networks via reactive power injection through distributed generators," *IEEE Transactions on smart grid*, vol. 3, no. 3, pp. 1226–1234, 2012.

[61] J. Barr and R. Majumder, "Integration of distributed generation in the volt/var management system for active distribution networks," *IEEE Transactions on Smart Grid*, vol. 6, no. 2, pp. 576–586, 2014.

[62] E. Demirok, P. C. Gonzalez, K. H. Frederiksen, D. Sera, P. Rodriguez, and R. Teodorescu, "Local reactive power control methods for overvoltage prevention of distributed solar inverters in low-voltage grids," *IEEE Journal of Photovoltaics*, vol. 1, no. 2, pp. 174–182, 2011.

[63] A. Kulmala, S. Repo, and P. Järventausta, "Coordinated voltage control in distribution networks including several distributed energy resources," *IEEE Transactions on Smart Grid*, vol. 5, no. 4, pp. 2010–2020, 2014.

[64] R. Tonkoski, L. A. Lopes, and T. H. El-Fouly, "Coordinated active power curtailment of grid connected pv inverters for overvoltage prevention," *IEEE Transactions on sustainable energy*, vol. 2, no. 2, pp. 139–147, 2010.

[65] A. Cagnano and E. De Tuglie, "Centralized voltage control for distribution networks with embedded pv systems," *Renewable Energy*, vol. 76, pp. 173–185, 2015.

[66] H. J. Liu, W. Shi, and H. Zhu, "Hybrid voltage control in distribution networks under limited communication rates," *IEEE Transactions on Smart Grid*, vol. 10, no. 3, pp. 2416–2427, 2018.

[67] Q. Yang, G. Wang, A. Sadeghi, G. B. Giannakis, and J. Sun, "Two-timescale voltage

control in distribution grids using deep reinforcement learning," *IEEE Transactions on Smart Grid*, vol. 11, no. 3, pp. 2313–2323, 2019.

[68] H. J. Liu, W. Shi, and H. Zhu, "Distributed voltage control in distribution networks: Online and robust implementations," *IEEE Transactions on Smart Grid*, vol. 9, no. 6, pp. 6106–6117, 2017.

[69] P. Papadopoulos, S. Skarvelis-Kazakos, I. Grau, L. M. Cipcigan, and N. Jenkins, "Predicting electric vehicle impacts on residential distribution networks with distributed generation," in *2010 IEEE Vehicle Power and Propulsion Conference*, pp. 1–5, IEEE, 2010.

[70] D. Singh, R. K. Misra, and D. Singh, "Effect of load models in distributed generation planning," *IEEE Transactions on Power Systems*, vol. 22, no. 4, pp. 2204–2212, 2007.

[71] M. Mokhtar, V. Robu, D. Flynn, C. Higgins, J. Whyte, C. Loughran, and F. Fulton, "Predicting the voltage distribution for low voltage networks using deep learning," in *2019 IEEE PES Innovative Smart Grid Technologies Europe (ISGT-Europe)*, pp. 1–5, IEEE, 2019.

[72] S. Munikoti, B. Natarajan, K. Jhala, and K. Lai, "Probabilistic voltage sensitivity analysis to quantify impact of high pv penetration on unbalanced distribution system," *IEEE Transactions on Power Systems*, vol. 36, no. 4, pp. 3080–3092, 2021.

[73] S. Dahale, H. S. Karimi, K. Lai, and B. Natarajan, "Sparsity based approaches for distribution grid state estimation - a comparative study," *IEEE Access*, vol. 8, pp. 198317–198327, 2020.

[74] E. Mulenga, M. H. Bollen, and N. Etherden, "A review of hosting capacity quantification methods for photovoltaics in low-voltage distribution grids," *International Journal of Electrical Power & Energy Systems*, vol. 115, p. 105445, 2020.

[75] M. Zain ul Abideen, O. Ellabban, and L. Al-Fagih, "A review of the tools and methods for distribution networks' hosting capacity calculation," *Energies*, vol. 13, no. 11, p. 2758, 2020.

[76] E. Mulenga, M. H. Bollen, and N. Etherden, "Solar pv stochastic hosting capacity in distribution networks considering aleatory and epistemic uncertainties," *International Journal of Electrical Power & Energy Systems*, vol. 130, p. 106928, 2021.

[77] A. Ali, K. Mahmoud, and M. Lehtonen, "Maximizing hosting capacity of uncertain photovoltaics by coordinated management of oltc, var sources and stochastic evs," *International Journal of Electrical Power & Energy Systems*, vol. 127, p. 106627, 2021.

[78] Y. Takenobu, N. Yasuda, S.-i. Minato, and Y. Hayashi, "Scalable enumeration approach for maximizing hosting capacity of distributed generation," *International Journal of Electrical Power & Energy Systems*, vol. 105, pp. 867–876, 2019.

[79] A. K. Jain, K. Horowitz, F. Ding, N. Gensollen, B. Mather, and B. Palmintier, "Quasi-static time-series pv hosting capacity methodology and metrics," in *2019 IEEE Power & Energy Society Innovative Smart Grid Technologies Conference (ISGT)*, pp. 1–5, IEEE, 2019.

[80] J. Smith and M. Rylander, "Stochastic analysis to determine feeder hosting capacity for distributed solar pv," *Electric Power Research Inst., Palo Alto, CA, Tech. Rep*, vol. 1026640, pp. 0885–8950, 2012.

[81] F. Ding and B. Mather, "On distributed pv hosting capacity estimation, sensitivity study, and improvement," *IEEE Transactions on Sustainable Energy*, vol. 8, no. 3, pp. 1010–1020, 2016.

[82] A. Dubey and S. Santoso, "On estimation and sensitivity analysis of distribution circuit's photovoltaic hosting capacity," *IEEE Transactions on Power Systems*, vol. 32, no. 4, pp. 2779–2789, 2016.

[83] M. Rylander, J. Smith, and W. Sunderman, "Streamlined method for determining distribution system hosting capacity," in *2015 IEEE Rural Electric Power Conference*, pp. 3–9, IEEE, 2015.

[84] Q. Xu, C. Kang, N. Zhang, Y. Ding, Q. Xia, R. Sun, and J. Xu, "A probabilistic method for determining grid-accommodable wind power capacity based on multiscenario system operation simulation," *IEEE Transactions on Smart Grid*, vol. 7, no. 1, pp. 400–409, 2014.

[85] H. Al-Saadi, R. Zivanovic, and S. F. Al-Sarawi, "Probabilistic hosting capacity for active distribution networks," *IEEE Transactions on Industrial Informatics*, vol. 13, no. 5, pp. 2519–2532, 2017.

[86] E. Mulenga, M. H. Bollen, and N. Etherden, "Distribution networks measured background voltage variations, probability distributions characterization and solar pv hosting capacity estimations," *Electric Power Systems Research*, vol. 192, p. 106979, 2021.

[87] R. Yan and T. K. Saha, "Voltage variation sensitivity analysis for unbalanced distribution networks due to photovoltaic power fluctuations," *IEEE Transactions on Power Systems*, vol. 27, no. 2, pp. 1078–1089, 2012.

[88] S. Kang, J. Kim, J.-W. Park, and S.-M. Baek, "Reactive power management based on voltage sensitivity analysis of distribution system with high penetration of renewable energies," *Energies*, vol. 12, no. 8, p. 1493, 2019.

[89] M. Brenna, E. De Berardinis, F. Foiadelli, G. Sapienza, and D. Zaninelli, "Voltage control in smart grids: An approach based on sensitivity theory," *Journal of Electromagnetic Analysis and Applications*, vol. 2010, 2010.

[90] B. B. Zad, J. Lobry, and F. Vallée, "A centralized approach for voltage control of mv distribution systems using dgs power control and a direct sensitivity analysis method," in *2016 IEEE International Energy Conference (ENERGYCON)*, pp. 1–6, IEEE, 2016.

[91] V. Klonari, B. B. Zad, J. Lobry, and F. Vallée, "Application of voltage sensitivity analysis in a probabilistic context for characterizing low voltage network operation," in *2016 International Conference on Probabilistic Methods Applied to Power Systems (PMAPS)*, pp. 1–7, IEEE, 2016.

[92] A. Kapoor, V. S. Patel, A. Sharma, and A. Mohapatra, "Centralized and decentralized pricing strategies for optimal scheduling of electric vehicles," *IEEE Transactions on Smart Grid*, vol. 13, no. 3, pp. 2234–2244, 2022.

[93] Y. Zhang, P. You, and L. Cai, "Optimal charging scheduling by pricing for ev charging station with dual charging modes," *IEEE Transactions on Intelligent Transportation Systems*, vol. 20, no. 9, pp. 3386–3396, 2018.

[94] Z. Liu, F. Wen, and G. Ledwich, "Optimal planning of electric-vehicle charging stations in distribution systems," *IEEE transactions on power delivery*, vol. 28, no. 1, pp. 102–110, 2012.

[95] S.-W. Park, K.-S. Cho, G. Hoefter, and S.-Y. Son, "Electric vehicle charging management using location-based incentives for reducing renewable energy curtailment considering the distribution system," *Applied Energy*, vol. 305, p. 117680, 2022.

[96] F. Ahmad, A. Iqbal, I. Ashraf, M. Marzband, *et al.*, "Optimal location of electric vehicle charging station and its impact on distribution network: A review," *Energy Reports*, vol. 8, pp. 2314–2333, 2022.

[97] Y. Wu, Z. Wang, Y. Huangfu, A. Ravey, D. Chrenko, and F. Gao, "Hierarchical operation of electric vehicle charging station in smart grid integration applications—an overview," *International Journal of Electrical Power & Energy Systems*, vol. 139, p. 108005, 2022.

[98] L. Luo, W. Gu, S. Zhou, H. Huang, S. Gao, J. Han, Z. Wu, and X. Dou, "Optimal planning of electric vehicle charging stations comprising multi-types of charging facilities," *Applied energy*, vol. 226, pp. 1087–1099, 2018.

[99] M. Z. Zeb, K. Imran, A. Khattak, A. K. Janjua, A. Pal, M. Nadeem, J. Zhang, and S. Khan, "Optimal placement of electric vehicle charging stations in the active distribution network," *IEEE Access*, vol. 8, pp. 68124–68134, 2020.

[100] P. Rajesh and F. H. Shajin, "Optimal allocation of ev charging spots and capacitors in distribution network improving voltage and power loss by quantum-behaved and gaussian mutational dragonfly algorithm (qgda)," *Electric Power Systems Research*, vol. 194, p. 107049, 2021.

[101] P. Saini and L. Gidwani, "An environmental based techno-economic assessment for battery energy storage system allocation in distribution system using new node voltage deviation sensitivity approach," *International Journal of Electrical Power & Energy Systems*, vol. 128, p. 106665, 2021.

[102] A. R. Kizhakkan, A. K. Rathore, and A. Awasthi, "Review of electric vehicle charging station location planning," in *2019 IEEE Transportation Electrification Conference (ITEC-India)*, pp. 1–5, IEEE, 2019.

[103] G. Zhou, Z. Zhu, and S. Luo, "Location optimization of electric vehicle charging stations: Based on cost model and genetic algorithm," *Energy*, vol. 247, p. 123437, 2022.

[104] S. Deb, X.-Z. Gao, K. Tammi, K. Kalita, and P. Mahanta, "A novel chicken swarm and teaching learning based algorithm for electric vehicle charging station placement problem," *Energy*, vol. 220, p. 119645, 2021.

[105] J. Cheng, J. Xu, W. Chen, and B. Song, "Locating and sizing method of electric vehicle charging station based on improved whale optimization algorithm," *Energy Reports*, vol. 8, pp. 4386–4400, 2022.

[106] S. R. Gampa, K. Jasthi, P. Goli, D. Das, and R. Bansal, "Grasshopper optimization algorithm based two stage fuzzy multiobjective approach for optimum sizing and placement of distributed generations, shunt capacitors and electric vehicle charging stations," *Journal of Energy Storage*, vol. 27, p. 101117, 2020.

[107] S. Nowak, L. Wang, and M. S. Metcalfe, "Two-level centralized and local voltage control in distribution systems mitigating effects of highly intermittent renewable generation," *International Journal of Electrical Power & Energy Systems*, vol. 119, p. 105858, 2020.

[108] E. Dall'Anese, S. V. Dhople, and G. B. Giannakis, "Optimal dispatch of photovoltaic inverters in residential distribution systems," *IEEE Transactions on Sustainable Energy*, vol. 5, no. 2, pp. 487–497, 2014.

[109] M. Farivar, C. R. Clarke, S. H. Low, and K. M. Chandy, "Inverter var control for distribution systems with renewables," in *2011 IEEE international conference on smart grid communications (SmartGridComm)*, pp. 457–462, IEEE, 2011.

[110] J. Li, Z. Xu, J. Zhao, and C. Zhang, "Distributed online voltage control in active distribution networks considering pv curtailment," *IEEE Transactions on Industrial Informatics*, vol. 15, no. 10, pp. 5519–5530, 2019.

[111] Y. Guo, Q. Wu, H. Gao, and F. Shen, "Distributed voltage regulation of smart distribution networks: Consensus-based information synchronization and distributed model predictive control scheme," *International Journal of Electrical Power & Energy Systems*, vol. 111, pp. 58–65, 2019.

[112] H. Almasalma and G. Deconinck, "Robust policy-based distributed voltage control provided by pv-battery inverters," *Ieee Access*, vol. 8, pp. 124939–124948, 2020.

[113] P. Šulc, S. Backhaus, and M. Chertkov, "Optimal distributed control of reactive power via the alternating direction method of multipliers," *IEEE Transactions on Energy Conversion*, vol. 29, no. 4, pp. 968–977, 2014.

[114] E. Dall'Anese, H. Zhu, and G. B. Giannakis, "Distributed optimal power flow for smart microgrids," *IEEE Transactions on Smart Grid*, vol. 4, no. 3, pp. 1464–1475, 2013.

[115] K. Baker, A. Bernstein, E. Dall'Anese, and C. Zhao, "Network-cognizant voltage droop

control for distribution grids," *IEEE Transactions on Power Systems*, vol. 33, no. 2, pp. 2098–2108, 2017.

[116] V. Nasirian, A. Davoudi, F. L. Lewis, and J. M. Guerrero, "Distributed adaptive droop control for dc distribution systems," *IEEE Transactions on Energy Conversion*, vol. 29, no. 4, pp. 944–956, 2014.

[117] P. P. Vergara, M. Salazar, T. T. Mai, P. H. Nguyen, and H. Slootweg, "A comprehensive assessment of pv inverters operating with droop control for overvoltage mitigation in lv distribution networks," *Renewable Energy*, vol. 159, pp. 172–183, 2020.

[118] X. Xie, X. Quan, Z. Wu, X. Cao, X. Dou, and Q. Hu, "Adaptive master-slave control strategy for medium voltage dc distribution systems based on a novel nonlinear droop controller," *IEEE Transactions on Smart Grid*, vol. 12, no. 6, pp. 4765–4777, 2021.

[119] M. Farivar, L. Chen, and S. Low, "Equilibrium and dynamics of local voltage control in distribution systems," in *52nd IEEE Conference on Decision and Control*, pp. 4329–4334, IEEE, 2013.

[120] H. Zhu and H. J. Liu, "Fast local voltage control under limited reactive power: Optimality and stability analysis," *IEEE Transactions on Power Systems*, vol. 31, no. 5, pp. 3794–3803, 2015.

[121] B. Zhang, A. D. Dominguez-Garcia, and D. Tse, "A local control approach to voltage regulation in distribution networks," in *2013 North American Power Symposium (NAPS)*, pp. 1–6, IEEE, 2013.

[122] N. Li, G. Qu, and M. Dahleh, "Real-time decentralized voltage control in distribution networks," in *2014 52nd Annual Allerton Conference on Communication, Control, and Computing (Allerton)*, pp. 582–588, IEEE, 2014.

[123] U. Sultana, A. B. Khairuddin, M. Aman, A. Mokhtar, and N. Zareen, "A review of optimum dg placement based on minimization of power losses and voltage stabil-

ity enhancement of distribution system," *Renewable and Sustainable Energy Reviews*, vol. 63, pp. 363–378, 2016.

[124] W. S. T. Fokui, M. J. Saulo, and L. Ngoo, "Optimal placement of electric vehicle charging stations in a distribution network with randomly distributed rooftop photovoltaic systems," *IEEE Access*, vol. 9, pp. 132397–132411, 2021.

[125] R. Piercy and S. L. Cress, "Recalculation of distribution system energy losses at hydro one," *Kinectrics Inc*, 2007.

[126] J. Dickert, M. Hable, and P. Schegner, "Energy loss estimation in distribution networks for planning purposes," in *2009 IEEE Bucharest PowerTech*, pp. 1–6, IEEE, 2009.

[127] R. Jackson, O. C. Onar, H. Kirkham, E. Fisher, K. Burkes, M. Starke, O. Mohammed, and G. Weeks, "Opportunities for energy efficiency improvements in the us electricity transmission and distribution system," *Oak Ridge National Laboratory Oak Ridge for the US Department of Energy*, pp. 3–9, 2015.

[128] A. S. Bretas, A. Rossoni, R. D. Trevizan, and N. G. Bretas, "Distribution networks nontechnical power loss estimation: A hybrid data-driven physics model-based framework," *Electric Power Systems Research*, vol. 186, p. 106397, 2020.

[129] N. Acharya, P. Mahat, and N. Mithulananthan, "An analytical approach for dg allocation in primary distribution network," *International Journal of Electrical Power & Energy Systems*, vol. 28, no. 10, pp. 669–678, 2006.

[130] A. Y. Abdelaziz, E. S. Ali, and S. Abd Elazim, "Flower pollination algorithm and loss sensitivity factors for optimal sizing and placement of capacitors in radial distribution systems," *International Journal of Electrical Power & Energy Systems*, vol. 78, pp. 207–214, 2016.

[131] K. Prakash and M. Sydulu, "A novel approach for optimal location and sizing of capacitors on radial distribution systems using loss sensitivity factors and/spl alpha/-

coefficients," in *2006 IEEE PES Power Systems Conference and Exposition*, pp. 1910–1913, IEEE, 2006.

[132] O. E. Olabode, I. K. Okakwu, A. S. Alayande, and T. O. Ajewole, "A two-stage approach to shunt capacitor-based optimal reactive power compensation using loss sensitivity factor and cuckoo search algorithm," *Energy Storage*, vol. 2, no. 2, p. e122, 2020.

[133] S. Kamel, A. Selim, F. Jurado, J. Yu, K. Xie, and T. Wu, "Capacitor allocation in distribution systems using fuzzy loss sensitivity factor with sine cosine algorithm," in *2019 IEEE Innovative Smart Grid Technologies-Asia (ISGT Asia)*, pp. 1276–1281, IEEE, 2019.

[134] S. Paul and W. Jewell, "Optimal capacitor placement and sizes for power loss reduction using combined power loss index-loss sensitivity factor and genetic algorithm," in *2012 IEEE Power and Energy Society General Meeting*, pp. 1–8, IEEE, 2012.

[135] J. Zhu, D. Hwang, and A. Sadjadpour, "Real time loss sensitivity calculation in power systems operation," *Electric power systems research*, vol. 73, no. 1, pp. 53–60, 2005.

[136] H. Abdel-mawgoud, S. Kamel, M. Tostado, J. Yu, and F. Jurado, "Optimal installation of multiple dg using chaotic moth-flame algorithm and real power loss sensitivity factor in distribution system," in *2018 International Conference on Smart Energy Systems and Technologies (SEST)*, pp. 1–5, IEEE, 2018.

[137] J. Z. Zhu, D. Hwang, and A. Sadjadpour, "Loss sensitivity calculation and analysis," in *2003 IEEE Power Engineering Society General Meeting (IEEE Cat. No. 03CH37491)*, vol. 2, pp. 962–967, IEEE, 2003.

[138] A. Singh and S. Parida, "Selection of load buses for dg placement based on loss reduction and voltage improvement sensitivity," in *2011 International Conference on Power Engineering, Energy and Electrical Drives*, pp. 1–6, IEEE, 2011.

[139] V. Murthy and A. Kumar, "Comparison of optimal dg allocation methods in radial distribution systems based on sensitivity approaches," *International Journal of Electrical Power & Energy Systems*, vol. 53, pp. 450–467, 2013.

[140] S.-J. Lee and S.-D. Yang, "Derivation of system loss sensitivity using optimization and application to improved eld computation," *International journal of electrical power & energy systems*, vol. 26, no. 6, pp. 461–464, 2004.

[141] V. Murty and A. Kumar, "Reactive power compensation in ubrds based on loss sensitivity appraoch," in *2014 6th IEEE Power India International Conference (PIICON)*, pp. 1–5, IEEE, 2014.

[142] A. Alburidy and L. Fan, "Loss locational sensitivity in distribution systems," in *2019 North American Power Symposium (NAPS)*, pp. 1–6, IEEE, 2019.

[143] J. Sardi, N. Mithulananthan, and D. Q. Hung, "A loss sensitivity factor method for locating es in a distribution system with pv units," in *2015 IEEE PES Asia-Pacific Power and Energy Engineering Conference (APPEEC)*, pp. 1–5, IEEE, 2015.

[144] N. Shaukat, S. Ali, C. Mehmood, B. Khan, M. Jawad, U. Farid, Z. Ullah, S. Anwar, and M. Majid, "A survey on consumers empowerment, communication technologies, and renewable generation penetration within smart grid," *Renewable and Sustainable Energy Reviews*, vol. 81, pp. 1453–1475, 2018.

[145] S. Dahale, H. S. Karimi, K. Lai, and B. Natarajan, "Sparsity based approaches for distribution grid state estimation-a comparative study," *IEEE Access*, vol. 8, pp. 198317–198327, 2020.

[146] H. S. Karimi and B. Natarajan, "Recursive dynamic compressive sensing in smart distribution systems," in *2020 IEEE Power & Energy Society Innovative Smart Grid Technologies Conference (ISGT)*, pp. 1–5, IEEE, 2020.

[147] R. Madbhavi, H. S. Karimi, B. Natarajan, and B. Srinivasan, "Tensor completion

based state estimation in distribution systems," in *2020 IEEE Power & Energy Society Innovative Smart Grid Technologies Conference (ISGT)*, pp. 1–5, IEEE, 2020.

[148] H. Farzin, M. Fotuhi-Firuzabad, and M. Moeini-Aghtaie, "Role of outage management strategy in reliability performance of multi-microgrid distribution systems," *IEEE Transactions on Power Systems*, vol. 33, no. 3, pp. 2359–2369, 2017.

[149] M. Zadsar, S. S. Sebtahmadi, M. Kazemi, S. Larimi, and M. Haghifam, "Two stage risk based decision making for operation of smart grid by optimal dynamic multi-microgrid," *International Journal of Electrical Power & Energy Systems*, vol. 118, p. 105791, 2020.

[150] C.-M. Jung, P. Ray, and S. R. Salkuti, "Asset management and maintenance: a smart grid perspective.," *International Journal of Electrical & Computer Engineering (2088-8708)*, vol. 9, no. 5, 2019.

[151] A. Arif, Z. Wang, J. Wang, and C. Chen, "Power distribution system outage management with co-optimization of repairs, reconfiguration, and dg dispatch," *IEEE Transactions on Smart Grid*, vol. 9, no. 5, pp. 4109–4118, 2017.

[152] H. T. Dinh, J. Yun, D. M. Kim, K.-H. Lee, and D. Kim, "A home energy management system with renewable energy and energy storage utilizing main grid and electricity selling," *IEEE Access*, vol. 8, pp. 49436–49450, 2020.

[153] M. Abujubbeh, F. Al-Turjman, and M. Fahrioglu, "Software-defined wireless sensor networks in smart grids: An overview," *Sustainable Cities and Society*, vol. 51, p. 101754, 2019.

[154] C. Li, X. Yu, W. Yu, G. Chen, and J. Wang, "Efficient computation for sparse load shifting in demand side management," *IEEE Transactions on Smart Grid*, vol. 8, no. 1, pp. 250–261, 2016.

[155] S. Sharda, M. Singh, and K. Sharma, "Demand side management through load shifting

in iot based hems: Overview, challenges and opportunities," *Sustainable Cities and Society*, p. 102517, 2020.

[156] R. Sivapriyan, K. M. Rao, and M. Harijyothi, "Literature review of iot based home automation system," in *2020 Fourth International Conference on Inventive Systems and Control (ICISC)*, pp. 101–105, IEEE, 2020.

[157] N. L. Dehghani, Y. M. Darestani, and A. Shafieezadeh, "Optimal life-cycle resilience enhancement of aging power distribution systems: A minlp-based preventive maintenance planning," *IEEE Access*, vol. 8, pp. 22324–22334, 2020.

[158] D. K. Asl, A. R. Seifi, M. Rastegar, and M. Mohammadi, "Optimal energy flow in integrated energy distribution systems considering unbalanced operation of power distribution systems," *International Journal of Electrical Power & Energy Systems*, vol. 121, p. 106132, 2020.

[159] V. Veeramsetty, V. Chintham, and D. M. V. Kumar, "Probabilistic locational marginal price computation in radial distribution system based on active power loss reduction," *IET generation, transmission & distribution*, vol. 14, no. 12, pp. 2292–2302, 2020.

[160] J. Zhu, Y. Yuan, and W. Wang, "An exact microgrid formation model for load restoration in resilient distribution system," *International Journal of Electrical Power & Energy Systems*, vol. 116, p. 105568, 2020.

[161] A. M. Imran, M. Kowsalya, and D. Kothari, "A novel integration technique for optimal network reconfiguration and distributed generation placement in power distribution networks," *International Journal of Electrical Power & Energy Systems*, vol. 63, pp. 461–472, 2014.

[162] S. Kalambe and G. Agnihotri, "Loss minimization techniques used in distribution network: bibliographical survey," *renewable and sustainable energy reviews*, vol. 29, pp. 184–200, 2014.

[163] A. Merlin, "Search for a minimal-loss operating spanning tree configuration for an urban power distribution system," *Proc. of 5th PSCC*, vol. 1, pp. 1–18, 1975.

[164] H. Fathabadi, "Power distribution network reconfiguration for power loss minimization using novel dynamic fuzzy c-means (dfcm) clustering based ann approach," *International Journal of Electrical Power & Energy Systems*, vol. 78, pp. 96–107, 2016.

[165] W. Dai, J. Yu, X. Liu, and W. Li, "Two-tier static equivalent method of active distribution networks considering sensitivity, power loss and static load characteristics," *International Journal of Electrical Power & Energy Systems*, vol. 100, pp. 193–200, 2018.

[166] J. Z. Zhu, "Optimal reconfiguration of electrical distribution network using the refined genetic algorithm," *Electric Power Systems Research*, vol. 62, no. 1, pp. 37–42, 2002.

[167] M. R. Kaveh, R.-A. Hooshmand, and S. M. Madani, "Simultaneous optimization of re-phasing, reconfiguration and dg placement in distribution networks using bf-sd algorithm," *Applied Soft Computing*, vol. 62, pp. 1044–1055, 2018.

[168] Q. Peng, Y. Tang, and S. H. Low, "Feeder reconfiguration in distribution networks based on convex relaxation of opf," *IEEE Transactions on Power Systems*, vol. 30, no. 4, pp. 1793–1804, 2014.

[169] B. Amanulla, S. Chakrabarti, and S. Singh, "Reconfiguration of power distribution systems considering reliability and power loss," *IEEE transactions on power delivery*, vol. 27, no. 2, pp. 918–926, 2012.

[170] K. Muthukumar and S. Jayalalitha, "Integrated approach of network reconfiguration with distributed generation and shunt capacitors placement for power loss minimization in radial distribution networks," *Applied Soft Computing*, vol. 52, pp. 1262–1284, 2017.

[171] J. Savier and D. Das, "Impact of network reconfiguration on loss allocation of radial distribution systems," *IEEE Transactions on Power Delivery*, vol. 22, no. 4, pp. 2473–2480, 2007.

[172] J. Wen, Y. Tan, L. Jiang, and K. Lei, "Dynamic reconfiguration of distribution networks considering the real-time topology variation," *IET Generation, Transmission & Distribution*, vol. 12, no. 7, pp. 1509–1517, 2017.

[173] S. Kansal, V. Kumar, and B. Tyagi, "Hybrid approach for optimal placement of multiple dgs of multiple types in distribution networks," *International Journal of Electrical Power & Energy Systems*, vol. 75, pp. 226–235, 2016.

[174] C. K. Das, O. Bass, G. Kothapalli, T. S. Mahmoud, and D. Habibi, "Overview of energy storage systems in distribution networks: Placement, sizing, operation, and power quality," *Renewable and Sustainable Energy Reviews*, vol. 91, pp. 1205–1230, 2018.

[175] P. S. Georgilakis and N. D. Hatziargyriou, "Optimal distributed generation placement in power distribution networks: models, methods, and future research," *IEEE Transactions on power systems*, vol. 28, no. 3, pp. 3420–3428, 2013.

[176] D. Q. Hung, N. Mithulananthan, and R. Bansal, "Analytical expressions for dg allocation in primary distribution networks," *IEEE Transactions on energy conversion*, vol. 25, no. 3, pp. 814–820, 2010.

[177] Y. Atwa, E. El-Saadany, M. Salama, and R. Seethapathy, "Optimal renewable resources mix for distribution system energy loss minimization," *IEEE Transactions on Power Systems*, vol. 25, no. 1, pp. 360–370, 2009.

[178] D. Q. Hung and N. Mithulananthan, "Multiple distributed generator placement in primary distribution networks for loss reduction," *IEEE Transactions on industrial electronics*, vol. 60, no. 4, pp. 1700–1708, 2011.

[179] S. G. Naik, D. Khatod, and M. Sharma, "Optimal allocation of combined dg and capacitor for real power loss minimization in distribution networks," *International Journal of Electrical Power & Energy Systems*, vol. 53, pp. 967–973, 2013.

[180] M. Kowsalya *et al.*, "Optimal distributed generation and capacitor placement in power distribution networks for power loss minimization," in *2014 International Conference on Advances in Electrical Engineering (ICAEE)*, pp. 1–6, IEEE, 2014.

[181] V. R. VC *et al.*, "Optimal renewable resources placement in distribution networks by combined power loss index and whale optimization algorithms," *Journal of Electrical Systems and Information Technology*, vol. 5, no. 2, pp. 175–191, 2018.

[182] K. Muthukumar and S. Jayalalitha, "Optimal placement and sizing of distributed generators and shunt capacitors for power loss minimization in radial distribution networks using hybrid heuristic search optimization technique," *International Journal of Electrical Power & Energy Systems*, vol. 78, pp. 299–319, 2016.

[183] P. V. Babu and S. Singh, "Optimal placement of dg in distribution network for power loss minimization using nlp & pls technique," *Energy Procedia*, vol. 90, pp. 441–454, 2016.

[184] A. Selim, S. Kamel, and F. Jurado, "Hybrid optimization technique for optimal placement of dg and d-statcom in distribution networks," in *2018 Twentieth International Middle East Power Systems Conference (MEPCON)*, pp. 689–693, IEEE, 2018.

[185] H. Abdel-mawgoud, S. Kamel, M. Ebeed, and A.-R. Youssef, "Optimal allocation of renewable dg sources in distribution networks considering load growth," in *2017 Nineteenth International Middle East Power Systems Conference (MEPCON)*, pp. 1236–1241, IEEE, 2017.

[186] D. Q. Hung, N. Mithulananthan, and K. Y. Lee, "Optimal placement of dispatchable and nondispatchable renewable dg units in distribution networks for minimizing energy loss," *International Journal of Electrical Power & Energy Systems*, vol. 55, pp. 179–186, 2014.

[187] Z. Ullah, M. Elkadeem, and S. Wang, "Power loss minimization and reliability en-

hancement in active distribution networks considering res uncertainty," *International Journal of Renewable Energy Research (IJRER)*, vol. 9, no. 3, pp. 1232–1240, 2019.

[188] S. Ganguly and D. Samajpati, "Distributed generation allocation on radial distribution networks under uncertainties of load and generation using genetic algorithm," *IEEE transactions on sustainable energy*, vol. 6, no. 3, pp. 688–697, 2015.

[189] A. Waqar, U. Subramaniam, K. Farzana, R. M. Elavarasan, H. U. R. Habib, M. Zahid, and E. Hossain, "Analysis of optimal deployment of several dgs in distribution networks using plant propagation algorithm," *IEEE Access*, vol. 8, pp. 175546–175562, 2020.

[190] R. Viral and D. K. Khatod, "An analytical approach for sizing and siting of dgs in balanced radial distribution networks for loss minimization," *International Journal of Electrical Power & Energy Systems*, vol. 67, pp. 191–201, 2015.

[191] S. M. Sajjadi, M.-R. Haghifam, and J. Salehi, "Simultaneous placement of distributed generation and capacitors in distribution networks considering voltage stability index," *International Journal of Electrical Power & Energy Systems*, vol. 46, pp. 366–375, 2013.

[192] J.-Y. Park, J.-M. Sohn, and J.-K. Park, "Optimal capacitor allocation in a distribution system considering operation costs," *IEEE Transactions on Power Systems*, vol. 24, no. 1, pp. 462–468, 2009.

[193] I. Ziari, G. Ledwich, A. Ghosh, D. Cornforth, and M. Wishart, "Optimal allocation and sizing of capacitors to minimize the transmission line loss and to improve the voltage profile," *Computers & Mathematics with Applications*, vol. 60, no. 4, pp. 1003–1013, 2010.

[194] S. Kannan, P. Renuga, S. Kalyani, and E. Muthukumaran, "Optimal capacitor placement and sizing using fuzzy-de and fuzzy-mapso methods," *Applied Soft Computing*, vol. 11, no. 8, pp. 4997–5005, 2011.

[195] S. Kola Sampangi and J. Thangavelu, "Optimal capacitor allocation in distribution networks for minimization of power loss and overall cost using water cycle algorithm

and grey wolf optimizer," *International Transactions on Electrical Energy Systems*, vol. 30, no. 5, p. e12320, 2020.

[196] M. Dixit, P. Kundu, and H. R. Jariwala, "Optimal integration of shunt capacitor banks in distribution networks for assessment of techno-economic asset," *Computers & Electrical Engineering*, vol. 71, pp. 331–345, 2018.

[197] M. Kasaei and M. Gandomkar, "Loss reduction in distribution network using simultaneous capacitor placement and reconfiguration with ant colony algorithm," in *2010 Asia-Pacific Power and Energy Engineering Conference*, pp. 1–4, IEEE, 2010.

[198] S. Pazouki, A. Mohsenzadeh, M.-R. Haghifam, and S. Ardalan, "Simultaneous allocation of charging stations and capacitors in distribution networks improving voltage and power loss," *Canadian Journal of Electrical and Computer Engineering*, vol. 38, no. 2, pp. 100–105, 2015.

[199] M. Ashari, R. Syahputra, *et al.*, "Power loss reduction strategy of distribution network with distributed generator integration," in *2014 The 1st International Conference on Information Technology, Computer, and Electrical Engineering*, pp. 404–408, IEEE, 2014.

[200] M. J. Mirzaei, A. Kazemi, and O. Homaee, "A probabilistic approach to determine optimal capacity and location of electric vehicles parking lots in distribution networks," *IEEE Transactions on industrial informatics*, vol. 12, no. 5, pp. 1963–1972, 2015.

[201] S. Sachan and N. Kishor, "Optimal location for centralized charging of electric vehicle in distribution network," in *2016 18th Mediterranean Electrotechnical Conference (MELECON)*, pp. 1–6, IEEE, 2016.

[202] G. Wang, Z. Xu, F. Wen, and K. P. Wong, "Traffic-constrained multiobjective planning of electric-vehicle charging stations," *IEEE Transactions on Power Delivery*, vol. 28, no. 4, pp. 2363–2372, 2013.

[203] S. Deb, A. K. Goswami, P. Harsh, J. P. Sahoo, R. L. Chetri, R. Roy, and A. S. Shekhawat, "Charging coordination of plug-in electric vehicle for congestion management in distribution system integrated with renewable energy sources," *IEEE Transactions on Industry Applications*, vol. 56, no. 5, pp. 5452–5462, 2020.

[204] S. Wang, Z. Y. Dong, F. Luo, K. Meng, and Y. Zhang, "Stochastic collaborative planning of electric vehicle charging stations and power distribution system," *IEEE Transactions on Industrial Informatics*, vol. 14, no. 1, pp. 321–331, 2017.

[205] G. Bharati and S. Paudyal, "Coordinated control of distribution grid and electric vehicle loads," *Electric Power Systems Research*, vol. 140, pp. 761–768, 2016.

[206] C. Wang, R. Dunn, and B. Lian, "Power loss reduction for electric vehicle penetration with embedded energy storage in distribution networks," in *2014 IEEE International Energy Conference (ENERGYCON)*, pp. 1417–1424, IEEE, 2014.

[207] E. Mortaz, A. Vinel, and Y. Dvorkin, "An optimization model for siting and sizing of vehicle-to-grid facilities in a microgrid," *Applied energy*, vol. 242, pp. 1649–1660, 2019.

[208] L. Luo, Z. Wu, W. Gu, H. Huang, S. Gao, and J. Han, "Coordinated allocation of distributed generation resources and electric vehicle charging stations in distribution systems with vehicle-to-grid interaction," *Energy*, vol. 192, p. 116631, 2020.

[209] A. Kavousi-Fard, M. A. Rostami, and T. Niknam, "Reliability-oriented reconfiguration of vehicle-to-grid networks," *IEEE transactions on industrial informatics*, vol. 11, no. 3, pp. 682–691, 2015.

[210] L. Wang and B. Chen, "Distributed control for large-scale plug-in electric vehicle charging with a consensus algorithm," *International Journal of Electrical Power & Energy Systems*, vol. 109, pp. 369–383, 2019.

[211] E. Veldman and R. A. Verzijlbergh, "Distribution grid impacts of smart electric vehicle charging from different perspectives," *IEEE Transactions on Smart Grid*, vol. 6, no. 1, pp. 333–342, 2014.

[212] S. Deilami, A. S. Masoum, P. S. Moses, and M. A. Masoum, "Real-time coordination of plug-in electric vehicle charging in smart grids to minimize power losses and improve voltage profile," *IEEE Transactions on Smart Grid*, vol. 2, no. 3, pp. 456–467, 2011.

[213] S. Yu, J. Zhang, and L. Wang, "Power management strategy with regenerative braking for fuel cell hybrid electric vehicle," in *2009 Asia-Pacific Power and Energy Engineering Conference*, pp. 1–4, IEEE, 2009.

[214] R. Xiong, J. Cao, and Q. Yu, "Reinforcement learning-based real-time power management for hybrid energy storage system in the plug-in hybrid electric vehicle," *Applied energy*, vol. 211, pp. 538–548, 2018.

[215] E. Apostolaki-Iosifidou, P. Codani, and W. Kempton, "Measurement of power loss during electric vehicle charging and discharging," *Energy*, vol. 127, pp. 730–742, 2017.

[216] G. J. Osório, M. Shafie-khah, P. D. Coimbra, M. Lotfi, and J. P. Catalão, "Distribution system operation with electric vehicle charging schedules and renewable energy resources," *Energies*, vol. 11, no. 11, p. 3117, 2018.

[217] J. Wang, G. R. Bharati, S. Paudyal, O. Ceylan, B. P. Bhattarai, and K. S. Myers, "Coordinated electric vehicle charging with reactive power support to distribution grids," *IEEE Transactions on Industrial Informatics*, vol. 15, no. 1, pp. 54–63, 2018.

[218] Z. Peng and L. Hao, "Decentralized coordination of electric vehicle charging stations for active power compensation," in *2017 IEEE 86th Vehicular Technology Conference (VTC-Fall)*, pp. 1–5, IEEE, 2017.

[219] S. M. B. Sadati, J. Moshtagh, M. Shafie-khah, and J. P. Catalão, "Smart distribution system operational scheduling considering electric vehicle parking lot and demand response programs," *Electric Power Systems Research*, vol. 160, pp. 404–418, 2018.

[220] R. Luthander, M. Shepero, J. Munkhammar, and J. Widén, "Photovoltaics and opportunistic electric vehicle charging in the power system–a case study on a swedish

distribution grid," *IET Renewable Power Generation*, vol. 13, no. 5, pp. 710–716, 2019.

[221] Z. A. Arfeen, A. B. Khairuddin, A. Munir, M. K. Azam, M. Faisal, and M. S. B. Arif, "En route of electric vehicles with the vehicle to grid technique in distribution networks: Status and technological review," *Energy Storage*, vol. 2, no. 2, p. e115, 2020.

[222] K. M. Tan, V. K. Ramachandaramurthy, and J. Y. Yong, "Optimal vehicle to grid planning and scheduling using double layer multi-objective algorithm," *Energy*, vol. 112, pp. 1060–1073, 2016.

[223] F. Mwasilu, J. J. Justo, E.-K. Kim, T. D. Do, and J.-W. Jung, "Electric vehicles and smart grid interaction: A review on vehicle to grid and renewable energy sources integration," *Renewable and sustainable energy reviews*, vol. 34, pp. 501–516, 2014.

[224] L. Ramesh, S. Chowdhury, S. Chowdhury, A. Natarajan, and C. Gaunt, "Minimization of power loss in distribution networks by different techniques," *International Journal of Electrical Power and Energy Systems Engineering*, vol. 2, no. 1, pp. 1–6, 2009.

[225] I. Power and E. Society, "Ieee pes amps dsas test feeder working group," 2021. https://site.ieee.org/pes-testfeeders/resources/.

[226] C. Muscas, M. Pau, P. A. Pegoraro, and S. Sulis, "Effects of measurements and pseudomeasurements correlation in distribution system state estimation," *IEEE Transactions on Instrumentation and Measurement*, vol. 63, no. 12, pp. 2813–2823, 2014.

[227] H. O. Lancaster and E. Seneta, "Chi-square distribution," *Encyclopedia of biostatistics*, vol. 2, 2005.

[228] L.-L. Chuang and Y.-S. Shih, "Approximated distributions of the weighted sum of correlated chi-squared random variables," *Journal of Statistical Planning and Inference*, vol. 142, no. 2, pp. 457–472, 2012.

[229] S.-C. Tsai, W.-G. Tzeng, and H.-L. Wu, "On the jensen-shannon divergence and variational distance," *IEEE transactions on information theory*, vol. 51, no. 9, pp. 3333–3336, 2005.

[230] A. Majtey, P. Lamberti, and D. Prato, "Jensen-shannon divergence as a measure of distinguishability between mixed quantum states," *Physical Review A*, vol. 72, no. 5, p. 052310, 2005.

[231] A. M. Joshua and K. P. Vittal, "Protection schemes for a battery energy storage system based microgrid," *Electric Power Systems Research*, vol. 204, p. 107701, 2022.

[232] S. Patel, K. Murari, and S. Kamalasadan, "Distributed control of distributed energy resources in active power distribution system for local power balance with optimal spectral clustering," *IEEE Transactions on Industry Applications*, 2022.

[233] K. Khan, I. El-Sayed, and P. Arboleya, "Multi-issue negotiation evs charging mechanism in highly congested distribution networks," *IEEE Transactions on Vehicular Technology*, 2022.

[234] A. M. Mathai and S. B. Provost, *Quadratic forms in random variables: theory and applications*. Dekker, 1992.

[235] "IEEE PES AMPS DSAS Test Feeder Working Group." https://site.ieee.org/pes-testfeeders/resources/. Accessed: 2021-08-10.

[236] S. Munikoti, K. Jhala, K. Lai, and B. Natarajan, "Analytical voltage sensitivity analysis for unbalanced power distribution system," in *2020 IEEE Power Energy Society General Meeting (PESGM)*, pp. 1–5, 2020.

[237] S. Dahale and B. Natarajan, "Joint matrix completion and compressed sensing for state estimation in low-observable distribution system," in *2021 IEEE PES Innovative Smart Grid Technologies Conference - Latin America (ISGT Latin America)*, pp. 1–5, 2021.

[238] S. D. Babacan, M. Luessi, R. Molina, and A. K. Katsaggelos, "Sparse bayesian methods for low-rank matrix estimation," *IEEE Transactions on Signal Processing*, vol. 60, no. 8, pp. 3964–3977, 2012.

[239] R. Tonkoski, D. Turcotte, and T. H. El-Fouly, "Impact of high pv penetration on voltage profiles in residential neighborhoods," *IEEE Transactions on Sustainable Energy*, vol. 3, no. 3, pp. 518–527, 2012.

[240] J. Vasilj, P. Sarajcev, and D. Jakus, "Pv power forecast error simulation model," in *2015 12th International Conference on the European Energy Market (EEM)*, pp. 1–5, IEEE, 2015.

[241] M. Nakagami, "The m-distribution—a general formula of intensity distribution of rapid fading," in *Statistical methods in radio wave propagation*, pp. 3–36, Elsevier, 1960.

[242] W. H. Kersting, "Radial distribution test feeders," *IEEE Transactions on Power Systems*, vol. 6, no. 3, pp. 975–985, 1991.

[243] "California Distributed Generation Statistics." https://www.californiadgstats.ca.gov/. Accessed: 2022-01-02.

[244] S. Maharjan, A. M. Khambadkone, and J. C.-H. Peng, "Robust constrained model predictive voltage control in active distribution networks," *IEEE Transactions on Sustainable Energy*, vol. 12, no. 1, pp. 400–411, 2020.

[245] P. Balram, O. Carlson, *et al.*, "Predictive voltage control of batteries and tap changers in distribution system with photovoltaics," in *2016 Power Systems Computation Conference (PSCC)*, pp. 1–7, IEEE, 2016.

[246] G. Qu and N. Li, "Optimal distributed feedback voltage control under limited reactive power," *IEEE Transactions on Power Systems*, vol. 35, no. 1, pp. 315–331, 2019.

[247] P. L. Donti, Y. Liu, A. J. Schmitt, A. Bernstein, R. Yang, and Y. Zhang, "Matrix

completion for low-observability voltage estimation," *IEEE Transactions on Smart Grid*, vol. 11, no. 3, pp. 2520–2530, 2020.

[248] G. Valverde and T. Van Cutsem, "Model predictive control of voltages in active distribution networks," *IEEE Transactions on Smart Grid*, vol. 4, no. 4, pp. 2152–2161, 2013.

[249] V. Calderaro, V. Galdi, F. Lamberti, and A. Piccolo, "A smart strategy for voltage control ancillary service in distribution networks," *IEEE Transactions on Power Systems*, vol. 30, no. 1, pp. 494–502, 2014.

[250] A. Dutta, S. Ganguly, and C. Kumar, "Mpc-based coordinated voltage control in active distribution networks incorporating cvr and dr," *IEEE Transactions on Industry Applications*, 2022.

[251] S. Boyd, S. P. Boyd, and L. Vandenberghe, *Convex optimization*. Cambridge university press, 2004.

[252] S. J. Wright, "Efficient convex optimization for linear mpc," in *Handbook of model predictive control*, pp. 287–303, Springer, 2019.

[253] M. S. Lau, S.-P. Yue, K. V. Ling, and J. M. Maciejowski, "A comparison of interior point and active set methods for fpga implementation of model predictive control," in *2009 European Control Conference (ECC)*, pp. 156–161, IEEE, 2009.

[254] Y. P. Agalgaonkar, B. C. Pal, and R. A. Jabr, "Stochastic distribution system operation considering voltage regulation risks in the presence of pv generation," *IEEE Transactions on Sustainable Energy*, vol. 6, no. 4, pp. 1315–1324, 2015.

[255] S. Dahale and B. Natarajan, "Bayesian framework for multi-timescale state estimation in low-observable distribution systems," *IEEE Transactions on Power Systems*, 2022.

[256] M. Farina, L. Giulioni, and R. Scattolini, "Stochastic linear model predictive control with chance constraints–a review," *Journal of Process Control*, vol. 44, pp. 53–67, 2016.

[257] "eGauge Monitoring Systems." https://www.egauge.net/home-energy-monitor/. Accessed: 2022-04-06.

Appendix A

Proof of Lemma 1

This proof derives the procedure for $\boldsymbol{\Delta I_e^h}$ decomposition.

Proof. The change in current flow for three phases (in Eq. (5.5)) due to one actor node can be written as,

$$\boldsymbol{\Delta I_e^h} \approxeq \left[\frac{\Delta S_A^{a*}}{V_A^{a*} + \Delta V_A^{a*}}, \frac{\Delta S_A^{b*}}{V_A^{b*} + \Delta V_A^{b*}}, \frac{\Delta S_A^{c*}}{V_A^{c*} + \Delta V_A^{c*}} \right]^T. \tag{A.1}$$

According to Eq. A.1, the change in current flow (ΔI_e^a) for phase a can be written in terms of the complex quantities of power change, nodal voltage, and voltage change as,

$$\Delta I_e^a \approxeq \frac{\Delta P_A^a - j\Delta Q_A^a}{V_A^{a,r} - jV_A^{a,i} + \Delta V_A^{a,r} - j\Delta V_A^{a,i}} \tag{A.2}$$

which can be rewritten as follows,

$$\Delta I_e^a \approxeq \frac{(\Delta P_A^a - j\Delta Q_A^a)\,\boldsymbol{\chi}}{[(V_A^{a,r} + \Delta V_A^{a,r}) - j\,(V_A^{a,r} + \Delta V_A^{a,r})]\,\boldsymbol{\chi}} \tag{A.3}$$

where, $\boldsymbol{\chi} \triangleq [(V_A^{a,r} + \Delta V_A^{a,r}) + j\,(V_A^{a,r} + \Delta V_A^{a,r})]$. Note that the quantity $\boldsymbol{\chi}$ helps to separate real and imaginary parts as shown in Eq. (A.3). Further simplification on Eq. (A.3) yields

Eq. (A.4).

$$\begin{aligned}\Delta I_e^a &\approx \frac{\Delta P_A^a\left(V_A^{a,r}+\Delta V_A^{a,r}\right)+\Delta Q_A^a\left(V_A^{a,i}+\Delta V_A^{a,i}\right)+j[\mathcal{G}]}{\left(V_A^{a,r}+\Delta V_A^{a,r}\right)^2+\left(V_A^{a,i}+\Delta V_A^{a,i}\right)^2} \\ &\approx \frac{\Delta P_A^a V_A^{a,r}\left(1+\frac{\Delta V_A^{a,r}}{V_A^{a,r}}\right)+\Delta Q_A^a V_A^{a,i}\left(1+\frac{\Delta V_A^{a,i}}{V_A^{a,i}}\right)+j[\mathcal{G}']}{\left(V_A^{a,r}\left(1+\frac{\Delta V_A^{a,r}}{V_A^{a,r}}\right)\right)^2+\left(V_A^{a,i}\left(1+\frac{\Delta V_A^{a,i}}{V_A^{a,i}}\right)\right)^2}\end{aligned} \tag{A.4}$$

where, $\mathcal{G} \triangleq \Delta P_A^a\left(V_A^{a,i}+\Delta V_A^{a,i}\right)-\Delta Q_A^a\left(V_A^{a,r}+\Delta V_A^{a,r}\right)$ and $\mathcal{G}' \triangleq \Delta P_A^a V_A^{a,i}\left(1+\frac{\Delta V_A^{a,i}}{V_A^{a,i}}\right)-\Delta Q_A^a V_A^{a,r}\left(1+\frac{\Delta V_A^{a,r}}{V_A^{a,r}}\right)$. Using Assumption 4, Eq. (A.4) reduces to,

$$\begin{aligned}\Delta I_e^{a,r}+j\Delta I_e^{a,i} \triangleq& \frac{\Delta P_A^a V_A^{a,r}+\Delta Q_A^a V_A^{a,i}}{(V_A^{a,r})^2+(V_A^{a,i})^2} \\ &+ j\frac{\Delta P_A V_A^{a,i}-\Delta Q_A V_A^{a,r}}{(V_A^{a,r})^2+(V_A^{a,i})^2}=\frac{\Delta S_A^{a*}}{V_A^{a*}}\end{aligned} \tag{A.5}$$

Hence, proved. This result is used to derive the expression for multiple actor nodes (Eq. (5.8)). Note that the expression in Eq. (A.4) can be similarly derived for phases b and c. □

Appendix B

Topology information vectors

The topology information vectors consist of the relationship between active and reactive power change, and real and imaginary parts of current change. Note that the elements of the topology information vector can be easily computed for every actor node in the system. Nodes where there is no power change, the influence indicator will be zero. Hence, will not contribute to the change in current flow. Eq. (B.1) and (B.2) contain the topology information vectors for phase b.

$$\boldsymbol{k}_r^b = \Bigg[\frac{\Psi_{M1}^b \cos\theta_1^b}{|V_1^b|}, \frac{\Psi_{M2}^b \cos\theta_1^b}{|V_2^b|}, \ldots, \frac{\Psi_{M\mathcal{N}}^b \cos\theta_{\mathcal{N}}^b}{|V_{\mathcal{N}}^b|}, -\frac{\Psi_{M1}^b \sin\theta_1^a}{|V_1^b|}, -\frac{\Psi_{M2}^b \sin\theta_1^a}{|V_2^b|}, \ldots, -\frac{\Psi_{M\mathcal{N}^b} \sin\theta_{\mathcal{N}}^b}{|V_{\mathcal{N}}^b|}\Bigg]^T \tag{B.1}$$

$$\boldsymbol{k}_i^b = \Bigg[-\frac{\Psi_{M1}^b \sin\theta_1^b}{|V_1^b|}, -\frac{\Psi_{M2}^b \sin\theta_1^b}{|V_2^b|}, \ldots, -\frac{\Psi_{M\mathcal{N}}^b \sin\theta_{\mathcal{N}}^b}{|V_{\mathcal{N}}^b|}, -\frac{\Psi_{M1}^b \cos\theta_1^b}{|V_1^b|}, -\frac{\Psi_{M2}^b \cos\theta_1^b}{|V_2^b|}, \ldots, -\frac{\Psi_{M\mathcal{N}^b} \cos\theta_{\mathcal{N}}^b}{|V_{\mathcal{N}}^b|}\Bigg]^T \tag{B.2}$$

Similarly, the topology information vectors can be computed for phase c as shown in Eq. (B.3) and (B.4),

$$\boldsymbol{k}_r^c = \Bigg[\frac{\Psi_{M1}^c \cos\theta_1^c}{|V_1^c|}, \frac{\Psi_{M2}^c \cos\theta_1^c}{|V_2^c|}, \ldots, \frac{\Psi_{M\mathcal{N}}^c \cos\theta_{\mathcal{N}}^c}{|V_{\mathcal{N}}^c|}, -\frac{\Psi_{M1}^c \sin\theta_1^c}{|V_1^c|}, -\frac{\Psi_{M2}^c \sin\theta_1^c}{|V_2^c|}, \ldots, -\frac{\Psi_{M\mathcal{N}^c} \sin\theta_{\mathcal{N}}^c}{|V_{\mathcal{N}}^c|}\Bigg]^T \tag{B.3}$$

$$\boldsymbol{k}_i^c = \Bigg[-\frac{\Psi_{M1}^c \sin\theta_1^c}{|V_1^c|}, -\frac{\Psi_{M2}^c \sin\theta_1^c}{|V_2^c|}, \ldots, -\frac{\Psi_{M\mathcal{N}}^c \sin\theta_{\mathcal{N}}^c}{|V_{\mathcal{N}}^c|}, \\ -\frac{\Psi_{M1}^c \cos\theta_1^c}{|V_1^c|}, -\frac{\Psi_{M2}^c \cos\theta_1^c}{|V_2^c|}, \ldots, -\frac{\Psi_{M\mathcal{N}^c} \cos\theta_{\mathcal{N}}^c}{|V_{\mathcal{N}}^c|} \Bigg]^T . \tag{B.4}$$

Appendix C

ST-PVSA derivation

The change in complex voltage at any phase (say phase a) of observation node O due to change in complex power at any phase of a single actor node A is given as [57],

$$\Delta V_{OA}^{a} \approx -\left[\frac{\Delta S_{A}^{a\star} Z_{OA}^{aa}}{V_{A}^{a\star}} + \frac{\Delta S_{A}^{b\star} Z_{OA}^{ab}}{V_{A}^{b\star}} + \frac{\Delta S_{A}^{c\star} Z_{OA}^{ac}}{V_{A}^{c\star}}\right], \tag{C.1}$$

On expanding the complex power and shared path impedance terms, we get the following equation,

$$\begin{aligned} \Delta V_{OA}^{a} &\approx -\left[\frac{(\Delta P_{A}^{a} - j\Delta Q_{A}^{a})(R_{OA}^{aa} + jX_{OA}^{aa})}{V_{A}^{a\star}} + ...\right], \\ &\approx -\left[\frac{(\Delta P_{A}^{a} R_{OA}^{aa} + Q_{A}^{a} X_{OA}^{aa}) + j(\Delta P_{A}^{a} X_{OA}^{aa} - R_{OA}^{aa} \Delta Q_{A}^{a})}{(V_{A}^{a,r} - jV_{A}^{a,i}) + (\Delta V_{A}^{a,r} - \Delta V_{A}^{a,i})} + ...\right], \end{aligned} \tag{C.2}$$

On normalizing the numerator and denominator, (C.2) reduces to

$$\Delta V_{OA}^{a} \approx -\frac{(\Delta P_{A}^{a} R_{OA}^{aa} + \Delta Q_{A}^{a} X_{OA}^{aa}) + j(\Delta P_{A}^{a} X_{OA}^{aa} - R_{OA}^{aa} \Delta Q_{A}^{a})}{(V_{A}^{a,r} + \Delta V_{A}^{a,r}) - j(V_{A}^{a,i} + \Delta V_{A}^{a,i})} \tag{C.3}$$

$$\times \frac{(V_{A}^{a,r} + \Delta V_{A}^{a,r}) + j(V_{A}^{a,i} + \Delta V_{A}^{a,i})}{(V_{A}^{a,r} + \Delta V_{A}^{a,r}) + j(V_{A}^{a,i} + \Delta V_{A}^{a,i})} + ..., \tag{C.4}$$

Normalization segregates (C.3) into real and imaginary parts as shown below,

$$\begin{aligned}\Delta V_{OA}^{a} \approx -\Bigg[&\frac{(\Delta P_A^a R_{OA}^{aa} + \Delta Q_A^a X_{OA}^{aa})(\hat{V}_A^{a,r}) - (\Delta P_A^a X_{OA}^{aa} - R_{OA}^{aa}\Delta Q_A^a)(\hat{V}_A^{a,i})}{(\hat{V}_A^{a,r})^2 + (\hat{V}_A^{a,i})^2} - \dots \\ &+ j\frac{(\Delta P_A^a R_{OA}^{aa} + \Delta Q_A^a X_{OA}^{aa})(\hat{V}_A^{a,i}) + (\Delta P_A^a X_{OA}^{aa} - R_{OA}^{aa}\Delta Q_A^a)(\hat{V}_A^{a,r})}{(\hat{V}_A^{a,r})^2 + (\hat{V}_A^{a,i})^2} - \dots\Bigg].\end{aligned} \tag{C.5}$$

Where, $\hat{V}_A^{a,r} \triangleq V_A^{a,r} + \Delta V_A^{a,r}$ and $\hat{V}_A^{a,i} \triangleq V_A^{a,i} + \Delta V_A^{a,i}$. The real part of the voltage change can be expressed as,

$$\Delta V_{OA}^{a,r} \approx -\left[\frac{(\Delta P_A^a R_{OA}^{aa} + \Delta Q_A^a X_{OA}^{aa})V_A^{a,r}\bar{V}_A^{a,r}}{(V_A^{a,r})^2(\bar{V}_A^{a,r})^2 + (V_A^{a,i})^2(\bar{V}_A^{a,i})^2} - \frac{(\Delta P_A^a X_{OA}^{aa} - \Delta Q_A^a R_{OA}^{aa})V_A^{a,i}\bar{V}_A^{a,i}}{(V_A^{a,r})^2(\bar{V}_A^{a,r})^2 + (V_A^{a,i})^2(\bar{V}_A^{a,i})^2} - \dots\right], \tag{C.6}$$

where, $\bar{V}_A^{a,r} \triangleq 1 + \frac{\Delta V_A^{a,r}}{V_A^{a,r}}$ and $\bar{V}_A^{a,i} \triangleq 1 + \frac{\Delta V_A^{a,i}}{V_A^{a,i}}$. Using the same assumptions as in [57], Eq. (C.6) can further be simplified as,

$$\Delta V_{OA}^{a,r} \approx -\left[\frac{(\Delta P_A^a R_{OA}^{aa} + \Delta Q_A^a X_{OA}^{aa})(V_A^{a,r})}{(V_A^{a,r})^2 + (V_A^{a,i})^2} - \frac{(\Delta P_A^a X_{OA}^{aa} - \Delta Q_A^a R_{OA}^{aa})(V_A^{a,i})}{(V_A^{a,r})^2 + (V_A^{a,i})^2} - \dots\right]. \tag{C.7}$$

Similarly, the imaginary part of the voltage change can be written as,

$$\Delta V_{OA}^{a,i} \approx -\left[\frac{(\Delta P_A^a X_{OA}^{aa} - \Delta Q_A^a R_{OA}^{aa})(V_A^{a,r})}{(V_A^{a,r})^2 + (V_A^{a,i})^2} + \frac{(\Delta P_A^a R_{OA}^{aa} + \Delta Q_A^a X_{OA}^{aa})(V_A^{a,i})}{(V_A^{a,r})^2 + (V_A^{a,i})^2} - \dots\right], \tag{C.8}$$

Equations (C.7) and (C.8) are rearranged by taking the common factor with power terms as shown below,

$$\begin{aligned}\Delta V_{OA}^{a,r} &\approx -\left[\frac{\Delta P_A^a(R_{OA}^{aa}V_A^{a,r} - X_{OA}^{aa}V_A^{a,i})}{(V_A^{a,r})^2 + (V_A^{a,i})^2} + \frac{\Delta Q_A^a(X_{OA}^{aa}V_A^{a,r} + R_{OA}^{aa}V_A^{a,i})}{(V_A^{a,r})^2 + (V_A^{a,i})^2} - \dots\right] \\ \Delta V_{OA}^{a,i} &\approx -\left[\frac{\Delta P_A^a(R_{OA}^{aa}V_A^{a,i} + X_{OA}^{aa}V_A^{a,r})}{(V_A^{a,r})^2 + (V_A^{a,i})^2} + \frac{\Delta Q_A^a(X_{OA}^{aa}V_A^{a,i} - R_{OA}^{aa}V_A^{a,r})}{(V_A^{a,r})^2 + (V_A^{a,i})^2} - \dots\right]\end{aligned} \tag{C.9}$$

Finally, the real and imaginary part of base voltages are expressed in polar magnitude form

(i.e., $V_A^{a,r} = |V_A^a| cos(\omega_A)$ $V_A^{a,i} = |V_A^a| sin(\omega_A)$) which reduces (C.9) to,

$$\Delta V_{OA}^{a,r} \approx -\left[\frac{\Delta P_A^a (R_{OA}^{aa} cos(\omega_A) - X_{OA}^{aa} sin(\omega_A))}{|V_A^a|} + \frac{\Delta Q_A^a (X_{OA}^{aa} cos(\omega_A) + R_{OA}^{aa} sin(\omega_A))}{|V_A^a|} - \dots\right]$$
$$\Delta V_{OA}^{a,i} \approx -\left[\frac{\Delta P_A^a (R_{OA}^{aa} sin(\omega_A) + X_{OA}^{aa} cos(\omega_A))}{|V_A^a|} + \frac{\Delta Q_A^a (X_{OA}^{aa} sin(\omega_A) - R_{OA}^{aa} cos(\omega_A))}{|V_A^a|} - \dots\right]. \tag{C.10}$$

Appendix D

Covariance matrix

The complete covariance matrix can be defined to capture the variance and covariance of complex power change at actor nodes as follows,

$$\boldsymbol{\Sigma_{\Delta S}} = \begin{bmatrix} \sigma^2_{p_1} & \dots & cov(p_n, p_1) & cov(q_1, p_1) & \dots & cov(q_n, p_1) \\ \vdots & \ddots & \vdots & \vdots & \ddots & \vdots \\ cov(p_1, p_n) & \dots & \sigma^2_{p_n} & cov(q_1, p_n) & \dots & cov(q_n, q_n) \\ cov(p_1, q_1) & \dots & cov(p_n, q_1) & \sigma^2_{q_1} & \dots & cov(q_n, p_1) \\ \vdots & \ddots & \vdots & \vdots & \ddots & \vdots \\ cov(p_1, q_n) & \dots & cov(p_n, q_n) & cov(q_1, q_n) & \dots & \sigma^2_{q_n} \end{bmatrix} \tag{D.1}$$

the diagonal terms represent the variance of active or reactive power change at actor nodes whereas the off-diagonal elements are the covariance between them due to geographical proximity.

Appendix E

Proof of Proposition 1

Proof. Solving Problem 2 with m control nodes, n voltage states and N time steps requires $\mathbb{O}(N(n+m)^3)$ flops [251]. Since $1 < \check{m} \leq m$, Problem 2 can be solved with $\mathbb{O}(N(n+\check{m})^3)$ flops, which yields a reduction in the computational complexity by a factor of $m - \check{m}$. Considering $\check{n} \subset n$ critical nodes to be monitored further reduces the computational complexity to $\mathbb{O}(N(\check{n}+\check{m})^3)$, i.e., a reduction factor of $(n-\check{n}) + (m-\check{m})$. Based on system topology and the amount of complex power changes at actor nodes $\mathcal{A}$, controlling the most dominant nodes in the system guarantees voltage stability margin [32]. Therefore, it is possible to reduce the computational complexity of Problem 1 by at least a factor of $(m-\check{m})$ for any SVI set of nodes with $1 < \check{m} \leq m$. □

Appendix F

Proof of Proposition 2

Proof. Consider one observation node $O \in \mathcal{O}$ and one actor node $A \in \mathcal{A}$. Let $\Delta x_{O.1}^{a,A}$ and $\Delta x_{O.2}^{a,A}$ be the real and imaginary parts of voltage change at phase a of observation node O due to reactive power change at A, respectively. According to (8.13), it is possible to induce small changes ($\Delta x_{O.1}^{a,A}$ and $\Delta x_{O.2}^{a,A}$) such that the voltage state vector in (8.15) satisfies safe operational limits, i.e., $0.95 < \mathbf{\Gamma x} < 1.05$ p.u. Pick two actor nodes d_O^1 and d_O^m (according to 8.21) such that they have ranks 1 and m based on their influence on voltage of node O, respectively. The DIVF paradigm states that [32],

$$D_{KL}(\Delta x_{O.\mathfrak{M}}^{a} || \Delta x_{O.\mathfrak{M}}^{a,d_O^1}) > D_{KL}(\Delta x_{O.\mathfrak{M}}^{a} || \Delta x_{O.\mathfrak{M}}^{a,d_O^m}). \tag{F.1}$$

From (8.14), The change in real and imaginary parts of voltage change can be written in terms of the reactive power change at A as $\Delta x_{O.1}^{a,A} = \mathbf{B}(\Delta x_{O.1}^{a,A}, A)\Delta q_A$, $\Delta x_{O.2}^{a,A} = \mathbf{B}(\Delta x_{O.2}^{a,A}, A)\Delta q_A$, respectively. Therefore,

$$\begin{aligned}
\Delta x_{O.1}^{d_O^1} &= \mathbf{B}(\Delta x_{O.1}^{d_O^1}, d_O^1)\Delta q_{d_O^1} \\
&> \Delta x_{O.1}^{d_O^m} = \mathbf{B}(\Delta x_{O.1}^{d_O^m}, d_O^m)\Delta q_{d_O^m} \\
\Delta x_{O.2}^{d_O^1} &= \mathbf{B}(\Delta x_{O.2}^{d_O^1}, d_O^1)\Delta q_{d_O^1} \\
&> \Delta x_{O.2}^{d_O^m} = \mathbf{B}(\Delta x_{O.2}^{d_O^m}, d_O^m)\Delta q_{d_O^m}.
\end{aligned} \tag{F.2}$$

Note that in (F.2), $\mathbf{B}(.,.)$ are scalar quantities since they relate the sensitivity of voltage change at one observation node due to one actor node. This means that the same change in real and imaginary parts of voltage $\Delta x_{O.1}^{d_O^1} = \Delta x_{O.1}^{d_O^m}$ and $\Delta x_{O.2}^{d_O^1} = \Delta x_{O.2}^{d_O^m}$ can be achieved but with a smaller control signal when using the dominant node d_O^1 instead of d_O^m, i.e., $\Delta q_{d_O^1} < \Delta q_{d_O^m}$. Now that the proof is shown for one observation node $O \in \mathcal{O}$, it is possible to generalize the concept to all observation nodes with voltage violations $\check{O} \subset \mathcal{O}$ and any SVI set with cardinality $\check{m}$ as in (8.36). Let $\mathbf{\Delta x}_{\check{O}.1}$ and $\mathbf{\Delta x}_{\check{O}.2}$ be the vectors of the change in real and imaginary parts of voltage at nodes $\check{O}$, respectively. Then, similarly, it is possible to induce small changes to each element $\Delta x_{i.1} \in \mathbf{\Delta x}_{\check{O}.1}$ and $\Delta x_{i.2} \in \mathbf{\Delta x}_{\check{O}.2}$ $\forall i \in \check{O}$ such that voltage magnitude at these location is brought within safe operational limits. Define $\{\mathfrak{D}_{\check{\mathcal{O}}}^*\}$ according to 8.36 and let $\hat{\mathfrak{D}}_{\check{\mathcal{O}}}^* \triangleq \mathfrak{D}_{\check{\mathcal{O}}} \backslash \{\mathfrak{D}_{\check{\mathcal{O}}}^*\}$. Then, it is evident from the CPF in (8.35) that,

$$\left\|\mathbf{\Delta x}_{\check{O}.1}^{\mathfrak{D}_{\check{\mathcal{O}}}^*}\right\|_2 > \left\|\mathbf{\Delta x}_{\check{O}.1}^{\hat{\mathfrak{D}}_{\check{\mathcal{O}}}^*}\right\|_2, \ \left\|\mathbf{\Delta x}_{\check{O}.2}^{\mathfrak{D}_{\check{\mathcal{O}}}^*}\right\|_2 > \left\|\mathbf{\Delta x}_{\check{O}.2}^{\hat{\mathfrak{D}}_{\check{\mathcal{O}}}^*}\right\|_2 \tag{F.3}$$

where, $\mathbf{\Delta x}_{\check{O}.1}^{i}$ and $\mathbf{\Delta x}_{\check{O}.2}^{i}$ represent vectors of the change in real and imaginary parts of voltage of nodes $\check{O}$ due to the change in reactive power at actor nodes within the sets $i \in \{\mathfrak{D}_{\check{\mathcal{O}}}^*, \hat{\mathfrak{D}}_{\check{\mathcal{O}}}^*\}$. In other words, it is possible to achieve equality between the norms in (F.3) with smaller reactive power changes (or cost of control) at any time k, i.e.,

$$\begin{aligned}&(V(\mathbf{x}_0, \mathbf{\Delta q}_k^*) \mid \mathbf{\Delta q}_k^* \in \mathfrak{D}_{\check{\mathcal{O}}}^*) \\ &\qquad < (V(\mathbf{x}_0, \mathbf{\Delta q}_k^*) \mid \mathbf{\Delta q}_k^* \in \hat{\mathfrak{D}}_{\check{\mathcal{O}}}^*) \ \forall k.\end{aligned} \tag{F.4}$$

Therefore, using the optimal DIVF set $\mathfrak{D}_{\check{\mathcal{O}}}^*$ helps reduce the cost of voltage control in Problem 1 compared to the non-optimal set $\hat{\mathfrak{D}}_{\check{\mathcal{O}}}^*$. □

Appendix G

Interior-point method

It is possible to rewrite voltage state and reactive power support vectors for the horizon $k \in [0, N_c - 1]$ as $\bar{\mathbf{x}} \triangleq [\mathbf{x}_1, ..., \mathbf{x}_{N_c}]^\intercal$ and $\boldsymbol{\Delta}\bar{\mathbf{q}} \triangleq [\boldsymbol{\Delta}\mathbf{q}_0, ..., \boldsymbol{\Delta}\mathbf{q}_{N_c-1}]^\intercal$, respectively. The resulting model constraints 8.27a and 8.27b can be rewritten as,

$$\bar{\mathbf{x}} = \bar{\mathbf{A}}\mathbf{x}_0 + \bar{\mathbf{D}}\boldsymbol{\Delta}\bar{\mathbf{p}} + \bar{\mathbf{B}}\boldsymbol{\Delta}\bar{\mathbf{q}} \tag{G.1}$$

$$\bar{\mathbf{H}}\bar{\mathbf{x}} + \bar{\mathbf{G}}\boldsymbol{\Delta}\bar{\mathbf{q}} \leq \bar{\mathbf{h}} \tag{G.2}$$

with the following cost function $V(\mathbf{x}_0, \boldsymbol{\Delta}\bar{\mathbf{q}}) \triangleq \boldsymbol{\Delta}\bar{\mathbf{q}}^\intercal\bar{\mathbf{R}}\boldsymbol{\Delta}\bar{\mathbf{q}}$ where, $\bar{\mathbf{A}}, \bar{\mathbf{D}}, \boldsymbol{\Delta}\bar{\mathbf{p}}, \bar{\mathbf{B}}, \bar{\mathbf{G}}, \bar{\mathbf{H}}, \bar{\mathbf{h}}$ and $\bar{\mathbf{R}}$ are defined as shown below. Substituting (G.1) into (G.2) yields, $\bar{\mathbf{H}}\bar{\mathbf{A}}\mathbf{x}_0 + \bar{\mathbf{H}}\bar{\mathbf{D}}\boldsymbol{\Delta}\bar{\mathbf{p}} + \bar{\mathbf{H}}\bar{\mathbf{B}}\boldsymbol{\Delta}\bar{\mathbf{q}} + \bar{\mathbf{G}}\boldsymbol{\Delta}\bar{\mathbf{q}} \leq \bar{\mathbf{h}}$ and therefore, Problem 1 reduces to,

$$V(\mathbf{x}_0, \boldsymbol{\Delta}\bar{\mathbf{q}}) = \min_{\boldsymbol{\Delta}\bar{\mathbf{q}}} \boldsymbol{\Delta}\bar{\mathbf{q}}^\intercal\bar{\mathbf{R}}\boldsymbol{\Delta}\bar{\mathbf{q}} \tag{G.3}$$

$$\text{s.t.} \quad [\bar{\mathbf{H}}\bar{\mathbf{B}} + \bar{\mathbf{G}}]\boldsymbol{\Delta}\bar{\mathbf{q}} \leq \bar{\mathbf{h}} - \bar{\mathbf{H}}\bar{\mathbf{A}}\mathbf{x}_0 - \bar{\mathbf{H}}\bar{\mathbf{D}}\boldsymbol{\Delta}\bar{\mathbf{p}} \tag{G.3a}$$

This quadratic program can be solved efficiently using the interior point or active set method [252].

$$\bar{\boldsymbol{x}} \triangleq \begin{bmatrix} \boldsymbol{x}_0 \\ \boldsymbol{x}_1 \\ \vdots \\ \boldsymbol{x}_N \end{bmatrix}, \bar{\boldsymbol{u}} \triangleq \begin{bmatrix} \boldsymbol{\Delta q}_0 \\ \boldsymbol{\Delta q}_1 \\ \vdots \\ \boldsymbol{\Delta q}_{N-1} \end{bmatrix}, \qquad \bar{\boldsymbol{h}} \triangleq \begin{bmatrix} \boldsymbol{h} \\ \boldsymbol{h} \\ \vdots \\ \boldsymbol{h} \\ \boldsymbol{h} \end{bmatrix}, \bar{\boldsymbol{A}} \triangleq \begin{bmatrix} \boldsymbol{A} \\ \boldsymbol{A^2} \\ \vdots \\ \vdots \\ \boldsymbol{A^N} \end{bmatrix} \tag{G.4}$$

$$\bar{\boldsymbol{B}} \triangleq \begin{bmatrix} \boldsymbol{B} & \boldsymbol{0} & \boldsymbol{0} & \dots & \boldsymbol{0} \\ \boldsymbol{AB} & \boldsymbol{B} & \boldsymbol{0} & \dots & \boldsymbol{0} \\ \boldsymbol{A^2B} & \boldsymbol{AB} & \boldsymbol{B} & \dots & \boldsymbol{0} \\ \vdots & \vdots & \vdots & \ddots & \vdots \\ \boldsymbol{A^{N-1}B} & \boldsymbol{A^{N-2}B} & \boldsymbol{A^{N-3}B} & \dots & \boldsymbol{B} \end{bmatrix} \tag{G.5}$$

$$\bar{\boldsymbol{R}} \triangleq \begin{bmatrix} \boldsymbol{R} & & & \\ & \boldsymbol{R} & & \\ & & \ddots & \\ & & & \boldsymbol{R} \end{bmatrix}, \bar{\boldsymbol{G}} \triangleq \begin{bmatrix} \boldsymbol{G} & & & \\ & \boldsymbol{G} & & \\ & & \ddots & \\ & & & \boldsymbol{G} \\ 0 & 0 & 0 & 0 \end{bmatrix},$$

$$\bar{\boldsymbol{D}} \triangleq \begin{bmatrix} \boldsymbol{D} & & & \\ & \boldsymbol{D} & & \\ & & \ddots & \\ & & & \boldsymbol{D} \end{bmatrix}, \bar{\boldsymbol{H}} \triangleq \begin{bmatrix} \boldsymbol{H} & & & \\ & \boldsymbol{H} & & \\ & & \ddots & \\ & & & \boldsymbol{H} \\ & & & & \boldsymbol{H} \end{bmatrix}.$$

Appendix H

Reuse permissions

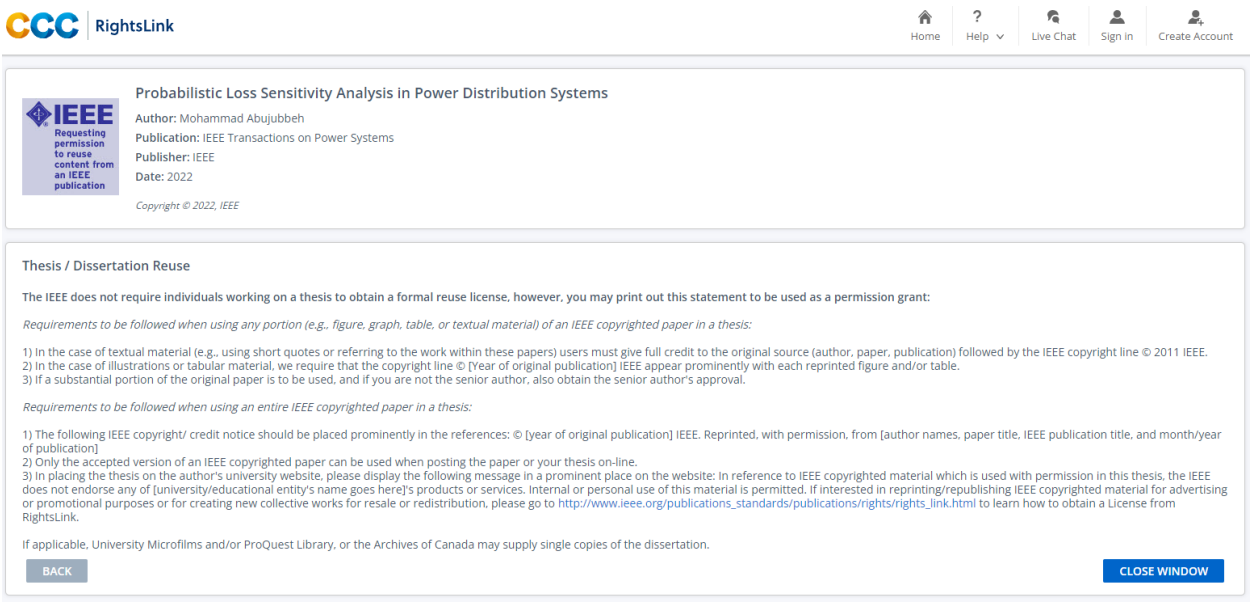

RightsLink

Home | Help | Live Chat | Sign in | Create Account

IEEE Requesting permission to reuse content from an IEEE publication

An Information Theoretic Approach to Identify Dominant Voltage Influencers for Unbalanced Distribution Systems

Author: Sai Munikoti
Publication: IEEE Transactions on Power Systems
Publisher: IEEE
Date: November 2022

Copyright © 2022, IEEE

Thesis / Dissertation Reuse

The IEEE does not require individuals working on a thesis to obtain a formal reuse license, however, you may print out this statement to be used as a permission grant:

Requirements to be followed when using any portion (e.g., figure, graph, table, or textual material) of an IEEE copyrighted paper in a thesis:

1) In the case of textual material (e.g., using short quotes or referring to the work within these papers) users must give full credit to the original source (author, paper, publication) followed by the IEEE copyright line © 2011 IEEE.
2) In the case of illustrations or tabular material, we require that the copyright line © [Year of original publication] IEEE appear prominently with each reprinted figure and/or table.
3) If a substantial portion of the original paper is to be used, and if you are not the senior author, also obtain the senior author's approval.

Requirements to be followed when using an entire IEEE copyrighted paper in a thesis:

1) The following IEEE copyright/ credit notice should be placed prominently in the references: © [year of original publication] IEEE. Reprinted, with permission, from [author names, paper title, IEEE publication title, and month/year of publication]
2) Only the accepted version of an IEEE copyrighted paper can be used when posting the paper or your thesis on-line.
3) In placing the thesis on the author's university website, please display the following message in a prominent place on the website: In reference to IEEE copyrighted material which is used with permission in this thesis, the IEEE does not endorse any of [university/educational entity's name goes here]'s products or services. Internal or personal use of this material is permitted. If interested in reprinting/republishing IEEE copyrighted material for advertising or promotional purposes or for creating new collective works for resale or redistribution, please go to http://www.ieee.org/publications_standards/publications/rights/rights_link.html to learn how to obtain a License from RightsLink.

If applicable, University Microfilms and/or ProQuest Library, or the Archives of Canada may supply single copies of the dissertation.

BACK | CLOSE WINDOW

RightsLink

Home | Help | Live Chat | Mohammad Abujubbeh

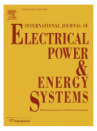

A novel framework for hosting capacity analysis with spatio-temporal probabilistic voltage sensitivity analysis

Author: Sai Munikoti,Mohammad Abujubbeh,Kumarsinh Jhala,Balasubramaniam Natarajan
Publication: International Journal of Electrical Power & Energy Systems
Publisher: Elsevier
Date: January 2022

© 2021 Elsevier Ltd. All rights reserved.

Journal Author Rights

Please note that, as the author of this Elsevier article, you retain the right to include it in a thesis or dissertation, provided it is not published commercially. Permission is not required, but please ensure that you reference the journal as the original source. For more information on this and on your other retained rights, please visit: https://www.elsevier.com/about/our-business/policies/copyright#Author-rights

BACK | CLOSE WINDOW

RightsLink

Home | Help | Live Chat | Mohammad Abujubbeh

IEEE Requesting permission to reuse content from an IEEE publication

Optimal Voltage Control in Low-Observable Unbalanced Distribution Systems

Conference Proceedings: 2022 IEEE Power & Energy Society Innovative Smart Grid Technologies Conference (ISGT)
Author: Mohammad Abujubbeh
Publisher: IEEE
Date: 24 April 2022

Copyright © 2022, IEEE

Thesis / Dissertation Reuse

The IEEE does not require individuals working on a thesis to obtain a formal reuse license, however, you may print out this statement to be used as a permission grant:

Requirements to be followed when using any portion (e.g., figure, graph, table, or textual material) of an IEEE copyrighted paper in a thesis:

1) In the case of textual material (e.g., using short quotes or referring to the work within these papers) users must give full credit to the original source (author, paper, publication) followed by the IEEE copyright line © 2011 IEEE.
2) In the case of illustrations or tabular material, we require that the copyright line © [Year of original publication] IEEE appear prominently with each reprinted figure and/or table.
3) If a substantial portion of the original paper is to be used, and if you are not the senior author, also obtain the senior author's approval.

Requirements to be followed when using an entire IEEE copyrighted paper in a thesis:

1) The following IEEE copyright/ credit notice should be placed prominently in the references: © [year of original publication] IEEE. Reprinted, with permission, from [author names, paper title, IEEE publication title, and month/year of publication]
2) Only the accepted version of an IEEE copyrighted paper can be used when posting the paper or your thesis on-line.
3) In placing the thesis on the author's university website, please display the following message in a prominent place on the website: In reference to IEEE copyrighted material which is used with permission in this thesis, the IEEE does not endorse any of [university/educational entity's name goes here]'s products or services. Internal or personal use of this material is permitted. If interested in reprinting/republishing IEEE copyrighted material for advertising or promotional purposes or for creating new collective works for resale or redistribution, please go to http://www.ieee.org/publications_standards/publications/rights/rights_link.html to learn how to obtain a License from RightsLink.

If applicable, University Microfilms and/or ProQuest Library, or the Archives of Canada may supply single copies of the dissertation.

BACK | CLOSE WINDOW

CCC RightsLink

Home | Help | Live Chat | Mohammad Abujubbeh

IEEE Requesting permission to reuse content from an IEEE publication

Voltage Violation Prediction in Unobservable Distribution Systems

Conference Proceedings: 2022 IEEE Power & Energy Society General Meeting (PESGM)
Author: Mohammad Abujubbeh
Publisher: IEEE
Date: 17 July 2022

Copyright © 2022, IEEE

Thesis / Dissertation Reuse

The IEEE does not require individuals working on a thesis to obtain a formal reuse license, however, you may print out this statement to be used as a permission grant:

Requirements to be followed when using any portion (e.g., figure, graph, table, or textual material) of an IEEE copyrighted paper in a thesis:

1) In the case of textual material (e.g., using short quotes or referring to the work within these papers) users must give full credit to the original source (author, paper, publication) followed by the IEEE copyright line © 2011 IEEE.
2) In the case of illustrations or tabular material, we require that the copyright line © [Year of original publication] IEEE appear prominently with each reprinted figure and/or table.
3) If a substantial portion of the original paper is to be used, and if you are not the senior author, also obtain the senior author's approval.

Requirements to be followed when using an entire IEEE copyrighted paper in a thesis:

1) The following IEEE copyright/ credit notice should be placed prominently in the references: © [year of original publication] IEEE. Reprinted, with permission, from [author names, paper title, IEEE publication title, and month/year of publication]
2) Only the accepted version of an IEEE copyrighted paper can be used when posting the paper or your thesis on-line.
3) In placing the thesis on the author's university website, please display the following message in a prominent place on the website: In reference to IEEE copyrighted material which is used with permission in this thesis, the IEEE does not endorse any of [university/educational entity's name goes here]'s products or services. Internal or personal use of this material is permitted. If interested in reprinting/republishing IEEE copyrighted material for advertising or promotional purposes or for creating new collective works for resale or redistribution, please go to http://www.ieee.org/publications_standards/publications/rights/rights_link.html to learn how to obtain a License from RightsLink.

If applicable, University Microfilms and/or ProQuest Library, or the Archives of Canada may supply single copies of the dissertation.

BACK CLOSE WINDOW

CCC RightsLink

Home | Help | Live Chat | Mohammad Abujubbeh

IEEE Requesting permission to reuse content from an IEEE publication

Analytical Power Loss Sensitivity Analysis in Distribution Systems

Conference Proceedings: 2021 IEEE Power & Energy Society General Meeting (PESGM)
Author: Mohammad Abujubbeh
Publisher: IEEE
Date: 26 July 2021

Copyright © 2021, IEEE

Thesis / Dissertation Reuse

The IEEE does not require individuals working on a thesis to obtain a formal reuse license, however, you may print out this statement to be used as a permission grant:

Requirements to be followed when using any portion (e.g., figure, graph, table, or textual material) of an IEEE copyrighted paper in a thesis:

1) In the case of textual material (e.g., using short quotes or referring to the work within these papers) users must give full credit to the original source (author, paper, publication) followed by the IEEE copyright line © 2011 IEEE.
2) In the case of illustrations or tabular material, we require that the copyright line © [Year of original publication] IEEE appear prominently with each reprinted figure and/or table.
3) If a substantial portion of the original paper is to be used, and if you are not the senior author, also obtain the senior author's approval.

Requirements to be followed when using an entire IEEE copyrighted paper in a thesis:

1) The following IEEE copyright/ credit notice should be placed prominently in the references: © [year of original publication] IEEE. Reprinted, with permission, from [author names, paper title, IEEE publication title, and month/year of publication]
2) Only the accepted version of an IEEE copyrighted paper can be used when posting the paper or your thesis on-line.
3) In placing the thesis on the author's university website, please display the following message in a prominent place on the website: In reference to IEEE copyrighted material which is used with permission in this thesis, the IEEE does not endorse any of [university/educational entity's name goes here]'s products or services. Internal or personal use of this material is permitted. If interested in reprinting/republishing IEEE copyrighted material for advertising or promotional purposes or for creating new collective works for resale or redistribution, please go to http://www.ieee.org/publications_standards/publications/rights/rights_link.html to learn how to obtain a License from RightsLink.

If applicable, University Microfilms and/or ProQuest Library, or the Archives of Canada may supply single copies of the dissertation.

BACK CLOSE WINDOW

CCC | RightsLink

Home | Help | Live Chat | Mohammad Abujubbeh

IEEE Requesting permission to reuse content from an IEEE publication

Probabilistic Voltage Sensitivity based Preemptive Voltage Monitoring in Unbalanced Distribution Networks

Conference Proceedings: 2020 52nd North American Power Symposium (NAPS)
Author: Mohammad Abujubbeh
Publisher: IEEE
Date: 11 April 2021

Copyright © 2021, IEEE

Thesis / Dissertation Reuse

The IEEE does not require individuals working on a thesis to obtain a formal reuse license, however, you may print out this statement to be used as a permission grant:

Requirements to be followed when using any portion (e.g., figure, graph, table, or textual material) of an IEEE copyrighted paper in a thesis:

1) In the case of textual material (e.g., using short quotes or referring to the work within these papers) users must give full credit to the original source (author, paper, publication) followed by the IEEE copyright line © 2011 IEEE.
2) In the case of illustrations or tabular material, we require that the copyright line © [Year of original publication] IEEE appear prominently with each reprinted figure and/or table.
3) If a substantial portion of the original paper is to be used, and if you are not the senior author, also obtain the senior author's approval.

Requirements to be followed when using an entire IEEE copyrighted paper in a thesis:

1) The following IEEE copyright/ credit notice should be placed prominently in the references: © [year of original publication] IEEE. Reprinted, with permission, from [author names, paper title, IEEE publication title, and month/year of publication]
2) Only the accepted version of an IEEE copyrighted paper can be used when posting the paper or your thesis on-line.
3) In placing the thesis on the author's university website, please display the following message in a prominent place on the website: In reference to IEEE copyrighted material which is used with permission in this thesis, the IEEE does not endorse any of [university/educational entity's name goes here]'s products or services. Internal or personal use of this material is permitted. If interested in reprinting/republishing IEEE copyrighted material for advertising or promotional purposes or for creating new collective works for resale or redistribution, please go to http://www.ieee.org/publications_standards/publications/rights/rights_link.html to learn how to obtain a License from RightsLink.

If applicable, University Microfilms and/or ProQuest Library, or the Archives of Canada may supply single copies of the dissertation.

BACK CLOSE WINDOW